

Applications of Surface Ligand Design to Flotation

Iria M. Río Echevarría



**Doctor of Philosophy
The University of Edinburgh**

2007

ABSTRACT

This thesis involves the design, synthesis and testing of organic hydrophobic ligands. They would act as co-collectors in froth flotation processes to enhance the recovery of sulfidic minerals which have undergone some oxidation on processing and are not efficiently collected by the commercial reagents used in froth flotation. Strong and selective binding to iron(III) oxide/hydroxide surfaces, e.g. goethite, over unwanted siliceous material was considered essential criteria for such new co-collectors.

A general overview of froth flotation processes is given in Chapter 1 as well as a description of the analytical techniques used in this thesis and the features that the ligands must have to act as co-collectors.

On the basis of the strong binding to iron(III) surfaces of the organic ligand Irgacor 419[®], used commercially as a corrosion inhibitor for iron, this compound was studied as a potential co-collector. Adsorption isotherms were determined by UV-Vis spectroscopy for two carboxylic acids that may also bind strongly to goethite, the results of which are discussed in Chapter 2.

Chapter 3 involves the measurement of the strength of binding of one the most widely used type of collectors for sulfide ores, potassium ethyl xanthate. Complications in the analysis of materials in solution by both ICP-OES and UV-Vis spectroscopy arose due to the instability of potassium ethyl xanthate in solution, making determination and interpretation of isotherms difficult. The determination of adsorption isotherms for 2-mercaptobenzothiazole, which showed weak binding to goethite as well as to silica, and the mode of binding of 2-mercaptobenzothiazole on copper(I) surfaces is reported in Chapter 4. A crystal structure was obtained in which four units of 2-mercaptobenzothiazole bridge two nickel atoms through the nitrogen atom and the exocyclic sulfur and is considered as a model for binding to sulfidic minerals.

Chapter 5 looks at the strength of binding to goethite and silica of various hydroxamic acids. Benzohydroxamic acid was initially selected for study since hydroxamates are known to act as collectors for oxidized materials. Unpredictably, benzohydroxamic acid showed strong binding to a goethite surface and did not release any iron from the surface into solution, which would have been predicted due to its known strong chelating abilities to iron(III). The X-ray structure determination of the first example of a dinuclear Fe(III) hydroxamate complex showed this to have μ -oxo bridge formed by the hydroxamate unit and supports multisite attachment between this ligand and the surface, as suggested by adsorption isotherms. Simple models based on this dinucleating motif provide plausible modes of multisite attachment to a goethite surface. Competitive binding studies provided a way of ranking the ability to bind to goethite of acetohydroxamic acid, which was not suitable for analyses by either ICP-OES or UV-Vis spectroscopy. Of the ligands studied in this chapter acetohydroxamic acid was found to bind most strongly to goethite followed by benzohydroxamic acid. In Chapter 6, the attachment to goethite and silica of a series of phosphonic acids is investigated. All show a very high binding strength to goethite.

Froth flotation experiments at a laboratory scale are described in Chapter 7. The types of ligand that showed strong binding to goethite in adsorption isotherms experiments were tested as co-collectors in different ores and conditions. There is not a simple correlation between adsorption isotherm data and flotation performance as co-collectors because other factors, besides strength of binding, affect the system. Benzohydroxamic acid was the ligand that increased the grade/recovery of the process in all the cases studied. Irgacor 419[®] enhances the grade/recovery curve for Palabora ore and phenyl malonic acid for Kennecott ore. These results support the original proposition that it may be possible to increase the recovery of oxidized particles substantially by using a blend of collectors which includes a compound to target the oxidized sites.

ACKNOWLEDGEMENTS

I would like to thank to my supervisor Prof. Peter Tasker for his guidance, encouragement, enthusiasm and motivation throughout my PhD. Working in his group offered me the opportunity to spend three stimulating years working on an interesting area of research.

I would also like to thank Prof. Jan Cilliers and his group, especially Dr. Nicolas Barbian, for all their help with flotation experiments and for making me feel very welcome when visiting the group.

Many thanks to Dr. Euan Brechin and Dr. Constantinos Milios for always being willing to give advice about crystal growing.

Thanks to Fraser White for solving crystal structures.

I wish to acknowledge also EPSRC and Rio Tinto for funding this project.

I would like to thank all my *Edinburgh* friends Andrea B. and K., Marco, Michele, Silvia, Myriam, Isa, Emiliano, Mike, Maria, Avgoustinos, Jone, Tijana, Marc, Christophe, Irene, Daniela, Pilar, Alex, Laurent, Filipa, Gaurav, Oscar, Pekka, Rosa, Leszek, Alessandro, Pepe, Javi and Luis for making my time in Edinburgh very enjoyable and with a fantastic social life! You made a difference all this time!

Thanks to all the members of the Tasker group and in particular to Dr. Jy Chartres for his valuable help in the lab and for reading some of my drafts and also to Dr. Rachel Cooper and Dr. David Henderson. Thanks also to all my lab mates for making the lab a great place to work.

I am especially grateful to my family for supporting and encouraging me during my studies.

*To my parents,
Magdalena and Ramón*

CONTENTS

Declaration.....	i
Abstract.....	ii
Acknowledgements.....	iv
Contents.....	vi
Ligand Index.....	xii
Abbreviations.....	xiv

Chapter 1. Introduction

1.1. Project overview.....	3
1.2. Copper.....	3
1.2.1. History and uses of copper.....	3
1.2.2. Natural occurrence of copper.....	5
1.3. Flotation processes in extractive metallurgy.....	6
1.3.1. Chemicals used in froth flotation.....	7
1.3.2. Problems in flotation.....	8
1.4. Mode of action of flotation agents.....	9
1.4.1. Sulfide mineral in flotation.....	10
1.5. Industrial practice.....	12
1.5.1. Characterization by chemical structure.....	12
1.5.2. Particle size interactions with sulfide collectors.....	16
1.5.3. Frother interactions with sulfide collectors.....	16
1.6. Adsorption modes: physical-chemical adsorption.....	16
1.6.1. Adsorption isotherms.....	17
1.6.1.1. Isotherm types.....	18
1.6.1.2. Interpretation of isotherms.....	20
1.7. Iron oxide and silica substrates.....	21
1.7.1. Iron oxides and oxyhydroxides.....	21
1.7.2. Silica.....	23
1.8. Surface ligands.....	24

1.9. UV-Vis spectroscopy.....	26
1.10. ICP-OES.....	28
1.11. Objectives.....	29
1.12. References.....	32

Chapter 2. Surface Binding Studies of Carboxylic Acids

2.1. Introduction.....	37
2.1.1. Outline.....	37
2.1.2. Background.....	37
2.1.3. Carboxylic acids.....	38
2.1.4. A corrosion inhibitor for iron: Irgacor 419®.....	38
2.1.5. Other ligands showing H-bond interactions and multisite attachment.....	41
2.2. Development of a suitable procedure to determine adsorption isotherms.....	43
2.3. Surface binding studies by adsorption isotherms.....	45
2.4. Conclusions.....	48
2.5. Experimental.....	49
2.5.1. Instrumentation.....	49
2.5.2. Solvents and reagents.....	49
2.5.3. Ligands.....	49
2.5.4. Extinction coefficient (ϵ) determination.....	49
2.5.5. Adsorption isotherm measurements.....	50
2.6. References.....	51

Chapter 3. Surface Binding Studies of Potassium Ethyl Xanthate

3.1. Introduction.....	54
3.1.1. Outline.....	54
3.1.2. Xanthates.....	54
3.1.3. Decomposition of xanthates.....	55
3.2. Surface binding studies by adsorption isotherms.....	57
3.3. Conclusions.....	67

3.4. Experimental.....	62
3.4.1. Instrumentation	62
3.4.2. Solvents and reagents.....	62
3.4.3. Ligand	62
3.4.4. Extinction coefficient (ϵ) determination	62
3.4.5. Adsorption isotherm measurements.....	62
3.5. References	64

Chapter 4. Surface Binding Studies of 2-Mercaptobenzothiazole

4.1. Introduction.....	67
4.1.1. Outline.....	67
4.1.2. Coordination chemistry of 2-mercaptobenzothiazole with copper	67
4.1.3. Coordination chemistry of 2-mercaptobenzothiazole with nickel	72
4.1.4. Copper(I).....	74
4.1.5. Copper(II).....	75
4.1.6. Nickel(II).....	75
4.2. Surface binding studies by adsorption isotherms.....	76
4.3. Investigating the mode of surface binding of 2-mercaptobenzothiazole (4).....	78
4.3.1. Attempts to synthesise copper(I) polynuclear complexes with ligand 4	78
4.3.2. Attempts to synthesise polynuclear complexes with ligand 4 and Ni(II) or Zn(II)	80
4.3.3. X-ray crystal structure of $[\text{Ni}_2(\mu_2\text{-mbt})_4]$ (4a).....	81
4.4. Conclusions	86
4.5. Experimental	86
4.5.1. Instrumentation	86
4.5.2. Solvents and reagents.....	87
4.5.3. Ligand	87
4.5.4. Extinction coefficient (ϵ) determination	87
4.5.5. Adsorption isotherm measurements.....	87
4.5.6. Attempted synthesis of the complex $[\text{Cu}_{x+y}(\text{hfac})_x(\text{mbt})_y]$	87
4.5.7. Synthesis of the complex $[\text{Ni}_2(\mu_2\text{-mbt})_4]$ (4a).....	89

4.6. References	90
-----------------------	----

Chapter 5. Surface Binding Studies of Hydroxamates

5.1. Introduction	93
5.1.1. Outline.....	93
5.1.2. Benzohydroxamic acid.....	93
5.1.3. Hydroxamic acids and their complexes with metal ions.....	94
5.1.4. The hydroxamic acid group and its metal-binding sites	95
5.1.5. Complexes of hydroxamic acids: mono hydroxamic acids as ligands.....	96
5.2. Surface binding studies by adsorption isotherms.....	100
5.2.1. Wavelengths and extinction coefficients used	100
5.3. Mono- and di-nuclear iron(III) complexes of benzohydroxamic acid (bhaH)..	102
5.3.1. X-ray crystal structure of $[\text{Fe}(\text{bha})_3] \cdot 1.5\text{MeOH}$ (5a).....	103
5.3.2. X-ray crystal structure of $[\text{Fe}_2(\mu_2\text{-bha})_2(\text{bha})_2\text{Br}_2]$ (5b).....	107
5.3.3. Infrared spectra of 5a and 5b	110
5.3.4. Magnetic susceptibility measurement of 5b	110
5.4. Hypothesis for mode of action of hydroxamates	111
5.5. Hydroxamate derivatives investigated	113
5.5.1. Investigating the effects of substitution on the hydroxamate group	116
5.5.2. Investigating the effects of substitution on the phenyl ring	117
5.5.3. Competitive binding studies.....	119
5.6. Conclusions	120
5.7. Experimental	121
5.7.1. Instrumentation	121
5.7.2. Solvents and reagents.....	122
5.7.3. Ligand synthesis.....	122
5.7.4. Synthesis of the complex $[\text{Fe}(\text{bha})_3] \cdot 1.5\text{MeOH}$ (5a).....	125
5.7.5. Synthesis of the complex $[\text{Fe}_2(\mu_2\text{-bha})_2(\text{bha})_2\text{Br}_2]$ (5b).....	125
5.7.6. Attempts to synthesise polynuclear complexes containing ligand 5 or 6 ..	125
5.7.7. Extinction coefficient (ϵ) determination	126
5.7.8. Adsorption isotherm measurements.....	126
5.8. References.....	128

Chapter 6. Surface Binding Studies of Phosphonic Acids

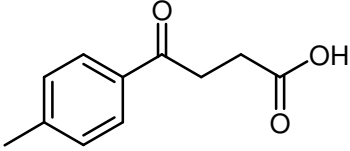
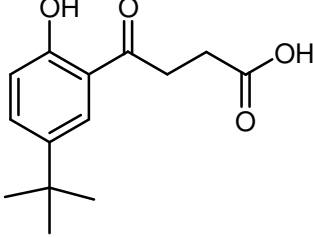
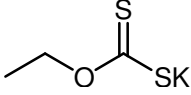
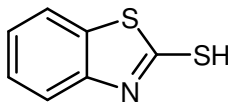
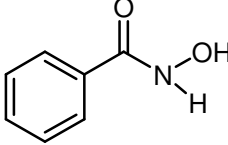
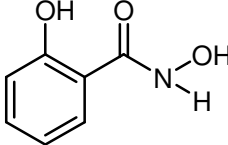
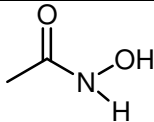
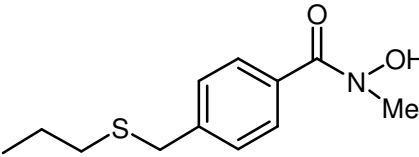
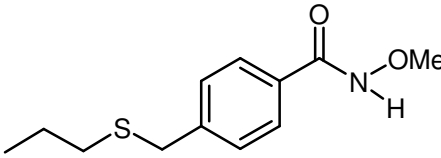
6.1. Introduction	132
6.1.1. Outline.....	132
6.1.2. Background	132
6.1.3. Phosphonic acids as passivating agents	132
6.2. Surface binding studies by adsorption isotherms.....	134
6.3. Conclusions	139
6.4. Experimental	140
6.4.1. Instrumentation	140
6.4.2. Solvents and reagents.....	140
6.4.3. Ligands.....	140
6.4.4. Adsorption isotherm measurements.....	140
6.5. References	141

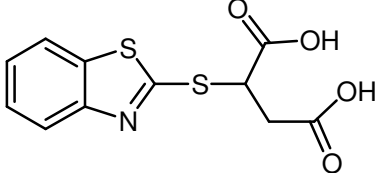
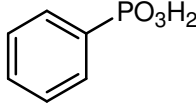
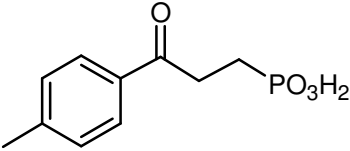
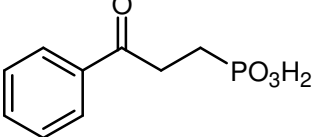
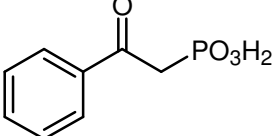
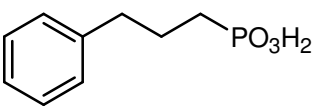
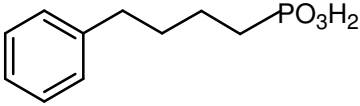
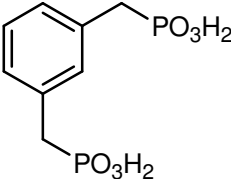
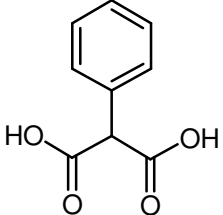
Chapter 7. Flotation tests of Selected Ligands

7.1. Introduction	144
7.1.1. Outline.....	144
7.1.2. Flotation variables and performance.....	144
7.1.3. Flotation equipment and procedures	148
7.2. Performance in laboratory tests of selected ligands on different substrates	150
7.2.1. Flotation tests with Amandelbult ore (UG2 Reef)	155
7.2.1.1. The influence of collector concentration.....	156
7.2.1.2. The influence of the air flowrate.....	158
7.2.2. Flotation tests with Kennecott ore (MZ2HE).....	160
7.2.2.1. The influence of collector concentration.....	161
7.2.2.2. The influence of surface-ligating groups	163
7.2.3. Flotation tests with Palabora ore	164
7.2.3.1. The influence of surface-ligating groups	165
7.3. Conclusions	168

7.4. Experimental	169
7.4.1. Materials.....	169
7.4.2. Solvents and reagents	169
7.4.3. Composition of the ores	170
7.4.4. Crushing processes.....	170
7.4.5. Flotation experimental processes	171
7.4.5.1. Flotation tests with Amandelbult ore (UG2 Reef)	172
7.4.5.2. Flotation tests with Kennecott ore (MZ2HE)	173
7.4.5.3. Flotation tests with Palabora ore	174
7.5. References	176
Chapter 8. Conclusions and Future Work.....	177
Appendix	
Appendix contents.....	180

LIGAND INDEX

Ligand number	Structural formula	Chemical Name
1		3-(4-Methylbenzoyl)-propionic acid (Irgacor 419 [®])
2		3-(5-tert-Butyl-2-hydroxybenzoyl)- propanoic acid
3		Potassium ethyl xanthate (KEX)
4		2-Mercaptobenzothiazole (mbtH)
5		Benzoic hydroxamic acid (bhaH)
6		Salicylic hydroxamic acid (shaH ₂)
7		Acetic hydroxamic acid
8		<i>N</i> -Hydroxy- <i>N</i> -methyl-4-propylthiomethyl-benzamide
9		<i>N</i> -Methoxy-4-propylthiomethyl-benzamide

10		Benzothiazol-2-ylthio-succinic acid (Irgacor 252 LD [®])
11		Phenylphosphonic acid
12		3-Oxo-3- <i>p</i> -tolylpropylphosphonic acid (P-419)
13		3-Oxo-3-phenylpropylphosphonic acid
14		2-Oxo-2-phenylethylphosphonic acid
15		3-Phenylpropylphosphonic acid
16		4-Phenylbutylphosphonic acid
17		2-Phosphonomethylbenzylphosphonic acid
18		Phenylmalonic acid (pmaH ₂)

ABBREVIATIONS

δ	chemical shift
$^{\circ}$	degrees
$^{\circ}\text{C}$	degree centigrade
%	percent
<	less than
λ	wavelength (UV)
ϵ	extinction coefficient (UV)
μm	micrometres
θ	fractional coverage
χ_{M}	molar susceptibility
\AA	Angstrom
Ar	aromatic (NMR)
ATH	aluminium trihydroxide
BC	Before Christ
br s	broad singlet (NMR)
<i>ca.</i>	<i>circa</i> (approximately)
ccp	cubic close-packed
CDCl_3	deuterated chloroform
<i>cf.</i>	compare
CFSE	crystal field stabilisation energy
<i>cis</i>	<i>cisoid</i>
cm^{-1}	wavenumber
CMC	critical micelle concentration
CSD	Cambridge Structural Database
d	doublet (NMR)
DCM	dichloromethane
dmp	2,9-dimethyl-1,10-phenanthroline
dppe	[1,2-bis(diphenylphosphino)ethane
dppm	1,2-bis(diphenylphosphino)methane
e.g.	for example
ES	electrospray
<i>et al.</i>	<i>et alli</i> (and others)
Et_3N	triethylamine
FAB	Fast Atom Bombardment
<i>fac</i>	<i>facial</i>
g	gram
g ton^{-1}	grams per tonne
h	hour
HCl	hydrochloric acid

hcp	hexagonal close-packed
hfach	1,1,1,5,5,5–hexafluoro-2,4-pentanedione
ICP-OES	Inductively Coupled Plasma Optical Emission Spectroscopy
ICSD	Inorganic Crystal Structure Database
<i>in vacuo</i>	under vacuum
IR	infrared
Irg 419 [®]	Irgacor 419 [®]
<i>J</i>	coupling constant (NMR)
<i>K</i>	equilibrium adsorption constant
K	Kelvin
kg	kilogram
l	litre
M	Molar
m	multiplet (NMR)
<i>m/z</i>	mass per unit charge
m ² g ⁻¹	metres squared per gram
Me	methyl
MeOH	methanol
<i>mer</i>	<i>meridional</i>
mg	milligrams
MHz	Mega Hertz
MIBC	4-methyl-2-pentanol
min	minute
ml	millilitres
mmol	millimoles
mol g ⁻¹	moles per gram
mol l ⁻¹	moles per litre
MS	Mass Spectrometry
nm	nanometre
NMR	Nuclear Magnetic Resonance
<i>p</i>	<i>para</i>
pH	-log ₁₀ [H ⁺]
Ph	phenyl
ppm	parts per million
r.p.m.	revolutions per minute
s	singlet (NMR)
SENKOL 5	sodium dialkyl dithiophosphate
SIBX	sodium isobutyl xanthate
t	triplet (NMR)
<i>trans</i>	<i>transoid</i>
U.S.A.	United States of America
UV-Vis	Ultraviolet-Visible
<i>via</i>	by way of

Chapter 1

Introduction

CONTENTS

1.1. Project overview.....	3
1.2. Copper.....	3
1.2.1. History and uses of copper.....	3
1.2.2. Natural occurrence of copper.....	5
1.3. Flotation processes in extractive metallurgy.....	6
1.3.1. Chemicals used in froth flotation.....	7
1.3.2. Problems in flotation.....	8
1.4. Mode of action of flotation agents.....	9
1.4.1. Sulfide mineral in flotation.....	10
1.5. Industrial practice.....	12
1.5.1. Characterization by chemical structure.....	12
1.5.2. Particle size interactions with sulfide collectors.....	16
1.5.3. Frother interactions with sulfide collectors.....	16
1.6. Adsorption modes: physical-chemical adsorption.....	16
1.6.1. Adsorption isotherms.....	17
1.6.1.1. Isotherm types.....	18
1.6.1.2. Interpretation of isotherms.....	20
1.7. Iron oxide and silica substrates.....	21
1.7.1. Iron oxides and oxyhydroxides.....	21
1.7.2. Silica.....	23
1.8. Surface ligands.....	24
1.9. UV-Vis spectroscopy.....	26
1.10. ICP-OES.....	28
1.11. Objectives.....	29
1.12. References.....	32

1.1. PROJECT OVERVIEW

This work is concerned with the design of ligating groups which bind strongly and selectively to the surface of particles of sulfide ores which have undergone some oxidation and are not effectively “collected” by existing reagents in froth flotation processes to “concentrate” copper-containing ores such as chalcopyrite (CuFeS_2).

The aim is to identify simple functional groups which form surface complexes with these oxidized particles selectively so that when incorporated into a hydrophobic ligand they will give “flotation agents” which allow separation of the oxidized ore from siliceous wastes (“gangues”). They could then be used in a mixture with concentrated reagents which address the surfaces of unoxidized ore particles to improve recovery. Currently up to 15 % of copper is lost from certain operations because the oxidized particles are not collected by froth flotation.¹

1.2. COPPER

1.2.1. HISTORY AND USES OF COPPER

Copper is the first element in the group number 11 of the periodic table occupying the same family as silver and gold. Its atomic number is 29 and it occurs in two natural isotopes, ^{63}Cu and ^{65}Cu and has a metallic reddish tone (Figure 1.1). The name copper and the symbol Cu come from the Greek *aes cyprium* (metal of Cyprus), called later *cuprum* by the Romans, as it was from Cyprus that during the Roman Empire copper metal was mainly mined.² In mythology and alchemy, copper was associated with the goddess Aphrodite/Venus. Early astronomers gave to copper a symbol consisting of a cross with a handle.³ Alchemists continued to use this sign as the symbol for copper which was known as the mirror of Venus too. Nowadays, this is still the symbol used for the planet Venus in astronomy and to indicate “female” in biology.



Figure 1.1. Copper flakes.

Copper, like silver and gold, are noble metals that can be found in nature in its elemental form. This group of metals is also known as the “coinage metals” due to their original usage.² All of them must have been used as primitive money before the introduction of gold coins in Egypt around 3400 BC. Copper is one of the most important and first metals known to man. It is unclear when copper started to be used, but there is recorded evidence indicating it was known in northern Iraq around 8700 BC. This metal was already being obtained in the Middle East by charcoal reduction of its ores around 3500 BC.² In India, Mesopotamia, and Greece they added tin to copper in order to produce bronze by 3000 BC and this marked the beginning of the “Bronze Age”. Copper was used in China around 2000 BC. Nowadays, copper is still playing an important role with more than 15 million tonnes of copper a year⁴ being used.

Copper is a ductile and malleable metal with great thermal and electrical conductivity, only surpassed by silver,² and which does not corrode easily. The major use of copper is as an electrical conductor but it is also extensively used in plumbing and in coinage alloys. Copper can be found as a component of Euro, Pound Sterling and U.S. dollar coins. It has biomedical applications, it is used as a fungicide and it is also found in musical instruments made of brass. Copper is also been used in technology and infrastructure. As a curiosity, 81.3 tonnes of copper were used to build The Statue of Liberty.

There are various alloys of copper^{2, 5} too such as bronze (a metal other than zinc or nickel in copper, being usually Sn the main additive), brass (up to 38% Zn in Cu) and Monel (Ni-Cu), also known as cupronickel.²

1.2.2. NATURAL OCURRENCE OF COPPER

The main copper ores are sulfide minerals, with chalcopyrite (CuFeS_2) being the one containing about 50% of all copper deposits.² Other secondary sulfide copper minerals are bornite (Cu_5FeS_4), covellite (CuS), chalcocite (Cu_2S); the oxide cuprite (Cu_2O); and the carbonate minerals, malachite ($\text{Cu}_2\text{CO}_3(\text{OH})_2$) and azurite ($\text{Cu}_3(\text{CO}_3)_2(\text{OH})_2$).

Large deposits of copper minerals are found in the United States, Mexico, Peru, Chile, Canada, Russia, Australia, Zambia and Zaire.^{2, 6} The majority of current supplies of copper are obtained from low-grade ores containing only about 1% copper. The largest copper deposit ever found⁴ was at Rio Tinto in Spain, giving its name to the mining company Rio Tinto. This deposit supplied the Roman Empire. The largest excavation in the world made by man is the open pit copper mine Kennecott Utah Copper in the U.S.A.^{4, 7, 8} (Figure 1.2). The Kennecott Utah Copper is wholly owned by Rio Tinto.^{3, 4} Mineral from this mine was used to carry out some of the flotation experiments described in Chapter 7.



Figure 1.2. Open pit copper mine, Kennecott Utah Copper Mine (U.S.A.).⁸

1.3. FLOTATION PROCESS IN EXTRACTIVE METALLURGY

Crushing and grinding⁹ are used to concentrate the mineral containing the metal values which are present in natural deposits as heterogeneous mixtures of solid materials. Differences in the physical properties of milled solid materials are the basis of their separation.

Minerals suffer oxidation after fresh surface area is created during grinding.¹⁰⁻¹² Nowadays, one of the challenges for the mineral scientists and engineers is to recover oxidized minerals^{10, 13} that do not respond to conventional sulfide mineral flotation and that is why identifying chemical reagents which make oxidized minerals hydrophobic is of great importance.

The process most commonly used to retrieve the ore “concentrates” is froth flotation.^{14, 15} This technique had its industrial beginning early last century in Australia making a major impact on the mineral industry.¹⁶ It is now used to treat around two billion tonnes of material per year,^{14, 17} mostly sulfide ores. Flotation is most effective for separating mineral particles in the size range between 10 and 100 μm .^{14, 16}

Froth flotation techniques^{9, 18, 19} to recover ore “concentrates” make use of differences in surface activities and the formation of complexes at the surface of the mineral particles.

An important feature in flotation chemistry¹⁴ is the control of wettability of the different mineral species present in the flotation pulp. The use of a series of organic reagents, called flotation agents or collectors, which are adsorbed onto the mineral surface changing hydrophilic materials into hydrophobic ones is the basis of separation by froth flotation.^{9, 20}

This process^{14, 21} consists of the capture of small mineral particles by bubbles (Figure 1.3). An oil-based froth collects the hydrophobic solids when bubbles rise and the “concentrate” is recovered from overflow. The gangue (undesired hydrophilic materials) accumulated in the aqueous suspension is eliminated from the separator.

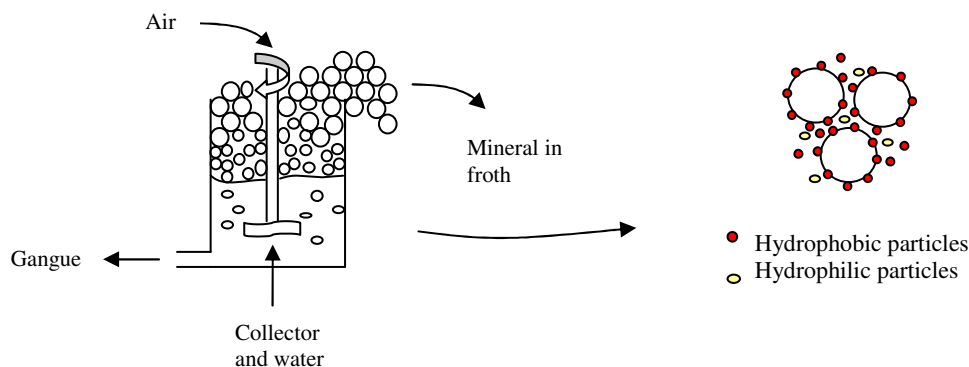


Figure 1.3. Representation of a froth flotation separator.

1.3.1. CHEMICALS USED IN FROTH FLOTATION

Chemicals that are used in froth flotation processes can be divided into three categories:

◆ **Flotation agents or collectors** are organic molecules containing nonpolar and polar chemical groups. The role of collectors²² is to induce flotability making valuable minerals hydrophobic. Sulfur atoms⁹ are present in the polar “head groups” of many of the more frequently used types of collectors which are used in the recovery of base metals from their sulfidic ores.

The formation of the bonds between collectors and mineral particles²² is via chemisorption through the polar end of the collector.

Redox properties of the collector⁹ determine the modes of chemisorption. Collectors have ligating head groups which could form polynuclear complexes. To suppress elimination of metal atoms from the surface, and transfer to the liquid phase

(rather than surface ligation, which is needed to generate hydrophobic particles) it is necessary to increase the stability of the complexes formed at the surface of the ore particles, relative to those formed in solution.

◆ **Frothers** are another important element in froth flotation. They are composed of a polar and nonpolar end and create stable bubbles necessary to carry the solid particles. The froth should also be stable enough to avoid froth breakage before the froth is collected, as undesired breakage would cause the return of the particles to the pulp. Another condition is that it should not adsorb on mineral particles, as this would reduce the selectivity of the collector used.¹⁶

◆ **Modifiers** control the selectivity of the flotation process.^{23, 24} They can be divided into four groups:

- *Activators* enhance the flotation increasing the interaction with collectors.
- *Depressants* increase hydrophilicity of the minerals and make the flotation more difficult.
- *Dispersants* break agglomerated particles into single ones which interact more efficiently with collectors and air bubbles.
- *pH regulators* control the optimal pH range of the system. This is important because hydrophobicity is generally optimal in a certain pH range.

1.3.2. PROBLEMS IN FLOTATION

Problems in flotation can come from fine particles smaller than 10 μm .¹⁴ New process development and old process enhancement for the recovery of fine particles is of increasing interest. One of the problems associated with flotation of fine particles is the large reagent consumption due to their high surface area.

The main approach to improving fine particle flotation types is based on increasing the probability of collision between gas bubbles and mineral particles.¹⁴ This is achieved when mineral particles are present as agglomerates or are attached to large hydrophobic particles which act as carrier particles. Agglomeration can be improved by chemisorbing collectors.

1.4. MODE OF ACTION OF FLOTATION AGENTS

The knowledge of the relation between the three elements that describe the flotation processing (Figure 1.4) is needed to process ores:¹⁴

- Mineralogical characteristics: soluble species, valuable and gangue minerals.
- Chemical variables: collectors, activators, depressants, modifiers and frothers.
- Process variables: feed preparation and cell design.

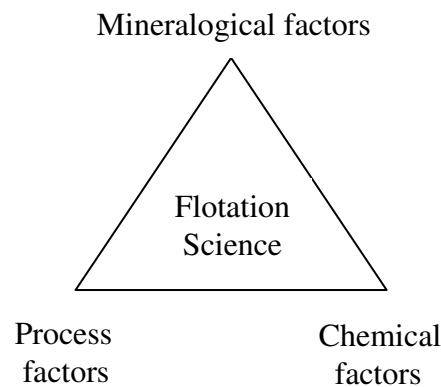


Figure 1.4. Representation of the elements of flotation science and engineering.¹⁴

Usually, in an industrial plant it is easier to change chemical factors than physical or mechanical factors.

The geology of the ore determines which minerals are possible to separate from each other and how this may be achieved.^{14, 25} Mineral forms (sulfide, oxidized and/or metallic species) are the main factors which have an effect on the selection of a collector. Another factor is liberation size, that is the size to which the ore must be milled to generate separate particles of either mineral value or gangue that can be removed efficiently from the ore. An additional consequence of ore mineralogy is the presence of soluble species and the nature and amount of slime particles generated.

The bulk chemistry of the pulp, which controls the surface chemistry of the particles and bubbles in the system using collectors, depressants, activators and modifiers, dominates the effective flotation processing of the ore. Process variables are dependent on the nature of the ore.

A key in industrial flotation separations is the design of specific chemical schemes for regulating the bulk and surface chemistry of the system,¹⁴ as well as the development of agents to aid or reduce mineral flotability.

1.4.1. SULFIDE MINERAL FLOTATION

The development of new collectors in sulfide mineral flotation is of special importance for commercial useful multicomponent ores which are difficult to recover selectively at a reasonable cost.^{26, 27}

Flotation characteristics of sulfide minerals¹⁴ can be considered depending on their natural or induced flotability. The two ways of inducing flotation are:

- Sulfidization: sulfur formation at the mineral surface by addition of a sulfidizing agent^{14, 18, 28, 29} as, for example, sodium sulfide (Na_2S), sodium hydrosulfide (NaSH) or ammonium sulfide ($(\text{NH}_4)_2\text{S}$).

This process is associated with disadvantages such as the difficulty of controlling the dosage of sulfidizing agent to get good recovery and not all the oxide minerals respond in the same way to sulfidization.

- Addition of collectors. This is the process carried out industrially.

In sulfide collector chemistry, the key donor is usually a sulfur atom attached either to a carbon or a phosphorus atom.²³ Adjacent groups and other donor atoms, such as N and O, will modify the bonding characteristics of the sulfur atom. Sulfide minerals can also be floated by collectors that do not contain sulfur, however, in order to get selectivity, a collector that contains sulfur is usually needed.

One of the mechanisms suggested to describe sulfide mineral flotation is by a chemical reaction with the ions of the mineral surface (chemisorption) or by electrostatic interaction to the mineral surface (physisorption).¹⁶

An essential condition for flotability of a mineral is that the hydrophobic substance is thermodynamically stable.

FLOTATION WITH A NONTHIOL CHELATING COLLECTOR

Flotation techniques use chelate-forming compounds as collectors¹⁴ due to the ability of this type of compounds to selectively complex metal cations on surfaces and, in some cases, even precipitate them as metal chelates on surfaces under certain conditions.

Chelate-forming collectors usually include electron donor atoms such as sulfur, nitrogen, oxygen and phosphorus within the chelating functional group. Hydroxamates are the most extensively studied nonthiol collectors.^{14, 23} Their structures are shown in Figure 1.5. Hydroxamates act as collectors for oxide minerals^{13, 14, 23} and for sulfide mineral flotation and thus can, in theory, be used in flotation for the mixed oxidized/unoxidized copper ores.

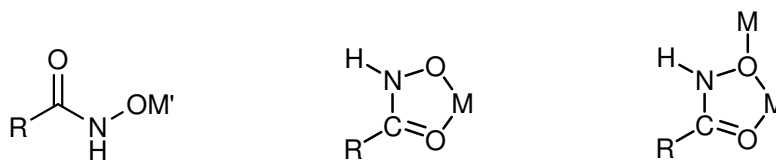


Figure 1.5. Hydroxamate and metal chelate structures.³⁰

Further discussion of hydroxamic acids and their metal complexes is included in Chapter 5. Characterization of a new type of polynuclear complex of iron(III) is described in Section 5.3. The significance of this type of structure and simple models providing plausible modes of binding of hydroxamic acids to surfaces is included in Sections 5.3 and 5.4.

COLLECTORLESS FLOTATION OF SULFIDES

This process takes advantage of the hydrophobicity of a sulfide in the absence of a collector to try to reduce reagent consumption.¹⁴ In practice, because of the difficulty to control such process³¹ and because the kinetics of this type of flotation are too slow,¹⁴ collectorless flotation has not been demonstrated to be effective industrially in spite of numerous possibilities which have been proposed.

1.5. INDUSTRIAL PRACTICE

Industrial sulfide mineral collector practice can be considered in different ways:²² by chemical structures, by influence of mineralogy, by collector dosage and particle size interaction, and by interactions between collectors and frothers.

1.5.1. CHARACTERIZATION BY CHEMICAL STRUCTURE

Over 90% of the reagents used today at the industrial level are represented by the collector reagents shown in Table 1.6. These compounds have been available since 1950s and, some of them, since the 1920s. They have been widely used due to

their low cost, extensive availability, strong sulfide mineral flotation ability, and improvements in applications technology.²²

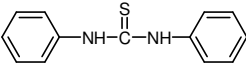
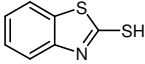
Chemical Name	Chemical Structure	Structure Identification
Alkyl Dithiocarbonates (xanthates)	$\text{R}-\text{O}-\overset{\text{S}}{\parallel}{\text{C}}-\text{SM}$	$\text{R} = \text{C}_2 \text{ to } \text{C}_6$
Alkyl or Aryl dithiophosphates	$\text{R}'-\text{O}-\overset{\text{S}}{\parallel}{\text{P}}(\text{R}'')-\text{SM}$	$\text{R} = \text{C}_2 \text{ to } \text{C}_6$ or $\text{R} = \text{Ar}$
Dialkyl thionocarbamates	$\text{R}'-\text{NH}-\overset{\text{S}}{\parallel}{\text{C}}-\text{O}-\text{R}''$	$\text{R} = \text{C}_2 \text{ to } \text{C}_5$
Thionocarbaniide		
Alkyl xanthogen formates	$\text{R}'-\text{O}-\overset{\text{S}}{\parallel}{\text{C}}-\text{S}-\overset{\text{S}}{\parallel}{\text{C}}-\text{O}-\text{R}''$	$\text{R} = \text{C}_2 \text{ to } \text{C}_5$
Alkyl xanthic esters	$\text{R}'-\text{O}-\overset{\text{S}}{\parallel}{\text{C}}-\text{S}-\text{R}''$	$\text{R} = \text{C}_2 \text{ to } \text{C}_6$
Mercaptobenzothiazole		
Alkyl or aryl dithiophosphinates	$\text{R}'-\overset{\text{S}}{\parallel}{\text{P}}(\text{R}'')-\text{SM}$	$\text{R} = \text{C}_2 \text{ to } \text{C}_6$ or $\text{R} = \text{Ar}$
Alkyl mercaptans	$\text{R}-\text{SH}$	$\text{R} = \text{C}_{10} \text{ to } \text{C}_{12}$
Dialkyl disulfides	$\text{R}'-\text{S}-\text{S}-\text{R}''$	$\text{R} = \text{C}_4 \text{ to } \text{C}_8$
Alkyl trithiocarbonates	$\text{R}-\text{S}-\overset{\text{S}}{\parallel}{\text{C}}-\text{SM}$	$\text{R} = \text{C}_2 \text{ to } \text{C}_6$

Table 1.6. Types of compounds generally used as collectors for sulfide minerals.²²

Collectors shown in Table 1.7 are more expensive and are only of interest when improved selectivity or enhanced recovery of secondary associated minerals is required.

Chemical Name	Chemical Structure	Structure Identification
Alkyl or aryl monothiophosphates		R = C ₂ to C ₅ or R = Ar
Alkyl or aryl monothiophosphinates		R = C ₂ to C ₅ or R = Ar
Allyl alkyl thionocarbamates		R' = CH ₂ -CH=CH ₂ R'' = C ₂ to C ₅
Alkoxy carbonyl Alkyl thionocarbamates		R = C ₂ to C ₅
Alkoxy carbonyl alkyl thioureas		R = C ₂ to C ₅
Dialkyl sulfides		R = C ₂ to C ₁₀
Alkyl thioethyl amines		R' = C ₄ to C ₈ R'' = C ₂ to C ₃
Dialkyl diphenyloxide sulfonates		R = C ₈ to C ₁₆

Table 1.7. Types of newer compounds used as collectors for sulfide minerals.²²

The characteristics of the three main collector families are:

XANTHATES

The major volume of any sulfide mineral collector corresponds to xanthates, which have been used in sulfide mineral flotation since the 1920s.^{22, 25} These compounds are among the least expensive sulfide mineral collectors.



Figure 1.8. Xanthate structure.²²

They are easy to make, completely water soluble in their salt forms when a short alkyl chain, R, is present, available in solid form with long shelf lives and in liquid form with a limited shelf life, and show high, although unselective, recovery

of sulfide minerals. Increasing the carbon chain length decreases the selectivity but increases the recovery power of the xanthate.

DITHIOPHOSPHATES

The second main group of sulfide collectors according to collector volume is the dithiophosphate family.²² They are liquids which can contain different active ingredient concentrations. These products are usually water-soluble and with reasonable shelf life if they are kept at high pH. In comparison with xanthates, dithiophosphates are less powerful and kinetically slower in the recovery of sulfides. Their recovery power is increased with the carbon content of the R groups. Dithiophosphates are used with other classes of collectors to obtain high recovery, and usually need high pH with lime for selectivity. In general, this family of collectors is usually more expensive than the xanthates but less expensive than most of the other classes of Table 1.6.

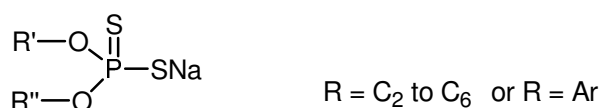


Figure 1.9. Dithiophosphate structure.²²

THIONOCARBAMATES

The thionocarbamate class^{22, 32} represents the third largest family from a collector volume viewpoint. They are liquids with very long shelf life and are water insoluble. In practice, they are emulsified or mixed with alcohols or added to the grinding step.

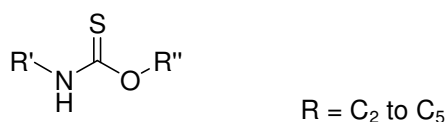


Figure 1.10. Thionocarbamate structure.²²

1.5.2. PARTICLE SIZE INTERACTIONS WITH SULFIDE COLLECTORS

In order to float larger particles it is necessary to control collector dosage.²² This is due to the smaller particles having a higher total surface area so they adsorb much of the initial collector added.

1.5.3. FROTHER INTERACTIONS WITH SULFIDE COLLECTORS

In the last 20 years one of the most important changes in industrial sulfide mineral flotation is that the dosage of frother used per ton of ore has increased and the dosage of collector used per ton of ore has decreased.²² This is due to the development of new frothers and also because collectors are more expensive than frothers.

1.6. ADSORPTION MODES: PHYSICAL - CHEMICAL ADSORPTION

Molecules are conventionally considered to bind to surfaces by two modes: physisorption and chemisorption.

Physisorption occurs when a surfactant ion is adsorbed as a counter ion in the double layer;^{7, 14, 19, 33} that is the surfactant ion is attracted electrostatically as its charge is opposite to the surface. In contrast, chemisorption involves chemical bond formation between polar head groups and metal sites on the mineral surface.^{7, 14, 19, 33} In this type of process, adsorption is usually limited to a monolayer.

1.6.1. ADSORPTION ISOTHERMS

Solute adsorption is fundamental in many industrial and life processes such as froth flotation of minerals, detergency, pollution control, purification processes for solutions and liquid solid chromatographic techniques.³⁴

A useful way of determining adsorption characteristics of an adsorbate onto a metal oxide surface is to use adsorption isotherms. In favourable cases they give us an adsorption/desorption equilibrium constant and information on:³⁵

- number of adsorption sites available for monolayer coverage
- strength of binding of a ligand
- surface coverage for a single ligand
- orientation of the ligand on the surface

Usually adsorption isotherms plot the amount of ligand adsorbed onto the surface of the solid against the amount left in solution at constant temperature and under equilibrium conditions³⁴ (Figure 1.11). The initial slope shows the strength of binding. The monolayer coverage is achieved at the plateau.

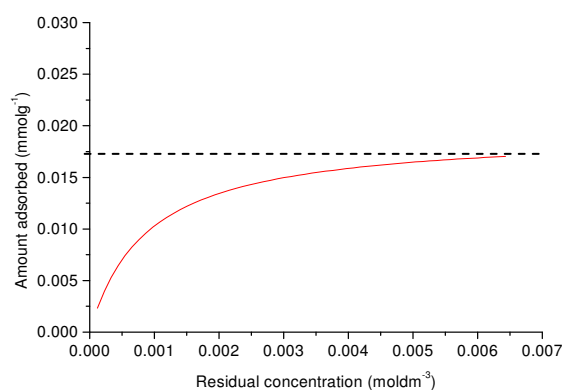


Figure 1.11. Typical Langmuir isotherm plot.

1.6.1.1. ISOTHERMS TYPES

The different isotherm types are result of the adsorption mechanism and will provide information on the nature of the adsorption.³⁴⁻³⁶ They fall into four classes, S (cooperative adsorption), L (Langmuir), H (high affinity) and C (constant partition), related to the initial shape of the isotherm. According to the form of the curve these types are divided in subgroups (Figure 1.12).

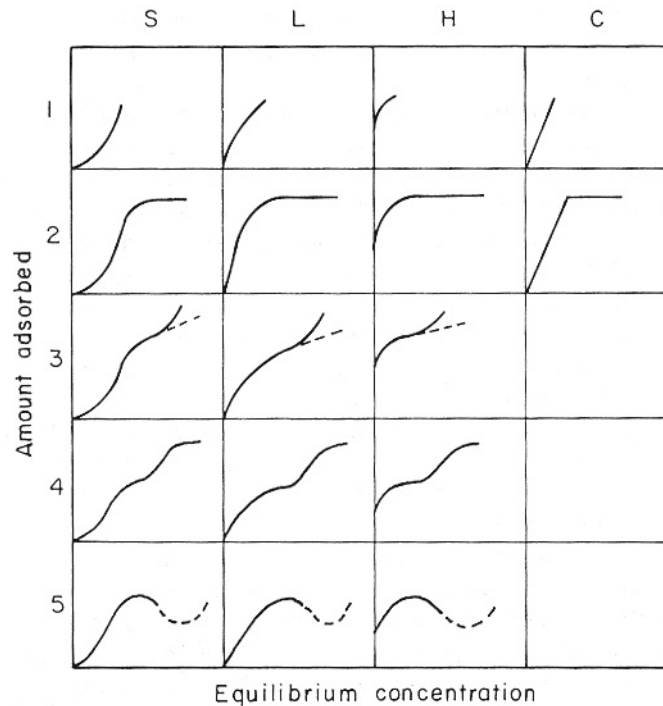


Figure 1.12. Classification of isotherm types.^{35, 36}

◆ In the S class the initial region is convex to the x-axis. Following this, an inflection point generates the S-shaped curve. For this type of curve raising the concentration, adsorption is favoured. This isotherm is found when:

- interactions between solute and adsorbent are not strong
- solute molecule is monofunctional with intermolecular interactions causing vertical packing in a regular arrangement (Figure 1.13)
- there is high competition between solute and solvent for the surface

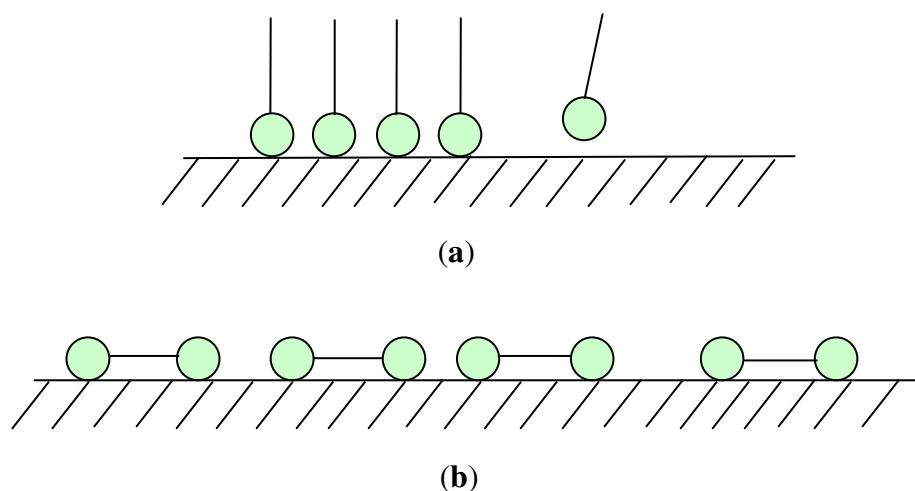


Figure 1.13. Difference between adsorption of a monofunctional solute **(a)**, which tends to be adsorbed vertically and in groups (S-shape), and a bifunctional solute **(b)**, which is more stable when adsorbed along the surface and equally stable in isolation or in aggregates (L-shape).

- ◆ For the L type, the initial slope is concave to the concentration axis. As the isotherm shows a plateau, this indicates saturation is completed since adsorption is more difficult as concentration increases due to fewer available sites left. In this class of isotherm, either the solute molecules adsorb along the surface (Figure 1.13) or if they adsorb vertically interactions between adsorbed molecules are insignificant. Monolayer coverage is considered. This type of isotherm is the most frequent.

- ◆ The H curve is found when very strong interactions between adsorbate and substrate occur at low concentrations.

- ◆ The C shape appears with microporous substrates and solutes with a constant number of sites for the different concentrations and higher affinity for the substrate than for the solvent.

1.6.1.2. INTERPRETATION OF ISOTHERMS

The Langmuir isotherm is one of the simplest and most used models to interpret adsorption isotherms.^{33,37} This model is based on the following assumptions:

- Adsorption cannot progress further than monolayer coverage
- All sites are equivalent
- The surface is uniform
- Binding is independent of the occupation of adjacent sites

The Langmuir isotherm is described by the equation in Figure 1.14. It is considered that an adsorbate, A, occupies the adsorption sites, S, on the surface of a solid (adsorbent). As a result, 1:1 stoichiometry is observed. SA is the adsorbate on surface sites. The units are usually expressed in mol dm⁻³.

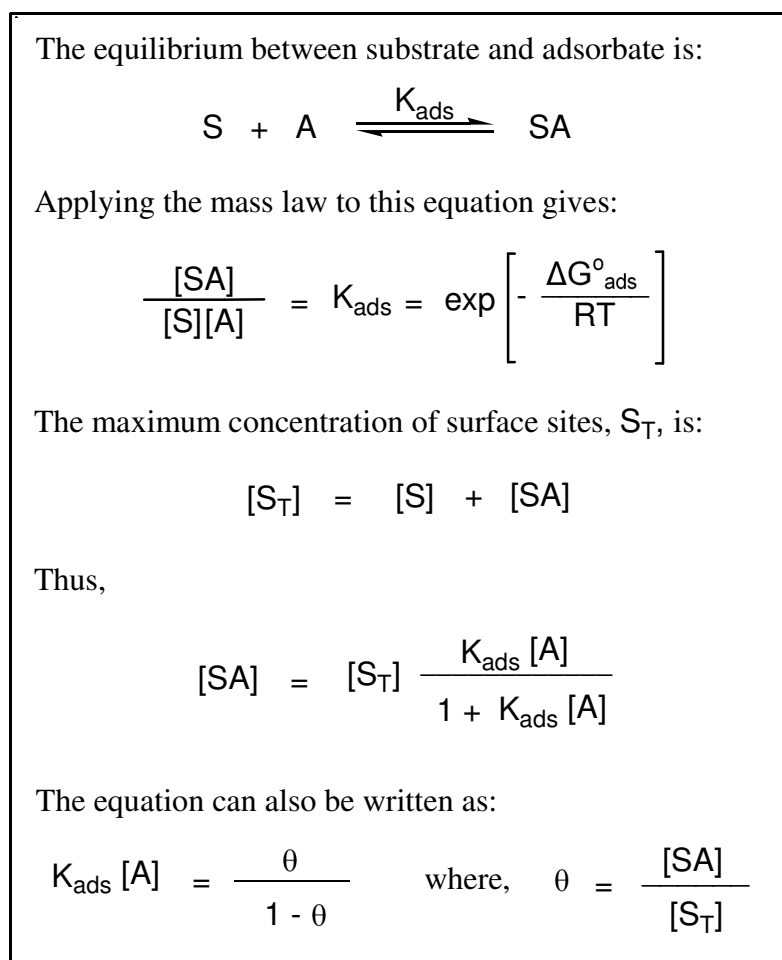


Figure 1.14. Derivation of the Langmuir Equation.³³

If the surface area of the substrate is known, the required surface area per ligand can be calculated using the value for S_T .

$$\text{Required surface area per molecule} = \frac{\text{surface area of substrate}}{S_T}$$

The Langmuir model has some limitations and complete monolayer coverage of the surface is only expected for strongly binding ligands. It will not apply when,

- there is more than one competing ligand in solution, and
- the ligand has two or more competing binding modes.

Additional equations have been developed but are not discussed here.

1.7. IRON OXIDE AND SILICA SUBSTRATES

A design feature of importance for the ligands studied in this thesis is their selectivity for strong binding to iron oxides over siliceous materials (see Section 1.8). Two substrates with relatively high surface area have been selected for the adsorption experiments to assess binding to these oxides; goethite, an iron(III) oxide, with a surface area of $22.50 \text{ m}^2 \text{ g}^{-1}$ and silica, whose surface area is $628.2 \text{ m}^2 \text{ g}^{-1}$. The surface areas of both materials were determined by Dr. Ronald Brown at University of Edinburgh.

1.7.1. IRON OXIDES AND OXYHYDROXIDES

The main forms of iron(III) oxides and oxyhydroxides are³⁸ goethite (α -FeOOH), lepidocrocite (γ -FeOOH), hematite (α -Fe₂O₃), maghemite (γ -Fe₂O₃) and magnetite (Fe₃O₄) are shown in Table 1.15. Due to their chemical stability, their non-toxic character and their inexpensive manufacture process; these compounds are used as inorganic pigments and raw materials for the production of permanent magnets.

Oxide / oxyhydroxide	Name	Oxidation state	Colour
α -FeOOH	goethite	Fe ^{III}	strong yellowish brown
γ -FeOOH	lepidocrocite	Fe ^{III}	light orange
α -Fe ₂ O ₃	hematite	Fe ^{III}	reddish brown
γ -Fe ₂ O ₃	maghemite	Fe ^{III}	dark yellowish brown
Fe ₃ O ₄	magnetite	Fe ^{II} /Fe ^{III}	black

Table 1.15. Different forms of iron(III) oxides and oxyhydroxides.^{2, 39}

Iron oxides and oxyhydroxides are built up by arrangements of oxide anions in close packing (either hcp or ccp)^{2, 38} with Fe³⁺ ions partially occupying the vacant sites. Goethite (α -FeOOH), which receives its name in honour to the German poet Goethe, has a diaspore structure⁴⁰ composed^{38, 41-43} by oxygen atoms in an hexagonal close packing, where Fe³⁺ ions fill half of the octahedral sites generating octahedral units of FeO₃(OH)₃ which spread along one direction (Figure 1.16).

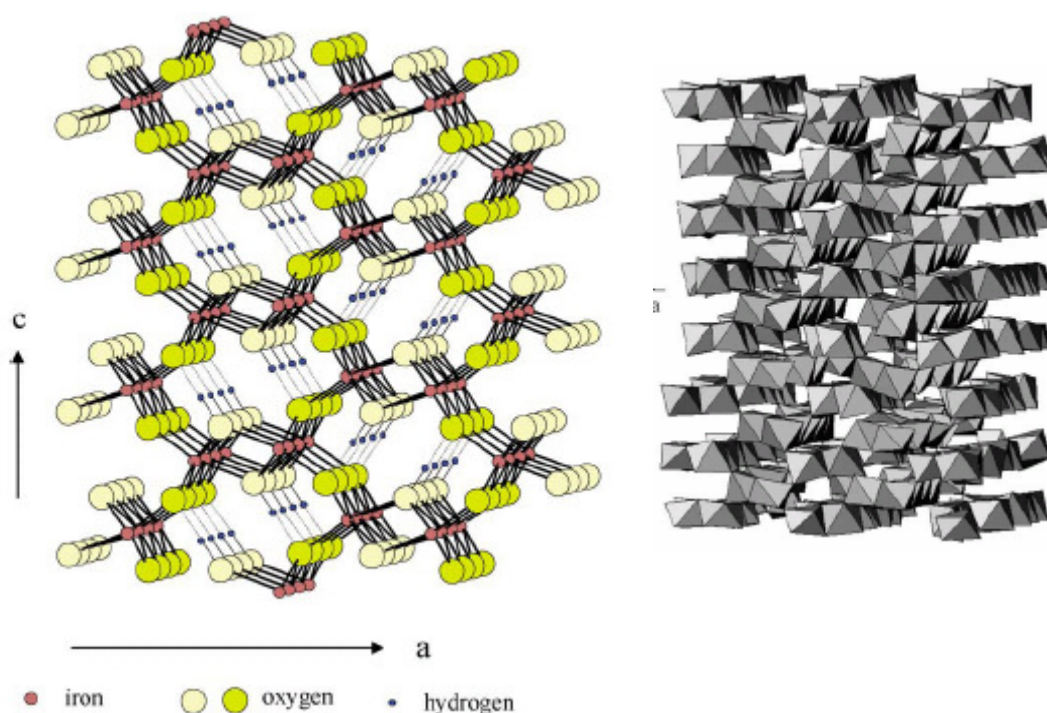


Figure 1.16. Representation of the structure³⁸ and packing⁴¹ of goethite (α -FeOOH).

1.7.2. SILICA

Silica (SiO_2) and silicates² have taken part in the progress of civilization from prehistoric times. Their names derive from the Latin *silex*, flint. Tools made of flint were developed in the paleolithic age about 500000 years ago.

About twelve polymorphs of “pure” SiO_2 are known² and, at least, 22 phases of silica have been described, though some of these depend on the presence of impurities or defects. α -quartz is the most common of the silica polymorphs and it is a key mineral constituent of numerous rocks such as granite and sandstone. It can also be found alone as a rock crystal and in impure forms as, for instance, rose quartz.

The main crystalline forms of SiO_2 consist of infinite arrays of SiO_4 tetrahedra sharing the vertices.² In α -quartz, which is thermodynamically the most stable form at room temperature, the tetrahedra form interlinked helical chains. Figure 1.17 depicts cristobalite⁴⁴ which is one the high temperature quartz polymorphs occurring in volcanic rocks. Cristobalite structure consists of layers of SiO_4 tetrahedra pointing up and down. Tetrahedra from one layer share oxygen atoms with the tetrahedra pointing in the opposite direction in the next layer.

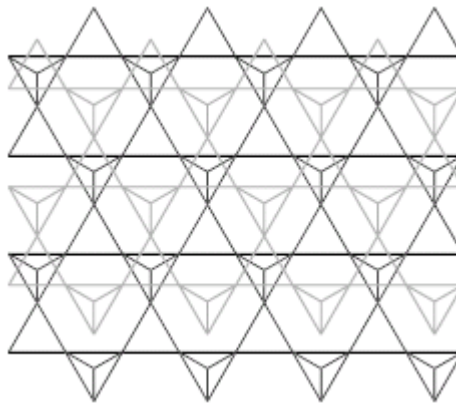


Figure 1.17. Representation of cristobalite⁴⁴ structure.

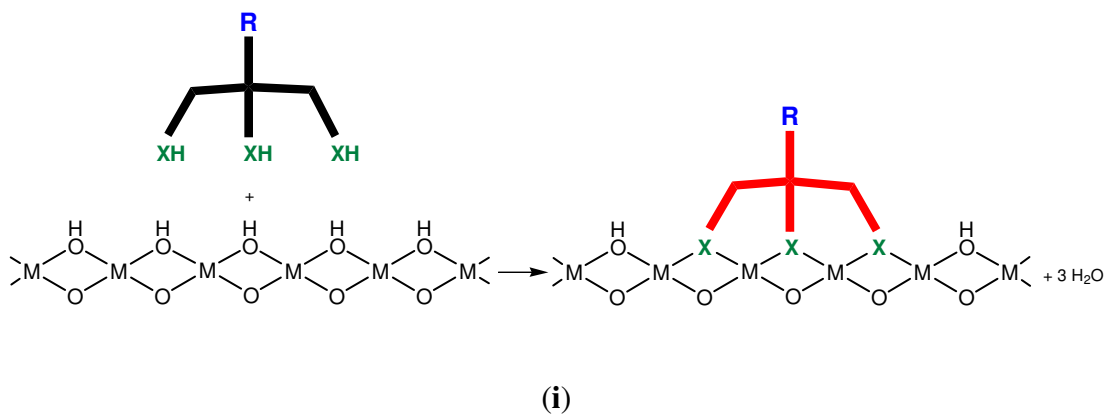
The main types of silica used in industry are α -quartz, vitreous silica, silica gel, fumed silica and diatomaceous earth.

1.8. SURFACE LIGANDS

Surface ligands are molecules which are design to bind strongly to a surface in question. To achieve this, such a ligand needs to have a “head group” functionalized to recognize the particular surface. The “tail group” is tailored according to the application of the ligand, in this case, the design of collector agents which provide hydrophobic characteristics to mineral particles.

Improving the attachment of the ligand to the surface involves designing a polynucleating ligand^{45, 46} to form a thermodynamic stable complex on the surface as shown in Figure 1.18.

It is also important, if the ligand is to be applied from solution, to design the structure to contain a rigid ligand backbone to avoid chelating properties of the ligand as much as possible, that is, to avoid getting two donor atoms attached to the same metal ion, because this could result in dissolution of metal ions from the surface.^{45, 46}



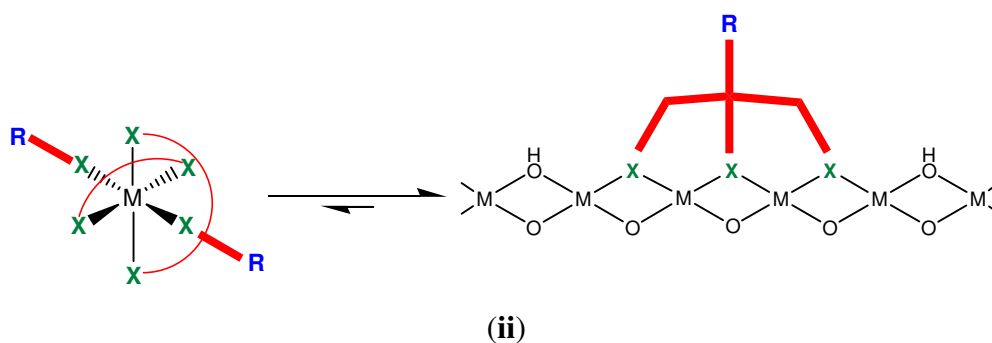


Figure 1.18. (i) Coordination of a polynucleating ligand to a metal oxide mineral surface (ii) Possible equilibrium between sequestration of metal ions in solution and an adsorbed ligand on the mineral surface.

The design of new ligands as collector agents is based on previous work at Edinburgh^{45, 46} on the mode of binding of the corrosion inhibitor Irgacor 419[®], 3-(4-methylbenzoyl)-propionic acid, on goethite. Irgacor 419[®] is used in waterborne coatings produced by Ciba Specialty Chemicals. Testing of this ligand and related derivatives without the methyl substituent or keto-group (**b** and **c**, respectively), shown in Figure 1.19, proved that the presence of both the methyl group in the *para* position of the aromatic ring and the carbonyl group increase the efficiency of this compound as a corrosion inhibitor. The mode of coordination is as a polynucleating ligand through the carboxylate functionality and the 3-keto group. The hydrophobic barrier on the surface is provided by the aromatic rings. As a consequence, Irgacor 419[®] may act as a good collector for the minerals with surface composition similar to goethite.

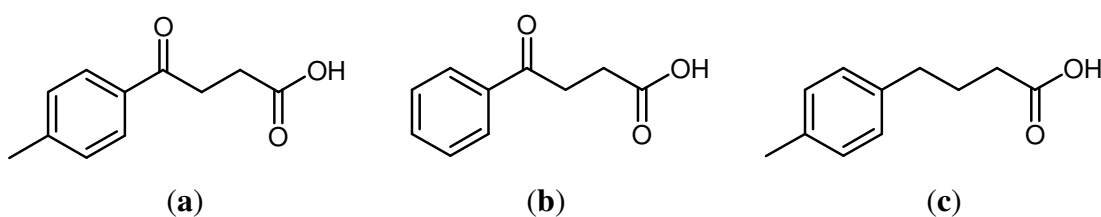


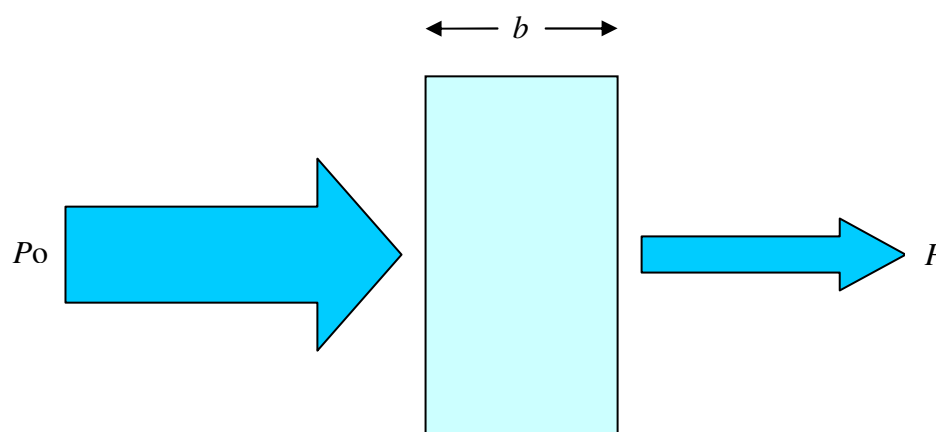
Figure 1.19. Structures of the ligands **(a)** 3-(4-methylbenzoyl)-propionic acid (Irgacor 419[®]), **(b)** 3-benzoyl propionic acid and **(c)** 4-*p*-tolyl-butyl-butyric acid.⁴⁶

1.9. UV-VIS SPECTROSCOPY

One of the techniques used in this thesis to determine the amount of ligand left in solution after an adsorption isotherm experiment is UV-Vis spectroscopy.

Absorption of longer-wavelength ultraviolet and visible radiation is limited to chromophores groups, which are functional groups containing valence electrons with relatively low excitation energies.⁴⁷

Scheme 1.20 illustrates a beam of parallel radiation that passes through a layer of solution having a thickness of b cm and a concentration c of an absorbing compound. As a consequence of interactions between the photons and absorbing particles, the intensity of the beam is attenuated from P_0 to P .^{47, 48}



Scheme 1.20. Attenuation of a beam of radiation by an absorbing solution of concentration c and thickness b .⁴⁷

The transmittance, T , of the solution is then the fraction of incident radiation transmitted by the solution and it is often expressed as a percentage.^{47, 48} That is,

$$T = P/P_0 \quad (1.1)$$

Transmittance can be plotted against the concentration, but the relationship is not linear. The negative log of the transmittance is, however, linear with the concentration. Hence the absorbance of a solution, represented by A , is defined by the equation,

$$A = -\log T = \log P_0/P \quad (1.2)$$

Absorbance is directly proportional to the path length through the solution and the concentration of the absorbing species. Therefore,

$$A = abc \quad (1.3)$$

where a is a proportionality constant called the absorptivity. When the concentration is given in moles per litre and the cell length is in centimetres, the absorptivity is called molar extinction coefficient; it is expressed by the symbol ϵ and has the units $\text{l cm}^{-1} \text{ mol}^{-1}$.^{47, 48}

$$A = \epsilon bc \quad (1.4)$$

$$\log P_0/P = A = \epsilon bc \quad (1.5)$$

Equation 1.5 is known as Beer-Lambert's Law. This law was formulated in 1852 and it tells us that absorbance depends on the totality of the absorbing species in the light path through the cuvette.

LIMITATIONS OF BEER-LAMBERT'S LAW

Some exceptions are found to the statement that absorbance is linearly related to concentration of an absorbing species.^{47, 49}

Beer-Lambert's law is successful in describing the absorption behaviour of dilute solutions only. This is as a result of deviations in absorptivity coefficients at

high concentrations, generally greater than 0.01 M, due to electrostatic interactions between molecules in close proximity can be observed.

Another limitation of Beer-Lambert's Law is that scattering of light can happen as a consequence of particulates in the sample.

1.10. ICP-OES

Inductively Coupled Plasma Optical Emission Spectrometry (ICP-OES) is one of the techniques used in this research work to determine the concentration of some of the ligands remaining in solution after running the adsorption isotherms.

Plasma sources were developed in the 1970s. ICP-OES is a technique that uses a high-temperature (*ca.* 6500 K) plasma to dissociate the sample into its constituent atoms or ions exciting them to a level where they emit light of a characteristic wavelength.⁴⁸ The emission energy released by the excited atoms provides specific quantitative data on the elements present.

Among the benefits of plasma sources are^{47, 48} their low interelement interference and thus the possibility of obtaining spectra of over 70 elements simultaneously. Plasma techniques also allow the analysis of low concentrations of elements. These are important features in the multielement determination of small samples.

The emission lines and detection limits for the elements determined by ICP-OES in this study are listed in Table 1.21.

Element	Emission line (nm)	Detection limit ($\mu\text{g ml}^{-1}$)
Phosphorus	213.617	0.03
Sulfur	180.669	
Iron	259.939	0.001
Silicon	212.412	0.01

Table 1.21. Emission lines and detection limits for the elements determined by ICP-OES.⁵⁰

1.11. OBJECTIVES

We aimed to identify polynucleating head groups for ligands that could be used as collector agents for oxidized sulfide minerals. The importance of the development of new collectors in enhancing efficiency of recovery can be demonstrated with an example relating to the recovery of copper. This flotation process was enhanced by 2% with the use of dialkylthiono carbamate (Dow's Z200) as a collector agent.¹⁴ Taking into consideration that ores worldwide contain average 1% Cu, 25000 additional tonnes of copper would have been recovered from ores already mined and processed previously by flotation.

A number of known collectors as well as potential new agents (Figure 1.22) have been studied to determine their relative binding strengths to mineral particles of interest. The iron corrosion inhibitor, Irgacor 419[®] (**1**), potassium ethyl xanthate (**3**), 2-mercaptobenzothiazole (**4**), benzohydroxamic acid and derivatives (**5**) as well as a series of phosphonic acids (**11**) were selected for study.

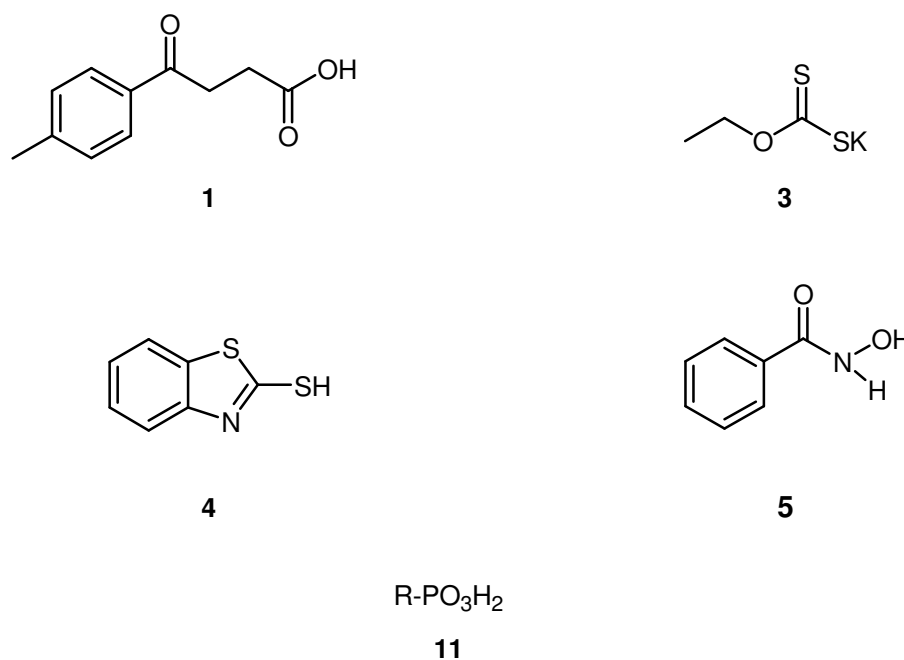


Figure 1.22. Structures of the ligands (1) 3-(4-methylbenzoyl)-propionic acid (Irgacor 419[®]), (3) potassium ethyl xanthate, (4) 2-mercaptobenzothiazole, (5) benzohydroxamic acid and (11) phosphonic acid.

Collector-agent development based on anticorrosive action has been reported before by Barbaro *et al.*,¹⁸ using an aminothiophenol, which shows anticorrosive action. This new flotation agent proposed for the flotation of chrysocolla consists of an aminothiophenol functional group and an alkoxy hydrocarbon chain (Figure 1.23). Chrysocolla is a copper silicate mineral, $((\text{Cu,Al})_2\text{H}_2\text{Si}_2\text{O}_5(\text{OH})_4 \cdot n\text{H}_2\text{O})$, whose solubility is controlled by the pH. Increased flotability of this mineral with the proposed collector is achieved in the pH range 5.5 to 7.

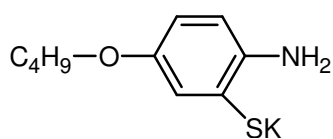


Figure 1.23. 5-n-butoxy-2-aminothiophenol structure.¹⁸

When chalcopyrite is oxidized,^{1, 15, 51-54} it forms iron oxides/hydroxides which make the mineral surface hydrophilic, therefore, goethite has been selected as a model for oxidized chalcopyrite. Silica is the model chosen for gangue. In principle,

it was also planned to use chalcopyrite or a very similar mineral as a substrate. The chalcopyrite used should have a surface area similar to the one of goethite, *ca.* $20 \text{ m}^2 \text{ g}^{-1}$, to obtain easily measurable uptake of ligand from solution. However, to obtain chalcopyrite of that surface area it was calculated that it would be necessary to mill it to a very small particle size, $4 \times 10^{-10} \text{ m}$ (calculations included in Appendix). It was recognized that it would be difficult to retain chemical composition typical of the bulk at this particle size. Another complication would be the difficulty to handle this mineral in isotherm experiments. Consequently, no sulfidic material was used in isotherm measurements. Although ideally this would have been preferred, for the general aim of this work it was not essential as new collectors are going to be used in *combination* with collectors commercially used for sulfidic ores and therefore they should only show selectivity for oxidized surfaces.

Adsorption isotherms run on high surface area goethite and silica are used to determine the adsorption characteristics of each adsorbate onto the metal oxide surface. New collectors should be selective for goethite over silica but need not bind to the sulfidic sites because it is assumed that it would be used in conjunction with a sulfidic collector. Chapters 2, 3, 4, 5 and 6 focus on binding strength studies using adsorption isotherms. Novel candidate flotation agents were identified which were then tested on flotation experiments in Chapter 7.

1.12. REFERENCES

- 1 B. Triffett and R. Shaw, Personal Communication, Rio Tinto, 2003.
2 N. N. Greenwood and A. Earnshaw, 'Chemistry of the Elements',
3 Butterworth-Heinemann, Oxford, 1994.
4 <http://www.kennecott.com/index.html>, 2007.
5 <http://www.riotinto.com/whatweproduce/copper.asp>, 2007.
6 P. Atkins, T. Overon, J. Rouke, M. Weller, and F. Armstrong, 'Inorganic
7 Chemistry', Oxford University Press, Oxford, 2006.
8 F. Habashi, 'A Textbook of Hydrometallurgy', Metallurgie Extractive
9 Quebec, Enr., Quebec, 1993.
10 J. M. Cases and F. Villieras, 'Innovations Flotation Technology', Kluwer
11 Academic Publishers, 1992.
12 <http://www.utah.com/attractions/kennecott.htm>, 2007.
13 P. A. Tasker, P. G. Plieger, and L. C. West, *Comprehensive Coordination
14 Chemistry II*, 2004, **9**, 759.
15 R. R. Klimpel, *International Journal of Mineral Processing*, 2000, **58**, 77.
16 Y. Peng, S. Grano, D. Fornasiero, and J. Ralston, *International Journal of
17 Mineral Processing*, 2003, **69**, 87.
18 G. Fairthorne, D. Fornasiero, and J. Ralston, *International Journal of Mineral
19 Processing*, 1997, **49**, 31.
20 K. K. Das and Pradip, *Process Technology Proceedings*, 1988, **7**, 305.
21 D. W. Fuerstenau, *Proceedings of the International Mineral Processing
22 Congress, 19th, San Francisco*, 1995, **3**, 3.
23 W. Tolley, D. Kotlyar, and R. Van Wagoner, *Minerals Engineering*, 1996, **9**,
24 603.
25 E. G. Kelly and D. J. Spottiswood, 'Introduction to mineral processing', John
26 Wiley & Sons, New York, 1982.
27 Pradip, *Metals, Materials and Processes*, 1998, **10**, 41.
28 M. Barbaro, R. Herrera Urbina, C. Cozza, D. Fuerstenau, and A. Marabini,
International Journal of Mineral Processing, 1997, **50**, 275.
B. P. Singh, *Langmuir*, 1994, **10**, 510.
J. A. Mielczarski, E. Mielczarski, and J. M. Cases, *International Journal of
Mineral Processing*, 1998, **52**, 215.
G. N. Andreev and A. Barzev, *Journal of Molecular Structure*, 2003, **661-
662**, 325.
R. R. Klimpel, 'A Review of Sulfide Mineral Collector Practice'.
D. R. Nagaraj, *Development of New Flotation Chemicals*, 1997, **50**, 355.
S. R. Grano, C. A. Prestidge, and J. Ralston, *International Journal of Mineral
Processing*, 1997, **52**, 161.
Cytotec Industries, 'Mining Chemicals Handbook', 2002.
A. M. Marabini, M. Barbaro, and V. Alesse, *International Journal of Mineral
Processing*, 1991, **33**, 291.
Pradip and B. Rai, *International Journal of Mineral Processing*, 2003, **72**, 95.
D. Orwe, S. R. Grano, and D. W. Lauder, *Minerals Engineering*, 1998, **11**,
171.

- 29 J. S. Lee, D. R. Nagaraj, and J. E. Coe, *Minerals Engineering*, 1998, **11**, 929.
30 C. J. Marmion, D. Griffith, and K. B. Nolan, *European Journal of Inorganic
Chemistry*, 2004, 3003.
- 31 R. R. Klimpel and B. S. Fee, *Publications of the Australasian Institute of
Mining and Metallurgy*, 1993, **3/93**, 569.
- 32 A. N. Mainza, S. Simukanga, and L. K. Witika, *Minerals Engineering*, 1999,
12, 571.
- 33 P. W. Atkins, 'Physical Chemistry', Oxford University Press, Oxford, 1995.
34 C. H. Giles, D. Smith, and A. Huitson, *Journal of Colloid and Interface
Science*, 1974, **47**, 755.
- 35 G. D. Parfitt and C. H. Rochester, 'Adsorption from Solution at the
Solid/Liquid Interface', Academic Press Inc., London, 1983.
- 36 C. H. Giles, A. P. D'Silva, and I. A. Easton, *Journal of Colloid and Interface
Science*, 1974, **47**, 766.
- 37 W. Stumm, 'Chemistry of the Solid-Water Interface', John Wiley & Sons,
New York, 1992.
- 38 Y. Cudennec and A. Lecerf, *Solid State Sciences*, 2005, **7**, 520.
- 39 A. C. Scheinost and U. Schwertmann, *Soil Science Society of America
Journal*, 1999, **63**, 1463.
- 40 S. Cornelius, J. R. Hurlbut, and C. Klein, 'Manual of Mineralogy 19 th Ed.
(after James D. Dana)', John Wiley & Sons, New York, 1977.
- 41 Y. Waseda, S. Suzuki, and M. Saito, *Journal of Alloys and Compounds*,
2005, **401**, 24.
- 42 A. F. Gualtieri and P. Venturelli, *American Mineralogist*, 1999, **84**, 895.
- 43 A. Manceau and J. M. Combes, *Physics and Chemistry of Minerals*, 1988, **15**,
283.
- 44 [http://www.science.smith.edu/departments/Geology/Minjb/SilicaPolymorphs.
pdf](http://www.science.smith.edu/departments/Geology/Minjb/SilicaPolymorphs.pdf), 2007.
- 45 M. Frey, S. G. Harris, J. M. Holmes, D. A. Nation, S. Parsons, P. A. Tasker,
S. J. Teat, and R. E. P. Winpenny, *Angewandte Chemie, International
Edition*, 1998, **37**, 3246.
- 46 M. Frey, S. G. Harris, J. M. Holmes, D. A. Nation, S. Parsons, P. A. Tasker,
and R. E. P. Winpenny, *Chemistry--A European Journal*, 2000, **6**, 1407.
- 47 D. A. Skoog, 'Principles of Instrumental Analysis', CBS College Publishing,
Philadelphia, 1985.
- 48 F. A. Settle, 'Handbook of Instrumental Techniques for Analytical
Chemistry', Prentice-Hall, New Jersey, 1997.
- 49 H. H. Perkampus, 'UV-Vis Spectroscopy and its Applications', Springer-
Verlag, Berlin, 1992.
- 50 <http://www.ivstandards.com>, 2007.
- 51 S. Chander and A. Khan, *International Journal of Mineral Processing*, 2000,
58, 45.
- 52 D. Fornasiero, D. Fullston, C. Li, and J. Ralston, *International Journal of
Mineral Processing*, 2001, **61**, 109.
- 53 S. R. Grano, M. Sollaart, W. Skinner, C. A. Prestidge, and J. Ralston,
International Journal of Mineral Processing, 1997, **50**, 1.

⁵⁴ A. J. H. Newell, D. J. Bradshaw, and P. J. Harris, *Minerals Engineering*, 2006, **19**, 675.

Chapter 2

Surface binding studies of carboxylic acids

CONTENTS

2.1. Introduction	37
2.1.1. Outline.....	37
2.1.2. Background	37
2.1.3. Carboxylic acids.....	38
2.1.4. A corrosion inhibitor for iron: Irgacor 419 [®]	38
2.1.5. Other ligands showing H-bond interactions and multisite attachment	41
2.2. Development of a suitable procedure to determine adsorption isotherms	43
2.3. Surface binding studies by adsorption isotherms.....	45
2.4. Conclusions	48
2.5. Experimental	49
2.5.1. Instrumentation	49
2.5.2. Solvents and reagents.....	49
2.5.3. Ligands	49
2.5.4. Extinction coefficient (ϵ) determination	49
2.5.5. Adsorption isotherm measurements.....	50
2.6. References	51

2.1. INTRODUCTION

2.1.1. OUTLINE

This chapter considers the adsorption of two carboxylic acids (ligands **1** and **2**, Figure 2.1) onto iron(III) oxide surfaces such as goethite, and onto siliceous surfaces, such as silica. The two ligands selected should show selectivity for binding goethite over silica. The commercial corrosion inhibitor for iron Irgacor 419[®] was used as a starting point of the investigation. In addition to attempting to confirm that the carboxylic acids bind more strongly to iron(III) oxides, the work described in this chapter was aimed at establishing protocols for determining isotherms reliably to allow comparisons to be made on both the strength of binding and the surface coverage shown by different ligands.

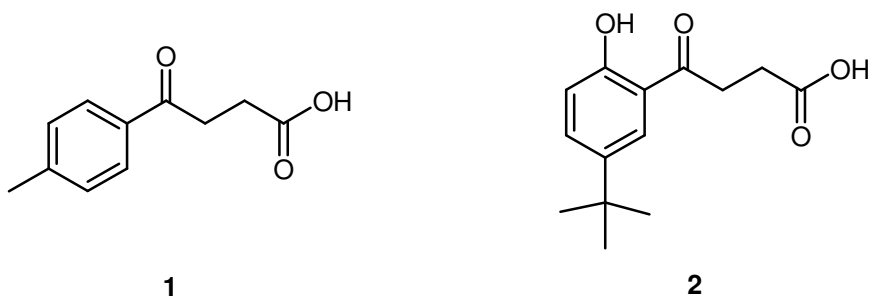


Figure 2.1. Ligands **1** and **2** studied in this chapter.

2.1.2. BACKGROUND

In previous studies carried out at the University of Edinburgh to develop new corrosion inhibitors for mild steel in waterborne coatings organic ligands that enhance anticorrosion properties have been identified.¹ The availability of such simple organic ligands which bind strongly and selectively to iron(III) oxides could provide a way of improving the recovery of oxidized sulfide mineral particles (see Section 1.11). Recovering oxidized minerals that are not effectively retrieved by the

existing sulfide mineral flotation reagents is one of the challenges in the mining industry at the moment^{2, 3} and therefore identifying chemical reagents which can make oxidized minerals hydrophobic by forming complexes at the surface of the mineral particles is of great importance.

2.1.3. CARBOXYLIC ACIDS

The general structure of carboxylic acids is shown in Figure 2.2. They include electronegative oxygen atoms and have both hydrogen bond donor and acceptors that form easily hydrogen bonds to other polarized molecules,⁴ such as water, alcohols, other carboxylic acids and amides (Figure 2.2).⁵ Carboxylic acids are usually held together as hydrogen-bonded dimers.

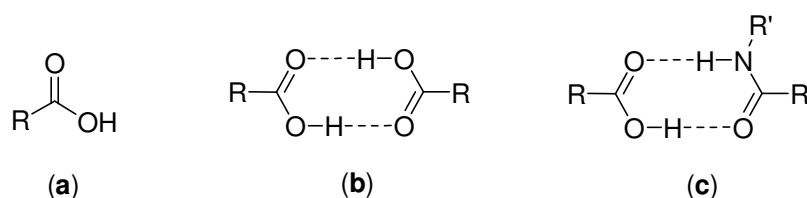


Figure 2.2. (a) General structure of carboxylic acids, (b) carboxylic acid dimer hydrogen bonded (c) hydrogen bonded acid-amide dimer.⁴

Carboxylate anions form complexes with a wide range of main group and transition metals, many of which are polynuclear with unusual properties.⁶⁻¹⁰ The different modes of coordination of carboxylates have been classified in earlier work in Edinburgh^{11, 12} and described in recent reviews.¹³

2.1.4. A CORROSION INHIBITOR FOR IRON: Irgacor 419®

The protection of metal surfaces against corrosion is of great industrial importance.¹ Concerns about the potential carcinogenic properties and ecological problems^{14, 15} associated with existing metal passivation treatments including

chromium(VI) have provided an encouragement for the development of environmentally friendly alternatives, such as organic ligands.¹ An example of a compound satisfying this requirement is 3-(4-methylbenzoyl)-propionic acid (see Figure 2.3), which is supplied by Ciba Specialty Chemicals under the trade name Irgacor 419[®], and is used in water-borne coatings. It was selected as a candidate co-collector for froth flotation due to the strong binding strength shown to iron(III) oxide surfaces in adsorption isotherm experiments¹ and its performance as a corrosion inhibitor for iron, that is described below.

Irgacor 419[®] and related derivatives (Figure 2.3) were studied to explain their effectiveness as corrosion inhibitors.¹ It was suggested that the presence of both the carbonyl group and the methyl group in the *para* position of the aromatic ring have a beneficial influence on the corrosion inhibition properties of Irgacor 419[®].

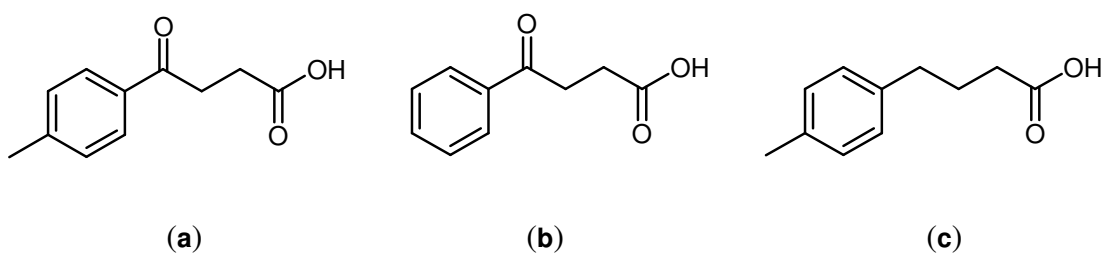


Figure 2.3. Structures of the ligands (a) 3-(4-methylbenzoyl)-propionic acid (Irgacor 419[®]), (b) 3-benzoyl propionic acid and (c) 4-*p*-tolyl-butyric acid.¹

In order to understand the mode of action of this ligand on iron oxide surfaces, polynuclear iron(III) complexes of Irgacor 419[®] were synthesized and their crystal structure characterized.^{1, 16} Structures of the ferric wheel of formula $[\{\text{Fe}(\text{OMe})_2(\text{Irg 419})\}_{10}]$ and the Fe_{11} cluster $[\text{Fe}_{11}(\text{O})_6(\text{OH})_6(\text{Irg 419})_{15}]$ show, in both cases, that the carboxylate ligand is dinucleating (see Figure 2.4 and 2.5). In the Fe_{11} cluster of Irgacor 419[®] in four cases the 3-keto functionalities hydrogen-bond to the hydroxide units on the surface of the cluster (Figure 2.4 and 2.5).

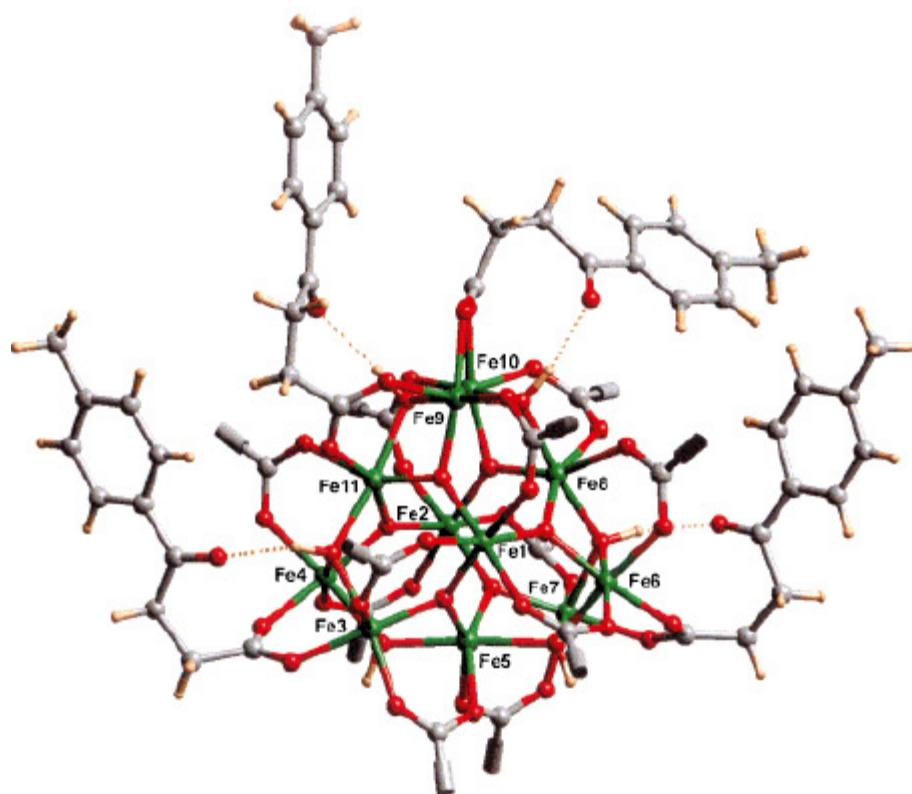


Figure 2.4. Structure of $[\text{Fe}_{11}(\text{O})_6(\text{OH})_6(\text{Irg 419})_{15}]$. Eleven of the Irg 419[®] ligands (but not their carboxylate groups) have been omitted for clarity. Only the four units of Irg 419[®] with hydrogen bonds to the hydroxide groups to the metal cage (represented as dotted lines) are shown.¹⁶

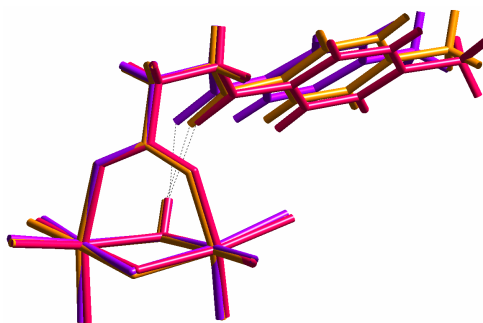


Figure 2.5. Conformation of the hydrogen-bonded carboxylates in $[\text{Fe}_{11}(\text{O})_6(\text{OH})_6(\text{Irg 419})_{15}]$. All carboxylates are dinucleating.¹

This proposed mode of action for corrosion protection was also supported by computer modelling.¹ The multisite attachment through the carboxylate group and

the hydrogen bonding of the 3-keto group to the hydroxyl groups of iron(III) oxy/hydroxides (Figure 2.6) help to account for the efficacy as a corrosion inhibitor of Irgacor 419[®] when compared to related compounds. The hydrophobic barrier on the surface is provided by the aromatic rings with the methyl groups filling in “gaps” in the packing, explaining its increased efficacy when compared with ligand **b** (Figure 2.3).¹

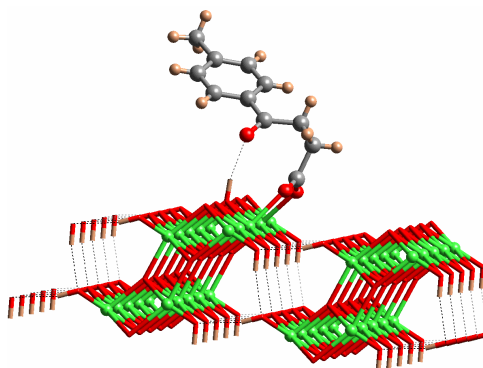


Figure 2.6. Multisite attachment and hydrogen bonding of a molecule of Irgacor 419[®] to the 021 surface of lepidocrocite.¹⁶

2.1.5. OTHER LIGANDS SHOWING H-BOND INTERACTIONS AND MULTISITE ATTACHMENT

Recently, work was carried out in our lab to explore how the presence of hydrogen bond donors and acceptors can enhance surface binding by multisite attachment.¹⁷

Hydrogen bonds are formed between an electronegative atom, such as nitrogen, oxygen or halogens, that has lone pair of electrons and a hydrogen atom bonded to another electronegative atom.¹⁸ H-bonds can be intermolecular, between different molecules, or intramolecular, within different atoms of a molecule. The strength of a hydrogen bond varies with the nature of heteroatoms involved and can vary¹⁹ from very weak, 1-2 kJ mol⁻¹, to strong, 40 kJ mol⁻¹.

This research demonstrated that carboxylic acids containing groups for secondary hydrogen bonding enhance the strength of binding to iron(III) oxide surfaces.¹⁷ Complementary bonding pairs such as amides, increase the stability of the surface complex. The inclusion of an additional hydrogen bond donor, such as a urea linkage, enhances this effect more distinctly.

Following a similar approach to that^{1, 16} described in the previous section for Irgacor 419[®], the binding of phenyl malonic acid, **18** (Figure 2.7), on goethite surfaces was also studied within the group at Edinburgh.¹⁷

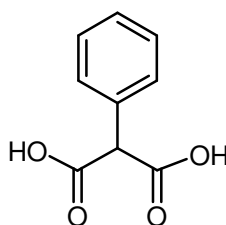


Figure 2.7. Structure of ligand **18**.

Adsorption isotherms of **18** on goethite (data in Appendix) showed that the malonate functionality increased the strength of binding in comparison to Irg 419[®], **1**. Consequently, malonic acids were considered to be good candidates for “surface” engineering of iron (oxide). Molecular modelling was used to account for its efficacy. The surface chosen for modelling was the 010 plane of goethite. The two most likely modes of binding consist of a binucleating mode which includes a free carboxylic acid group available for hydrogen bonding to hydroxyl groups on the goethite surface (Figure 2.8 (a)) and a dianionic malonate trinucleating mode (Figure 2.8 (b)).

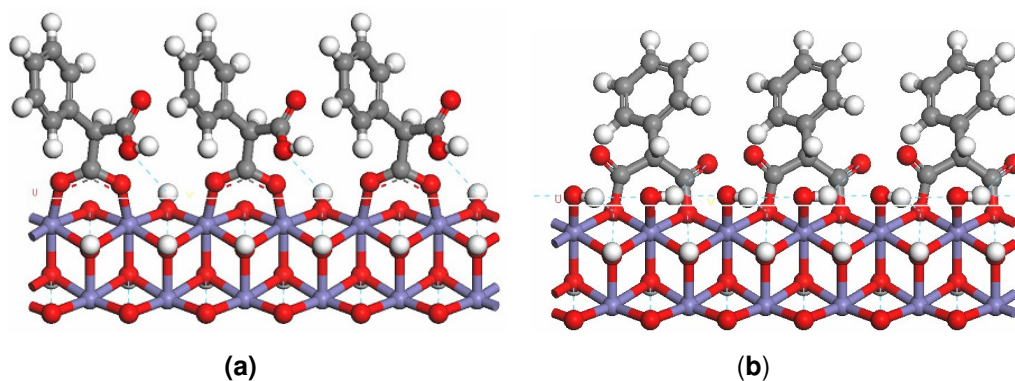


Figure 2.8. Molecular modelling simulations of malonate binding to the 010 surface of goethite, illustrating (a) binucleating mode with a free carboxylic acid group hydrogen bonding to hydroxyl groups on the goethite surface and (b) dianionic malonate trinucleating mode.¹⁷

2.2. DEVELOPMENT OF A SUITABLE PROCEDURE TO DETERMINE ADSORPTION ISOTHERMS

A series of experiments were undertaken to establish the most suitable method to determine adsorption isotherms as it was observed that errors could arise from several factors:

- automated pipettes showing irreproducibility when delivering solutions
- evaporation occurring when filtering
- high scatter being observed in the region of the isotherm with high residual ligand concentrations due to errors associated with the high dilution factors necessary to analyse samples of higher concentrations by UV-Vis spectroscopy
- a new batch of goethite, with surface area $22.50 \text{ m}^2 \text{ g}^{-1}$, being used. Its composition seems not to be homogeneous and it showed

differences when comparing the isotherms of Irgacor 419[®] obtained using the two batches.

It was observed that some unknown substance is released from the mineral surface when the goethite is stirred with the solvent used to run the adsorption isotherms in this project, methanol/water (95:5 v/v). Table 2.9 records the absorbance values of the supernatant liquor. Since no ligand had been added, it indicates that a ligand has been transferred to solution.

Ligand (wavelength / nm) ^a						
	1 (252)	2 (254)	3 (301)	4 (321)	5 (224)	6 (300)
Abs	0.254	0.246	0.151	0.086	0.511	0.163

Table 2.9. Background correction data: Absorbance values of methanol/water (95:5 v/v) stirred with goethite at 25°C for 2 h.

^a Absorbance values are recorded at the wavelengths used for the ligands studied in this thesis whose concentrations after contact with goethite were determined by UV-Vis spectroscopy.

When analysing adsorption isotherm data, each measurement of the absorbance of the supernatant was corrected by subtracting this background absorbance for the unknown material at the wavelength of interest according to Table 2.9. If this correction is not applied, calculated values of concentration of ligand remaining in solution are higher than they should be and for very low added ligand concentration the “residual” values are higher than those added.

When corrections are not applied adequately difficulties arise in plotting and interpreting isotherms because they do not pass through the coordinate origin.

Problems associated with release of UV-Vis absorbing materials were not observed either when goethite is stirred with water prior to conducting an isotherm or

with a previous batch of goethite used by the group although similar behaviour has been observed in related studies on aluminium trihydroxide.²⁰ From now on in this thesis, this phenomenon will be referred to as the “background correction factor”. A similar process was undertaken for silica measurements. The possibility of a similar problem arising when using high surface area silica in adsorption measurements was examined but proved not to be of concern.

The optimised adsorption isotherm technique incorporated:

- filtering the aliquot of known volume of supernatant solution to make up the solutions to the required dilution factor,
- a filtration procedure to minimise evaporation by covering the volumetric flasks with parafilm into which the filtered solution was delivered,
- running overlapping points for solutions prepared from different stock solutions to check concentrations of stock solutions and dilution errors and
- applying the background correction factor in each case when using UV-Vis spectroscopy to determine ligand uptake from solution (Table 2.9).

2.3. SURFACE BINDING STUDIES BY ADSORPTION ISOTHERMS

The binding characteristics of ligands **1** and **2** (Figure 2.1) are discussed below. The Beer-Lambert Law (Section 1.9) and the background correction factor (see Section 2.2) were applied to determine the concentration remaining in solution

after contact with goethite by UV-Vis spectroscopy (see Section 2.5.5) after an adsorption isotherm is run. Data are displayed in Table 2.10.

Ligand	Wavelength (nm)	Extinction coefficient ($l \text{ mol}^{-1} \text{ cm}^{-1}$)	Background correction factor
1	252	15890	0.254
2	254 ^a , 334	10889 ^a , 3860	0.246 (at 254)

Table 2.10. Extinction coefficient data and background correction factors for **1** and **2** determined in methanol/water (95:5 v/v) at room temperature.

^a Wavelength used in the adsorption isotherm determination.

A comparison of the behaviour of each ligand on the two substrates, goethite and silica, is shown in the graph (Figure 2.11). The solid lines correspond to the theoretical fit to the Langmuir adsorption equation and squares or crosses to experimental values.

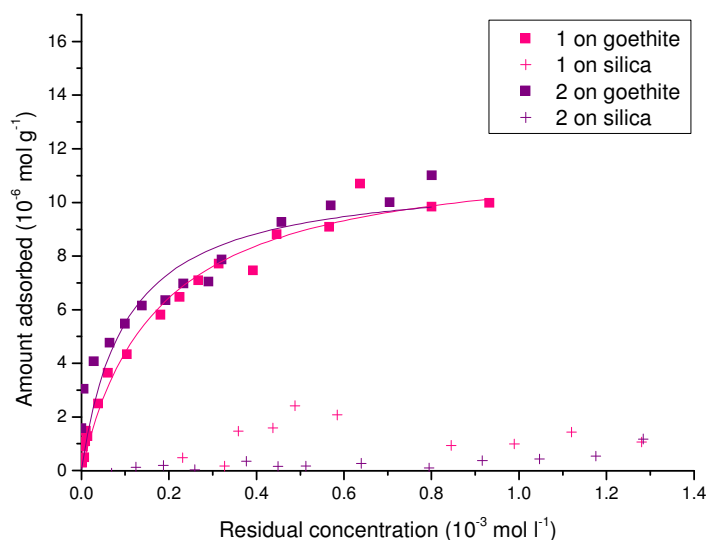


Figure 2.11. Adsorption isotherms of ligands **1** and **2** on goethite and silica in methanol/water (95:5 v/v) at 25 °C.

Ligand	Equilibrium adsorption constant (K) 10^3	Surface coverage (10^{-6} mol g^{-1})	Required surface area (\AA^2 molecule $^{-1}$)
1	5.8(8)	12.0(5)	300(10)
2	9.9(3)	11(1)	340(30)

Table 2.12. Adsorption isotherm data for ligand **1** and **2** (errors in parentheses) on goethite. For definitions of K , surface coverage, required surface area and their determination see Section 1.6.1.

The isotherms for **1** and **2** (Figure 2.11) show very similar shapes and the data in Table 2.12 reflect this. Surface coverages, 12.0(5) and 11(1) $\times 10^{-6}$ mol g^{-1} for **1** and **2**, respectively are the same within experimental error. This suggests that the mode of surface binding and of packing is similar and the presence of the bulky group, *t*-butyl, on the aromatic ring of **2** does not create any steric effects. The binding strength is proportional to the slope of the early part of the isotherm which is linear at low equilibrium concentrations (lower than *ca.* 5×10^{-4} mol l^{-1} in this case). Visual comparison of the slopes shows them to be similar. The equilibrium adsorption constant for **2** [$9.9(3) \times 10^3$] calculated by curve fitting assuming Langmuir behaviour is slightly greater than that of **1** [$5.8(8) \times 10^3$]. This suggests that the surface attachment is due to the 4-keto acid group present in both ligands and that the extra OH functionality on the phenyl ring may allow H-bonding interactions between ligands or with hydroxyl groups of the iron(III) oxide/hydroxide surface. Consequently, the binding mode of **2** on goethite may essentially occur in the same way as it does for **1**, via multisite attachment through bonds from the carboxylic group to the iron(III) centres and hydrogen bonding from surface groups to the keto function, as described by Frey *et al.*¹

A small difference in the strength of binding of **1** to goethite was observed in this work when using a new batch of goethite with a different surface area. The value of K given by Frey *et al.*¹ was $1.4(1) \times 10^3$ whilst the one found in this research was

$5.8(8) \times 10^3$. All results quoted in the thesis were obtained with the same batch of goethite (see Section 2.5.2).

As desired, the binding to silica of **1** and **2** is very weak, which will help to obtain separation of sulfidic from oxidic minerals in froth flotation.

2.4. CONCLUSIONS

The work described in this chapter has confirmed that it is possible to follow the uptake of carboxylic acids with aromatic substituents onto high surface area inorganic oxides by using UV-Vis spectroscopy to determine the residual concentration of the ligand after contacting with the solid oxide. For the two test case carboxylic acids **1** and **2** a Langmuir model was used successfully to estimate equilibrium adsorption constants and surface coverage on goethite. Slight modifications of procedures used previously were needed to improve the reproducibility of data and to correct for the release of materials from the goethite surface which absorb light in the UV-Visible regions.

1 and **2** show very similar binding strengths and surface coverage on goethite suggesting that it is the common keto acid functionality which is responsible for surface attachment. The bulky *t*-butyl groups appended to **2** clearly present no problems in surface packing and the additional OH group on pendant benzene ring may be responsible for the slightly more favourable bonding constant by favouring H-bonding interactions with ligand or surface oxygen chains.

1 and **2** bind much more strongly to goethite than to silica, confirming their potential to function as co-collectors for minerals with oxidized surfaces, a criterion which is needed to avoid increased collection of siliceous materials.

2.5. EXPERIMENTAL

2.5.1. INSTRUMENTATION

UV-Vis absorption spectra were measured in methanol/water (95:5 v/v) on a Perkin-Elmer Lambda 900 UV-Vis-NIR spectrophotometer with 1 cm path length quartz cuvettes. Curve fitting was performed using the program Origin 7.5 © Microcal Software Inc.

2.5.2. SOLVENTS AND REAGENTS

Solvents were of analytical reagent grade, laboratory reagent grade or HPLC grade. High surface area goethite (Bayferrox[®] 415) was obtained from Bayer. Silica 60A was supplied by Fisher. Water was purified using a Milli-Q[®] water purification system.

2.5.3. LIGANDS

1 (Irgacor 419[®]) was supplied by Ciba Specialities. **2** was prepared by Mr. R. Forgan.²¹

2.5.4. EXTINCTION COEFFICIENT (ϵ) DETERMINATION

UV-Visible spectra of solutions of ligand in methanol/water (95:5 v/v) with concentrations in the range of 3.0×10^{-6} to 3.0×10^{-5} mol l⁻¹ were measured and concentration of ligands determined using Beer-Lambert plots obtained with solutions of known concentration.

2.5.5. ADSORPTION ISOTHERM MEASUREMENTS

Different concentrations of each of the ligands in methanol/water (10 ml, 95:5 v/v) were added to accurately weighed samples of goethite (0.40 g) in polycarbonate centrifuge tubes. The suspensions were stirred for 2 h at 25 °C and then centrifuged. The aliquot of known volume of supernatant solution necessary to make up the solutions to the required dilution factor was filtered through glass microfibre filter paper which was then washed (3 x 0.5 ml) with the solvent used methanol/water (95:5 v/v) and the sample was made up to volume. The absorbance was measured by UV-Vis spectroscopy at the appropriate wavelengths to determine the concentration of the ligand remaining in solution. The difference between the initial and the residual concentration in solution provides the amount of ligand adsorbed on the substrate, which was plotted against the residual concentration in solution using Origin V7.5 to fit data to a non-linear curve (rectangular hyperbole or double rectangular hyperbole). Surface coverage and equilibrium adsorption constants were calculated from these curves. Equations are gathered in the introduction (Section 1.6.1) and data for adsorption isotherms are collected in the Appendix.

Adsorption isotherms of the ligands using silica as an adsorbate were obtained following the procedure described above but making up the solutions to 100 ml in glass jars.

2.6. REFERENCES

- 1 M. Frey, S. G. Harris, J. M. Holmes, D. A. Nation, S. Parsons, P. A. Tasker,
2 and R. E. P. Winpenny, *Chemistry--A European Journal*, 2000, **6**, 1407.
- 3 R. R. Klimpel, *International Journal of Mineral Processing*, 2000, **58**, 77.
- 4 K. K. Das and Pradip, *Process Technology Proceedings*, 1988, **7**, 305.
- 5 K. P. C. Vollhardt and N. E. Schore, 'Organic Chemistry. Structure and
6 Function', W. H. Freeman and Company, New York, 1998.
- 7 A. Parkin, G. Barr, W. Dong, C. J. Gilmore, and C. C. Wilson, *Crystal
8 Engineering Communications*, 2006, **8**, 257.
- 9 K. S. Gavrilenko, S. V. Punin, O. Cador, S. Golhen, L. Ouahab, and V. V.
10 Pavlishchuk, *Journal of the American Chemical Society*, 2005, **127**, 12246.
- 11 R. H. Laye, F. K. Larsen, J. Overgaard, C. A. Muryn, E. J. L. McInnes, E.
12 Rentschler, V. Sanchez, S. J. Teat, H. U. Guedel, O. Waldmann, G. A.
13 Timco, and R. E. P. Winpenny, *Chemical Communications*, 2005, 1125.
- 14 N. L. Rosi, J. Kim, M. Eddaoudi, B. Chen, M. O'Keeffe, and O. M. Yaghi,
15 *Journal of the American Chemical Society*, 2005, **127**, 1504.
- 16 E. K. Brechin, G. Christou, M. Soler, M. Helliwell, and S. J. Teat, *Dalton
17 Transactions*, 2003, 513.
- 18 C. N. R. Rao, S. Natarajan, and R. Vaidhyanathan, *Angewandte Chemie,
19 International Edition*, 2004, **43**, 1466.
- 20 F. J. White, 'PhD work in progress', University of Edinburgh, 2007.
- 21 S. G. Harris, 'Crystallographic and modelling studies of organic ligands on
metal surfaces', PhD Thesis, University of Edinburgh, 1999.
- R. K. Hocking and T. W. Hambley, *Dalton Transactions*, 2005, 969.
- H. J. Gibb, P. S. Lees, P. F. Pinsky, and B. C. Rooney, *American Journal of
Industrial Medicine*, 2000, **38**, 115.
- D. E. Kimbrough, Y. Cohen, A. M. Winer, L. Creelman, and C. Mabuni,
Critical Reviews in Environmental Science and Technology, 1999, **29**, 1.
- M. Frey, S. G. Harris, J. M. Holmes, D. A. Nation, S. Parsons, P. A. Tasker,
S. J. Teat, and R. E. P. Winpenny, *Angewandte Chemie, International
Edition*, 1998, **37**, 3246.
- R. Renz, 'Design and synthesis of benign, N- and O-containing organic
ligands for surface engineering', PhD Thesis, University of Edinburgh, 2007.
- C. E. Housecroft and A. G. Sharpe, 'Inorganic Chemistry', Pearson Education,
Harlow, 2nd Ed., 2005.
- G. R. Desiraju and T. Steiner, 'The weak Hydrogen Bond', Oxford University
Press, Oxford, 2001.
- J. Robertson, 'Studies of the Binding Strengths and Modes of Action of
Organic Ligands on Aluminium Trihydroxide Surfaces', PhD Thesis,
University of Edinburgh, 2001.
- R. S. Forgan, S. Parsons, P. A. Tasker, and F. J. White, *Acta
Crystallographica, Section E: Structure Reports Online*, 2007, **E63**, o3249.

Chapter 3

Surface binding studies of potassium ethyl xanthate

CONTENTS

3.1. Introduction	54
3.1.1. Outline.....	54
3.1.2. Xanthates.....	54
3.1.3. Decomposition of xanthates.....	55
3.2. Surface binding studies by adsorption isotherms.....	57
3.3. Conclusions	61
3.4. Experimental	62
3.4.1. Instrumentation	62
3.4.2. Solvents and reagents.....	62
3.4.3. Ligand	62
3.4.4. Extinction coefficient (ϵ) determination	62
3.4.5. Adsorption isotherm measurements.....	62
3.5. References	64

3.1. INTRODUCTION

3.1.1. OUTLINE

This chapter discusses the adsorption characteristics of potassium ethyl xanthate on goethite and silica. Initially it was intended also to test the adsorption of ligands on chalcopyrite. However, in practice it was not possible to obtain sulfidic material milled to the required size to obtain a measurable uptake from solution, as discussed in Section 1.11.

Xanthates are one of the families of collectors most frequently used in mineral flotation. Ethyl xanthate is the most commonly used,¹ and consequently, was selected as a model for testing in adsorption isotherm experiments. Unlike other collectors, there is evidence¹⁻⁴ that xanthates undergo hydrolysis and oxidation reactions under the conditions of flotation, making it more difficult to carry out and interpret binding studies.

3.1.2. XANTHATES

Xanthate collectors (Figure 3.1) were introduced in 1925⁵ and they dominated the sulfide collector market until not long ago. They are some of the most inexpensive material used as collectors and their global consumption is estimated to be around 60000 tonnes per year.¹ They can be used individually or in combination with other collectors.^{5, 6} They are also used in the production of viscose rayon and pesticides.²

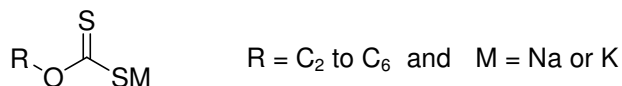


Figure 3.1. Xanthate structure.⁶

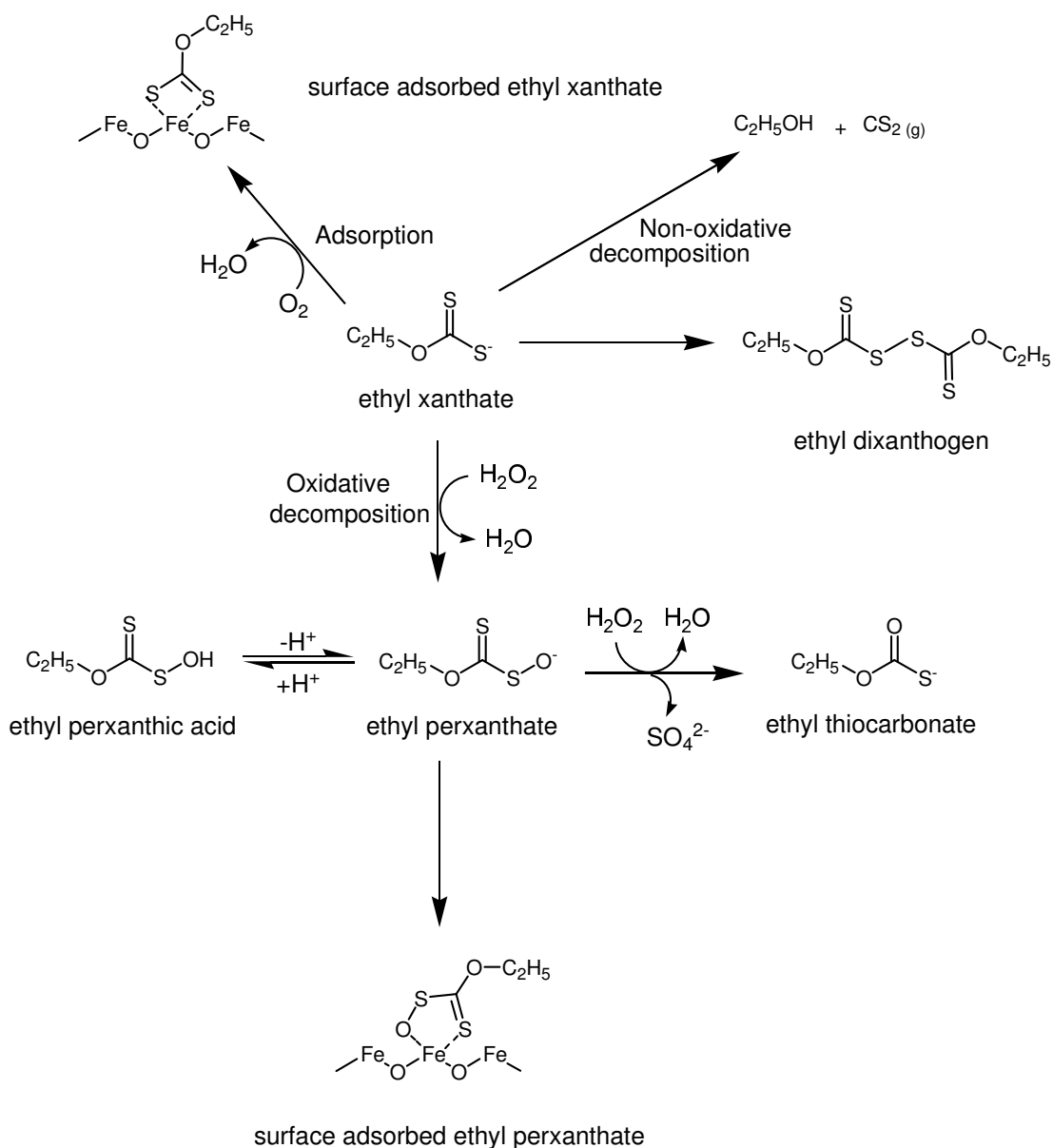
After more than fifty years investigating the interactions between xanthates and mineral surfaces, the mechanisms involved are still not totally understood.³ This is due to their instability in solution,^{3,7} forming a range of derivatives with different properties on the mineral surface (see Section 3.1.3) and also because their interactions with minerals are both time and pH dependent.^{1,3,8,9}

3.1.3. DECOMPOSITION OF XANTHATES

The role of xanthates in froth flotation processes is to selectively adsorb on the sulfide mineral surface of value conferring hydrophobic character to the mineral to be separated.²

As mentioned above, oxidative decomposition (Scheme 3.2) is one of the major reaction pathways undergone by xanthates. Hao *et al.*⁴ suggested decomposition on surface minerals involves O₂. However, in a following paper² they proposed that oxidation requires H₂O₂. They report that the nature of the mineral surface has an influence on the xanthate species generated as shown in Scheme 3.2. In the cases of pyrite (FeS₂) and galena (PbS), it has been observed² that one of the products of dissolved oxygen is hydrogen peroxide which reacts with xanthate in solution giving perxanthate which on further oxidation forms thiocarbonate. The authors also conclude that the involvement of H₂O₂ in the generation of these two compounds has never been proved conclusively. They investigated the oxidative decomposition of xanthates in solution using UV-Vis spectroscopy and HPLC.

It must also be emphasised that evidence of generation of H₂O₂ by dioxygen reduction is limited to laboratory electrochemical experiments.² The presence of H₂O₂ in mineral processing waste streams has not been reported although perxanthates have been found in various flotation plants, an indication of this type of reaction may occur in real processes. Other xanthate degradation products have not been detected in flotation sites.¹



Scheme 3.2. Possible reaction pathways of the oxidation of ethyl xanthate, **3**, and ethyl perxanthate.^{1,2}

Other researchers have studied the decomposition pathways of xanthates. Montalti *et al.*³ investigated the adsorption of ethyl xanthate on pyrite using UV-Vis spectroscopy to detect the species left in solution after adsorption occurred. Based on the absorption spectra, they concluded that ethyl perxanthate and ethyl dixanthogen were the main species generated under acidic conditions and ethyl monothiocarbonate under basic conditions. They also reported that under the

conditions studied dixanthogen was the species adsorbed on the pyrite surface. The reaction occurring depends on time and pH.

HPLC techniques to identify xanthate mixtures were developed¹⁰ in the 1970's. In later investigations, HPLC was also used to study dixanthogen species with long alkyl chains.¹¹

None of the papers referred to above presents very convincing evidence for the nature of the adsorbed species or for the mechanisms involved in oxidation and oxygenation of xanthates. However, it is clear that interconversion of species is promoted by mineral surfaces and it is likely that such reactions will be observed when contacting xanthates with goethite because oxidized pyrite has been shown³ to promote reactions.

3.2. SURFACE BINDING STUDIES BY ADSORPTION ISOTHERMS

The first attempts to measure the concentration remaining in solution of potassium ethyl xanthate, **3**, were made by ICP-OES. These analyses presented problems because the ligand or its decomposition products containing sulfur are retained by the plastic tubes used to deliver the solution to the nebulizer. This led to low determined values of initial samples and desorption over time led to artificially high determined values in subsequent samples. An attempt was made to use HNO₃ (5%) to clean the tubing between samples but did not lead to successful results as the sulfur-containing products continued being retained by the tubing.

UV-Vis spectroscopy was chosen as an alternative to determine the concentration of ligand **3** in solution. The Beer-Lambert Law (Section 1.9) and the background correction factor were applied as described in Section 2.2 to determine the concentration of ligand left in solution after an adsorption isotherm. Data are

listed in Table 3.3. The extinction coefficient value determined compares favourably with the ones found in literature.^{2, 3, 8, 12}

Ligand	Wavelength (nm)	Extinction coefficient ($l \text{ mol}^{-1} \text{ cm}^{-1}$)	Background correction factor
3	301	17583	0.151

Table 3.3. Extinction coefficient data and background correction factor for **3** determined in methanol/water (95:5 v/v) at room temperature.

Preliminary attempts to determine the adsorption isotherms for ligand **3** are shown in Figure 3.4. It was not possible to fit this adsorption isotherm on goethite using conventional methods. It does not pass through the coordinate origin even when the correction factor was applied and consequently, values of binding constant and surface coverage cannot be obtained to compare with other ligands. However, the data displayed in Figure 3.4 clearly suggest that either xanthate or a derivative/decomposition product are taken up by the goethite. In contrast very little uptake is observed on silica.

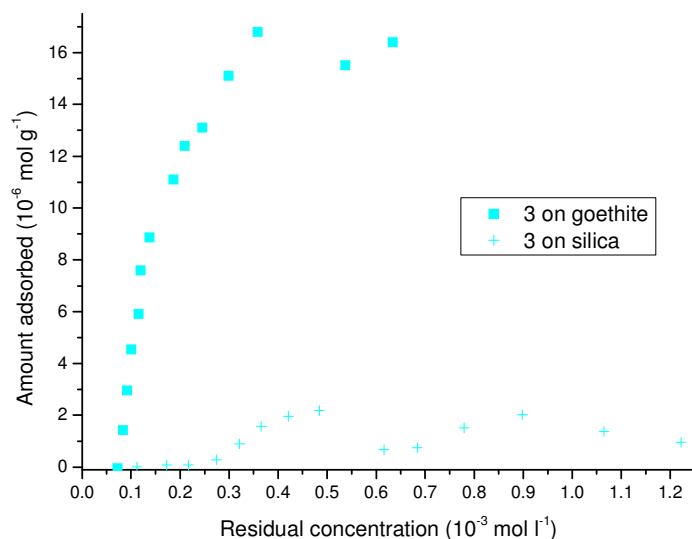


Figure 3.4. Adsorption isotherms of **3** on goethite and silica in methanol/water (95:5 v/v) at 25°C.

The instability of potassium ethyl xanthate in solution (Section 3.1.3) and decomposition to give various derivatives,^{1, 7, 13-15} will complicate attempts to determine adsorption isotherms by using UV-Vis spectra to monitor uptake. The main products are CS₂, ethyl perxanthate, diethyl dixanthogen and ethyl monothiocarbonate which show absorption peaks at 210 nm;⁹ 301, 348 nm;^{2, 13, 15} 238, 288 nm;^{3, 13, 15} and 221 nm^{3, 15} respectively. As a consequence of this decomposition, the interaction between the ligand and the mineral will also be dependent on time and pH, and the decrease in the intensity of the ethyl xanthate peak at 301 nm will not necessarily correspond to the amount adsorbed.

In light of these concerns some experiments were carried out to establish the reactivity of potassium ethyl xanthate under conditions similar to those used in this thesis for isotherm determination. It was found that when UV-Vis measurements were compared for the same sample containing potassium ethyl xanthate, a decrease in absorbance value at 301 nm and an increase in absorbance in the region of 226 nm with time occurred (Table 3.5). These data suggested the formation of other species in solution in methanol/water (95:5 v/v).

Time/h	Abs (potassium ethyl xanthate 7.5 x 10 ⁻³ M)		
	206 nm	226 nm	301 nm
0	-	0.323	0.527
1.40	0.371	0.315	0.501
4.40	0.540	0.315	0.464
8.40	0.533	0.344	0.466

Table 3.5. Time dependence of UV-Vis spectroscopy of ethyl xanthate, **3**, in methanol/water (95:5 v/v) at room temperature.

The half-life of xanthate in aqueous media was reported⁹ to be greater in basic solutions, showing two maximum ranges of half-life at the pH range 7 – 8 and at pH 12. A rapid decomposition of xanthate was observed between pH 9 - 10. The reason for this behaviour is unknown. In this work we looked at the behaviour in

methanol/water (95:5 v/v) to determine whether would be possible to stabilize the xanthate solution for a period of time long enough that would allow us to run adsorption isotherms. These experiments showed that the addition of alkali (potassium hydroxide) to a potassium ethyl xanthate solution stabilizes it for around 1.40 hours (Table 3.6) which is not long enough for the purpose of this study.

Time/h	Abs (potassium ethyl xanthate 7.5×10^{-3} M + KOH 1.6×10^{-3} M)		
	206 nm	226 nm	301 nm
0	-	0.338	0.547
1.40	-	0.341	0.541
4.40	0.356	0.323	0.518
8.40	0.414	0.354	0.523
24	1.068	-	0.312

Table 3.6. Time dependence of UV-Vis spectra of potassium ethyl xanthate, **3**, with addition of alkali in methanol/water (95:5 v/v) at room temperature.

Attempts to reverse the decomposition process by addition of potassium hydroxide to the supernatant solutions obtained after the adsorption on goethite was not successful. No significant change in the adsorption peak at 301 nm was observed (Table 3.7) indicating it is not possible to convert the materials in solution back to potassium ethyl xanthate after the decomposition process is completed, as Iwasaki *et al.*⁷ had reported.

V_{KOH}/ml added	Abs (potassium ethyl xanthate $7.0 \times 10^{-4} \text{ M}$)		
	206 nm	226 nm	301 nm
0	0.800	0.692	0.417
1	0.900	0.773	0.499
3	0.800	0.707	0.418
Excess	0.200	0.750	0.518

Table 3.7. UV-Vis spectra of potassium ethyl xanthate, **3**, with addition of alkali after adsorption process in methanol/water (95:5 v/v) at room temperature.

Another possibility in these experiments is that oxidation by atmospheric oxygen occurs, although this is unlikely to occur as it has been reported that such reactions are very slow.^{7, 12}

3.3. CONCLUSIONS

One interpretation of isotherm experiments carried out in this chapter is that xanthate binds fairly strongly to goethite surfaces. However, this observation is based on the disappearance of the absorption band at 301 nm which is characteristic of xanthate in solution. If the xanthate ion were converted to another species in solution which fails to absorb at 301 nm, it is possible that very high uptake at the goethite surface is occurring. Evidence in the literature, largely with aqueous rather than methanolic solutions is consistent with conversion of xanthates to other species but it is generally assumed that these are surface active and become attached to mineral surfaces. If this is the case, it is curious that xanthates appear to be ineffective as collectors for some of the “oxidized” minerals of interest to Rio Tinto. It is possible that the degradation products fail to generate surfaces with a level of hydrophobicity which is useful for flotation. This, however, is mere speculation and is not directly relevant to this thesis in which we aim to identify co-collectors which do address the oxidized surfaces and when used in conjunction with conventional collectors will give good recovery of partially oxidized minerals. Candidate surface ligands to meet this criterion are discussed within following chapters.

3.4. EXPERIMENTAL

3.4.1. INSTRUMENTATION

General information for instrumentation used for UV-Vis spectroscopy is provided in Section 2.5.1. Inductively coupled plasma optical emission spectroscopy (ICP-OES) analysis measurements were obtained on aqueous samples using a Thermo Jarrell Ash IRIS ICP-OES. Data was processed using the software programme, WinLab32 for ICP-OES, version 3.0.0.0103, 2004.

3.4.2. SOLVENTS AND REAGENTS

General information on solvents and reagents used is given in Section 2.5.2.

3.4.3. LIGAND

3 was supplied by Aldrich and was used as received.

3.4.4. EXTINCTION COEFFICIENT (ϵ) DETERMINATION

Procedure described in Section 2.5.4.

3.4.5. ADSORPTION ISOTHERM MEASUREMENTS

Adsorption isotherms were performed following the procedure described in Section 2.5.5. The concentration of ligand in the supernatant solutions was analysed using both UV-Vis spectroscopy and by ICP-OES. To use ICP-OES the solvent of the filtered solutions was removed *in vacuo* and these solutions were made up to the equivalent volume with water. Calibration standards were made up by weight and the

instrument was calibrated using 1, 15, 40, 70 and 100 ppm sulfur solutions. Data gathered was processed as explained in Section 2.5.5.

3.5. REFERENCES

- ¹ E. Silvester and F. P. Hao, *Publications of the Australasian Institute of Mining and Metallurgy*, 2002, **4/2002**, 259.
- ² E. Silvester, D. Truccolo, and F. P. Hao, *Journal of the Chemical Society, Perkin Transactions 2*, 2002, 1562.
- ³ M. Montalti, D. Fornasiero, and J. Ralston, *Journal of Colloid and Interface Science*, 1991, **143**, 440.
- ⁴ F. P. Hao, E. Silvester, and G. D. Senior, *Analytical Chemistry*, 2000, **72**, 4836.
- ⁵ Cytec Industries, 'Mining Chemicals Handbook', 2002.
- ⁶ R. R. Klimpel, 'A Review of Sulfide Mineral Collector Practice'.
- ⁷ I. Iwasaki and S. R. B. Cooke, *Journal of the American Chemical Society*, 1958, **80**, 285.
- ⁸ E. Klein, J. K. Bosarge, and I. Norman, *Journal of Physical Chemistry*, 1960, **64**, 1666.
- ⁹ Z. Sun and W. Forsling, *Minerals Engineering*, 1997, **10**, 389.
- ¹⁰ R. A. Hasty, *Analyst*, 1977, **102**, 519.
- ¹¹ C. Zhou, A. Bahr, and G. Schwedt, *Fresenius' Journal of Analytical Chemistry*, 1990, **338**, 908.
- ¹² R. N. Tipman and J. Leja, *Colloid and Polymer Science*, 1975, **253**, 4.
- ¹³ S. R. Grano, C. A. Prestidge, and J. Ralston, *International Journal of Mineral Processing*, 1997, **52**, 161.
- ¹⁴ S. R. Grano, N. W. Johnson, and J. Ralston, *Minerals Engineering*, 1997, **10**, 17.
- ¹⁵ S. R. Grano, C. A. Prestidge, and J. Ralston, *International Journal of Mineral Processing*, 1997, **52**, 1.

Chapter

4

Surface binding studies of 2-mercaptobenzothiazole

CONTENTS

4.1. Introduction	67
4.1.1. Outline.....	67
4.1.2. Coordination chemisty of 2-mercaptobenzothiazole with copper	67
4.1.3. Coordination chemistry of 2-mercaptobenzothiazole with nickel	72
4.1.4. Copper(I).....	74
4.1.5. Copper(II).....	75
4.1.6. Nickel(II).....	75
4.2. Surface binding studies by adsorption isotherms.....	76
4.3. Investigating the mode of surface binding of 2-mercaptobenzothiazole (4)... 78	
4.3.1. Attempts to synthesise copper(I) polynuclear complexes with ligand 4 . 78	
4.3.2. Attempts to synthesise polynuclear complexes with ligand 4 and Ni(II) or Zn(II)	80
4.3.3. X-ray crystal structure of $[\text{Ni}_2(\mu_2\text{-mbt})_4]$ (4a).....	81
4.4. Conclusions	86
4.5. Experimental	86
4.5.1. Instrumentation	86
4.5.2. Solvents and reagents.....	87
4.5.3. Ligand	87
4.5.4. Extinction coefficient (ϵ) determination	87
4.5.5. Adsorption isotherm measurements.....	87
4.5.6. Attempted synthesis of the complex $[\text{Cu}_{x+y}(\text{hfac})_x(\text{mbt})_y]$	87
4.5.7. Synthesis of the complex $[\text{Ni}_2(\mu_2\text{-mbt})_4]$ (4a).....	89
4.6. References	90

4.1. INTRODUCTION

4.1.1. OUTLINE

This chapter concerns the surface binding properties of 2-mercaptobenzothiazole, ligand **4**, (Figure 4.1). It was also hoped that the structures of some polynuclear copper(I) or metal(II) structures could be determined to clarify its mode of action as a collector for sulfide minerals, recognizing that adsorption studies on high surface area sulfides could not be carried out (see Section 1.11).

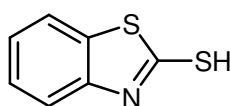


Figure 4.1. Structure of ligand **4**, 2-mercaptobenzothiazole, mbtH.

4.1.2. COORDINATION CHEMISTRY OF 2-MERCAPTOBENZOTHIAZOLE WITH COPPER

2-Mercaptobenzothiazole, also known as benzo-1,3-thiazole-2-thione, and its derivatives are used in processes of vulcanization of rubber.¹ It is also used as a corrosion inhibitor of copper^{1, 2} and as a flotation agent.³ In the solid state 2-mercaptobenzothiazole exists as the thione tautomer rather than the thiol form (Figure 4.2).

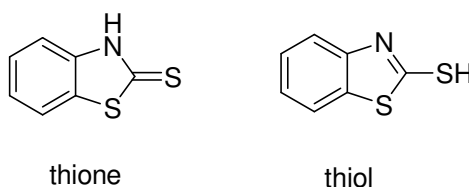


Figure 4.2. Tautomers of ligand **4**, 2-mercaptobenzothiazole.^{4, 5}

The most common ^{1, 2, 6-10} oxidation state of copper in complexes with heterocyclic thiones as ligands is +1. The number of donor atoms that 2-mercaptobenzothiazole uses when reacting with copper is 1; the coordination sphere of copper in the complexes reported in literature^{1, 2, 6-10} has always the exocyclic sulfur atom as a donor in a terminal or bridging mode. No cases in which the endocyclic sulfur atom or the nitrogen are coordinated to the copper have been reported. Usually the coordination sphere is completed by phosphines or halogen atoms. In summary, the known structures of complexes of heterocyclic thiones with copper are monomers,^{6, 7, 9} S-bridged dimers,¹⁰ halogen-bridged dimers⁸ or phosphine-bridged dimers.¹ Some representative structures are discussed below.

In all the complexes reported in literature, the copper atoms have a distorted tetrahedral geometry. As has been said above, 2-mercaptobenzothiazole adopts a monodentate coordination mode in all cases. The only case that has been reported in which it coordinates to copper also through the nitrogen atom is an oxidized form of the ligand 2-mercaptobenzothiazole in which an additional sulfur atom has been inserted (Figure 4.3).² This new central sulfur atom and the nitrogen atom are coordinated to the metal.

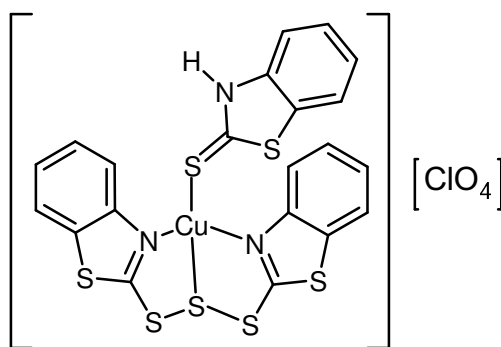


Figure 4.3. Structure of a copper(I)-mercaptobenzothiazole complex containing a ligand generated by an unusual sulfur insertion.²

The crystal structure of $[\text{Cu}_2(\text{mbt})_2(\text{dppe})_3]$,¹ dppe = 1,2-bis(diphenylphosphino)ethane, is a dimer with a bridging dppe ligand (Figure 4.4). The distorted tetrahedral coordination sphere of each copper atom is completed by a

chelating dppe ligand and an anionic 2-mercaptobenzothiazole ligand binding through the exocyclic sulfur atom.

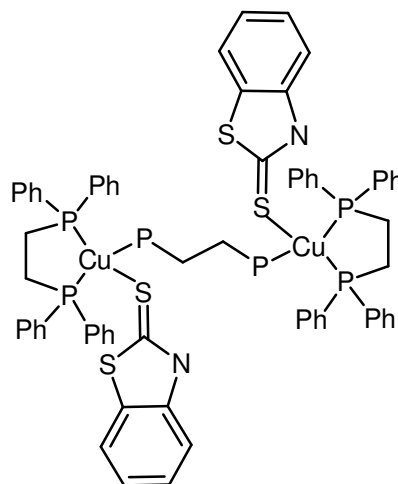


Figure 4.4. Structure of $[\text{Cu}_2(\text{mbt})_2(\text{dppe})_3]$.¹

Another example⁶ of a mixed mbtH/phosphine system is the material claimed to be $\{[\text{Cu}(\text{PPh}_3)_2(\text{mbtH})\text{Cl}][\text{Cu}(\text{PPh}_3)_2(\text{mbtH})_2]\}$ (Figure 4.5). The $[\text{Cu}(\text{PPh}_3)_2(\text{mbtH})\text{Cl}]$ complex has a distorted tetrahedral geometry, in this case with two phosphorus, one sulfur atom and one chloride ion bonded to the copper(I) atom (Molecule **b** in Figure 4.5).

In their description of the structure containing $[\text{Cu}(\text{PPh}_3)_2(\text{mbtH})_2]$ (Molecule **a** in Figure 4.5), the authors imply that the complex contains a zero valent Cu atom. In the CSD data the mbt units are deprotonated which implies that the complex contains a divalent Cu atom which is unlikely to give the tetrahedral geometry and it is highly probable that one of the mbt ligands is in fact protonated as $[\text{Cu}(\text{PPh}_3)_2(\text{mbt})(\text{mbtH})]$.

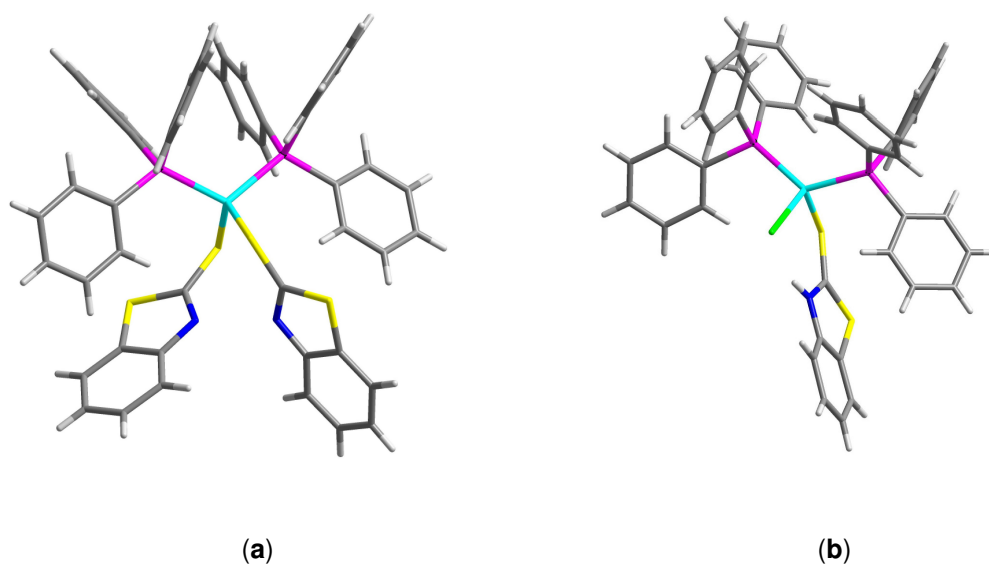


Figure 4.5. Crystal structure of $\{[\text{Cu}(\text{PPh}_3)_2(\text{mbtH})\text{Cl}][\text{Cu}(\text{PPh}_3)_2(\text{mbtH})_2]\}$.⁶

Intramolecular hydrogen bonding is observed⁷⁻⁹ in some cases between halogen atoms and the heterocyclic nitrogen atoms as discussed below.

Cox *et al.*⁷ describe the crystal structure of $[\text{CuI}(\text{PPh}_3)_2(\text{mbtH})]$ (Figure 4.6). It is a mononuclear tetrahedral complex with a $\text{P}_2\text{S}\Gamma$ donor set. Hydrogen bonding is observed between the NH group and the iodide ion.

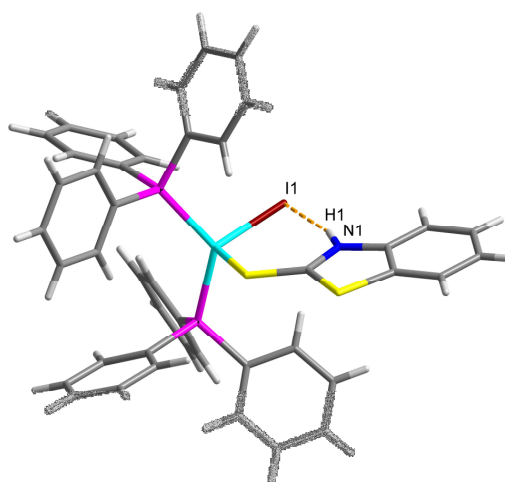


Figure 4.6. Structure of the copper(I)-mercaptobenzothiazole complex $[\text{CuI}(\text{PPh}_3)_2(\text{mbtH})]$.⁷

A similar structure, $[\text{CuCl}(\text{PPh}_3)_2(\text{mbtH})]\text{CH}_3\text{COCH}_3$, with an intramolecular hydrogen bond between the chloride ion and the NH group was reported by Voutsas *et al.*⁹

In the chloro-bridged dinuclear structure $[\text{Cu}_2\text{Cl}_2(\text{PPh}_3)_2(\text{mbtH})_2]$ hydrogen bonds are formed between heterocyclic NH atoms and the bridging chloride ions (Figure 4.7).⁸

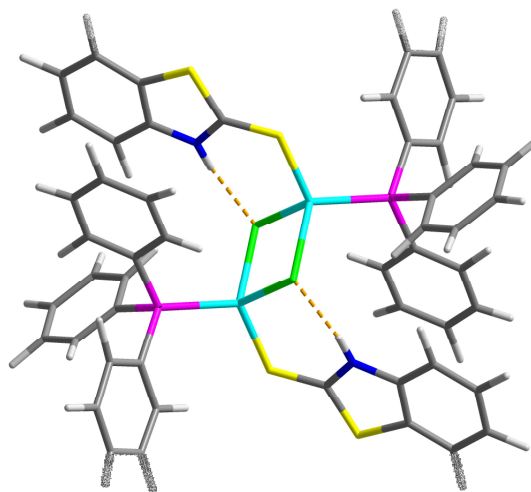


Figure 4.7. Structure of the 2-mercaptobenzothiazole dimer with chloride bridges, $[\text{Cu}_2\text{Cl}_2(\text{PPh}_3)_2(\text{mbtH})_2]$.⁸

The crystal structure¹⁰ of $[\text{Cu}(\text{PPh}_3)(\text{mbtH})\text{Br}]_2$ contains a planar Cu_2S_2 moiety and the copper atoms have a distorted tetrahedral geometry (Figure 4.8). The 2-mercaptobenzothiazole ligands are monodentate, where the sulfur atoms bridge two copper atoms. Two other positions of the tetrahedron are occupied by phosphorus of PPh_3 and bromine atoms.

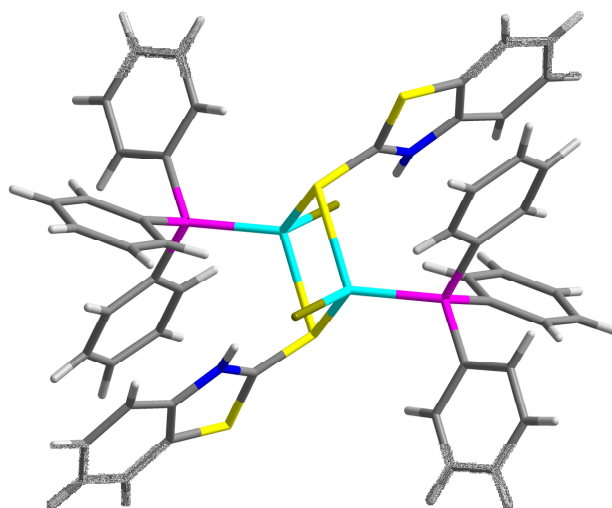


Figure 4.8. Structure of $[\text{Cu}(\text{PPh}_3)(\text{mbtH})\text{Br}]_2$.¹⁰

4.1.3. COORDINATION CHEMISTRY OF 2-MERCAPTOBENZOTHIAZOLE WITH NICKEL

In metal(II) complexes, 2-mercaptobenzothiazole usually coordinates in a bidentate mode through the exocyclic sulfur atom and the nitrogen atom and three X-ray structures showing these features have been reported in the CSD.^{4, 5, 11}

As an example, in $[\text{Ni}(\text{mbt})_2(\text{dmp})]$,⁴ dmp = 2,9-dimethyl-1,10-phenanthroline, two 2-mercaptobenzothiazolate ligands coordinate in a bidentate manner a nickel(II) ion with *pseudo*-octahedral geometry, is displayed in Figure 4.9.

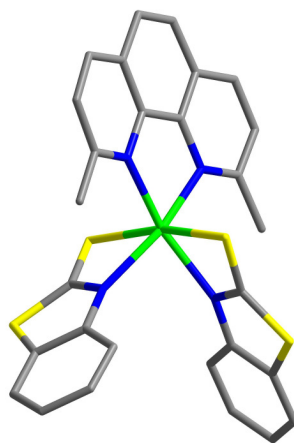


Figure 4.9. Structure of $[\text{Ni}(\text{mbt})_2(\text{dmp})]$.⁴

Recently, Jian *et al.*¹¹ reported the first series of clusters containing 2-mercaptobenzothiazole in which the ligand uses the nitrogen atom and the exocyclic sulfur to coordinate to two different metal(II) ions, these being two Fe, two Co or two Ni atoms. The three complexes have analogous geometries and all the metal(II) ions show distorted tetrahedral environment (Figure 4.10). The four metal ions form a tetrahedral structure with a tetracoordinated O^{2-} in the centre of the tetrahedron as depicted in Figure 4.11.

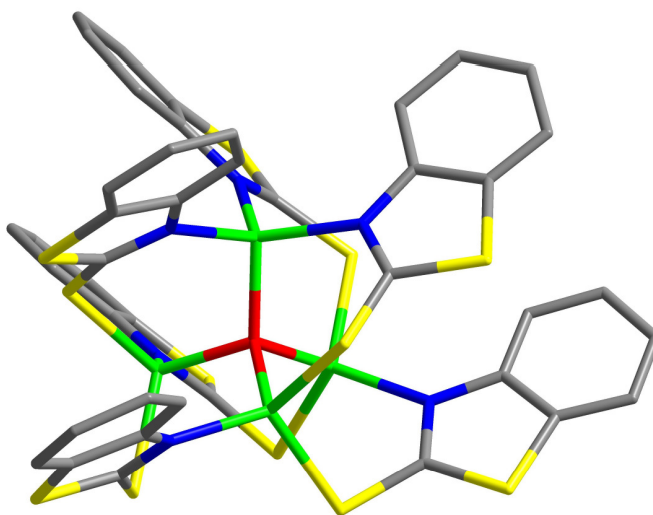


Figure 4.10. X-ray structure of $[\text{M}_4\text{O}(\text{mbt})_6]$, $\text{M} = \text{Fe}, \text{Co}, \text{Ni}$.¹¹

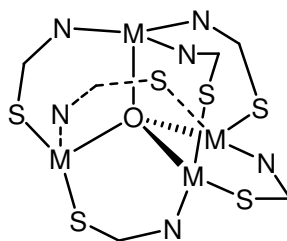


Figure 4.11. Core of the structure $[M_4O(mbt)_6]$, $M = Fe, Co, Ni$.

4.1.4. COPPER(I)

In ionic forms copper exists mainly in the 1+ and 2+ oxidation states. The electronic configuration of the copper(I) ion is $[Ar]3d^{10}$ and it forms diamagnetic compounds.¹² In the absence of stabilizing ligands the copper(I) ion is very unstable with respect to disproportionation in aqueous solution. It can be stabilized by complexing it with ligands having π -acceptor character. The stability of different valence states of copper is given by the following standard reduction potentials:^{12, 13}



$$E^0 (Cu^+/Cu) = +0.52 V$$

$$E^0 (Cu^{2+}/Cu) = +0.34 V$$

$$E^0 (Cu^{2+}/Cu^+) = +0.15 V$$

As observed above, the most common geometry for copper(I) is tetrahedral although some linear and trigonal planar compounds have been reported.¹² It is categorised as a soft metal ion.

4.1.5. COPPER(II)

The copper(II) ion has electronic configuration $[\text{Ar}]3d^9$ and generally forms green or blue paramagnetic compounds.¹² This is the most abundant oxidation state for copper and it usually forms water-soluble salts. The most common coordination numbers 4, 5 and 6, tend to have either a square-planar, a square-pyramidal or tetragonally distorted octahedral configuration. This is because of the Jahn-Teller effect, where an ion in a degenerate electronic state will be unstable and will undergo a geometrical distortion by elongation of metal-ligand bonds in the z -direction and compression in the x - and y -direction to remove degeneracy and achieve a lower energy. The stabilizing influence of the Jahn-Teller distortion lowers the ligand field stabilization energy compared to the pure octahedral ligand field and increases the value of the formation constants, explaining why copper(II) complexes have the largest formation constants of all the divalent cations in the first row of the transition metals given by the Irving-Williams series. Copper(II) is classified as a borderline hard acid.

4.1.6. NICKEL(II)

The most stable oxidation state for nickel is the divalent ion Ni^{2+} and its chemistry is very extensive. Its electronic configuration is $[\text{Ar}]3d^8$. The most frequent coordination numbers of nickel(II) are 4 and 6, whose configurations are square-planar and octahedral, respectively. A small number of complexes of nickel(II) with tetrahedral, bipyramidal and square pyramidal geometries are known as well.¹²

- Square-planar complexes of nickel(II) are very abundant due to the splitting of the orbitals according to the CFSE theory.¹² They are diamagnetic and normally red to yellow. $[\text{Ni}(\text{CN})_4]^{2-}$ is an example.

- Octahedral complexes of nickel(II) are typically form with neutral *N*-donor ligands such as NH₃, en, bipy, NCS⁻, NO₂⁻ and DMSO. They are paramagnetic and green to blue, in general.
- Tetrahedral complexes of nickel(II) are less common. These complexes are blue and paramagnetic, having two unpaired electrons. Some examples are this type of compounds [NiL₂X₂] (L = PR₃, AsR₃, OPR₃, OAsR₃, X = Cl, Br, I).

4.2. SURFACE BINDING STUDIES BY ADSORPTION ISOTHERMS

2-Mercaptobenzothiazole, **4**, was selected as a model of sulfide mineral collector due to the difficulties in the determination of adsorption isotherms with potassium ethyl xanthate, **3**, which is described in Chapter 3. The binding of **4** to goethite and silica is investigated in this chapter. The wavelength and extinction coefficients used to determine the concentration of **4** left in solution after an adsorption isotherm experiment by UV-Vis spectroscopy (see Section 2.5.4) were worked out using the Beer-Lambert Law (Section 1.9). A background correction factor (see Section 2.2) was applied when determining the concentration of ligand remaining in solution. Data are listed in Table 4.12.

Ligand	Wavelength (nm)	Extinction coefficient (l mol ⁻¹ cm ⁻¹)	Background correction factor
4	237, 321 ^a	14922, 26586 ^a	0.086 (at 321 nm)

Table 4.12. Extinction coefficient data and background correction factor for **4** determined in methanol/water (95:5 v/v) at room temperature.

^aWavelength used in the adsorption isotherm determination.

The adsorption isotherms of **4** on goethite and silica are shown in Figure 4.13 and Table 4.14. It shows weak binding to goethite, as expected, since **4** is a ligand with soft atoms in its head group that do not tend to bind to the hard iron(III) atoms found on the goethite surface. It reaches a surface coverage of $3.5 \times 10^{-6} \text{ mol g}^{-1}$. The binding to silica is weak, as expected and will help to ensure separation of sulfidic from oxidic minerals in flotation.

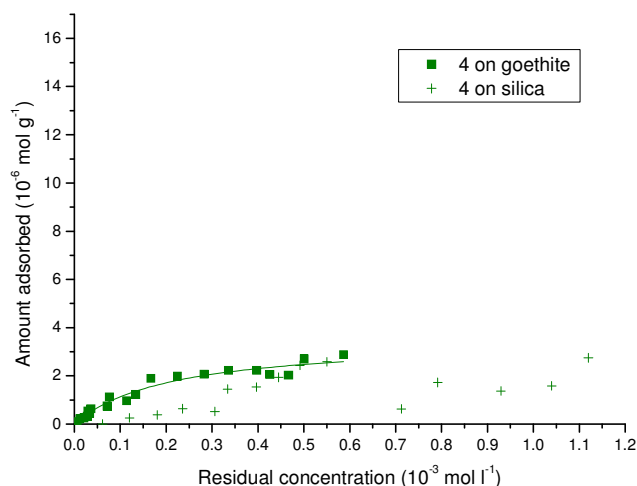


Figure 4.13. Adsorption isotherms of ligand **4** on goethite and silica in methanol/water (95:5 v/v) at 25°C.

Ligand	Equilibrium adsorption constant (K) 10^3	Surface coverage ($10^{-6} \text{ mol g}^{-1}$)	Required surface area ($\text{\AA}^2 \text{ molecule}^{-1}$)
4	4.7(10)	3.5(3)	1060(90)

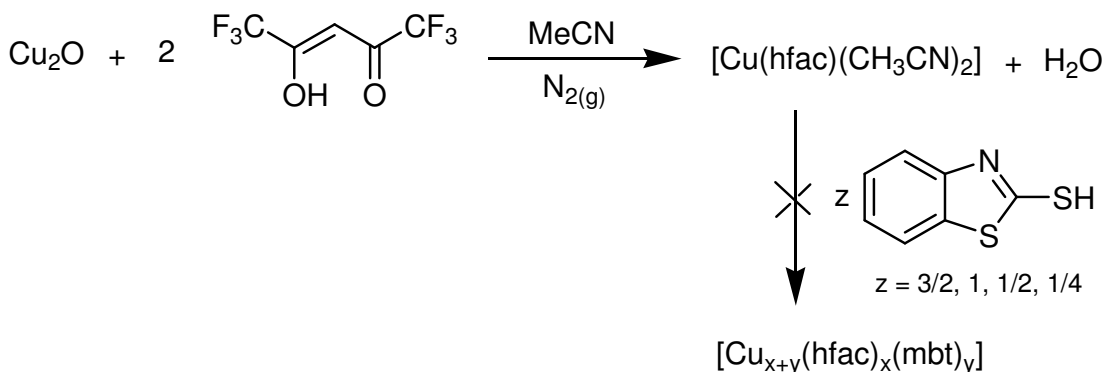
Table 4.14. Adsorption isotherm data for ligand **4** (errors in parentheses) on goethite. For definitions of K , surface coverage, required surface area and their determination see Section 1.6.1.

4.3. INVESTIGATING THE MODE OF SURFACE BINDING OF 2-MERCAPTOBENZOTHAZOLE (4)

It was expected to obtain polynuclear copper complexes containing 2-mercaptobenzothiazole, **4**, to provide information on the binding motif of such ligand to copper(I)-containing surfaces. Many attempts were made and finally one crystal containing a dinuclear nickel(II) complex bridged by four 2-mercaptobenzothiazolate units was grown.

4.3.1. ATTEMPTS TO SYNTHESISE COPPER(I) POLYNUCLEAR COMPLEXES WITH LIGAND **4**

The synthesis of polynuclear clusters with copper(I) was attempted using the approach shown in Scheme 4.15.



Scheme 4.15. General reaction scheme for the attempted preparation of $[\text{Cu}_{x+y}(\text{hfac})_x(\text{mbt})_y]$.

Such a scheme had proved successful in obtaining copper(I) alkyne clusters earlier at University of Edinburgh.¹⁴⁻¹⁸ Alkynyl ligands have a high tendency of forming aggregates and generate polymeric materials. However, in our group large clusters containing up to twenty six copper centres were characterized.¹⁸ Copper ions were contained in discs containing polynucleating ligands; such as alkynes which are orientated perpendicular to the faces of the disc. Anionic hfac^- ligands confer

stability to the system by “blocking” the rims of the cluster and that way preventing polymerization (Figure 4.16).

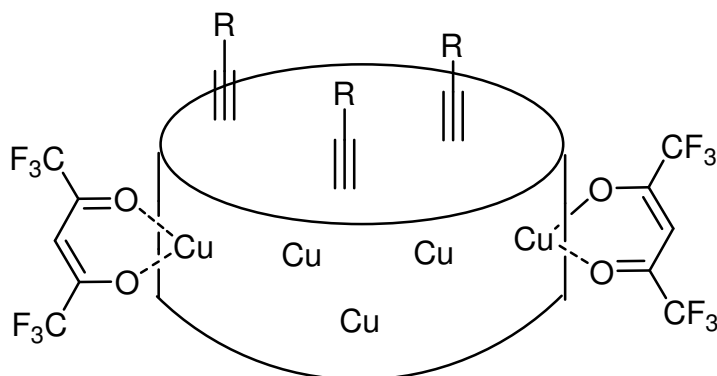


Figure 4.16. Schematic arrangement of $[\text{Cu}_{x+y}(\text{hfac})_x(\text{C}\equiv\text{CR})_y]$ clusters.

The largest cluster molecule of this series was $[\text{Cu}_{26}(\text{hfac})_{11}(1\text{-pentynyl})_{15}]$.¹⁸ It is a neutral cluster with a disc shape in which its 26 ligands are monoanionic and with 25 copper centres distributed in four concentric annuli as is shown in Figure 4.17. All the pentynyl ligands bridge copper atoms and are located in the faces of the disc and all the terminal anionic hfac⁻ ligands are distributed on the edge of the disc.

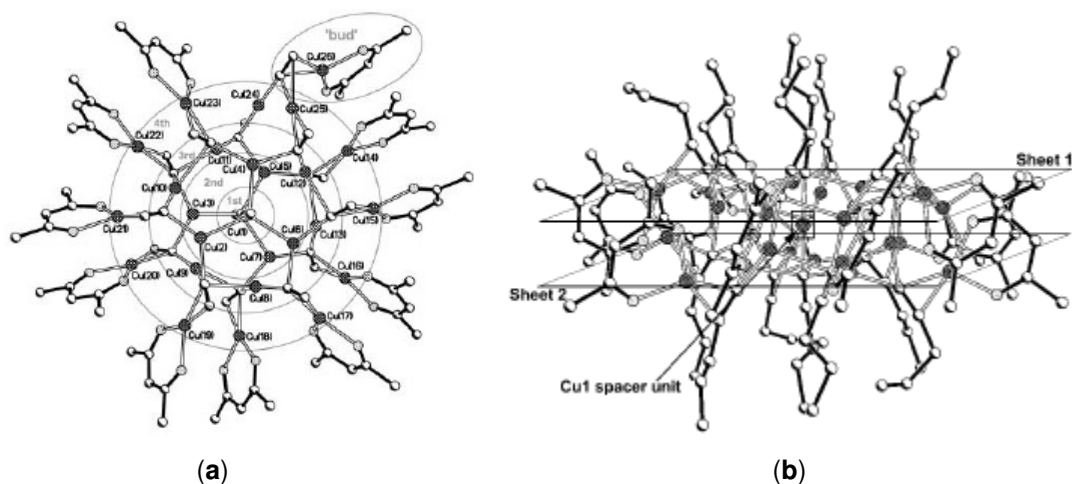


Figure 4.17. (a) Representation of the cluster $[\text{Cu}_{26}(\text{hfac})_{11}(1\text{-pentynyl})_{15}]$ and (b) its lateral view.¹⁸

In this project, we attempted to use 2-mercaptobenzothiazole as the polynucleating ligand. The fluorinated acacH derivative, hfacH, has a highly electron withdrawing effect due to the $-CF_3$ groups that decrease the hard character of the oxygen atoms, favouring binding of Cu(I) which it was hoped would also be bond to soft sulfur atom in 2-mercaptobenzothiazole.

Several attempts using different ratios of ligand **4** as well as variations in the methodology (see Section 4.5.6) were made. None of these experiments was successful. In all cases an insoluble and uncharacterizable material was obtained.

4.3.2. ATTEMPTS TO SYNTHESISE POLYNUCLEAR COMPLEXES WITH LIGAND 4 AND Ni(II) or Zn(II)

Consistent with the lack of success in characterising copper(I) polynuclear complexes of ligand **4** and because no structures of such polynuclear complexes were found in the Cambridge Crystallographic Data Base, it was thought that synthesis of complexes featuring other metals, such as nickel or zinc, might illustrate the binding modes of ligand **4** in surface complexes.

A total of 86 different reactions to grow clusters containing ligand **4** and either Ni(II) or Zn(II) salts were attempted. All were run at room temperature and using either methanol or acetonitrile as solvent. Different combinations of metal salts, bases, alcohol tripodal co-ligands such as 1,1,1-tris(hydroxymethyl)ethane, 1,1,1-tris(hydroxymethyl)propane, pentaerythritol and other co-ligands (carboxylates) were prepared. Only one crystalline complex, $[Ni_2(\mu_2\text{-mbt})_4]$, was obtained (see Section 4.3.3).

The infra-red spectrum of the free ligand shows a band at 3111 cm^{-1} corresponding to the $\nu(\text{NH})$ absorption. This and the absence of the $\nu(\text{SH})$ absorption band in the region of $2500\text{-}2600\text{ cm}^{-1}$ indicate that the free ligand is in its thione and not in the enethiol form.⁴⁻⁶

The $\nu(\text{NH})$ band at 3111 cm^{-1} is not present in the spectra of the complex as coordination through the nitrogen to the metal ion has happened. The band at 1399 cm^{-1} in the metal complex is shifted when compared to the one of the free ligand at 1595 cm^{-1} , indicating coordination through the nitrogen atom.¹¹ The band at 423 cm^{-1} in **4a** is assigned to the $\nu(\text{Ni}-\text{N})$.¹¹

4.3.3. X-RAY CRYSTAL STRUCTURE OF $[\text{Ni}_2(\mu_2\text{-mbt})_4]$ (**4a**)

Suitable crystals for X-ray crystallography were isolated by dissolving ligand **4** with $\text{Ni}(\text{OAc})_2 \cdot 4\text{H}_2\text{O}$, NaOOCCH_3 , tetrabutylammonium bromide and Et_3N in methanol. The structure of **4a** contains three crystallographically independent units of the complex. The complexes are dimers containing four bridging units of ligand **4** and two nickel(II) ions (Figure 4.18 and 4.19). The geometry around each of the nickel ions is *pseudo* square-planar with the sulfur atoms *trans* to each other around the metal, as well as the nitrogen atoms. Each of the 2-mercaptobenzothiazolate units is coordinated to the nickel ion through the exocyclic sulfur atom and the nitrogen atom.

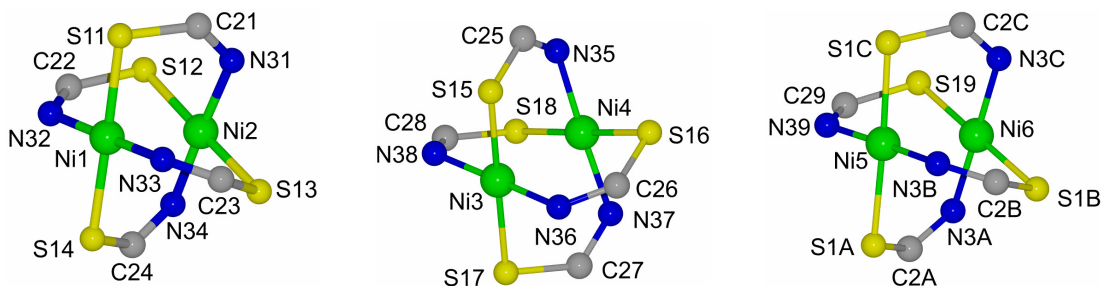


Figure 4.18. Core of the structures of the three crystallographically independent molecules of $[\text{Ni}_2(\mu_2\text{-mbt})_4]$ (**4a**) showing the atom labelling scheme used in tables (data are available in detail in the Appendix CD).

The two NiN_2S_2 coordination planes are twisted by approximately 19° relative to each other (Figure 4.19). The twist angles are shown in Table 4.20.

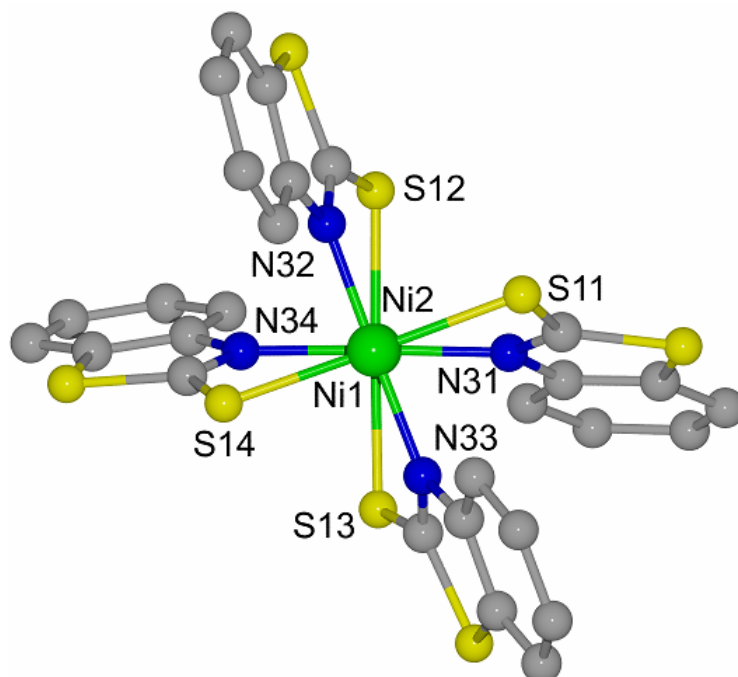


Figure 4.19. One of the three crystallographically independent molecules of $[\text{Ni}_2(\mu_2\text{-mbt})_4]$ viewed down the $\text{Ni}\cdots\text{Ni}$ axis.

Angles ($^\circ$) about $\text{Ni}(1)\cdots\text{Ni}(2)$ defined by			
S(11), N(31)	N(32), S(12)	S(14), N(34)	N(33), S(13)
21.70(9)	20.37(9)	18.99(9)	20.39(9)
Angles ($^\circ$) about $\text{Ni}(3)\cdots\text{Ni}(4)$ defined by			
S(15), N(35)	N(36), S(16)	S(17), N(37)	N(38), S(18)
19.74(10)	18.75(9)	19.23(9)	19.09(9)
Angles ($^\circ$) about $\text{Ni}(5)\cdots\text{Ni}(6)$ defined by			
N(39), S(19)	S(1A), N(3A)	N(3B), S(1B)	S(1C), N(3C)
18.20(10)	18.35(10)	18.15(10)	17.97(10)

Table 4.20. Twist angles between the coordination planes in the three units of $[\text{Ni}_2(\mu_2\text{-mbt})_4]$, as defined by torsion angles $\text{S} - \text{Ni}\cdots\text{Ni} - \text{N}$ ($^\circ$).

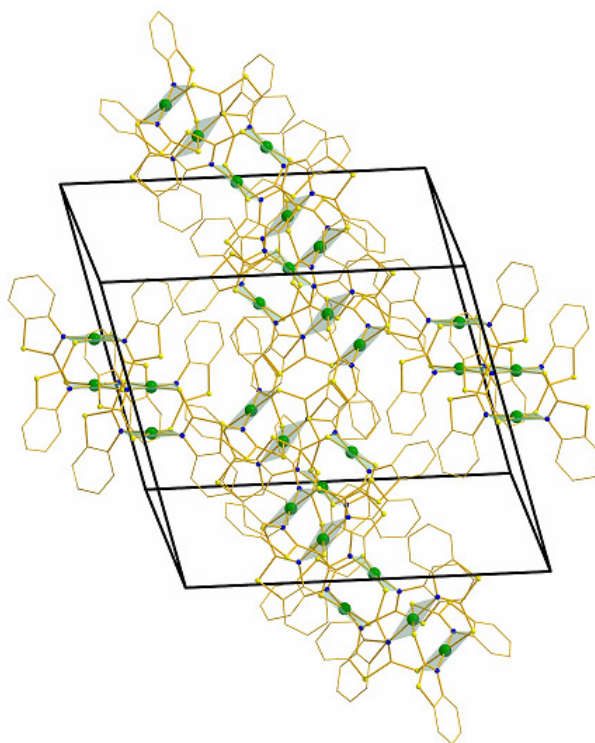


Figure 4.21. Crystal packing of $[\text{Ni}_2(\mu_2\text{-mbt})_4]\text{Et}_3\text{N}$ (**4a**). Colour code: Ni: green; S: yellow; N: blue.

The Ni - N bond lengths range from 1.881(3) to 1.895(3) Å and the Ni - S range from 2.2340(9) to 2.2403(10) Å (Table 4.22).

Bond lengths (Å) in the coordination spheres					
Ni(1)	Ni(2)	Ni(3)	Ni(4)	Ni(5)	Ni(6)
N(32)	N(31)	N(36)	N(35)	N(32)	N(31)
1.893(3)	1.881(3)	1.889(3)	1.889(3)	1.893(3)	1.881(3)
N(33)	N(34)	N(38)	N(37)	N(33)	N(34)
1.895(3)	1.895(3)	1.900(3)	1.894(3)	1.895(3)	1.895(3)
S(11)	S(12)	S(15)	S(16)	S(11)	S(12)
2.2340(9)	2.2358(11)	2.2156(11)	2.2286(9)	2.2340(9)	2.2358(11)
S(14)	S(13)	S(17)	S(18)	S(14)	S(13)
2.2363(9)	2.2403(10)	2.2447(10)	2.2369(10)	2.2363(9)	2.2403(10)

Table 4.22. Bond lengths (Å) (with estimated standard deviations in parentheses) in the inner coordination spheres of $[\text{Ni}_2(\mu_2\text{-mbt})_4]$ (**4a**).

The bond angles are all close to 90° or 180° (Table 4.23), with values ranging from 87.79(9) to 91.82(9) and from 176.95(4) to 179.00(4).

Bond angles (°) in the coordination spheres					
Ni(1)	Ni(2)	Ni(3)	Ni(4)	Ni(5)	Ni(6)
N(32), N(33) 178.41(13)	N(31), N(34) 177.64(13)	N(36), N(38) 178.42(13)	N(35), N(37) 177.66(13)	N(3B), N(39) 178.45(14)	N(3A), N(3C) 178.46(13)
N(32), S(11) 89.80(9)	N(31), S(12) 91.13(9)	N(36), S(15) 88.33(9)	N(35), S(16) 89.32(9)	N(3B), S(1A) 89.79(10)	N(3A), S(1B) 89.87(9)
N(32), S(14) 89.28(9)	N(31), S(13) 87.79(9)	N(36), S(17) 89.07(9)	N(35), S(18) 90.46(9)	N(3B), S(1C) 91.43(10)	N(3A), S(19) 89.13(9)
N(33), S(11) 89.10(9)	N(34), S(12) 90.68(9)	N(38), S(15) 91.12(9)	N(37), S(18) 91.59(9)	N(39), S(1A) 89.18(10)	N(3C), S(1B) 91.62(10)
N(33), S(14) 91.82(9)	N(34), S(13) 90.39(9)	N(38), S(17) 91.43(9)	N(37), S(16) 88.61(9)	N(39), S(1C) 89.56(10)	N(3C), S(19) 89.37(10)
S(11), S(14) 179.00(4)	S(12), S(13) 178.83(4)	S(15), S(17) 176.95(4)	S(16), S(18) 178.59(4)	S(1A), S(1C) 177.49(5)	S(1B), S(19) 177.75(5)

Table 4.23. Bond angles (°) (with estimated standard deviations in parentheses) in the inner coordination spheres of $[\text{Ni}_2(\mu_2\text{-mbt})_4]$ (**4a**).

Ni···Ni distance (Å)		
Ni(1)···Ni(2)	Ni(3)···Ni(4)	Ni(5)···Ni(6)
2.5639(6)	2.5586(6)	2.5678(7)

Table 4.24. Ni···Ni distance (Å) (with estimated standard deviations in parentheses) in the three units of $[\text{Ni}_2(\mu_2\text{-mbt})_4]$ (**4a**).

It is of interest to consider whether the Ni···Ni separations in the $[\text{Ni}_2(\mu_2\text{-mbt})_4]$ complexes provide support for models for how mbt^- could bind to the surfaces of sulfidic minerals. It appears that these *nickel* complexes do not provide a good model because the $[\text{Ni}_2(\mu_2\text{-mbt})_4]$ units have the feature that the mbt^- ligands define square-planar geometries at the two metal centres and consequently (Figure 4.25 (i)) the N – Ni – N, S – Ni – S bond angles are close to 180°. In such an arrangement the

Ni \cdots Ni separation will be similar to the N \cdots S distance in a mbt $^-$ unit. When bringing two metals with tetrahedral geometries such as Cu(I) or Fe(II) in chalcopyrite, the preferred N – M – N or S – M – S angles at the metal centres will be *ca.* 109° (Figure 4.25 (ii)) and much longer M \cdots M separations are expected. This was found to be the case when the CSD was mined for data for structures containing the moiety depicted in Figure 4.26 when the TM \cdots TM distance was found to be *ca.* 3.20 Å. For instance, in the metal(II) clusters described in Section 4.1.3 the Fe(II) or Ni(II) ions are disposed in a tetrahedral geometry where the M – M distance is 3.209 and 3.207 Å, respectively.¹¹

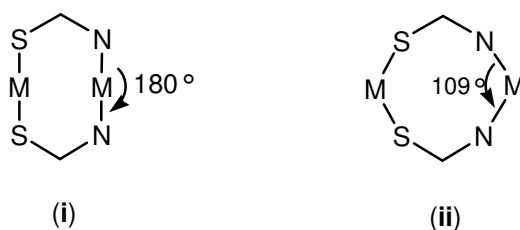


Figure 4.25. (i) Bis square-planar geometry showing N – M – N or S – M – S bond angles close to 180° and (ii) bis tetrahedral geometry showing N – M – N or S – M – S bond angles close to 109°.

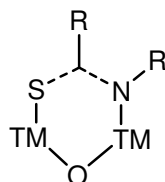


Figure 4.26. A fragment searched on CSD representing a possible moiety of mbt $^-$ on a metal oxide surface, where TM represents any transition metal.

The Fe \cdots Fe distance, 3.024 Å, in the goethite models discussed earlier (Section 2.1.4) is considerably shorter than this whilst typical M \cdots M separations in chalcopyrite like minerals are considerably longer and range between 3.713 and 3.740 Å.

This indicates that a possible binding mode of **4** to both sulfidic and oxidized surfaces may be through the nitrogen atom and the exocyclic sulphur to two different metal centres as illustrated in Figure 4.27.

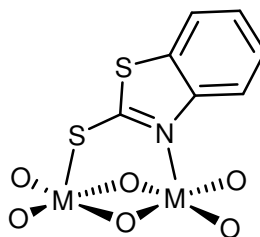


Figure 4.27. Possible binding mode of **4** on sulfidic or oxidized surfaces.

4.4. CONCLUSIONS

The work described in this chapter indicates weak binding of ligand **4** to goethite as well as to silica. The latter is consistent with **4** giving a good separation of the sulfidic minerals of interest from the siliceous gangue. X-ray structure of the complex **4a** and data from CSD show that multisite attachment of **4** to both chalcopyrite and goethite surfaces is possible through the nitrogen atom and the exocyclic sulfur to two different metal centres.

4.5. EXPERIMENTAL

4.5.1. INSTRUMENTATION

Refer to Section 2.5.1 for general instrumentation. Infra-red (IR) spectra were recorded on a JABCO FT/IR-410 spectrometer using potassium bromide discs.

4.5.2. SOLVENTS AND REAGENTS

For general information on solvents and reagents, refer to Section 2.5.2. All commercially available materials were used as received from Aldrich, Fluka, Acros, Lancaster and Fisher.

4.5.3. LIGAND

4 was obtained from Aldrich and was used as received.

4.5.4. EXTINCTION COEFFICIENT (ϵ) DETERMINATION

The extinction coefficient determination is explained in Section 2.5.4.

4.5.5. ADSORPTION ISOTHERM MEASUREMENTS

Adsorption isotherms using UV-Vis spectroscopy were carried out according to the procedure described in Section 2.5.5.

4.5.6. ATTEMPTED SYNTHESIS OF THE COMPLEX



1) *Addition of ligand 4 to $[\text{Cu}(\text{hfac})(\text{MeCN})_2]$*

Cu_2O (2.224 g, 15.54 mmol) was weighed into a 250 ml Schlenk flask under $\text{N}_2(\text{g})$. 60 ml of anhydrous MeCN was then transferred into the flask via syringe forming a bright red suspension. hfacH (3 ml, 28.26 mmol) was added dropwise into the flask containing the suspension causing an instant change in colour, turning

darker. The mixture was stirred for 90 min at room temperature. Ligand **4** (4.73 g, 28.26 mmol) was then added to the mixture, causing an instant colour change to yellow/orange, before being stirred overnight under nitrogen at room temperature. The solution was cannula-filtered, and immediately after a yellow precipitate formed in the orange filtrate. The filtrate was stored at -30 °C and the precipitate was dried *in vacuo*. The resulting product was an insoluble unidentifiable material. As a result, variations in the procedure were made.

2) *Slow diffusion method*

Cu₂O (1.5 g, 10.48 mmol) was weighed into a 250 ml Schlenk flask under N₂(g). 50 ml of anhydrous MeCN was then transferred into the flask via syringe forming a bright red suspension. Dropwise addition of previously degassed hfacH (2.20 ml, 15.73 mmol) caused a change in colour of the solution to bright red. The mixture was stirred at room temperature under N₂(g) for 90 min. The mixture was then frozen in a Dewar containing N₂(l). A yellow layer was formed on top. A solution of ligand **4** (0.438 g, 2.62 mmol) in anhydrous MeCN was added via cannula to the previously frozen solution. The mixture was left in the nitrogen bath overnight so the layers diffused slowly into each other. The resulting yellow/orange solution was filtered via cannula. The residue was washed with degassed hexane (3 x 10 ml) and the washings combined with the filtrate, which was reduced *in vacuo*. MeCN was added to the residue and heated. The filtrate was placed in the fridge at -30 °C. No suitable crystals for X-ray diffraction were obtained.

3) *Variations in stoichiometry on method 2*

Method 2 was repeated using different ratios (1:1:1/2) and (1:1:1/4) of the reagents Cu₂O, hfacH and ligand **4**. However, no crystals were obtained that were suitable for X-ray diffraction.

4.5.7. SYNTHESIS OF THE COMPLEX $[Ni_2(\mu_2\text{-mbt})_4]$ (4a)

Ni(OAc)₂·4H₂O (0.300 g, 1.21 mmol), NaOOCCH₃ (0.099 g, 1.21 mmol), Et₃N (1.25 mmol), tetrabutylammonium bromide (0.389 g, 1.21 mmol) and 2-mbtH (ligand **4**) (0.202 g, 1.21 mmol) were dissolved in methanol (20 ml) with stirring. The resultant green solution was stirred for 90 minutes at room temperature and filtered giving a colourless solution. The solid retained in the filter paper was washed with DCM. Black crystals grew upon slow evaporation after 2 weeks. Yield 22 %.

4.6. REFERENCES

- 1 E. W. Ainscough, E. N. Baker, A. G. Bingham, A. M. Brodie, and C. A. Smith, *Dalton Transactions*, 1989, 2167.
- 2 S. Jeannin, Y. Jeannin, and G. Lavigne, *Inorganic Chemistry*, 1979, **18**, 3528.
- 3 Cytec Industries, 'Mining Chemicals Handbook', 2002.
- 4 L. Ballester, A. Gutierrez, M. F. Perpnan, T. Rico, E. Gutierrez-Puebla, and A. Monge, *Polyhedron*, 1994, **13**, 2277.
- 5 S. Banerji, R. E. Byrne, and S. E. Livingstone, *Transition Metal Chemistry*, 1982, **7**, 5.
- 6 P. J. Cox, P. Aslanidis, P. Karagiannidis, and S. K. Hadjikakou, *Polyhedron*, 1999, **18**, 1501.
- 7 P. J. Cox, P. Aslanidis, P. Karagiannidis, S. K. Hadjikakou, and C. D. Antoniadis, *European Journal of Inorganic Chemistry*, 2002, 2216.
- 8 T. Shibahara, S. Kobayashi, D. Long, and X. Xin, *Acta Crystallographica, Section C: Crystal Structure Communications*, 1997, **C53**, 58.
- 9 G. P. Voutsas, S. C. Kokkou, C. J. Cheer, P. Aslanidis, and P. Karagiannidis, *Polyhedron*, 1995, **14**, 2287.
- 10 J. Lang, K. Tatsumi, and D. Yu, *Polyhedron*, 1996, **15**, 2127.
- 11 F. Jian, H. Xiao, Z. Bai, and P. Zhao, *Journal of Materials Chemistry*, 2006, **16**, 3746.
- 12 N. N. Greenwood and A. Earnshaw, 'Chemistry of the Elements', Butterworth-Heinemann, Oxford, 1994.
- 13 P. Atkins, T. Overon, J. Rouke, M. Weller, and F. Armstrong, 'Inorganic Chemistry', Oxford University Press, Oxford, 2006.
- 14 C. W. Baxter, T. C. Higgs, A. C. Jones, S. Parsons, P. J. Bailey, and P. A. Tasker, *Dalton Transactions*, 2002, 4395.
- 15 T. C. Higgs, S. Parsons, A. C. Jones, P. J. Bailey, and P. A. Tasker, *Dalton Transactions*, 2002, 3427.
- 16 T. C. Higgs, S. Parsons, P. J. Bailey, A. C. Jones, F. McLachlan, A. Parkin, A. Dawson, and P. A. Tasker, *Organometallics*, 2002, **21**, 5692.
- 17 C. W. Baxter, T. C. Higgs, P. J. Bailey, S. Parsons, F. McLachlan, M. McPartlin, and P. A. Tasker, *Chemistry--A European Journal*, 2006, **12**, 6166.
- 18 T. C. Higgs, P. J. Bailey, S. Parsons, and P. A. Tasker, *Angewandte Chemie, International Edition*, 2002, **41**, 3038.

Chapter 5

Surface binding studies of hydroxamates

CONTENTS

5.1. Introduction	93
5.1.1. Outline.....	93
5.1.2. Benzohydroxamic acid.....	93
5.1.3. Hydroxamic acids and their complexes with metal ions.....	94
5.1.4. The hydroxamic acid group and its metal-binding sites	95
5.1.5. Complexes of hydroxamic acids: mono hydroxamic acids as ligands.....	96
5.2. Surface binding studies by adsorption isotherms.....	100
5.2.1. Wavelengths and extinction coefficients used	100
5.3. Mono- and di-nuclear iron(III) complexes of benzohydroxamic acid (bhaH)..	102
5.3.1. X-ray crystal structure of $[\text{Fe}(\text{bha})_3] \cdot 1.5\text{MeOH}$ (5a).....	103
5.3.2. X-ray crystal structure of $[\text{Fe}_2(\mu_2\text{-bha})_2(\text{bha})_2\text{Br}_2]$ (5b).....	107
5.3.3. Infrared spectra of 5a and 5b	110
5.3.4. Magnetic susceptibility measurement of 5b	110
5.4. Hypothesis for mode of action of hydroxamates	111
5.5. Hydroxamate derivatives investigated	113
5.5.1. Investigating the effects of substitution on the hydroxamate group	116
5.5.2. Investigating the effects of substitution on the phenyl ring	117
5.5.3. Competitive binding studies.....	119
5.6. Conclusions	120
5.7. Experimental	121
5.7.1. Instrumentation	121
5.7.2. Solvents and reagents.....	122
5.7.3. Ligand synthesis	122
5.7.4. Synthesis of the complex $[\text{Fe}(\text{bha})_3] \cdot 1.5\text{MeOH}$ (5a).....	125
5.7.5. Synthesis of the complex $[\text{Fe}_2(\mu_2\text{-bha})_2(\text{bha})_2\text{Br}_2]$ (5b).....	125
5.7.6. Attempts to synthesise polynuclear complexes containing ligand 5 or 6 ..	125
5.7.7. Extinction coefficient (ϵ) determination	126
5.7.8. Adsorption isotherm measurements.....	126
5.8. References	128

5.1. INTRODUCTION

5.1.1. OUTLINE

This chapter investigates the ability of a series of hydroxamic acid derivatives to bind to iron(III) oxide/hydroxide surfaces. This class of ligand is claimed to be an effective flotation agent¹⁻³ and therefore presumably is surface active. However, it is also known to form very stable mononuclear iron(III) complexes in solution⁴ and consequently it was not expected to bind strongly to high surface area iron(III) oxides but, instead, sequester iron(III) ions, transferring them to the liquid phase.

5.1.2. BENZOHYDROXAMIC ACID

Whilst alkyl hydroxamates^{1, 5} and in particular, octyl hydroxamate,^{2, 3} are most commonly used as collector-agents for oxide minerals, benzohydroxamic acid (structure displayed in Figure 5.1) was selected for study in this thesis because it has a chromophore group that allows the analysis of the supernatant solutions by UV-Vis spectroscopy after an adsorption isotherm experiment.

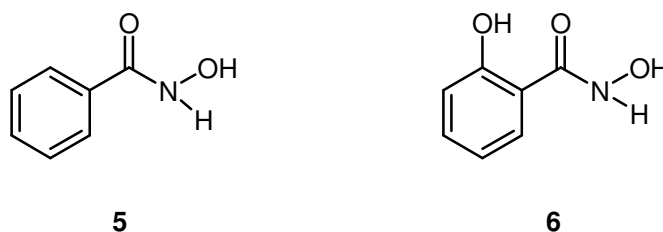


Figure 5.1. Structure of ligand **5**, benzohydroxamic acid, and its hydroxy substituted analogue **6**.

5.1.3. HYDROXAMIC ACIDS AND THEIR COMPLEXES WITH METAL IONS

Monohydroxamic acids of the general formula $RCONR'OH$ are one of the major classes of naturally occurring metal complexing agents. This family of compounds has been subject to considerable study due to its many biological and medical applications.^{4, 6} Hydroxamic acid-containing compounds are strongly implicated in iron-transport processes *in vivo*.⁶ Selectivity is crucial in such phenomena as several metal ions, which might not be essential or which may be toxic to the organism, are present in the environment.

In addition, hydroxamic acid is known as a component of food additives, antibiotics, tumour inhibitors, antifungal agents,⁶⁻⁸ HIV and Alzheimer's disease therapeutic agents^{9, 10} as well as a specific inhibitor of different enzyme activities,¹¹ such as urease.^{6-8, 12} This role is of special importance due to therapeutic applications. The mechanism of inhibition usually involves chelation of metals at the enzymatic active sites by the hydroxamate function ($RCONR'OH$). Most of their versatile biological activity is associated to the strong capacity of hydroxamic acids to chelate metals, and iron especially,^{13, 14} in particular because most naturally occurring iron-complexing agents are hydroxamic acids which complex as trihydroxamic acids with octahedral coordination to iron(III).

Marmion *et al.*¹⁵ have suggested that the biomedical applications of hydroxamic acids may also be a result of their ability to release nitric oxide (NO), which is involved in many biological processes.

As mentioned above, one of the physiological roles of hydroxamic acids is associated with their use as siderophores,¹⁶⁻²⁰ a class of low molecular-weight iron-sequestering agents, produced by microorganisms which solubilize iron(III) from the environment to transport it across the cell membrane when a cell needs an iron supply.²¹ Solubilization of iron(III) by siderophores is necessary due to the

insolubility of ferric hydroxide which would make it impossible to get iron by the microorganisms.²²

Furthermore, hydroxamic acids are used as reagents for solvent extraction.⁶ Their use in analytical chemistry^{6, 13, 23} is based on their ability to react selectively with metal ions forming low-solubility and strongly coloured complexes. Many studies to date have been undertaken in solution and focus on the determination of metal complex stability constants.^{13, 22}

The only reference to hydroxamates being used in “surface engineering” is, as mentioned in the opening paragraph, in mineral collection. Alkyl hydroxamates in combination with xanthates have shown collector properties for the beneficiation of mixed sulfide-oxide ore deposits.²

5.1.4. THE HYDROXAMIC ACID GROUP AND ITS METAL-BINDING SITES

In solution, hydroxamic acids can exist as two tautomers (Figure 5.2),⁶ the keto form, which is predominant in acidic media, and the enol tautomer, which is more stable under basic conditions. Each tautomer can exist in (*E*) and (*Z*) forms.

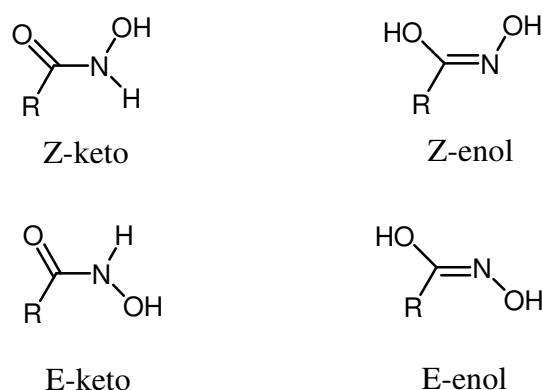


Figure 5.2. Tautomeric forms of hydroxamic acid.¹⁹

5.1.5. COMPLEXES OF HYDROXAMIC ACIDS: MONO HYDROXAMIC ACIDS AS LIGANDS

The complexing ability of the hydroxamic functionality was predicted in 1908.²³ Complexes of iron(III) with hydroxamate ligands are very stable. For instance, some trishydroxamate siderophores, such as desferrioxamine B²⁴ (Figure 5.3), which is involved in the treatment of Cooley's anemia, have a formation constant $\log \beta = 30.4$.¹⁹

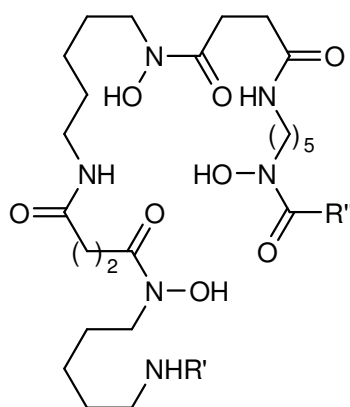


Figure 5.3. Hydroxamate siderophore. Desferrioxamine B.¹⁹

The hydroxamate group usually functions as a bidentate monoanionic donor system that can be effectively bound to a range of metal ions,⁶ forming very stable five-membered chelates (Figure 5.4). The delocalization of the double bond within the chelate ring enhances stability.⁶

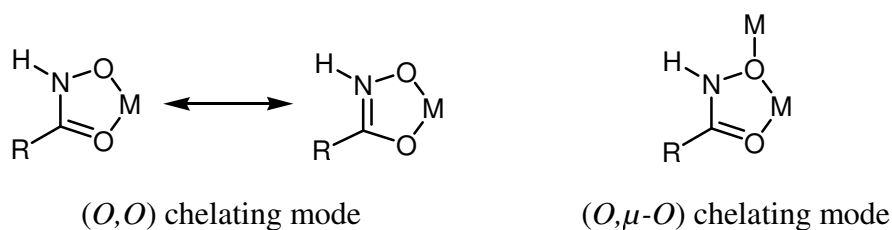


Figure 5.4. Modes of hydroxamate binding.¹⁹

A critical factor in the selectivity of this family of ligands as enzyme inhibitors could be the different sites for potential hydrogen-bond interactions that the hydroxamate moiety possesses.¹⁹

It has been shown by single crystal X-ray analysis that monohydroxamic acids usually coordinate in a bidentate mode to various metal ions, such as iron(III), cobalt(II) and nickel(II)^{6, 8, 19, 25, 26} giving octahedral complexes with 3:1 stoichiometry ligand:metal.

The structure of tris(benzohydroxamato)iron(III) trihydrate, shown in Figure 5.5, was first published in 1969.²⁷ It shows coordination of the central metal atom by the oxygen atoms of the ligand.^{27, 28} In both cases they obtained the *fac*- isomer.

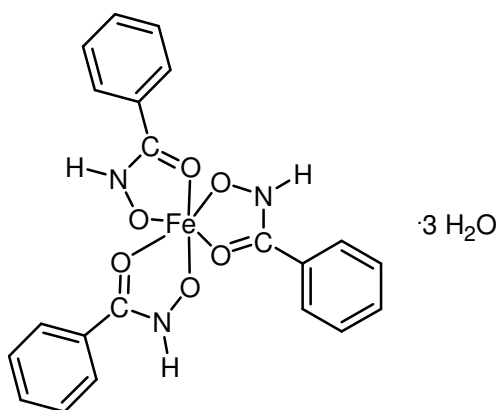


Figure 5.5. Structure of tris(benzohydroxamato)iron(III) trihydrate.²⁷⁻²⁹

Seven tris(hydroxamato)iron(III) structures have been reported in the CSD.²⁷⁻³⁰ Six are the *fac*- isomer, and one is the *mer*-; of these seven structures, three contain the benzohydroxamate ligands,²⁷⁻²⁹ and all of these are the *fac*- isomer.

Recently, complexes of hydroxamic acids with the softer ruthenium(III),³¹ platinum(II)³² and palladium(II)³³ have been structurally characterised. In ruthenium(III)-hydroxamate complex hydrate, [Ru(H₂edta)(2-OMe-Pha)], where 2-OMe-Pha = 2-methoxyphenylhydroxamate, the hydroxamate ligand shows normal (O,O) bidentate coordination (Figure 5.6).³¹

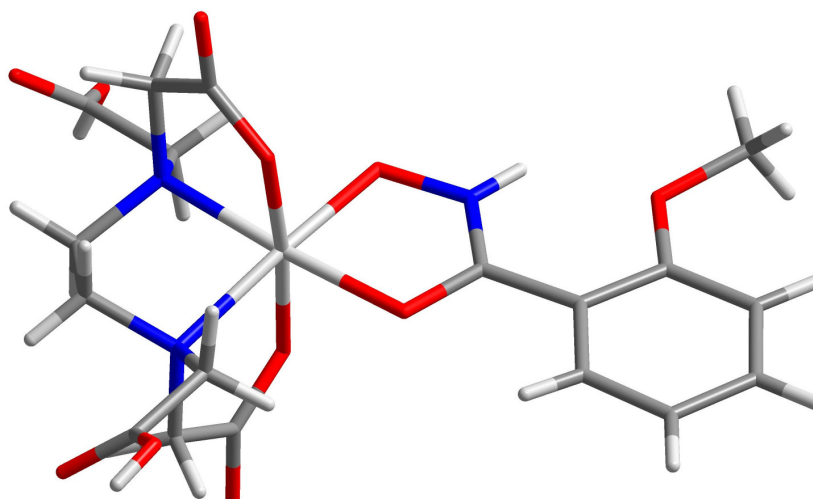


Figure 5.6. Crystal structure of $[\text{Ru}(\text{H}_2\text{edta})(2\text{-OMe-Pha})]$.³¹

The structures of two dinuclear platinum(II)-hydroxamate complexes have been recently determined.³² The complexes $[\{\text{Pt}(\text{en})\}_2(\mu\text{-bha})]\text{ClO}_4\cdot\text{H}_2\text{O}$ and $[\{\text{Pt}(\text{R,R-chxn})\}_2(\mu\text{-bha})]\text{NO}_3\cdot 2\text{H}_2\text{O}$ where en = ethylene diamine, bha = benzohydroxamate and chxn = cyclohexane-1,2-diamine, have two platinum atoms bridged by the benzohydroxamate ligand via (O,O), as expected, and (C,N) coordination fashion. Unexpectedly, the latter mode occurs through deprotonation of the *ortho* carbon of the phenyl ring to a second Pt(en) moiety as it is shown in Figure 5.7.

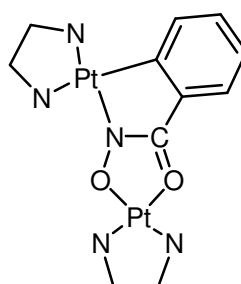


Figure 5.7. Structure of $[\{\text{Pt}(\text{en})\}_2(\mu\text{-bha})]\text{ClO}_4\cdot\text{H}_2\text{O}$.³²

Examples of complexes $[M_2(\mu\text{-OAc})(\mu\text{-aha})_2(\text{tmen})_2]^+$ where $M = \text{Co},^{34} \text{Ni},^{35}$ $\text{OAc} = \text{CH}_3\text{COO}^-$, $\text{aha} =$ deprotonated acetohydroxamic acid, $\text{tmen} =$ tetramethylethylenediamine, have been reported. The deprotonated hydroxyl oxygen of the hydroxamic acid bridges the two metal centres with the carbonyl oxygen bonding to one metal centre only, in contrast to normal (O,O) chelation of a metal ion by a hydroxamic acid as is shown in Figure 5.8. Other examples of complexes can be found in literature where this sort of binding in which hydroxamic acids act as a bridge between two metal atoms, but significantly in the context of this thesis there are no examples where the group bridges Fe(III) ions.

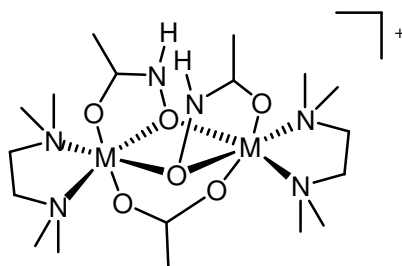


Figure 5.8. $[M_2(\mu\text{-OAc})(\mu\text{-aha})_2(\text{tmen})_2]^+$ structure where $M = \text{Co},^{34} \text{Ni},^{35}$

The hydroxamate complex, $^{36} [Zn_2(\mu\text{-OAc})_2(\text{OAc})(\mu\text{-bha})(\text{tmen})]$ where $\text{OAc} = \text{CH}_3\text{COO}^-$, $\text{bha} =$ deprotonated benzohydroxamic acid, $\text{tmen} =$ tetramethylethylenediamine, also has the oximato oxygen atom bridging the zinc atoms and the carbonyl oxygen bonding only to one zinc atom. This structure (Figure 5.9) shows the ability of hydroxamic acids to mimic the inhibition of related dinuclear metalloenzymes. 36,37

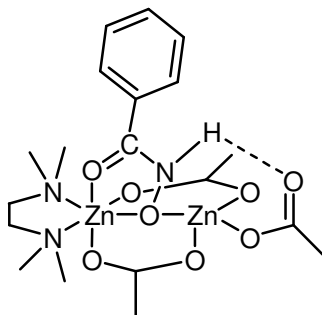


Figure 5.9. $[Zn_2(\mu\text{-OAc})_2(\text{OAc})(\mu\text{-bha})(\text{tmen})]$ structure. 36

5.2. SURFACE BINDING STUDIES BY ADSORPTION ISOTHERMS

Adsorption isotherm studies of a series of hydroxamic acids are presented in this section. The initial testing was done with ligand **5**, benzohydroxamic acid, which was not expected to bind strongly to iron(III) oxide/hydroxide surfaces as it forms very stable mononuclear iron(III) complexes and consequently sequestration of iron into solution was expected. As a result of the tests showing very strong binding to goethite (see below) a range of structurally related compounds (see Section 5.6) was also investigated. Initially adsorption isotherms were measured on **5** and its hydroxyl-substituted analogue **6** (Figure 5.27) because these have strong UV-Visible adsorption bands.

5.2.1. WAVELENGTHS AND EXTINCTION COEFFICIENTS USED

The extinction coefficients of ligands **5** and **6** were determined by UV-Vis spectroscopy to calculate the concentration of ligand in solution in isotherm determination (see Section 2.5.4) using the Beer-Lambert Law (Section 1.9). Table 5.10 shows the data for ligands **5** and **6**. The background correction factor (see Section 2.2) was applied when determining the concentration of ligand left in solution.

Ligand	Wavelength (nm)	Extinction coefficient ($\text{l mol}^{-1} \text{cm}^{-1}$)	Background correction factor
5	224	9318	0.511
6	300	7273	0.163

Table 5.10. Extinction coefficient data and background correction factors for **5** and **6** determined in methanol/water (95:5 v/v) at room temperature.

The adsorption isotherms of **5** on goethite and silica are shown in Figure 5.11 and data about its binding constant and surface coverage on goethite are displayed in Table 5.12.

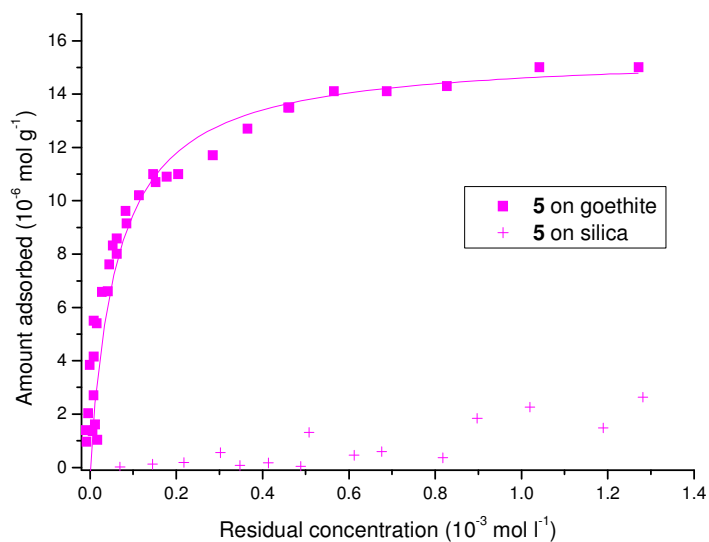


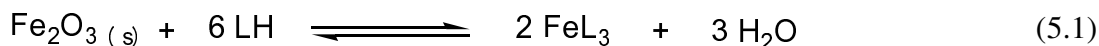
Figure 5.11. Adsorption isotherms of ligand **5** on goethite and silica in methanol/water (95:5 v/v) at 25°C.

Ligand	Equilibrium adsorption constant (K) 10^3	Surface coverage (10^{-6} mol g^{-1})	Required surface area (\AA^2 molecule $^{-1}$)
5	16(3)	15.5(8)	240(12)

Table 5.12. Adsorption isotherm data for ligand **5** (errors in parentheses) on goethite. For definitions of K , surface coverage, required surface area and their determination see Section 1.6.1.

The starting point of the investigation was benzohydroxamic acid, **5**, as alkyl hydroxamates have been identified as collector agents for oxide minerals. As stated above, benzohydroxamic acid is known as a strong chelating agent and, as a result, it was not expected to bind strongly to iron(III) oxide/hydroxide surfaces. Instead

iron(III) sequestration into solution (see Equation 5.1) as well as the degradation of the surface were predicted:



$\text{Log } \beta = 27.20$, for LH = benzohydroxamic acid.⁴

Unexpectedly, the adsorption isotherm of ligand **5** on goethite shows strong binding (Figure 5.11). The remaining supernatant solutions were analyzed by ICP-OES to check that the steep slope observed was not due to removal of free ligand form to the solution phase by dissolution of iron ions from the mineral surface which creates a complex with UV-Vis absorption bands in different regions from those of the free ligand. No iron was found in the colourless supernatant solutions. In view of these results, it is of considerable interest to establish how the hydroxamate binds to iron(III) oxide surfaces and consequently attempts were made to prepare and characterize polynuclear complexes to provide models for how a hydroxamate unit can bridge more than one iron centre. No polynuclear iron(III) complexes had previously been structurally characterized (Section 5.1.5).

5.3. MONO- AND DI-NUCLEAR IRON(III) COMPLEXES OF BENZOHYDROXAMIC ACID (*bhaH*)

Following the observations that benzohydroxamic acid (*bhaH*, **5**) binds strongly to high surface area goethite, we attempted to prepare polynuclear Fe(III) complexes and to determine their X-ray crystal structures in the hope that these would provide structural motifs which indicated how attachment to the surface is achieved. Different reagents and techniques, such as solvothermolysis and microwave techniques, were used to attempt to synthesize polynuclear complexes containing either ligand **5** or **6**. The salicylic acid analogue **6** was included in these studies because it was hoped that the additional phenyl OH group which is known to function as a good bridging unit in Fe(III)-O-Fe(III) units would favour formation of

polynuclear complexes. Whilst many of these experiments yielded solid materials, very few gave crystalline products suitable for crystal X-ray structure determination.

Various Fe(II) and Fe(III) salts, iron(III) triangles as $[\text{Fe}_3\text{O}(\text{OAc})_6(\text{H}_2\text{O})_3]\text{Cl}$, bases, alcohol tripodal co-ligands such as 1,1,1-tris(hydroxymethyl)ethane, 1,1,1-tris(hydroxymethyl)propane, pentaerythritol and *cis*, *cis*-1,3,5-cyclohexanetriol dihydrate, other co-ligands such as carboxylates and solvents [methanol, acetonitrile, pyridine] were investigated. All of the reactions were carried out at room temperature and most were repeated using

- solvothermal reaction conditions (sealed Teflon container, 120 °C, 12 h or 150 °C, 5 h) (see Section 5.7.6). This technique allows the use of high temperatures in reactions in low boiling solvents³⁸ or
- microwave techniques (120 °C, 130 psi and 200 W) (see Section 5.7.6). This method results in superheating phenomena due to high frequency oscillating electric and magnetic fields.³⁹

In total 439 experiments to prepare crystalline samples of polynuclear complexes were attempt in this manner. Two were successful (see Sections 5.3.1 and 5.3.2).

5.3.1. X-RAY CRYSTAL STRUCTURE OF $[\text{Fe}(\text{bha})_3] \cdot 1.5\text{MeOH}$ (5a)

Red crystals suitable for single crystal X-ray diffraction were obtained from a methanolic solution upon diffusion of diethyl ether. The structure of **5a** was determined by Mr. Fraser White and contains two crystallographically independent units and three solvent methanols in the asymmetric unit. One of the $[\text{Fe}(\text{bha})_3]$ tris(benzohydroxamato)iron(III) units is the *fac*- isomer and the other is the *mer*-isomer. Of the seven tris(hydroxamato)iron(III) structures reported in the CSD,²⁷⁻³⁰

six are the *fac*- isomer whereas only one the *mer*-isomer. The numbering schemes for atoms in the coordination spheres are shown in Figure 5.14.

The *pseudo*-octahedral environment around the Fe(III) atoms is defined in Table 5.15. The bonds from the hydroxamato oxygen atoms are slightly shorter (mean 1.9924 Å) than those for the carbonyl oxygen atoms (mean 2.0375 Å). There appears not be any systematic difference between Fe - O bond lengths in the *fac*- and *mer*- isomers but the lower symmetry of the *mer*- complex is reflected in a slightly wider range of bond angles; the *trans* angles fall in the range 155.37(6) – 163.33(6)° compared with 159.56(6) – 167.38(6)° and the *cis* – angles (non-chelate) 84.14(6) – 108.51(6)° *cf.* 85.92(6) – 106.17(6)°. As would be expected, the chelate “bite” angles show only very small variations, and no systematic differences between the *fac*- and *mer*- isomers, 78.35(6) – 79.09(6)° and 77.84(6) – 79.32(6)° respectively. The average value of these “bite” angles, 78.50°, falls within the range 78.23 – 79.67° for the six *fac*- and one *mer*- isomers of tris(hydroxamato)iron(III) complexes recorded in the CSD.²⁷⁻³⁰

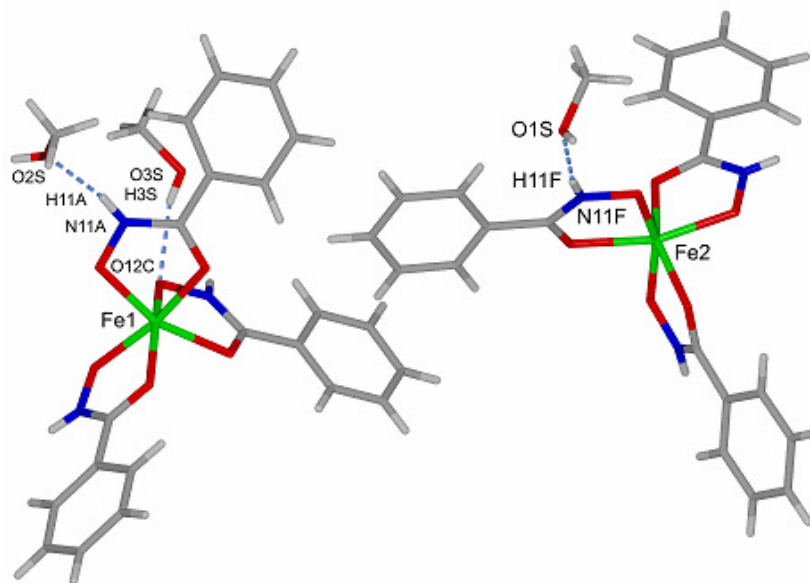


Figure 5.13. Structure of **5a** in the solid state showing the atom labelling scheme used in the table of H-bond lengths (available in detail in the Appendix CD).

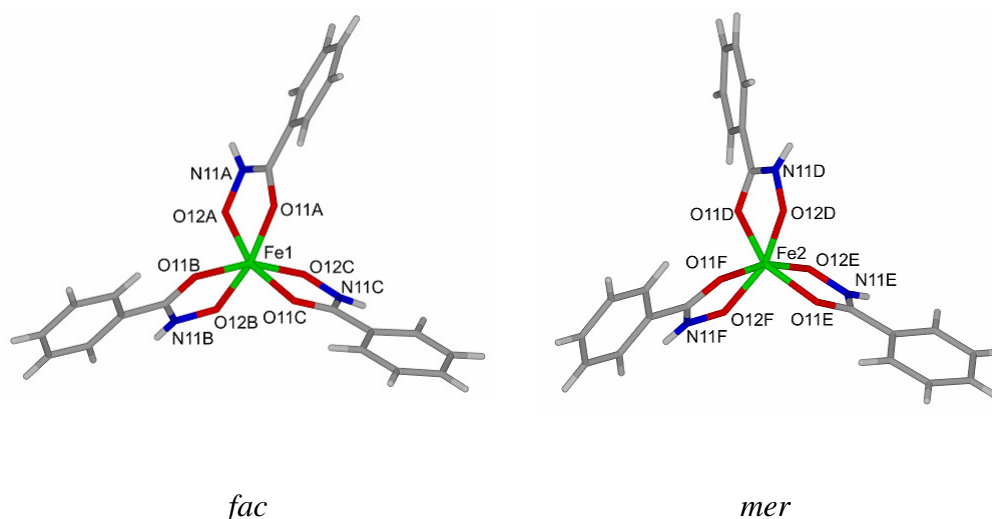


Figure 5.14. Structures of the *fac*- and *mer*- isomers contained in **5a**, showing the atom labelling scheme of the inner coordination spheres used in the following tables (data available in detail in the Appendix CD).

Bond lengths (Å) in the coordination spheres			
Fe(1)		Fe(2)	
O(11A)	2.0486(14)	O(11D)	2.0234(14)
O(11B)	2.0118(14)	O(11E)	2.0382(14)
O(11C)	2.0588(14)	O(11F)	2.0439(14)
O(12A)	1.9966(14)	O(12D)	1.9878(14)
O(12B)	1.9843(14)	O(12E)	1.9853(14)
O(12C)	2.0015(14)	O(12F)	1.9988 (14)
Bond angles (°) in the coordination spheres			
Fe(1)		Fe(2)	
O(11A), O(11B)	98.19(6)	O(11D), O(11E)	155.37(6)
O(11A), O(11C)	86.18(6)	O(11D), O(11F)	108.47(6)
O(11A), O(12A)	78.35(6)	O(11D), O(12D)	79.32(6)
O(11A), O(12B)	167.38(6)	O(11D), O(12E)	84.14(6)
O(11A), O(12C)	99.36(6)	O(11D), O(12F)	94.69(6)
O(11B), O(11C)	92.36(6)	O(11E), O(11F)	94.95(6)
O(11B), O(12A)	100.83(6)	O(11E), O(12D)	89.18(6)
O(11B), O(12B)	79.09(6)	O(11E), O(12E)	78.94(6)

O(11B), O(12C)	159.56(6)	O(11E), O(12F)	103.19(6)
O(11C), O(12A)	160.89(6)	O(11F), O(12D)	85.04(6)
O(11C), O(12B)	106.17(6)	O(11F), O(12E)	163.33(6)
O(11C), O(12C)	78.46(5)	O(11F), O(12F)	77.84(5)
O(12A), O(12B)	89.99(6)	O(12D), O(12E)	108.51(6)
O(12A), O(12C)	92.92(6)	O(12D), O(12F)	159.06(6)
O(12B), O(12C)	85.92(6)	O(12E), O(12F)	90.57(6)

Table 5.15. Bond lengths (Å) and bond angles (°) in the inner coordination spheres of the two crystallographically independent [Fe(bha)₃] complexes in **5a**.

Bond angle values in the chelate rings of complex **5a** correlate well with the ones found in literature.³⁴

A 3-dimensional H-bond network of MeOH solvent molecules and hydroxamic acids NH, C = O and N – O units is shown in the solid state structure. Layers of tris(benzohydroxamato)iron(III) units are observed with gaps between layers where hydrophobic phenyl rings are located. Hydrogen bond lengths are shown in Table 5.16.

H-bond for unit 1 (Å)		H-bond for unit 2(Å)	
N(11A) – H(11A)···O(2S)	2.733	N(11D) – H(11D)···O(3S)	2.888
N(11B) – H(11B)···O(12D)	2.894	N(11E) – H(11E)···O(12E)	2.733
N(11C) – H(11C)···O(12A)	2.775	N(11F) – H(11F)···O(1S)	2.755
O(2S) – H(2S)···O(12B)	2.883	O(1S) – H(1S)···O(12F)	2.690
O(3S) – H(3S)···O(12C)	2.731		

Table 5.16. Hydrogen bond donor-acceptor distances (Å) for complex **5a**.

5.3.2. X-RAY CRYSTAL STRUCTURE OF $[\text{Fe}_2(\mu_2\text{-bha})_2(\text{bha})_2\text{Br}_2]$ (**5b**)

Black crystals of the complex **5b** suitable for a single crystal X-ray diffraction were obtained by diffusion of diethyl ether into a methanolic solution.

The crystalline complex **5b** was characterised by an X-ray structure determination. Elemental analysis data are consistent with formulation as $[\text{Fe}_2(\mu_2\text{-bha})_2(\text{bha})_2\text{Br}_2]$ and infra-red data with monodeprotonation of each of the hydroxamic acid units.

The asymmetric unit of the crystal structure of **5b** contains half of the centrosymmetric dimer shown in Figure 5.17. This Figure also defines the labelling scheme used for the atoms in the inner coordination spheres of the dinuclear Fe(III) complex. The dimer contains hydroxamato ligands which operate in two different modes. One, containing O1B and O11B in Figure 5.17, forms a conventional 5-membered chelate ring with the oximato and carboxamato Fe-O bond lengths, 1.9554(13) and 2.0166(13) Å respectively, being similar to those in **5a** (Table 5.15). The chelate bite angle ($79.69(5)^\circ$) in this hydroxamato unit is slightly larger than those in the mononuclear tris(benzohydroxamato) complexes of **5a** (see Table 5.15). This is consistent with the other ligands in the coordination sphere of the iron atom in the dimer being disposed very differently from those in a tris(hydroxamato) complex (see below).

The other crystallographically independent hydroxamato group, containing O1A and O11A, operates as a chelating unit to one iron atom and additionally forms a bridge via the oximato oxygen atom to the other iron atom. As a consequence, the bond lengths and angles defined by this hydroxamate are slightly different from those showing the “simple” chelating mode. The bite angle, O1A-Fe1-O11A, is smaller, $76.75(5)$ *c.f.* $79.65(5)^\circ$, and the oximato oxygen atom to iron bond is significantly longer, $2.0873(15)$ *c.f.* $1.9554(13)$ Å.

Most importantly in the context of forming dinuclear complexes at a surface the bonds to the two iron atoms, Fe(1) and Fe(1A), formed by the bridging hydroxamate oxygen atom O(1) are similar in length, 2.0930(13) and 2.0873(15) Å. This implies that both these bridging bonds are relatively strong. They are only slightly longer than the oximate to Fe bonds in the tris(hydroxamate) complexes (mean 1.9924 Å) and very similar in length to the carbonyl to Fe bonds in the tris(hydroxamate) complexes (mean 2.0375 Å).

The phenyl group associated with the bridging hydroxamate is disordered over two sites (see Figure 5.17). This could be of significance when considering how the benzohydroxamates would pack across a surface defined by oxo-bridged iron units corresponding to the Fe(1), O(1), Fe(1A), O(1A) plane in Figure 5.17.

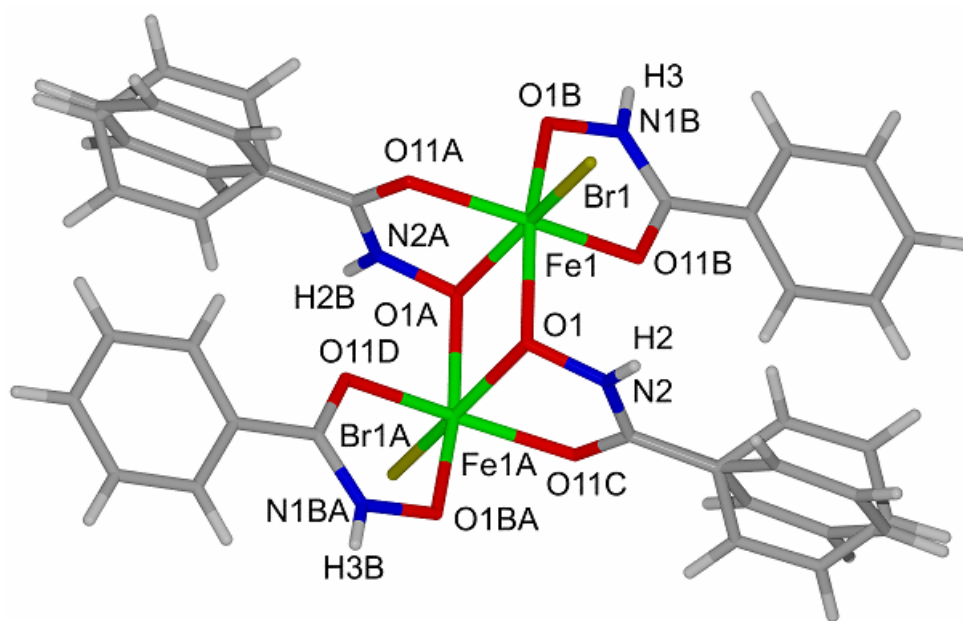


Figure 5.17. Structure of **5b** in the solid state showing the atom labelling scheme used in the following tables (data available in detail in the Appendix CD).

Selected bond lengths (Å)			
Fe(1) – O(1)	2.0930(13)	Fe(1) – Br(1)	2.4448(4)
Fe(1) – O(1B)	1.9554(13)	Fe(1) – O(1A)	2.0873(15)
Fe(1) – O(11A)	2.0152(13)	Fe(1) – O(11B)	2.0166(13)
Fe(1)···Fe(1A)	3.298		
Selected bond angles (°)			
O(1) – Fe(1) – O(1A)	75.83(6)	O(1) – Fe(1) – O(1B)	164.55(5)
O(1) – Fe(1) – O(11A)	100.31(5)	O(1) – Fe(1) – O(11B)	87.03(5)
O(1) – Fe(1) – Br(1)	89.90(4)	Br(1) – Fe(1) – O(1B)	100.20(5)
Br(1) – Fe(1) – O(11A)	95.40(4)	Br(1) – Fe(1) – O(11B)	100.46(4)
O(1A) – Fe(1) – O(11A)	76.75(5)	O(1B) – Fe(1) – O(11B)	79.69(5)
O(1A) – Fe(1) – O(11B)	89.93(5)	O(1B) – Fe(1) – O(11A)	90.43(5)
O(1A) – Fe(1) – O(1B)	96.13(6)	O(11A) – Fe(1) – O(11B)	162.54(6)
O(1A) – Fe(1) – Br(1)	161.95(4)		

Table 5.18. Selected bond lengths (Å) and angles (°) in the inner coordination sphere of complex **5b**.

There are intermolecular hydrogen bonds N(2)-H(2)···O(1B) and O(1)···N(1B)-H(3) linking the two units of benzohydroxamato ligands (Figure 5.17 and Table 5.19). A Br(1)···N(1B)-H(3) close contact is also seen.

H-bond length (Å)	
N(2)–H(2)···O(1B)	2.915
O(1)···N(1B)–H(3)	2.981

Table 5.19. Hydrogen bond lengths (Å) for complex **5b**.

The hydroxamate moiety has been seen before acting as a bridge between two metal centres, in Co, Ni and Zn complexes,³⁴⁻³⁶ as described in Section 5.1.5. Unlike **5b**, in the Co and Ni complexes reported in literature both of the hydroxamato units

lie on the same side of the N₂O₂ plane in the molecule and the Zn complex contains only one bridging benzohydroxamato unit per dinuclear complex.

5.3.3. INFRARED SPECTRA OF 5a AND 5b

The infrared spectra of benzohydroxamic acid, **5a** and **5b** were recorded in the range 4000 – 400 cm⁻¹. Key bands compare closely with those reported in literature.³⁵ On metal complexation, the carbonyl vibration band assigned to the free ligand at 1644 cm⁻¹ shifts about 40 – 60 cm⁻¹ to 1596 cm⁻¹, indicating chelation by the ketonic oxygen atom.^{4, 7, 40} In complexes **5a** and **5b** a band corresponding to $\nu(\text{Fe} - \text{O})$ can be observed around 555 cm⁻¹.⁴¹

5.3.4. MAGNETIC SUSCEPTIBILITY MEASUREMENT OF 5b

The temperature dependence of the molar magnetic susceptibility of **5b** was studied in the temperature range of 2 – 300 K (Figure 5.20). The $\chi_{\text{M}}T$ value decreases upon cooling from approximately 9 cm³ K mol⁻¹ at 300 K to 2 cm³ K mol⁻¹ at 0 K, which is indicative of a $S = 0$ ground state and intramolecular antiferromagnetic exchange interactions between the iron(III) ($S = 5/2$) ions in the dimer.

The data were fitted assuming a 1J model. Use of the Hamiltonian in Equation 5.2 afforded, $J = -6.8 \text{ cm}^{-1}$, $g = 2.06$.

$$\hat{H} = -2J\hat{S}_1\hat{S}_2 \quad (5.2)$$

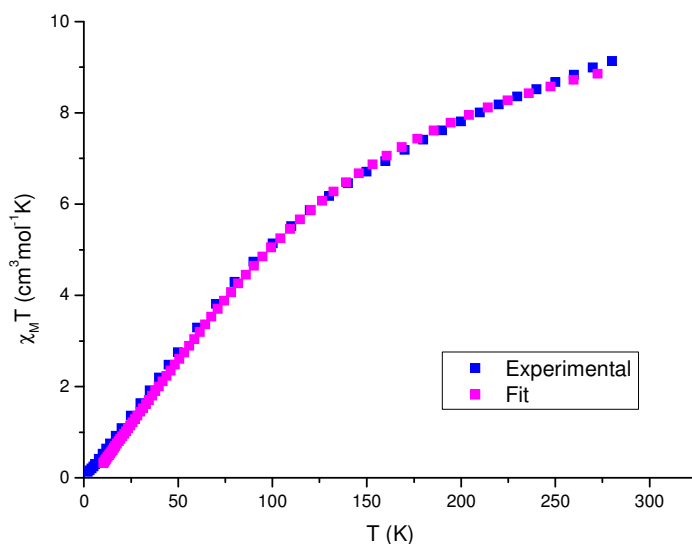


Figure 5.20. Thermal variation of $\chi_M T$ in ranges 300 - 2 K at 1 T for complex **5b**.

5.4. HYPOTHESIS FOR MODE OF ACTION OF HYDROXAMATES

The strong isotherm obtained for benzohydroxamic acid, **5**, on goethite and the crystal structure of **5b** in which the hydroxamato moiety bridges two iron ions provides an incentive to consider the potential modes of surface attachment of benzohydroxamic acid. Figure 5.21 illustrates two binding modes on iron(III) oxide/hydroxide surfaces that use the motif present in $[\text{Fe}_2(\mu_2\text{-bha})_2(\text{bha})_2\text{Br}_2]$ with a raft of edge-shared Fe(III) octahedral representing the surface. Edges are defined by $\mu\text{-OH}$ and by bridging oximato oxygen atoms. The carbonyl oxygen atoms then occupy axial positions as in $[\text{Fe}_2(\mu_2\text{-bha})_2(\text{bha})_2\text{Br}_2]$.

- In Figure 5.21 (a) the oximato oxygen chains are arranged *trans* about each Fe(III) centre and consequently adjacent hydroxamate chelate rings are mutually perpendicular.

- In Figure 5.21 (b) the oximato oxygen atoms are *cis* to each other and the hydroxamates are parallel to each other.

In both cases, the suggested multisite attachment implies that the deprotonated N-OH oxygen of the hydroxamate functionality is embedded in the mineral surface which would confer additional kinetic stability to the proposed model in comparison to the one for carboxylic acids of the Irgacor 419[®] type.^{42, 43} In the latter the multisite attachment involves the carboxylate group spanning axial sites on adjacent iron(III) atoms and hydrogen bonding of the 3-keto group to the hydroxyl groups of the mineral surface (see Section 2.1.4) and the ligand is not embedded in the surface but lies above it.

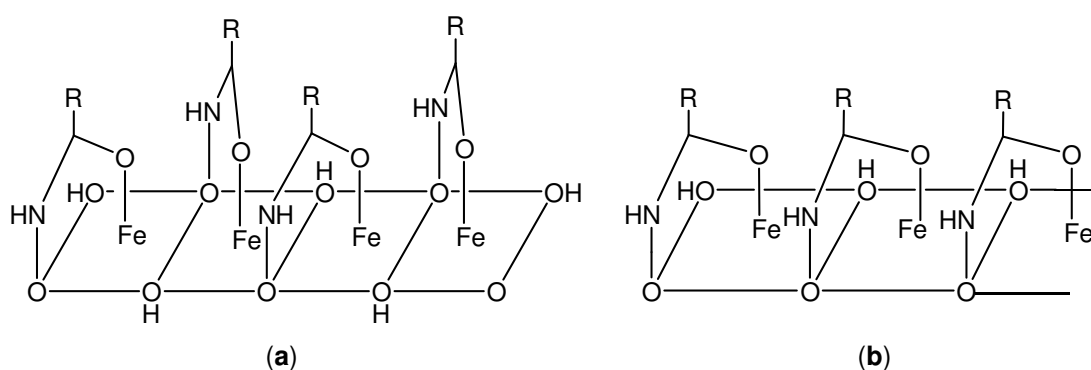


Figure 5.21. Schematic representation of possible modes of binding of hydroxamates on iron(III) oxide/hydroxide surfaces.

To investigate whether these models for binding were valid, other hydroxamates derivatives were synthesised and their strength of binding to goethite was studied. Other packing arrangements are possible and are being modelled⁴⁴ by methods similar to those described for iron corrosion inhibitors.^{42, 43}

5.5. HYDROXAMATE DERIVATIVES INVESTIGATED

Further investigations to corroborate or refute the assumptions made above about mode of binding were based on the ligands shown in Figure 5.22.

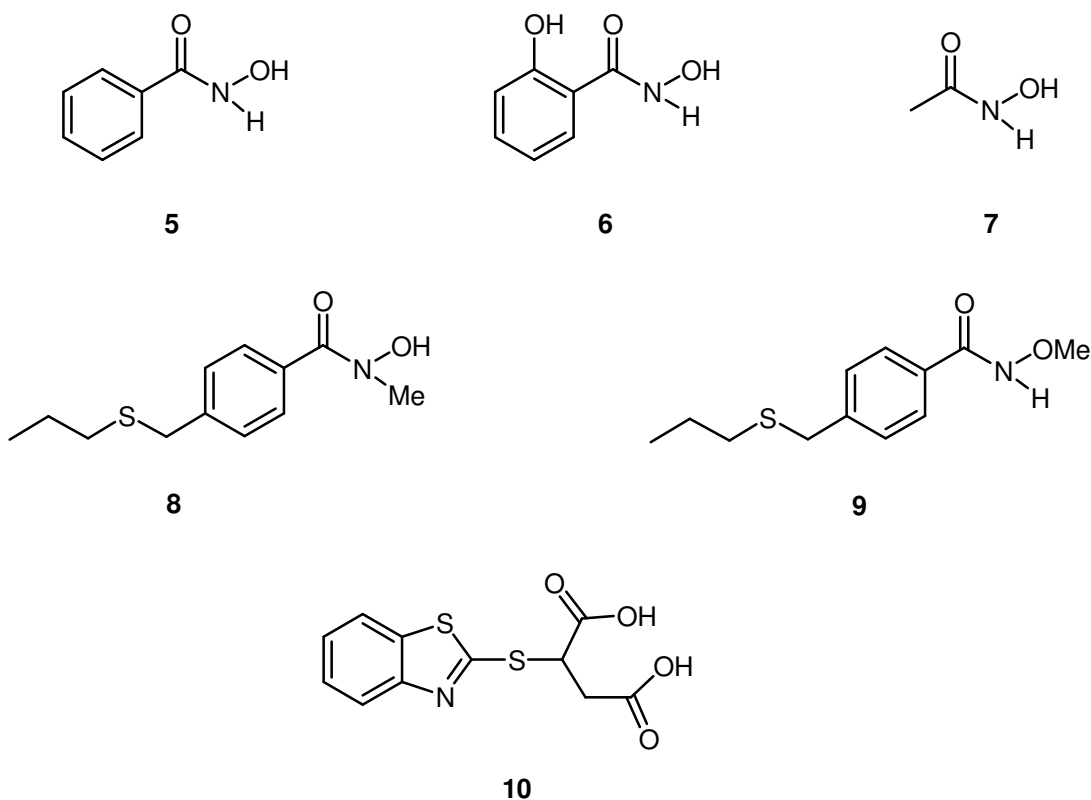


Figure 5.22. Ligands **5**, **6**, **7**, **8**, **9** and **10** investigated in this chapter.

- Ligand **9** is a compound offering no possibility of forming μ -oxygen bridges between the iron centres due to the bulk of the N-OMe unit and the impossibility of this being deprotonated to provide an anionic oxygen atom.
- The steric bulk of the nitrogen atom is greater in ligand **8** than in **5** and may disfavour the binding strength on goethite.

Ligands **8** and **9** incorporate a sulfur-containing tail as an atom label for ICP-OES analysis. Details of their preparation and characterization are given in Section 5.7.

- Ligand **6** has an additional hydroxyl group on the phenyl ring which makes this ring bulkier thus disfavoring binding or could provide an additional group for surface attachment by forming additional Fe-O bonds or promote H-bonding to coordinated OH units on the surface.
- Ligand **7** was chosen to investigate the influence of the size of the tail group. It contains a methyl group instead of the phenyl ring of benzohydroxamic acid, **5**. As it does not have an ICP label or a chromophore group, its binding abilities were investigated using competitive binding studies.
- Ligand **10** was used as a control in competitive binding studies of ligands **5** and **7** on iron(III) oxide surfaces as **10** had already been shown to bind strongly to such surfaces.⁴⁵ Additionally its sulfur containing tail facilitates analysis by ICP-OES in adsorption isotherm determination.

X-RAY CRYSTAL STRUCTURE OF 9

The reaction product from 4-(propylthiomethyl)benzoic acid, oxalyl chloride and *O*-methylhydroxylamine hydrochloride was chromatographed and recrystallised from diethyl ether to yield colourless blocks of **9** suitable for X-ray crystallography, confirming its characterization by ¹H and ¹³C NMR, ES-MS and elemental analysis.

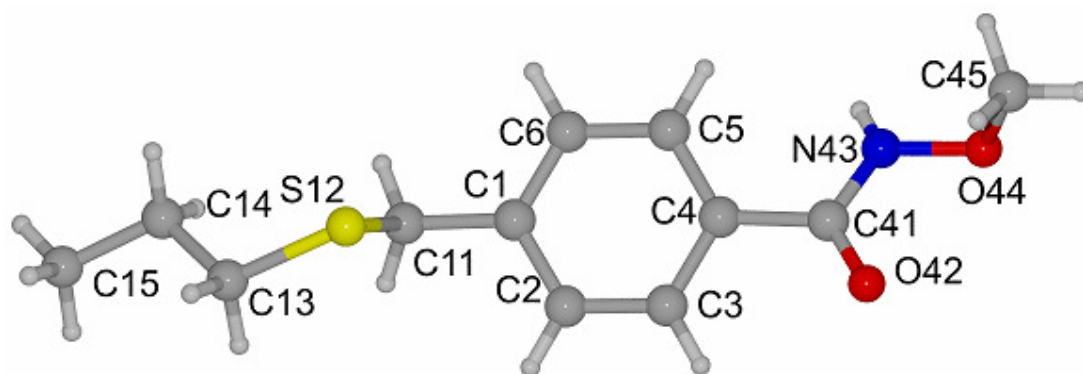


Figure 5.23. Structure of ligand **9** in the solid state showing the atom labelling scheme (data available in detail in the Appendix CD).

There is one strong intermolecular hydrogen bond (2.8105(14) Å) per molecule, between the keto oxygen O42 and the hydrogen on the amino group N43 (Figure 5.24).

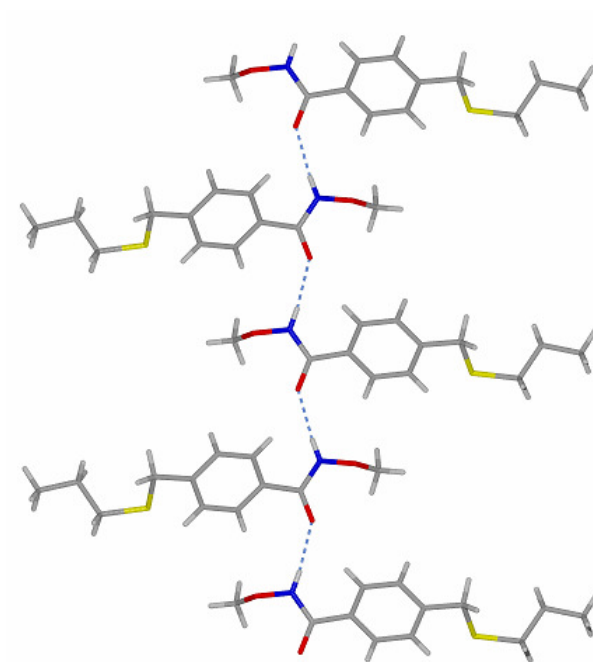


Figure 5.24. Crystal packing of **9** showing H-bonding between the keto oxygen and the H on the amino group.

5.5.1. INVESTIGATING THE EFFECTS OF SUBSTITUTION ON THE HYDROXAMATE GROUP

Isotherms of ligands **8** and **9** were run using ICP-OES as the technique to determine the amount of ligand remaining in solution based on the sulfur content. Isotherms in Figure 5.25 compare the binding of **8**, in which the hydrogen atom of the nitrogen of the hydroxamate functionality has been substituted for a methyl group, and **9**, in which a methyl group has replaced hydrogen of the hydroxyl group of the hydroxamate moiety. This methoxy group was expected to make the binding of **9** to the surface more difficult because the OMe group is too large to insert between two adjacent Fe(III) atoms on the surface and indeed the binding to either goethite or silica was found to be very weak (Figure 5.25). In contrast, the binding of **8** to goethite is much stronger than **9** but weaker than **5** (Table 5.26) which has no substituent on the N atom.

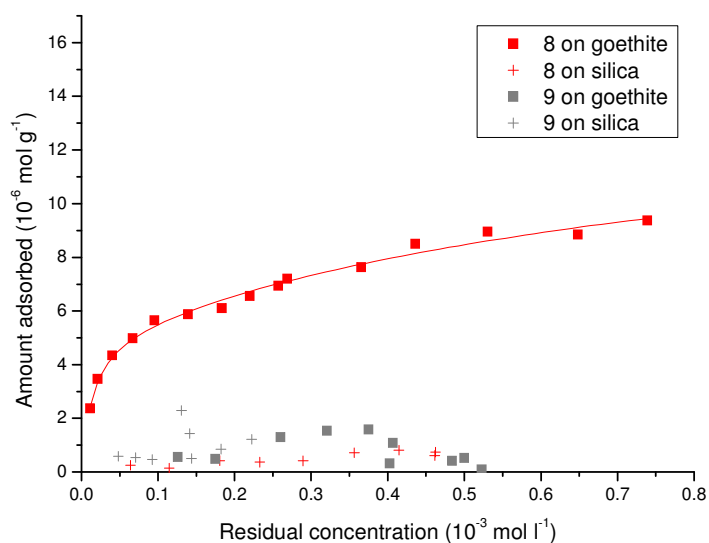


Figure 5.25. Adsorption isotherms comparing ligands **8** and **9** on goethite and silica in methanol/water (95:5 v/v) at 25 °C.

Ligand	Equilibrium adsorption constant (K) 10^3	Surface coverage (10^{-6} mol g^{-1})	Required surface area (\AA^2 molecule $^{-1}$)
5	16(3)	15.5(8)	240(10)
6	18(7)	10(1)	360(40)
8^a	75(250)	5.1(6)	700(90)
	1.1(1.5)	10(3)	400(100)
9	-	-	-

Table 5.26. Adsorption isotherm data for ligands **5**, **6**, **8** and **9** (errors in parentheses) on goethite. For definitions of K , surface coverage, required surface area and their determination see Section 1.6.1.

^a Ligand **8** required the double Langmuir equation to fit the data. Consequently, two equilibrium adsorption constants are quoted.

The adsorption isotherms obtained for **8** and **9** on goethite support the binding hypotheses discussed in Section 5.5. For **9**, preventing the N-OMe oxygen from embedding into the surface decreases the binding strength considerably and consequently suggests that it is the presence of the N-O⁻ oxygen atom which allows strong surface binding. The adsorption isotherm of **8** indicates that including a bulkier group on the N atom the binding abilities are diminished in comparison to **5**.

5.5.2. INVESTIGATING THE EFFECTS OF SUBSTITUTION ON THE PHENYL RING

Salicylhydroxamic acid, **6**, was studied to see whether the presence of a hydroxyl group on the phenyl ring had any influence on the binding strength. Isotherms are compared in Figure 5.27 for ligands **5** and **6**. The values of the adsorption constants of **5** and **6** are similar, 16000(3000) and 18000(7000), respectively, indicating that it is possible that **5** and **6** bind to the surface in the same polynucleating mode illustrated in Figure 5.28, (a) and (b), respectively. Figure 5.27 and Table 5.26 show that the surface coverage of ligands **5** and **6** differ slightly,

suggesting that there is an adverse steric effect of the phenolic OH group which reduces the efficiency of surface packing. There is no evidence that the presence of the additional OH group provides beneficial surface binding by interacting with more Fe centres (as in Figure 5.28, (c)) or by forming ligand···ligand or ligand···surface H-bonding. Both ligands **5** and **6** show weak binding to silica, as desired.

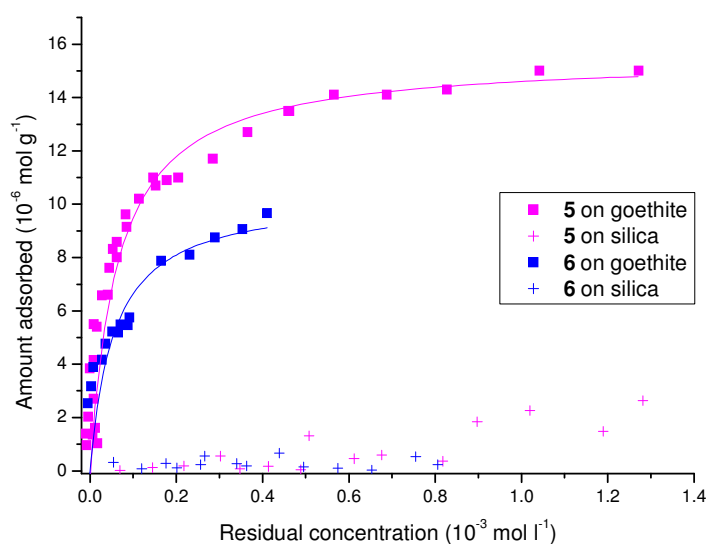


Figure 5.27. Adsorption isotherms comparing ligands **5** and **6** on goethite and silica in methanol/water (95:5 v/v) at 25 °C.*

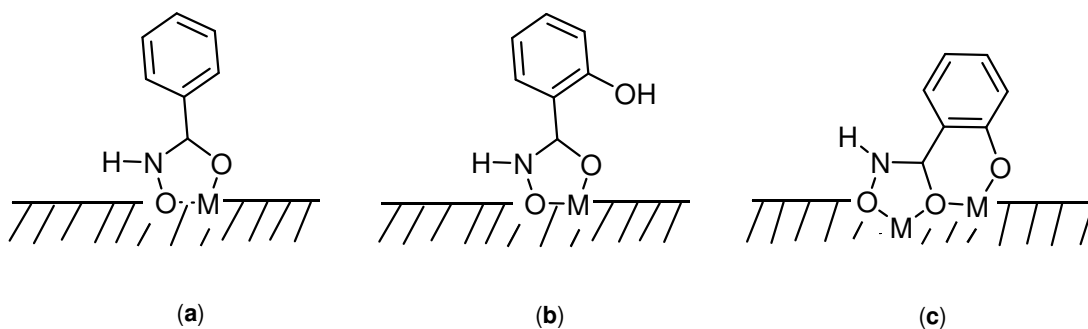


Figure 5.28. Schematic representation of the binding modes commented for **5** and **6** on goethite.

* The gap in the points observed in the isotherm of **6**, as well as the lowering of the points in the region of $0.25 \times 10^{-3} \text{ mol l}^{-1}$ of isotherm **5**, is due to an inconsistency between the two different stock solutions prepared which are necessary to cover the region from 0 to 1.4 mol l^{-1} .

5.5.3. COMPETITIVE BINDING STUDIES

Due to the lack of either a chromophore group for analysis by UV-Vis spectroscopy or a suitable atom for excitation and analysis by ICP-OES in acetohydroxamic acid, ligand **7**, competitive binding studies were carried out relative to a ligand known to bind fairly strongly to iron(III) oxide surfaces,⁴⁵ **10**. The ability of ligand **5** (binding strength on an iron(III) oxide/hydroxide surface studied in Section 5.3.2) to compete with **10** for the surface sites, when co-adsorbed from methanol/water onto the iron(III) oxide/hydroxide surface, goethite, was also tested. This allowed us to rank the binding affinities of ligands **5** and **7** for the iron(III) oxide/hydroxide surface. A strong competitor will bind preferentially to the goethite surface over ligand **10**, resulting in a lower concentration of **10** on the surface.

The experiment is identical to the adsorption isotherms described previously, but a fixed amount of the competing ligands of quantities corresponding approximately to the highest molar concentration of ligand **10** used in the isotherm were added (see Section 5.8.8).

The isotherm for ligand **10** (Figure 5.29, black data) indicates a high affinity of this ligand for the iron(III) oxide/hydroxide surface. The more effective competitor is **7** as this depresses the isotherm of ligand **10** more significantly, reducing the surface coverage of ligand **10** onto goethite. Although both ligands bind very strongly. As a result of these data, the conclusion can be made that the substitution of the phenyl ring for a smaller group, as a methyl group, allows a better disposition of the molecules on the surface, generating a higher surface coverage.

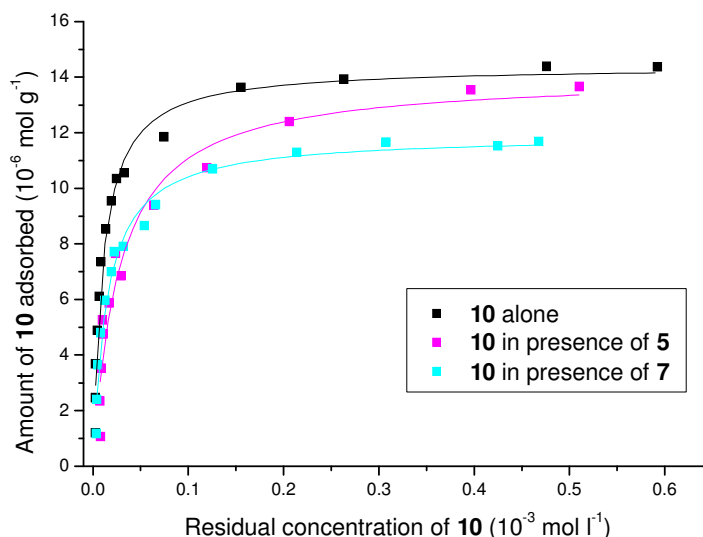


Figure 5.29. Adsorption isotherms of **10** showing the competitive binding of **5** and **7** relative to **10** onto goethite in methanol/water (95:5 v/v) at 25°C.

5.6. CONCLUSIONS

The research in this chapter has confirmed that the commercial collector agents, hydroxamates, bind strongly to iron(III) oxide surfaces.

Benzohydroxamic acid, **5**, was selected for study by adsorption isotherm measurement initially as it has strong UV-Vis chromophore. As it is a known chelating agent⁴ it was not expected to bind strongly to goethite but, instead iron sequestration into solution would be favoured. Strong binding at goethite was observed and consequently models for surface binding were investigated. The X-ray structures of $[\text{Fe}(\text{bha})_3]$, and the dinuclear complex, $[\text{Fe}_2(\mu_2\text{-bha})_2(\text{bha})_2\text{Br}_2]$ were obtained. The dimer is the first polynuclear complex in which hydroxamate bridges two iron(III) centres that has been fully characterized. Its isolation proves that hydroxamates can function in a bridging mode and support the hypothesis that multisite attachment to oxide surfaces is possible.

Different packing arrangements of hydroxamate ligands on oxide surfaces showing multisite attachment can be proposed. To compare the validity of these models adsorption isotherm studies with different hydroxamate derivatives were undertaken.

The availability of the N-OH oxygen to bind to the surface proved to be very important, as very weak binding on goethite was observed with ligand **9**, which contains an N-OMe group.

Increasing the bulk either on the nitrogen atom of the hydroxamate moiety or on the phenyl ring decreased the strength of binding to goethite. Competitive binding studies also showed this feature when the tail phenyl ring is substituted by a smaller methyl group.

In all cases binding to silica was weak, as desired, in order not to collect waste material during the froth flotation process. The work described above proves the ability of hydroxamates to show multisite attachment on iron(III)oxide/hydroxide surfaces and encouraged us to include hydroxamates as co-collectors in flotation tests (Chapter 7).

5.7. EXPERIMENTAL

5.7.1. INSTRUMENTATION

Refer to Section 4.5.1 for general instrumentation used. Inductively coupled plasma optical emission spectroscopy (ICP-OES) analysis measurements were obtained on aqueous samples using a Perkin-Elmer Optima 5300 DV. Data was processed using the software programme, WinLab32 for ICP-OES, version 3.0.0.0103, 2004. Fast atom bombardment (FAB) mass spectrometry was performed on a Kratos MS50TS machine using a 3-nitrobenzyl alcohol (NOBA) or thioglycol

matrix. Elemental analysis for C, H and N content were obtained on a CE-440 elemental analyzer. Magnetic data was fitted using the program MAGPACK.⁴⁶

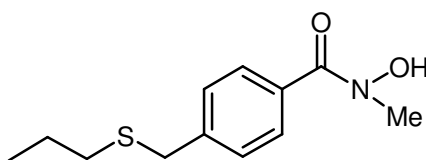
5.7.2. SOLVENTS AND REAGENTS

General information on solvents and reagents is given in Section 2.5.2. All commercially available materials were used as received from Aldrich, AlfaAesar, and Fisher.

5.7.3. LIGAND SYNTHESIS

Benzohydroxamic acid **5** and salicylhydroxamic acid **6** were supplied by AlfaAesar. Acetohydroxamic acid **7** was obtained from Acros. Benzothiazol-2-ylthio-succinic acid (Irgacor 252 LD[®]) **10** was provided by Ciba Specialties.

SYNTHESIS OF LIGAND 8



1) Synthesis of 4-(propylthiomethyl)benzoic acid

To a suspension of 60% sodium hydride in paraffin oil (1.86 g, 46.6 mmol) in tetrahydrofuran (100 ml) was added propanethiol (5.31 g, 69.8 mmol) and the mixture was stirred until the evolution of hydrogen had ceased. To the resulting white suspension was added a solution of 4-(bromomethyl)benzoic acid (5.0 g, 23.3 mmol) in tetrahydrofuran (50 ml) and the reaction mixture was refluxed for 1 hour. Methanol (100 ml) was added to dissolve the solid and the solution was refluxed for a further 16 hours. The reaction mixture was cooled and concentrated hydrochloric

acid (5 ml) was added before being adsorbed onto silica gel and the solvent evaporated. The resulting solids were loaded onto a silica gel column which was eluted with 0% to 5% methanol/dichloromethane to give 4-(propylthiomethyl)benzoic acid as a white solid (4.5 g, 92%). ^1H NMR (250.1 MHz, CDCl_3) δ 11.71 (br s, 1H, OH), 8.07 (AA'XX', 2H, ArH *ortho* to the carboxylic acid), 7.42 (AA'XX', 2H, ArH *ortho* to the propylthiomethyl group), 3.75 (s, 2H, CH_2Ar), 2.40 (t, $J = 7$ Hz, 2H, SCH_2CH_2), 1.58 (m, 2H, SCH_2CH_2), 0.96 (t, $J = 7$ Hz, 3H, CH_3). ^{13}C NMR (62.9 MHz, CDCl_3) δ 172.1, 145.2, 130.4, 128.9, 127.9, 36.0, 33.5, 22.5, 13.4. MS (FAB, +ve) m/z 211.1 $[\text{M}+\text{H}]^+$.

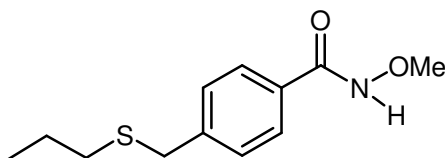
2) Synthesis of 8: *N*-hydroxy-*N*-methyl-4-propylthiomethyl-benzamide

To a solution of 4-(propylthiomethyl)benzoic acid (4.21 g, 20.0 mmol) (see Section 5.7.3, 1) in chloroform (100 ml) was added oxalyl chloride (3.0 ml, 36.0 mmol) plus a drop of DMF and the mixture was heated at 60°C for 2 hours. The solvent was removed under reduced pressure and chloroform (50 ml) was added and again removed. This process was repeated and the resulting residue was placed under high vacuum.

The preparation follows the method of Coates *et al.*⁴⁷ A solution of *N*-methylhydroxylamine (0.146 g, 1.75 mmol) in water was added to a solution of Na_2CO_3 (0.214 g, 2.02 mmol) in 10 ml of water. The resultant solution was covered with 5 ml of ether. The mixture was stirred and cooled in an ice-bath, as 4-(propylthiomethyl)benzoyl chloride earlier prepared (0.40 g, 1.75 mmol) and previously dissolved in 5 ml of ether, was added dropwise. After stirring and cooling for additional 45 minutes, 4.5 ml of 20% NaOH were added. The aqueous layer was neutralized to pH 7 with 6M HCl and extracted five times with chloroform. The organic layer was dried with MgSO_4 , filtered and evaporated under reduced pressure leaving a pale yellow viscous solid in 86 % yield. ^1H -NMR (250.1 MHz, CDCl_3) δ 7.40 (d, 2H, ArH *ortho* to the amide group), 7.30 (d, 2H, ArH *ortho* to the propylthiomethyl group), 3.65 (s, 2H, CH_2Ar), 3.35 (s, 3H, NCH_3), 2.30 (t, $J = 7$ Hz, 2H, SCH_2CH_2), 1.50 (m, 2H, SCH_2CH_2), 0.90 (t, $J = 7$ Hz, 3H, CH_3). ^{13}C -NMR

(62.9 MHz, CDCl₃) δ 166.3, 141.1, 130.0, 128.1, 127.8, 37.4, 34.9, 32.5, 21.5, 12.4. MS (FAB, +ve) m/z 240.0 [M+H]⁺. Elemental analysis for C₁₂H₁₇NO₂S: Calc.: C, 60.22 %; H, 7.16 %; N, 5.85 %. Found: C, 60.25 %; H, 7.27 %; N, 5.53 %.

SYNTHESIS OF LIGAND 9



To a solution of 4-(propylthiomethyl)benzoic acid (4.21 g, 20.0 mmol) (see Section 5.7.3, 1) in chloroform (100 ml) was added oxalyl chloride (3.0 ml, 36.0 mmol) plus a drop of DMF and the mixture was heated at 60°C for 2 hours. The solvent was removed under reduced pressure and chloroform (50 ml) was added and again removed. This process was repeated and the resulting residue was placed under high vacuum. The residue was dissolved in ethyl acetate (150 ml) and a mixture of *O*-methylhydroxylamine hydrochloride (2.01 g, 24.0 mmol) and potassium carbonate (6.91 g, 50.0 mmol) in water (100 ml) was added and the two phases were intimately stirred for 16 hours. The organic layer was separated and the aqueous phase was extracted with ethyl acetate (2 x 50 ml). The combined organic layers were evaporated and the residue was chromatographed eluting with 0% to 3% methanol/dichloromethane. The resulting white solid (3.4 g) was recrystallised from diethyl ether to give *N*-methoxy-4-propylthiomethyl-benzamide as colourless crystals. Yield (2.2 g, 46 %). ¹H NMR (250.1 MHz, CDCl₃) δ 9.11 (br s, 1H, NH), 7.69 (d, J = 8 Hz, 2H, ArH *ortho* to the amide group), 7.36 (d, J = 8 Hz, 2H, ArH *ortho* to the propylthiomethyl group), 3.85 (s, 3H, CH₃O), 3.70 (s, 2H, CH₂Ar), 2.36 (t, J = 7 Hz, 2H, SCH₂CH₂), 1.56 (m, 2H, SCH₂CH₂), 0.93 (t, J = 7 Hz, 3H, CH₃). ¹³C NMR (62.9 MHz, CDCl₃) δ 166.3, 143.3, 130.3, 129.1, 127.3, 64.5, 35.9, 33.5, 22.4, 13.4. MS (ES, +ve) m/z 240.0 [M+H]⁺. Elemental analysis for C₁₂H₁₇NO₂S: Calc.: C, 60.22 %; H, 7.16 %; N, 5.85 %. Found: C, 60.40 %; H, 6.99 %; N, 5.79 %.

5.7.4. SYNTHESIS OF THE COMPLEX $[Fe(bha)_3] \cdot 1.5MeOH$ (5a)

$FeCl_3$ (0.250 g, 1.54 mmol), $NaOOCPh$ (0.444 g, 3.08 mmol), $NaOMe$ (0.166 g, 3.08 mmol) and $bhaH$ (ligand **5**) (0.211 g, 1.54 mmol) were dissolved in methanol (20 ml) with stirring. The resultant dark orange solution was stirred overnight at room temperature and filtered. Red crystals grew upon diffusion of diethyl ether during 3 weeks. Yield 17 %. This complex can also be prepared from $FeBr_2$ (0.300 g, 1.39 mmol), $NaOOCPh$ (0.400 g, 2.78 mmol), $bhaH$ (ligand **5**) (0.191 g, 1.39 mmol) dissolved in methanol (20 ml) with stirring. The solution was stirred overnight and filtered. Diffusion of diethyl ether into the solution gave orange crystals after 3 weeks.

5.7.5. SYNTHESIS OF THE COMPLEX $[Fe_2(\mu_2-bha)_2(bha)_2Br_2]$ (5b)

$FeBr_2$ (0.300 g, 1.39 mmol), $NaOOCPh$ (0.200 g, 1.39 mmol) and $bhaH$ (ligand **5**) (0.191 g, 1.39 mmol) were dissolved in methanol (20 ml) with stirring. The resulting purple solution was stirred overnight at room temperature, after which a purple precipitate was obtained and removed by filtration. Layering of the filtrate with diethyl ether gave black crystals of **5b**, $[Fe_2(\mu_2-bha)_2(bha)_2Br_2]$, after 4-5 weeks. Yield 5 %. Elemental analysis for $C_{28}H_{24}Br_2Fe_2N_4O_8$: C, 41.21 %; H, 2.96 %; N, 6.87 %. Found: C, 41.26 %; H, 3.04 %; N, 6.78 %.

5.7.6. ATTEMPTS TO SYNTHESISE POLYNUCLEAR COMPLEXES CONTAINING LIGAND 5 or 6

A similar procedure to the ones described in Sections 5.6.7 and 5.6.8 was followed to attempt the preparation of Fe(III) clusters using different combinations of reagents (Section 5.4.1).

1) Procedure for solvothermal synthesis

[NEt₄]₂[Fe₂OCl₆] (0.300 g, 0.500 mmol), NaOMe (0.054 g, 1.000 mmol), bhaH (ligand **5**) (0.068 g, 0.500 mmol) and *ca.* 7 ml of methanol were sealed in a Teflon container 150 °C for 5 h.

2) Procedure for microwave synthesis

FeBr₂ (0.100 g, 0.464 mmol), NaOMe (0.100 g, 1.856 mmol), 1,1,1-tris(hydroxymethyl)ethane (0.056 g, 0.464 mmol), tetrabutylammonium bromide (0.149 g, 0.464 mmol), bhaH (ligand **5**) (0.064 g, 0.464 mmol) and methanol (20 ml) were placed in a test tube and microwaved at 120 °C, 130 psi and 200 W.

The procedures described in paragraphs 1) and 2) illustrate what was done in all cases when these techniques were used.

5.7.7. EXTINCTION COEFFICIENT (ϵ) DETERMINATION

Section 2.5.4 provides details of the extinction coefficient determination.

5.7.8. ADSORPTION ISOTHERM MEASUREMENTS

Adsorption isotherm experiments were run as described in Section 2.5.5 (analysis done by UV-Vis spectroscopy, ligands **5** and **6**) and Section 3.4.5 (analysis done by ICP-OES, ligands **8** and **9**). Calibration standards were made up by weight and the instrument was calibrated using, 1, 15, 40, 70 and 100 ppm sulfur solutions, 1, 5 and 15 ppm iron solutions and 1, 5 and 15 ppm silicon. The iron and silicon content in solution was measured to check that degradation of the substrate had not occurred; no significant levels (< 1 ppm) were detected in the aqueous phase after adsorption experiments.

COMPETITIVE BINDING ADSORPTION ISOTHERMS

To carry out competitive binding studies the procedure was followed as described in Section 3.4.5. Adsorption isotherms of ligand **10** (1.4×10^{-3} M) on goethite were run and used as the control experiment. Further adsorption isotherms were performed according to the same experimental procedure and in addition to **10**, also in each of the tubes were added as a competitor ligand 1 ml of either ligand **5** or **7** (1.4×10^{-2} M) to ensure a final competitor concentration of 1.4×10^{-3} M.

5.8. REFERENCES

- 1 D. R. Nagaraj, *Development of New Flotation Chemicals*, 1997, **50**, 355.
- 2 D. W. Fuerstenau, *Proceedings of the International Mineral Processing*
3 *Congress, 19th, San Francisco*, 1995, **3**, 3.
- 4 K. K. Das and Pradip, *Process Technology Proceedings*, 1988, **7**, 305.
- 5 E. C. O'Brien, E. Farkas, M. J. Gil, D. Fitzgerald, A. Castineras, and K. B.
6 Nolan, *Journal of Inorganic Biochemistry*, 2000, **79**, 47.
- 7 Cytec Industries, 'Mining Chemicals Handbook', 2002.
- 8 B. Kurzak, H. Kozlowski, and E. Farkas, *Coordination Chemistry Reviews*,
9 1992, **114**, 169.
- 10 D. A. Brown, W. K. Glass, N. J. Firzpatrick, T. J. Kemp, W. Errington, G. J.
11 Clarkson, W. Haase, F. Karsten, and A. H. Mahdy, *Inorganica Chimica Acta*,
12 2005, **358**, 2454.
- 13 D. A. Brown, W. K. Glass, and S. J. C. McGardle, *Inorganica Chimica Acta*,
14 1983, **80**, 13.
- 15 C. Mulcahy, F. M. Dolgushin, K. A. Krot, D. Griffith, and C. J. Marmion,
16 *Dalton Transactions*, 2005, 1993.
- 17 I. Ekelchik, J. Gun, O. Lev, R. Shelkov, and A. Melman, *Dalton*
18 *Transactions*, 2006, 1285.
- 19 A. Vannini, C. Volpari, G. Filocamo, E. C. Casavola, M. Brunetti, D.
20 Renzoni, P. Chakravarty, C. Paolini, R. De Francesco, P. Gallinari, C.
21 Steinkuehler, and S. Di Marco, *Proceedings of the National Academy of*
22 *Sciences of the United States of America*, 2004, **101**, 15064.
- M. A. Pearson, L. O. Michel, R. P. Hausinger, and P. A. Karplus,
Biochemistry, 1997, **36**, 8164.
- D. A. Brown, D. McKeith, and W. K. Glass, *Inorganica Chimica Acta*, 1979,
35, 5.
- J. El Yazal and Y.-P. Pang, *Journal of Physical Chemistry A*, 1999, **103**,
8346.
- C. J. Marmion, T. Murphy, K. B. Nolan, and J. R. Docherty, *Chemical*
Communications, 2000, 1153.
- M. Gaspar, R. Grazina, A. Bodor, E. Farkas, and M. A. Santos, *Dalton*
Transactions, 1999, 799.
- M. A. Santos, M. Gaspar, and M. T. Amorim, *Inorganica Chimica Acta*,
1999, **284**, 20.
- C. P. Brink and A. L. Crumbliss, *Inorganic Chemistry*, 1984, **23**, 4708.
- C. J. Marmion, D. Griffith, and K. B. Nolan, *European Journal of Inorganic*
Chemistry, 2004, 3003.
- R. J. Bergeron, J. Wiegand, J. S. McManis, W. R. Weimar, and G. Huang,
Advances in Experimental Medicine and Biology, 2002, **509**, 167.
- K. J. Wallace, M. Gray, Z. Zhong, V. M. Lynch, and E. V. Anslyn, *Dalton*
Transactions, 2005, 2436.
- W. R. Harris, C. J. Carrano, S. R. Cooper, S. R. Sofen, A. E. Avdeef, J. V.
McArdle, and K. N. Raymond, *Journal of the American Chemical Society*,
1979, **101**, 6097.

- 23 F. Baroncelli and G. Grossi, *Journal of Inorganic and Nuclear Chemistry*,
1965, **27**, 1085.
- 24 D. A. Brown, K. M. Herlihy, and S. K. O'Shea, *Inorganic Chemistry*, 1999,
38, 5198.
- 25 J. Leong and K. N. Raymond, *Journal of the American Chemical Society*,
1974, **96**, 6628.
- 26 J. Leong and K. N. Raymond, *Journal of the American Chemical Society*,
1974, **96**, 1757.
- 27 H. J. Lindner and S. Goettlicher, *Acta Crystallographica, Section B:*
Structural Crystallography and Crystal Chemistry, 1969, **25**, 832.
- 28 C. J. Marmion, T. Murphy, Z. Starikova, and K. B. Nolan, *Acta*
Crystallographica, Section C: Crystal Structure Communications, 2000, **C56**,
E491.
- 29 T. W. Failes and T. W. Hambley, *Australian Journal of Chemistry*, 2000, **53**,
879.
- 30 A. Dietrich, K. A. Fidelis, D. R. Powell, D. Vander Helm, and D. L. Eng-
Wilmot, *Dalton Transactions*, 1991, 231.
- 31 J. Comiskey, E. Farkas, K. A. Krot-Lacina, R. G. Pritchard, C. A. McAuliffe,
and K. B. Nolan, *Dalton Transactions*, 2003, 4243.
- 32 T. W. Failes, M. D. Hall, and T. W. Hambley, *Dalton Transactions*, 2003,
1596.
- 33 M. D. Hall, T. W. Failes, D. E. Hibbs, and T. W. Hambley, *Inorganic*
chemistry, 2002, **41**, 1223.
- 34 D. A. Brown, W. Errington, W. K. Glass, W. Haase, T. J. Kemp, H. Nimir, S.
M. Ostrovsky, and R. Werner, *Inorganic chemistry*, 2001, **40**, 5962.
- 35 M. Arnold, D. A. Brown, O. Deeg, W. Errington, W. Haase, K. Herlihy, T. J.
Kemp, H. Nimir, and R. Werner, *Inorganic Chemistry*, 1998, **37**, 2920.
- 36 D. A. Brown, W. Errington, N. J. Fitzpatrick, W. K. Glass, T. J. Kemp, H.
Nimir, and A. T. Ryan, *Chemical Communications*, 2002, 1210.
- 37 M. A. Holmes and B. W. Matthews, *Biochemistry*, 1981, **20**, 6912.
- 38 D. M. Low, L. F. Jones, A. Bell, E. K. Brechin, T. Mallah, E. Riviere, S. J.
Teat, and E. J. L. McInnes, *Angewandte Chemie, International Edition*, 2003,
42, 3781.
- 39 C. J. Millos, A. G. Whittaker, and E. K. Brechin, *Polyhedron*, 2007, **26**, 1927.
- 40 D. A. Brown and A. L. Roche, *Inorganic Chemistry*, 1983, **22**, 2199.
- 41 D. A. Brown, D. McKeith, and W. K. Glass, *Inorganica Chimica Acta*, 1979,
35, 57.
- 42 M. Frey, S. G. Harris, J. M. Holmes, D. A. Nation, S. Parsons, P. A. Tasker,
S. J. Teat, and R. E. P. Winpenny, *Angewandte Chemie, International*
Edition, 1998, **37**, 3246.
- 43 M. Frey, S. G. Harris, J. M. Holmes, D. A. Nation, S. Parsons, P. A. Tasker,
and R. E. P. Winpenny, *Chemistry-A European Journal*, 2000, **6**, 1407.
- 44 F. J. White, 'PhD work in progress', University of Edinburgh, 2007.
- 45 D. A. Nation, 'Unpublished work', University of Edinburgh, 2003.
- 46 J. J. Borrás-Almenar, J. M. Clemente-Juan, E. Coronado, and B. S.
Tsukerblat, *Inorganic Chemistry*, 1999, **38**, 6081.
- 47 R. M. Coates and S. J. Firsan, *Journal of Organic Chemistry*, 1986, **51**, 5198.

Chapter 6

Surface binding studies of phosphonic acids

CONTENTS

6.1. Introduction	132
6.1.1. Outline.....	132
6.1.2. Background	132
6.1.3. Phosphonic acids as passivating agents	132
6.2. Surface binding studies by adsorption isotherms.....	134
6.3. Conclusions	139
6.4. Experimental	140
6.4.1. Instrumentation	140
6.4.2. Solvents and reagents.....	140
6.4.3. Ligands	140
6.4.4. Adsorption isotherm measurements.....	140
6.5. References	141

6.1. INTRODUCTION

6.1.1. OUTLINE

The strength of binding of a series of phosphonic acids is explored in this chapter. Background information concerning their applications and earlier studies is given below.

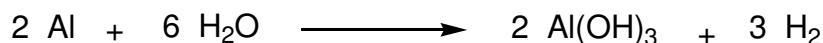
6.1.2. BACKGROUND

The range of phosphonic acids studied in this thesis was used by other members of the Tasker group in various research projects investigating their binding properties onto aluminium trihydroxide [Al(OH)₃] and on iron oxide surfaces in aqueous media in all cases.¹⁻³ Phosphonic acids show strong binding to such systems. Portet *et al.*⁴ report the use of phosphonic acids as a coating for colloidal iron oxide particles. Based on the data generated by other members of the group, it was decided to investigate their uptake on goethite and silica surfaces from methanol/water (95:5 v/v) and whether these ligands would have a positive effect in recovering oxidized material in froth flotation processes.

6.1.3. PHOSPHONIC ACIDS AS PASSIVATING AGENTS

Environmental issues and the fact that chromium(VI) is known to be very toxic and carcinogenic⁵ make necessary the replacement of chromates constituting the solvent-based paints by water-borne systems.⁶ Organic coatings have proved to be an effective alternative in preventing corrosion. They should not allow water, ions and oxygen to pass through. Additionally, they must provide passivating properties to prevent surface oxidation when in contact with water.

Aluminium flake pigments are used to achieve sheen in metallic paints used in the automobile industry.⁷ Due to the reactivity of aluminium with water a necessary condition for a noble water-borne coating is low hydrogen gas generation.³ A passivating agent, currently involving chromates, is added to avoid flake degradation and hydrogen evolution.



A variety of *mono*- and *di*-phosphonic acids were studied at Edinburgh as passivating agents for aluminium.³ These studies involved the comparison of strength of binding of phosphonic acids to aluminium trihydroxide [Al(OH)₃] (ATH) and suppression of hydrogen evolution. The approach followed the one used in the development of corrosion inhibitors for iron⁸ (see Section 2.1.4). It was based on information obtained from previous studies to improve the wet fastness of water-borne dyes in an ink formulation on aluminium oxyhydroxide coated papers^{1,2} where it was concluded that phosphonate-functionalised dyes bind more strongly to ATH than carboxylates and sulfonates.

In this study to develop new benign passivating agents for aluminium,³ it was demonstrated that a combination of strong binding of the phosphonic acid ligands to the ATH surface and hydrophobicity, provided by the pendant group, were necessary conditions for good passivating performance. Of the phosphonic acids tested the most efficient passivating agents were those with long hydrophobic chains (Figure 6.1).

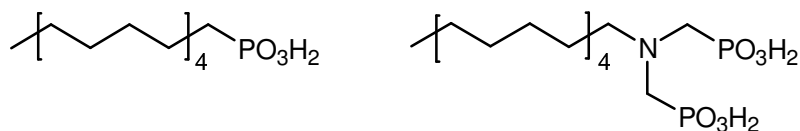


Figure 6.1. Structures of the phosphonic acids that showed the most efficient passivating abilities.³ [The structure of these compounds are incorrectly displayed in reference 3].

6.2. SURFACE BINDING STUDIES BY ADSORPTION ISOTHERMS

Adsorption isotherm measurements to study the binding of ligands **11** - **17** (Figure 6.2) onto goethite and silica were run following the procedures described in Section 3.4.5. Only two of the ligands, **11** and **14**, were used in isotherm experiments on silica to confirm weak binding.

In this chapter ICP-OES was used to determine the concentration of the different ligands remaining in solution by analysis of phosphorus content.

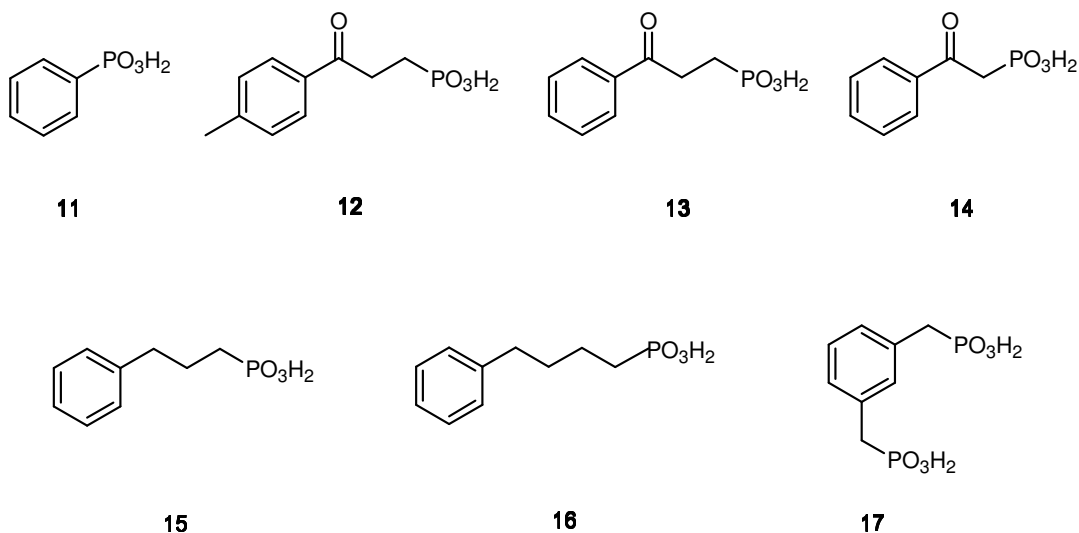


Figure 6.2. Ligands **11** - **17** studied in this chapter.

A source of error in the analysis of phosphonic acids by ICP-OES may be due to the impossibility of using the solvent system in which the adsorption isotherms were run (methanol/water (95:5 v/v)) as the ICP-OES torch does not ignite in the presence of methanol. As a consequence, it was necessary to remove the solvent and make up the solutions with water to the previous volume (Section 3.4.5). This may have introduced certain error in the analyses and could also be the reason why no good adsorption isotherm points for **17** were obtained.

Curve fitting of adsorption isotherm data for phosphonic acids presented difficulties because of the strong uptake of these ligands at low concentrations which caused values of ligand remaining in solution to be close to zero. Consequently large errors are associated with curve fitting in this region needed to obtain the binding constants (Table 6.5). This is clearly illustrated by comparing the plots for **12** and **13** shown in Figure 6.3. The initial slopes for these plots should be very similar but the curve fitting procedures in Origin (Section 6.4.1) generate very different curves and the calculated adsorption constants are approximately one order of magnitude different, $50(20) \times 10^3$ and $6(5) \times 10^3$ respectively. Nevertheless it is clear that binding constants for goethite are consistently higher than most of the other ligands studied in this thesis.

Ligands **12**, **13** and **14** [$44(3) \times 10^{-6}$, $48(7) \times 10^{-6}$ and $43(3) \times 10^{-6}$] reach a similar surface coverage (Figure 6.3, Table 6.5) and these values are slightly higher than **11**, [$35(4) \times 10^{-6}$]. The higher surface coverage reached by **12**, **13** and **14** could be due to the presence of the 3-keto group in these three ligands allowing intramolecular H-bonding interactions between ligands to form a better packing arrangement.

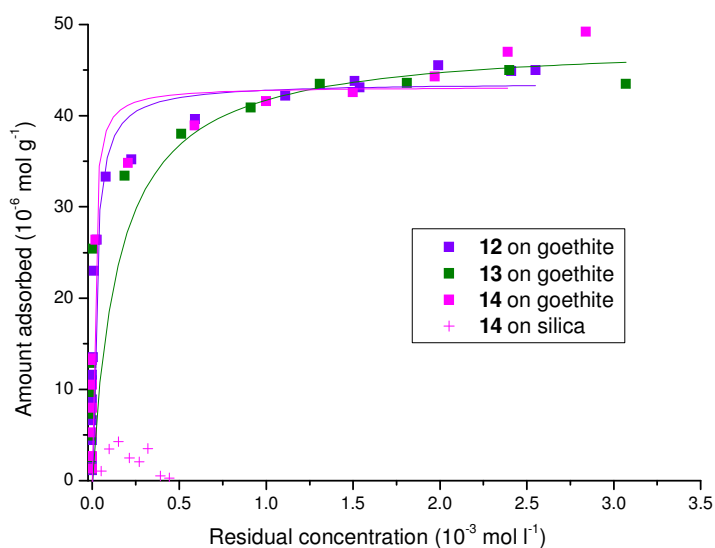


Figure 6.3. Isotherms comparing the binding to goethite and silica of the phosphonic acids **12**, **13** and **14** in methanol/water (95:5 v/v) at 25°C.

Ligands **15** and **16** (Figure 6.4, Table 6.5) show higher surface coverage than **11** but the statistical significance of the data are questionable. This may occur due to stabilising interactions between the alkyl chains in the tail groups.

11 and **14** show weak binding to silica as required in order not to collect any siliceous waste materials during froth flotation processes.

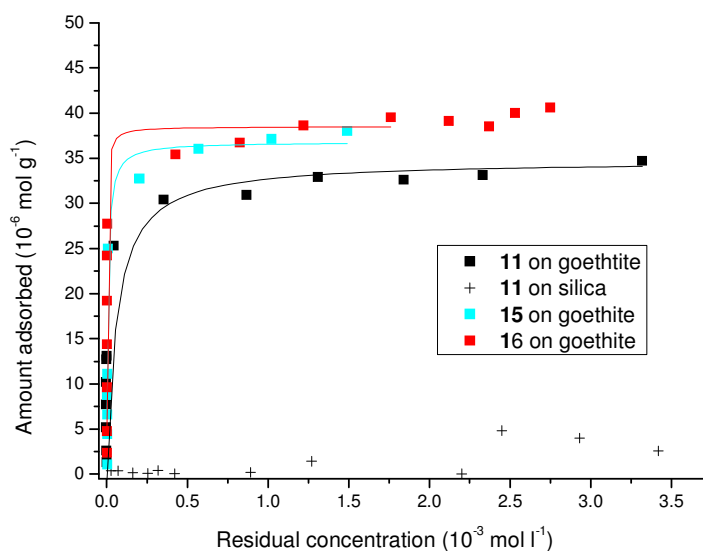


Figure 6.4. Isotherms comparing the binding to goethite and silica of the phosphonic acids **11**, **15** and **16** in methanol/water (95:5 v/v) at 25 °C.

Ligand	Surface coverage ($10^{-6} \text{ mol g}^{-1}$)	Required surface area ($\text{\AA}^2 \text{ molecule}^{-1}$)
11	35(4)	110(10)
12	44(3)	86(5)
13	48(7)	80(10)
14	43(3)	90(5)
15	40(2)	100(6)
16	40(3)	100(6)

Table 6.5. Adsorption isotherm data for ligand **11**, **12**, **13**, **14**, **15** and **16** (errors in parentheses) on goethite. For definitions of surface coverage, required surface area and their determination see Section 1.6.1.*

Phosphonic acids were studied in different systems earlier in the group.⁹⁻¹¹ The substrates used previously were ATH (aluminium trihydroxide) and goethite, and the solvent was always water.

It was observed⁹ that phosphonic acids show considerably steeper initial slopes and higher binding constants on goethite than on ATH, when using water as a solvent. The adsorption isotherm data for phosphonic acids obtained in this work with methanol/water (95:5 v/v) as the solvent system also shows significantly higher surface coverage values on goethite.

A reason for the weaker binding observed in water may be due to pH influence as similar tendencies were observed in Edinburgh before.⁹ In adsorption isotherm experiments of phosphonic acids in water the pH was adjusted⁹ to *ca.* 8 prior to isotherm analysis to enhance the solubility of these ligands. With their double deprotonation at basic pH the surface coverage dropped to about a quarter of the value observed with no pH adjustment (Figure 6.7). It was suggested⁹ that the double deprotonation of the phosphonate groups generates electrostatic repulsion

* The equilibrium adsorption constants calculated by the poor curve fitting procedures are **11**, $16(15) \times 10^3$; **12**, $50(20) \times 10^3$; **13**, $6(5) \times 10^3$; **14**, $100(70) \times 10^3$; **15**, $140(40) \times 10^3$; **16**, $500(200) \times 10^3$.

increasing P-O⁻·····O-P contact distances and as a consequence the surface coverage fell. At lower pH (3) the phosphonate group is expected to be only singly deprotonated. P-O-H·····O-P hydrogen bonding contacts optimize packing arrangements, although P-O⁻·····O-P repulsions are also present.

As a consequence, the higher surface coverage values of approximately $4.1 \times 10^{-5} \text{ mol g}^{-1}$ observed in this work should be expected when compared to the surface coverage of phosphonic acids on goethite in water with pH adjustment ($1.0 \times 10^{-5} \text{ mol g}^{-1}$).⁹

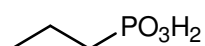


Figure 6.6. Structure of propylphosphonic acid.

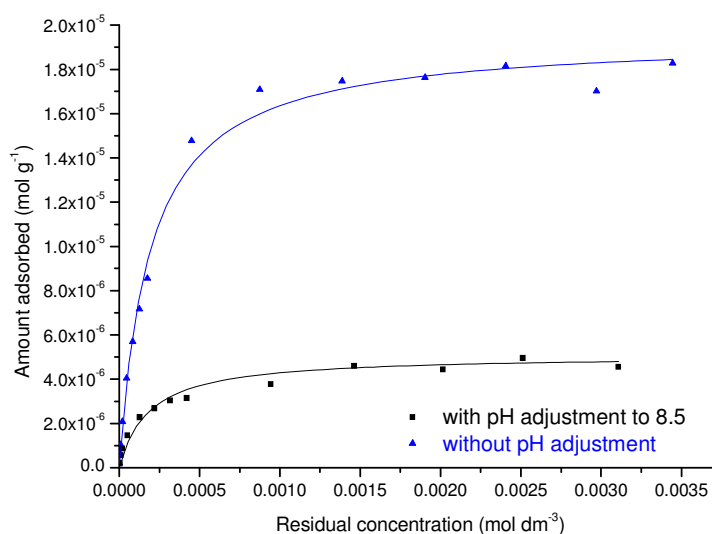


Figure 6.7. The uptake of propylphosphonic acid on ATH, in water, with and without pH adjustment (ca. pH 8.5 and 3), 25 °C.⁹

In Figure 6.8 a comparison between **12** and its carboxylic acid analogue, **1**, (see Section 2.3) is shown, illustrating the significantly stronger binding and surface coverage of the phosphonic acid on goethite.

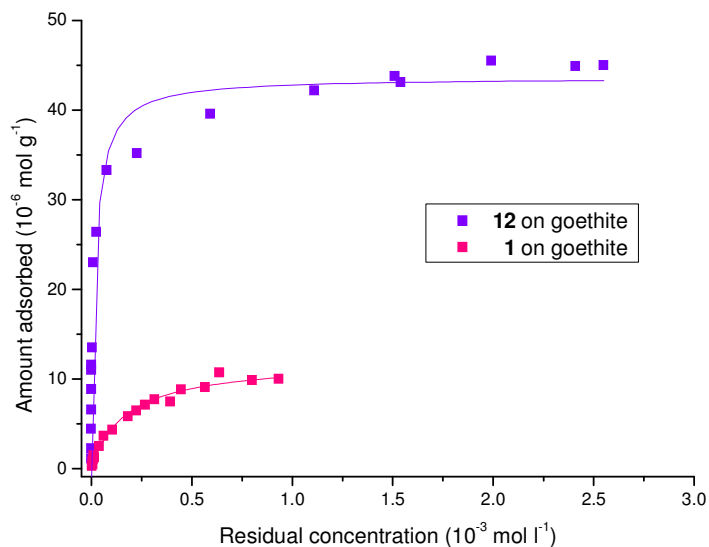


Figure 6.8. Isotherms showing the binding to goethite of the carboxylic acid **1** and its phosphonic acid analogue **12** in methanol/water (95:5 v/v) at 25°C.

6.3. CONCLUSIONS

The phosphonic acids investigated in this chapter all showed very strong binding to goethite and weak binding to silica, as desired, and consequently it was appropriate to consider using one in flotation tests (Chapter 7) to assess performance as a co-collector. As they all showed comparably strong binding to goethite, the selection of which compound to use in these tests was made on the grounds of the structural analogy of **12** to the carboxylic acid **1**. In addition, as they bind so strongly to iron(III) oxide surfaces, a very small amount of any of the phosphonic acid ligands could offer a good performance as a co-collector in froth flotation.

6.4. EXPERIMENTAL

6.4.1. INSTRUMENTATION

For general information on ICP-OES equipment refer to Section 5.7.1.

6.4.2. SOLVENTS AND REAGENTS

General information on solvents and reagents is provided in Section 2.5.2. All commercially available materials were used as received from Aldrich.

6.4.3. LIGANDS

Phenylphosphonic acid, **11**, was obtained from Aldrich. **12** and **14** were prepared by Dr D. Henderson, **13**, **15** and **16** by Dr R. Cooper³ and **17** by Dr P. Lowat,¹² at the University of Edinburgh.

6.4.4. ADSORPTION ISOTHERM MEASUREMENTS

Section 3.4.5 provides of the general adsorption isotherm procedure when using ICP-OES as the technique to determine the amount of ligand remaining in solution. Calibration standards were made up by weight and the instrument was calibrated using 1, 50, 100, 150 and 200 ppm or 1, 12, 25, 37 and 50 ppm phosphorus solutions; 1, 5 and 15 ppm iron solutions and 1, 5 and 15 ppm silicon solutions.

6.5. REFERENCES

- 1 S. S. De Silva, P. J. Camp, D. K. Henderson, D. C. R. Henry, H. McNab, P.
A. Tasker, and P. Wight, *Chemical Communications*, 2003, 1702.
- 2 R. J. Cooper, P. J. Camp, R. J. Gordon, D. K. Henderson, D. C. R. Henry, H.
McNab, S. S. De Silva, D. Tackley, P. A. Tasker, and P. Wight, *Dalton*
Transactions, 2006, 2785.
- 3 R. J. Cooper, P. J. Camp, D. K. Henderson, P. A. Lovatt, D. A. Nation, S.
Richards, and P. A. Tasker, *Dalton Transactions*, 2007, 1300.
- 4 D. Portet, B. Denizot, E. Rump, J.-J. Lejeune, and P. Jallet, *Journal of*
Colloid and Interface Science, 2001, **238**, 37.
- 5 H. J. Gibb, P. S. Lees, P. F. Pinsky, and B. C. Rooney, *American Journal of*
Industrial Medicine, 2000, **38**, 115.
- 6 B. del Amo, R. Romagnoli, C. Deya, and J. A. Gonzalez, *Progress in*
Organic Coatings, 2002, **45**, 389.
- 7 http://www.silberline.com/silberline_sll/markets/automotive/index.html.
- 8 M. Frey, S. G. Harris, J. M. Holmes, D. A. Nation, S. Parsons, P. A. Tasker,
and R. E. P. Winpenny, *Chemistry--A European Journal*, 2000, **6**, 1407.
- 9 R. J. Cooper, 'Surface Engineering of Metal Oxides Using Polynucleating
Ligands', PhD Thesis, University of Edinburgh, 2006.
- 10 S. S. De Silva, 'Dye Binding Studies on Alumina coated Surfaces', PhD
Thesis, University of Edinburgh, 2004.
- 11 D. K. Henderson, 'The Design of Ligands for Aluminium Oxy/hydroxide
Surfaces', PhD thesis, University of Edinburgh, 2001.
- 12 P. A. Lowatt, 'Synthesis of Novel Polynucleating Lignads for Lightly
Oxidised Aluminium Surfaces', Project Report, University of Edinburgh,
1998.

Chapter 7

Flotation tests of selected ligands

CONTENTS

7.1. Introduction	144
7.1.1. Outline.....	144
7.1.2. Flotation variables and performance.....	144
7.1.3. Flotation equipment and procedures	148
7.2. Performance in laboratory tests of selected ligands on different substrates	150
7.2.1. Flotation tests with Amandelbult ore (UG2 Reef).....	155
7.2.1.1. The influence of collector concentration.....	156
7.2.1.2. The influence of the air flowrate.....	158
7.2.2. Flotation tests with Kennecott ore (MZ2HE)	160
7.2.2.1. The influence of collector concentration.....	161
7.2.2.2. The influence of surface-ligating groups	163
7.2.3. Flotation tests with Palabora ore	164
7.2.3.1. The influence of surface-ligating groups	165
7.3. Conclusions	168
7.4. Experimental	169
7.4.1. Materials.....	169
7.4.2. Solvents and reagents.....	169
7.4.3. Composition of the ores	170
7.4.4. Crushing processes.....	170
7.4.5. Flotation experimental processes	171
7.4.5.1. Flotation tests with Amandelbult ore (UG2 Reef)	172
7.4.5.2. Flotation tests with Kennecott ore (MZ2HE).....	173
7.4.5.3. flotation tests with Palabora ore.....	174
7.5. References	176

7.1. INTRODUCTION

7.1.1. OUTLINE

Froth flotation experiments at laboratory scale were carried out in order to test the performance of some of the ligands studied in adsorption experiments. The main objective of this work was to establish whether a mixture of a conventional collector and one of the new ligands (co-collector) studied in Chapters 2 and 6 which were shown to bind very strongly to high surface area goethite performs better than the collectors currently used commercially. It was hoped that this would be the case because various forms of iron(III) oxides are thought to be present on the surfaces of oxidized minerals¹⁻⁴ and a blend of conventional collector and one of the new ligands (co-collector) should then be able to address both the sulfidic and oxidic areas of the mineral surfaces.

Details concerning of the equipment and procedures used are described in Section 7.4. The flotation experiments were carried out initially on a Platinum Group Metal ore (PGM) to establish a test protocol because samples of this were readily available, and afterwards, on chalcopyrite-containing ores.

7.1.2. FLOTATION VARIABLES AND PERFORMANCE

In flotation processes each mineral feed is unique and usually only a specific set of conditions and chemicals provides efficient *recovery*. Consequently even when the same valued mineral is present, e. g. chalcopyrite, systems which have worked well previously are often only useful as a starting point when developing a successful process for a new site.⁵ Also variations in crushing and grinding processes used at different sites are likely to influence the best combination of conditions required for froth flotation. Differences in the level of oxidation of the ore (Section 1.3) often result in significant differences in flotation behaviour. An outline of the basic features of froth flotation processes is given in Sections 1.3, 1.4 and 1.5.

A characteristic of mineral separations is that they are never ideal, and non valuable material (gangue) will always be found in the concentrate, and vice versa.

The air flowrate and the frother concentration are two manipulated variables. The two parameters used to express the efficiency of the flotation process are:⁵

- the **grade of the concentrate (G)** which refers to the content of the mineral(s) of value in the concentrate. It is defined by the equation:⁵

$$G = \frac{\text{mineral value in concentrate}}{\text{mass of mineral value and waste in concentrate}} \times 100 \quad (7.1)$$

- and the **recovery of valuable material (R)** which is the fraction of the mineral(s) of value contained in the feed that is recovered in the concentrate. It is given as a percentage by the equation:⁵

$$R = \frac{\text{mineral value in concentrate}}{\text{mineral value in the feed}} \times 100 \quad (7.2)$$

In metallic ores, *grades* are usually given as a percentage of metal, whilst the metal actually exists as a mineral. Consequently the maximum value of the *grade* of concentrate (G) that can be obtained cannot exceed that defined by the stoichiometric composition of the mineral. For example, for chalcopyrite (CuFeS_2) the highest concentrate would contain a maximum of 35 % of copper by weight and also a maximum of 35 % of sulfur. If the mineral is chalcocite (Cu_2S), the greatest concentrate would contain 80 % of copper and 20 % of sulfur. The metal content is directly proportional to the sulfur content in a sulfide mineral, so that in the flotation tests reported in this work the *grade* is indicated as the sulfur content given by the analyser (see Section 7.2) following the convention in the industry.

By plotting the cumulative concentrate *grade* against cumulative *recovery*, we get a curve which gives another way of describing the efficiency of the process.⁵ This curve is known as *grade/recovery* curve. It shows the fact that it is usually not

possible to achieve simultaneously high *grade* and high *recovery* and one can often be optimised at the expense of the other. Lower quantity of material is obtained when the process is run to obtain the maximum *recovery*. Typical *grade/recovery* curves ((a) and (b) in Figure 7.1) represent graphs and *recoveries* under two different operating conditions. Curve (b) reaches higher *grade* and *recovery* than curve (a) and therefore conditions in (b) would be preferred.

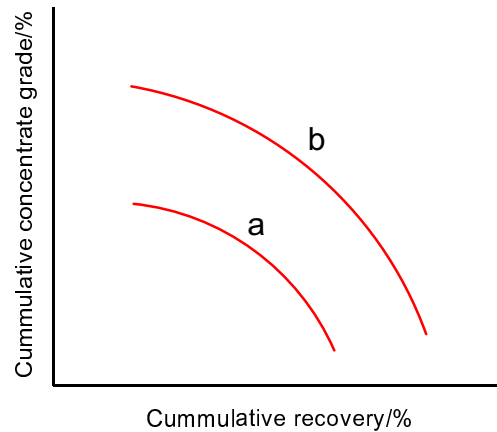


Figure 7.1. The typical form of *grade/recovery* curves.

An example where a *grade/recovery* curve is used to show the efficiency of the process is found in the work of Barbian *et al.*⁶ They studied the froth stability and structure using a froth stability column, which measures the froth rise rate and its height, as a way of determining the flotation performance. They looked at the influence of the froth structure and stability in the system by modifying the air flowrate and the frother concentration. It has been observed before⁵⁻⁷ that small bubbles entrain more water and with it more unwanted hydrophilic particles as well as hydrophobic particles. Also the air flowrate has a major impact on formation of bubbles as high aeration generates more bubbles, which leads to increase the water entrainment. In addition, it has been demonstrated that a bubble rising slowly increases the probability of the contact between hydrophobic particles of interest and bubbles.⁸ Figure 7.2 (i) shows how, under the same conditions, by decreasing the air flowrate the *grades* rise, as expected.⁶ A change in the froth behaviour is shown in

the *grade/recovery* curves in Figure 7.2 (ii). The use of a deep froth decreases the *recovery* for all flowrates. The best results are observed for low air flowrate and standard frother addition.

They found out that variations in the measured froth stability are related to flotation performance, concluding that a froth stability column can be applied at industrial scale.

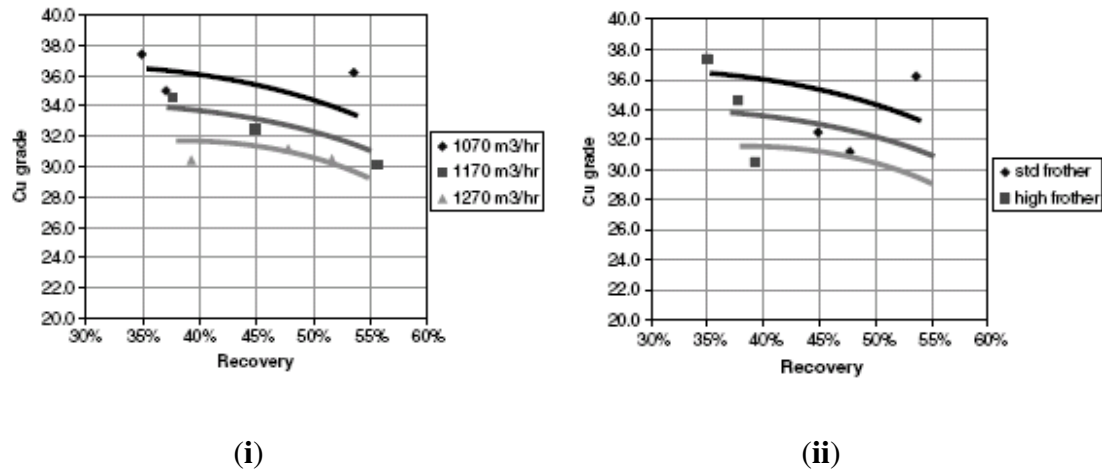


Figure 7.2. *Grade/recovery* curves showing (i) the influence of the air flowrate and (ii) the influence of frother concentration.⁶

The flotation performance can also be characterised by other parameters as

- the **water recovery (W)** in the concentrate refers to the amount of water entrained by the froth, and can also be considered as a measure of the entrainment of hydrophilic waste particles.

$$W = \frac{\text{amount of water in concentrate}}{\text{amount of water in feed}} \times 100 \quad (7.3)$$

In the case of the froth flotation tests carried out in this research work, the *recoveries* of valuable material are expressed by cumulative *recoveries* as a function of time.

7.1.3. FLOTATION EQUIPMENT AND PROCEDURES

A general description of the procedure to undertake froth flotation experiments is provided at this stage to make it easier to follow the results section. Full details are given in the experimental section, 7.4.

Froth flotation experiments were carried out in a Denver laboratory flotation machine and a specially constructed cell, designed to contain a pulp volume of approximately 1 litre, depicted in Figure 7.3. The agitator operated at a constant speed of 1500 rpm. Compressed air was introduced to the system through the cell agitator at constant pressure which is regulated by an air flowrate control system.

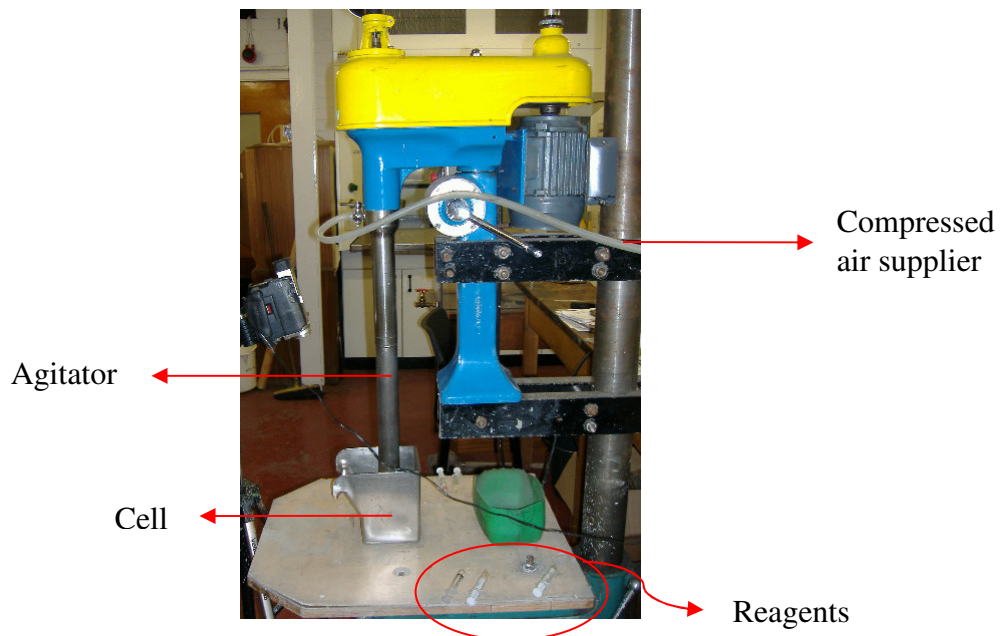


Figure 7.3. The Denver laboratory flotation machine used in the flotation tests.

The general procedure for the froth flotation experiments involved crushing the ore to a suitable size. The ore was then milled in a rod mill (Figure 7.4) for further 40 minutes in all the tests until the size distribution was 50% passing through a 75 μm screen. Several tests were carried out in order to establish the milling time required to achieve this distribution size. The time was determined to be 40 or 45 minutes depending on the ore and was kept constant for all experiments on a given

ore. 1 kg of ore was milled each time and divided in a rotary sample splitter (Figure 7.5). The specific amount of ore is put in the rotary sample splitter which spins dividing the sample into smaller fractions that fall into the different containers. This method ensures the use of representative fractions from heterogeneous mineral that are suitable for flotation tests. In most of the cases these flotation tests involved two different conditions where only the concentration of ligand added was changed.



(a)



(b)

Figure 7.4. The container and rods (a) and the rod mill (b) used in the final milling of the ores.



Figure 7.5. Rotary sample splitter.⁹

Several trials with each of the ores were carried out to establish appropriate flotation conditions. The factors considered were the amount of ore and water to place in the flotation cell, the concentration of reagents, the flotation time as well as the air flowrate to supply.

The ore was placed in the flotation cell and water, the collector, co-collectors and frother were added. The reagents used are shown in Table 7.7. The froth overflow to containers and the concentrates were collected at timed intervals. The solids were dried to determine their sulfur content.

7.2. PERFORMANCE IN LABORATORY TESTS OF SELECTED LIGANDS ON DIFFERENT SUBSTRATES

The performance in froth flotation processes at laboratory scale of five different ligands (Figure 7.6) was tested. Four of these ligands were selected on the basis of their relatively strong binding to Fe(III) oxides demonstrated in the adsorption isotherm experiments described in Chapters 2, 5 and 6:

- Of the two carboxylic acids tested in adsorption isotherms in Chapter 2, ligand **1** was chosen instead **2** as the both of them show similar binding characteristics but **1** is cheap and commercially available.
- Ligand **5** was selected among the series of hydroxamates tested in Chapter 5 because it showed the strongest binding and the highest surface coverage. Ligand **6** was also selected for flotation experiments to check the correlation of the results obtained for a same family of ligands as **6** was showed poorer binding features than **5**.

- Of the phosphonates studied earlier ligand **12** was chosen because it has a structure which is otherwise the same as the carboxylic acid **1** (all the phosphonic acids investigated in Chapter 6 show very similar binding strength).
- Ligand **18**, phenylmalonic acid, was also included in these tests because it was shown to bind strongly to Fe(III) oxides in other research work in the group at the University of Edinburgh.¹⁰ Adsorption isotherm data for ligand **18** can be found in the Appendix.

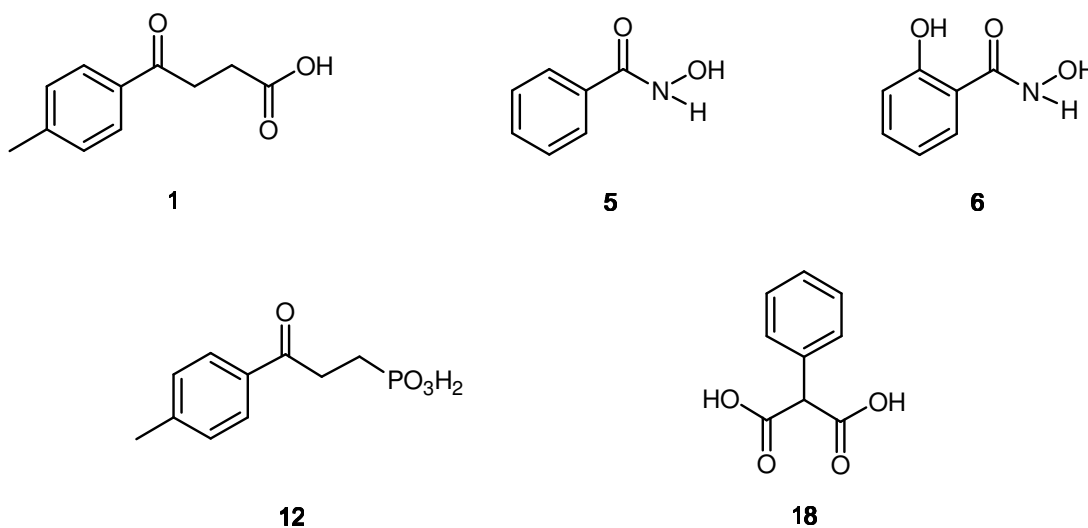


Figure 7.6. Ligands studied in froth flotation experiments.

The ligands shown in Figure 7.6 were intended to function as co-collectors, being used in conjunction with collectors (Table 7.7) which are known to address sulfidic surfaces effectively. The frothers used in the tests are also shown in Table 7.7. One platinum group metal ore and two copper ores were used.

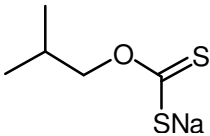
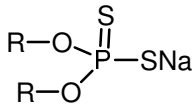
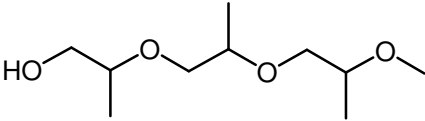
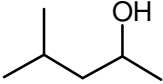
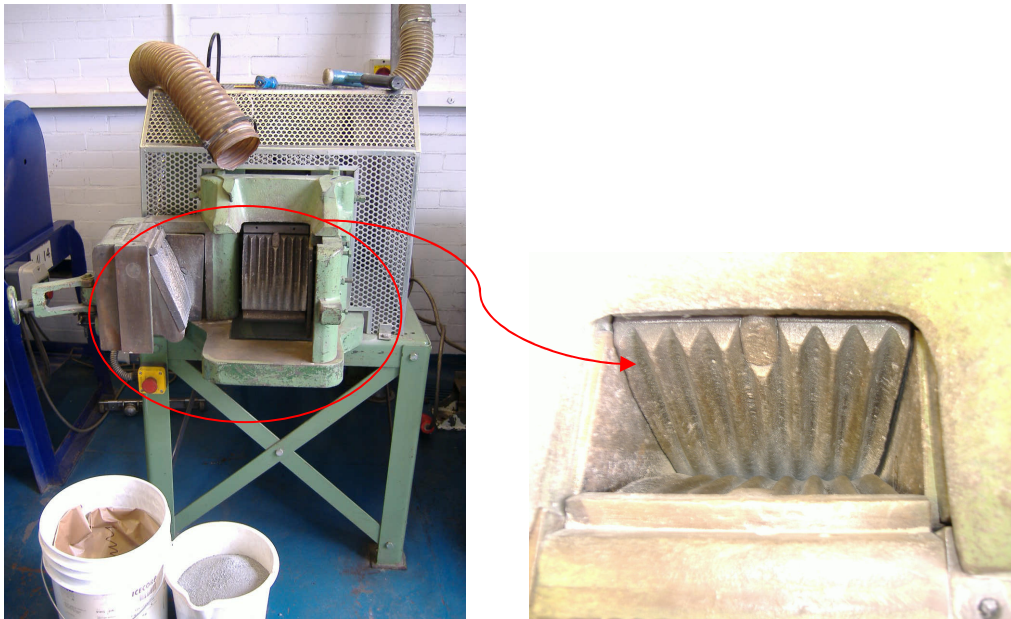
Function	Structural formula	Chemical name
Collector		Sodium isobutyl xanthate (SIBX)
		Sodium dialkyl dithiophosphate (Senkol 5)
Frother		Tripropylene glycol methyl ether (Dow 200)
		4-Methyl-2-pentanol (MIBC)

Table 7.7. Reagents used in froth flotation experiments.

The Kennecott and Palabora ores were processed in a jaw crusher (Figure 7.8) until the material passed through a 4.75 mm sieve. In order to determine the particle size distribution of the minerals, 25 to 30 kg of each of the ores were divided down into sub-samples of *ca.* 130 g using sample splitters of different sizes (Figure 7.9) to get representative fractions of the mineral. To carry out this, approximately half of the initial amount of ore, 12 – 15 kg, was divided into two fractions. A specific amount of material was passed through the sample splitter falling into two different containers, one of which was always disregarded and the other one was continuously being split until fractions of *ca.* 130 g were obtained. The same procedure was undertaken for the other half of the ore.

One of the fractions of ore of approximately 130 g was placed on the top of a series of 14 mesh sieves. These sieves were piled with their meshes ranging from 2.36 mm to <38 μm (see Figure 7.10) and were vibrated for twenty minutes. The amount of ore retained in each of the sieves was collected and weighed. The cumulative % passing each sieve was determined. This process was repeated for other sample of *ca.* 130 g coming from the other initial half of the ore.



(a)

(b)

Figure 7.8. (a) The jaw crusher used to crush the ores and (b) a close up of the jaw.



Figure 7.9. Picture of a sample splitter.⁹



Figure 7.10. The sieves used to determine the particles size distribution.

When plotting the cumulative mass passing each mesh for the two subsamples coming from the two halves of the same ore, curves overlapped indicating that samples had a homogeneous particle size distribution. The particle size distribution charts obtained for the Kennecott and the Palabora ores are shown in Figure 7.11. The different shapes of the curves are due to the different particle size distribution for each of the ores. The Kennecott ore contains coarser particles than Palabora ore. For the Kennecott ore approximately 40 % of the material had a particle size less than 1000 μm whereas 70 % passed through this mesh for the Palabora ore. This difference in the particle size distribution was not relevant to the flotation tests as prior to them, the ores were milled again in a rod mill (Figure 7.9) until 50% passed through the 75 μm mesh (see Section 7.1.3).

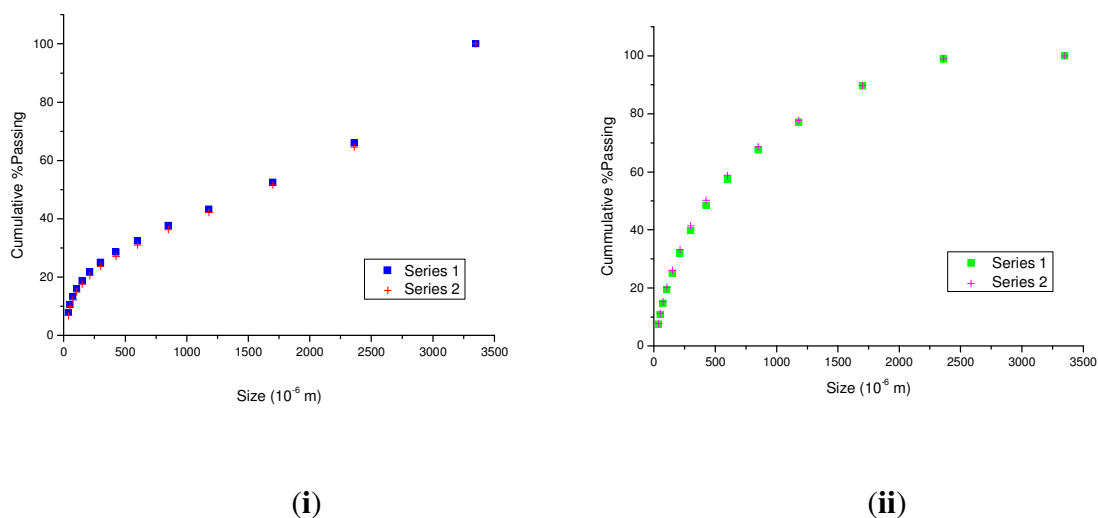


Figure 7.11. Sizing distribution charts of (i) Kennecott (MZ2HE) ore and (ii) Palabora ore.

7.2.1. FLOTATION TESTS WITH AMANDELBULT ORE (UG2 REEF)

In order to establish a basic methodology for froth flotation experiments, ligands **1**, **5**, **6**, **12** and **18** were tested on a Platinum Group Metal ore from Amandelbult (UG2 reef) in South Africa. This ore was selected because samples of this were immediately available and it took time to acquire samples and specifications of the ores which were more directly relevant to the objectives of this thesis.

The ligands in their free acid form have a low solubility in water and, as there were no “pH regulators” available in the testing laboratory which could have been used to convert the ligands to their more soluble salts, they had to be dissolved in the minimum amount of ethanol which was different for each ligand. The corresponding amount of ethanol was also added to each of the control tests (containing no ligand) to have the same conditions for all sets of experiments. As a result, the tests are not very relevant to the aims of this research work. However they were useful in helping us to understand the experimental protocols which were then

improved for use on the two more relevant minerals. The tests on Amandelbult ore highlighted the need of using water-soluble co-collectors in trials, for instance by forming a salt of the candidate ligand. Concentrates were collected after 1 and 4 minutes of flotation. The content of sulfur of the Amandelbult ore feed is 0.02 % by mass.

As described in Section 7.1.2, both the copper *grade* in the concentrate and the copper *recovery* provide an indication of performances in the flotation experiment. An ideal combination of operating parameters and reagents gives both a high *grade* and high *recovery*.

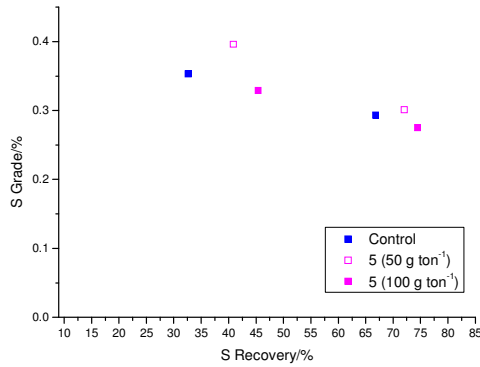
7.2.1.1. THE INFLUENCE OF COLLECTOR CONCENTRATION

Ligands **5**, **6**, **12** and **18** were tested in a series of froth flotation experiments at concentrations, which would correspond to 50 g ton⁻¹ or 100 g ton⁻¹, and results were compared with a control with no ligand added. A depressant was added to avoid natural hydrophobic particles in the ore being floated instead of the mineral of interest. In the control experiments the same amount of ethanol which was needed to dissolve a particular ligand was added to match the conditions used for a particular ligand (co-collector) (see Section 7.4.5.1). Comparisons of the control for a specific ligand and flotation experiments at two different concentrations are made in the four graphs shown in Figure 7.12.

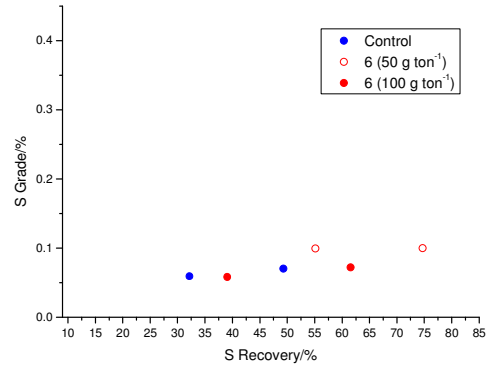
It was not possible to carry out tests on ligand **1** as a large amount of ethanol was needed to prepare a solution H₂O/EtOH. This is inconvenient in flotation experiments because of the frothing properties of alcohols^{5, 11} that causes more hydrophilic particles (wastes) to be entrained with the froth.

The best performance of ligand **5** was seen at the lower concentration (50 g ton⁻¹) giving 0.4 % *grade* and 74 % *recovery* (Figure 7.12, Table 7.13). This ligand at high concentration offers results similar to the ones of the control test.

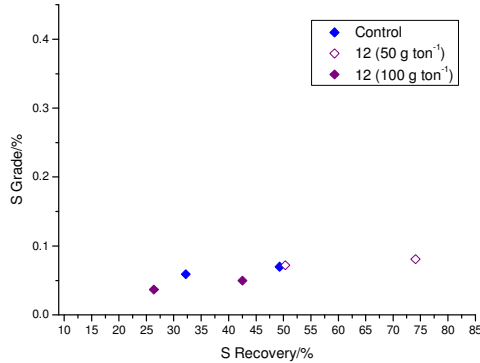
The comparison of the *grade/recovery* curves for Amandelbult ore for ligands **5**, **6**, **12** and **18** tested at two different concentrations shows that, in general, it is unnecessary to use a high concentration of a ligand to get a better performance. At low concentration (50 g ton^{-1}), ligand **5** improves both the *grade* and the *recovery* compared to the control. Whilst ligands **6** and **12**, improve just the *recovery* relative to the control.



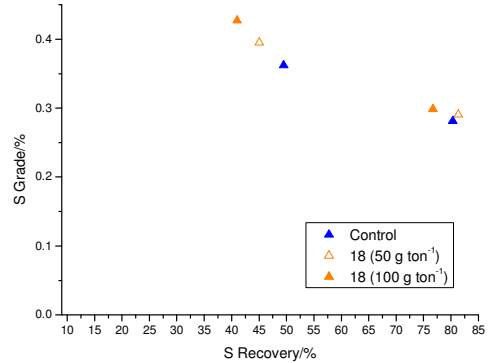
(Ligand 5)



(Ligand 6)



(Ligand 12)



(Ligand 18)

Figure 7.12. *Grade/Recovery* curves for the control tests and ligands **5**, **6**, **12** and **18** at two different concentrations, 50 g ton^{-1} and 100 g ton^{-1} , and an airflow rate of 6 l min^{-1} , with Amandelbult ore (concentrates collected after 1 and 4 minutes of flotation).

Ligand (conc. in g ton ⁻¹)	Grade ^a at collection times (min)		Recovery ^b at collection times (min)		Solids Recovery ^c at collection times (min)		
	1	4	1	4	1	4	
5	-	0.35	0.29	32.7	66.8	1.85	4.56
	(50)	0.40	0.30	40.9	72.1	2.07	4.79
	(100)	0.33	0.28	45.4	74.5	2.76	5.42
6	-	0.06	0.07	32.2	49.3	10.9	14.1
	(50)	0.10	0.10	55.2	74.7	11.1	15.0
	(100)	0.06	0.07	39.1	61.6	13.5	17.1
12	-	0.06	0.07	32.2	49.3	10.9	14.1
	(50)	0.07	0.08	50.4	74.1	14.0	18.3
	(100)	0.04	0.05	26.4	42.5	14.3	17.1
18	-	0.36	0.28	49.5	80.3	2.74	5.71
	(50)	0.40	0.29	45.0	81.3	2.28	5.60
	(100)	0.43	0.30	41.0	76.7	1.92	5.14

Table 7.13. Grade, recoveries and solids recoveries for flotation of Amandelbult ore using ligands **5**, **6**, **12** and **18** as co-collectors.^d

^a Grades are recorded as a percentage of the mineral(s) of value found in the concentrate.

^b Recoveries are recorded as a percentage of the mineral value in the feed that is recovered in the concentrate.

^c Solids recoveries are recorded as a percentage of the total amount of solids recovered in relation to the total mineral mass.

^d SIBX and SENKOL 5 were added at 50 g ton⁻¹ in all cases.

7.2.1.2. THE INFLUENCE OF THE AIR FLOWRATE

As discussed previously (Section 7.1.2), the air flowrate is an important variable in defining the efficiency of a flotation process and often needs to be optimised for each mineral supplied.⁵

Two different air flowrates, 2 and 6 l min⁻¹, were used in flotation tests with ligand **12** on the Amandelbult ore. Control tests were also carried out for these air flowrates. The control test at 2 l min⁻¹ reached 0.15 % grade and 47 % recovery (Figure 7.14, Table 7.15). A better grade/recovery curve was observed when using an air flowrate of 2 l min⁻¹ for ligand **12** at a concentration of 50 g ton⁻¹ than when

the same concentration of ligand is used at 6 l min^{-1} (Figure 7.14, Table 7.15). These data confirm that variations in air flowrate result in changes in flotation performance. The *grade* increases and the *recovery* decreases when aeration is reduced. This is because with low air flowrate, the water *recovery* drops as the rate of bubbles passing through the pulp-froth interface decreases.^{6, 7} Consequently a poor *grade* (separation) is obtained with high aeration as the *recovery* is mainly obtained by entrainment (water carried by the froth containing both hydrophilic and hydrophobic particles). Low air flowrates also promote a more selective separation by generation a higher coverage of the bubbles by the valuable mineral.¹²

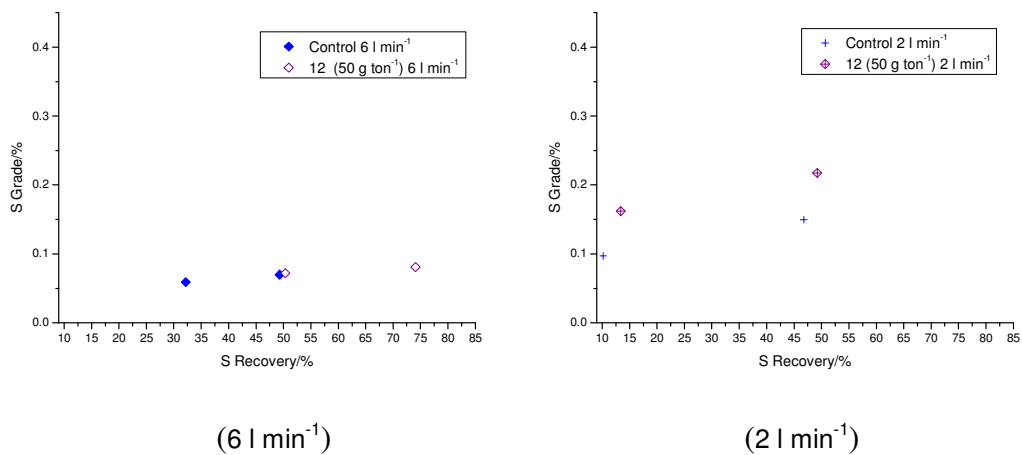


Figure 7.14. Grade/Recovery curves for the control tests and ligand **12** at 50 g ton^{-1} and two different airflow rates of 6 and 2 l min^{-1} with Amandelbult ore (concentrates were collected after 1 and 4 minutes of flotation).

Air flowrate in l min ⁻¹	Ligand 12 (conc. in g ton ⁻¹)	Grade ^a at collection times (min)		Recovery ^b at collection times (min)	
		1	4	1	4
2	-	0.10	0.15	10.2	46.8
	50	0.16	0.22	13.4	49.2
6	-	0.06	0.07	32.2	49.3
	50	0.07	0.08	50.4	74.1

Table 7.15. Grade and recoveries for flotation of Amandelbult ore using ligand 12 (50 g ton⁻¹) as a co-collector^c at two different air flowrates, 2 and 6 l min⁻¹.

^a Grades are recorded as a percentage of the mineral(s) of value found in the concentrate.

^b Recoveries are recorded as a percentage of the mineral value in the feed that is recovered in the concentrate.

^c SIBX and SENKOL 5 were added at 50 g ton⁻¹ in all cases.

In summary, data obtained from tests with Amandelbult ore are inconclusive in ranking the ligands because ethanol had to be added to enhance solubility and this has a frothing effect, increasing the amount of froth in the cell. The generation of so much froth caused more hydrophilic material to be entrained with the froth. This effect prevented the grades from increasing although it improved the recoveries as with the water, apart from hydrophilic material, some hydrophobic particles are also entrained.

7.2.2. FLOTATION TESTS WITH KENNECOTT ORE (MZ2HE)

Ligands 1, 5, 12 and 18 in their sodium salt form were tested on Kenecott ore (Monazite – MZ2HE) from U.S.A. using two different concentrations of ligands corresponding to 30 and 60 g ton⁻¹ of ore and an air flowrate of 10 l min⁻¹. A control experiment with no ligand was carried out. Concentrates were collected at timed intervals: 1st, 2nd and 3rd concentrates after 1 minute, 3 minutes and 5 minutes of flotation. The sulfur content of Kenecott ore feed is 0.99 % by mass.

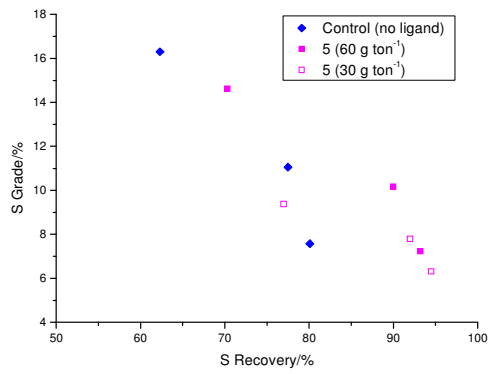
7.2.2.1. THE INFLUENCE OF COLLECTOR CONCENTRATION

A control test, where no ligand was added, was run obtaining a *grade* of 16 % and a *recovery* of 80 %. In each of the graphs shown in Figure 7.16 the control test and a ligand at two different concentrations are compared. Data are available in Table 7.17.

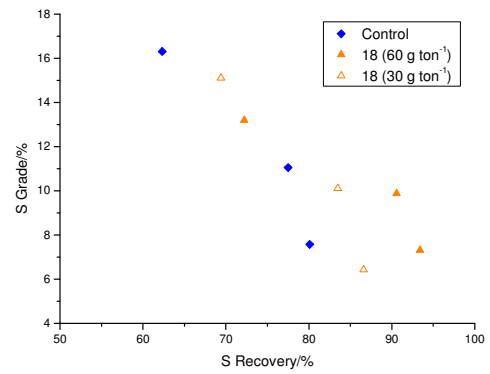
Ligand **5** at 60 g ton⁻¹ achieves better results than the control test. When a low concentration of ligand **5** was added, about the same *recovery* as at high concentration was obtained but it gave a lower final *grade*. (Figure 7.16, Table 7.17).

Both tests, at high and low concentration of ligand **18**, show a better performance than the control test. *Grade/recovery* curve of ligand **18** shifted upwards towards higher *recovery* (93 %) at 60 g ton⁻¹. (Figure 7.16, Table 7.17).

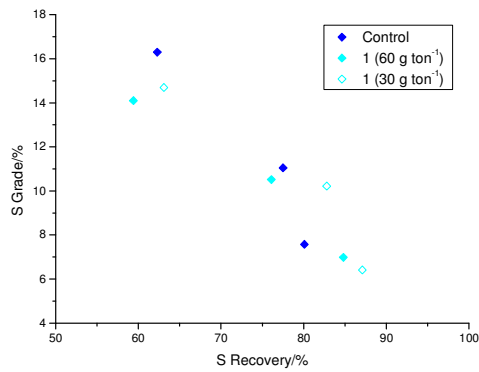
Both ligands, **1** and **12**, work better at a low than at a high concentration (Figure 7.16, Table 7.17), although neither gave a better *grade/recovery* curve than the control. A possible reason for these ligands performing better at low than at high concentrations may be due to a “micellization” effect.⁵ The concentration in solution of collectors is limited by their association or micellization. This phenomenon occurs at a specific concentration for each chemical species and this concentration is called the critical micelle concentration (CMC). When the concentration of a collector added to a solution is larger than the CMC, micellization happens and the concentration of collector available for mineral adsorption is reduced.



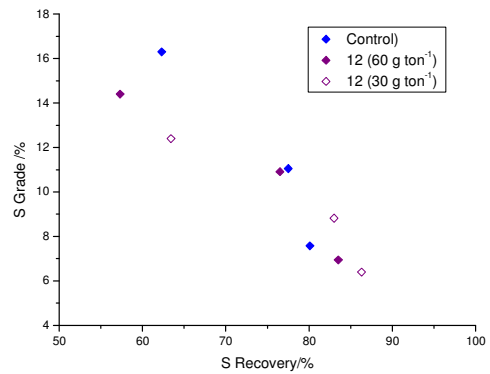
(Ligand 5)



(Ligand 18)



(Ligand 1)



(Ligand 12)

Figure 7.16. *Grade/Recovery* curves for the control test and ligands **1**, **5**, **12** and **18** at two different concentrations, 30 g ton^{-1} and 60 g ton^{-1} , and an airflow rate of 10 l min^{-1} , with Kennecott ore (concentrates were collected after 1, 3 and 5 minutes of flotation).

Ligand (conc. in g ton ⁻¹)	Grade ^a at collection times (min)			Recovery ^b at collection times (min)			Solids Recovery ^c at collection times (min)			
	1	3	5	1	3	5	1	3	5	
-	16.3	11.1	7.9	62.3	77.5	80.1	3.8	7.0	10.5	
1	(60)	14.1	10.5	7.0	59.4	76.1	84.8	4.2	7.2	12.0
	(30)	14.7	10.2	6.4	63.1	82.8	87.1	4.3	8.0	13.5
5	(60)	14.6	10.2	7.2	70.3	90.0	93.2	4.8	8.8	12.8
	(30)	9.4	7.8	6.3	77.0	92.0	94.5	8.2	11.7	14.9
12	(60)	14.4	10.9	7.0	57.3	76.5	83.5	4.0	7.0	12.0
	(30)	12.4	8.8	6.4	63.4	83.0	86.3	5.1	9.3	13.4
18	(60)	13.2	9.9	7.3	72.2	90.6	93.4	5.4	9.1	12.7
	(30)	15.1	10.1	6.4	69.4	83.5	86.6	4.6	8.2	13.4

Table 7.17. Grade, recoveries and solids recoveries for flotation of Kennecott ore (MZ2HE) using ligands **1**, **5**, **12** and **18** as co-collectors.^d

^a Grades are recorded as a percentage of the mineral(s) of value found in the concentrate.

^b Recoveries are recorded as a percentage of the mineral value in the feed that is recovered in the concentrate.

^c Solids recoveries are recorded as a percentage of the total amount of solids recovered in relation to the total mineral mass.

^d SIBX was added at 30 g ton⁻¹ in all cases.

Overall comparison of the *grade/recovery* curves for the four ligands studied indicate that the dosage of ligand (co-collector) to use depends on the ligand used in each case and a pattern cannot be established in this particular case study. Ligands **5** and **18** at high concentration (60 g ton⁻¹) produced a higher *recovery* for the same final *grade* as the control, which means that more material is being collected.

7.2.2.2. THE INFLUENCE OF SURFACE-LIGATING GROUPS

A comparison of the *grade/recovery* curves at different concentrations of the polyfunctional surface ligand **18** and the monofunctional ligand **5**, which showed the best performance in the flotation test undertaken with this ore (see Section 7.2.2.1) is made.

As discussed in the previous section, both ligands **5** and **18** at 60 g ton^{-1} showed higher *recovery* for about the same final *grade* as the control experiment. Data of the control test are omitted for clarity in Figure 7.18.

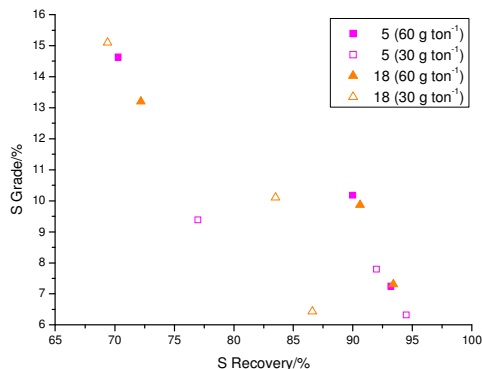


Figure 7.18. *Grade/Recovery* curves for ligands **5** and **18** at two different concentrations, 60 and 30 g ton^{-1} , and an airflow rate of 10 l min^{-1} with Kennecott ore (concentrates collected after 1, 3 and 5 minutes of flotation).

At 60 g ton^{-1} , ligands **5** and **18** showed a very similar behaviour (Figure 7.18, Table 7.17). It is at 30 g ton^{-1} when the difference between these two ligands is remarkable; ligand **5** gave a higher *recovery* than ligand **18**.

From the data collected for Kennecott ore, it can be concluded that a *monofunctional* ligand at low concentration gives a better *grade/recovery* curve than a *polyfunctional* ligand at low concentration and also a better curve than the control experiment.

7.2.3. FLOTATION TESTS WITH PALABORA ORE

Palabora ore (South Africa) was tested with ligands **1**, **5**, **12** and **18** in their sodium salt form, with a concentration of ligand of 30 g ton^{-1} and an air flowrate 6 l min^{-1} in all the cases. Because of the limited time when visiting Imperial College London, it was decided to run the tests only at low concentrations of ligand (equal dosage of collector used) as high concentration of ligand could imply additional

problems to the process such as micellization (see Section 7.2.2.1) and also because the use of lowest concentrations of collectors are desired at industrial scale to reduce the cost of the process. Concentrates were collected at timed intervals: 1st, 2nd and 3rd concentrates after 30 seconds, 90 seconds and 5 minutes of flotation. Because not much froth was overflowing, timed intervals of collection of 1st and 2nd concentrates were shortened for tests with Palabora ore compared with the Kennecott ore. The overall flotation time of 5 minutes was maintained to allow comparison to be made with the Kennecott ore. The sulfur content of the feed ore is 0.48 % by mass.

7.2.3.1. THE INFLUENCE OF SURFACE-LIGATING GROUPS

A control test with no ligand added was run, obtaining a *grade* of 12 % and a *recovery* of 67 %.

Results for the control test and ligands **1** and **5** are shown in Figure 7.19 and Table 7.20. Data for ligand **5** show a higher final *recovery* for a slightly higher *grade* than the control test. The good performance of **5** in Kennecott and Palabora ores might result from the singular surface ligating properties that this compound has shown, and are described in Section 5.4, such as the penetration in the surface of the oxygen atom attached to the nitrogen in the hydroxamate moiety which seems to confer stability to the system. **5** could therefore work on all iron(III) oxides as these contain the sequence Fe-O-Fe.

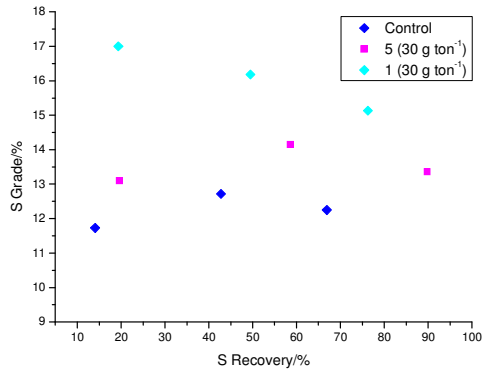
Ligand **1** produces an initial concentrate up to 17 % *grade*. Results for ligand **1** are significant as **1** increases the *grade* of all the concentrates which also produces a higher sulfur *recovery*, although the actual solids *recovery* is lower than for the control (Table 7.20). This could be due to the mineral attachment being so strong to the bubbles that it makes them burst more than in the control test, therefore, reducing the *recovery* of solids in the concentrate. However the bubbles which still manage to overflow are very rich in sulfide mineral giving high *recovery* and *grade*. This effect

could be supported by investigations reporting that very hydrophobic particles destabilize the froth.^{7, 13}

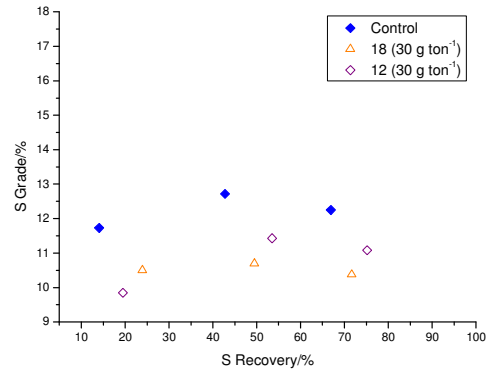
Figure 7.19 compares the results obtained for the control test and ligands **12** and **18**. The *grade/recovery* curves for ligands **12** and **18** fall under the curve of the control test indicating poor performances relative to a situation where no ligand was added.

A possible explanation for the poor performance of **12** in all the flotation tests carried out in this research work could be that phosphonic acids are known to be good surfactants, allowing the formation of stable bubbles. These could have two effects: one of them is that it generates smaller bubbles which increase water entrainment, carrying more hydrophilic particles, and therefore decreasing the *grades*. Although entrainment caused the *recoveries* to increase slightly as the water also carries some unattached hydrophobic particles of interest. The other consequence may be that a micellization effect (see Section 7.2.2.1) is happening, lowering the concentration of collector available in solution by the formation of micelles. It would have been interesting to test lower concentrations of **12** to see if these effects could have been minimised.

For Palabora ore, *monofunctional* surface-ligating groups work better than *polynuclear* surface-ligating groups. Ligands **1** and **5** work well and increase *recovery* and *grade* respect of the control test.



(Ligands 1 and 5)



(Ligands 12 and 18)

Figure 7.19. Grade/Recovery curves of control test and ligands 1, 5, 18 and 12, at concentration 30 g ton^{-1} and an air flowrate of 6 l min^{-1} , with Palabora ore (concentrates collected after 30 seconds, 90 seconds and 5 minutes of flotation).

Ligand (conc. 30 g ton^{-1})	Grade ^a at collection times			Recovery ^b at collection times			Solids Recovery ^c at collection times		
	30 sec	90 sec	5 min	30 sec	90 sec	5 min	30 sec	90 sec	5 min
-	11.7	12.7	12.3	14.1	42.7	66.9	0.6	1.6	2.6
1	17.0	16.2	15.1	19.4	49.5	76.3	0.5	1.5	2.4
5	13.1	14.2	13.4	19.7	58.6	89.8	0.7	2.0	3.2
12	9.9	11.4	11.1	19.5	53.5	75.1	0.9	2.2	3.2
18	10.5	10.7	10.4	23.9	49.5	71.7	1.1	2.2	3.3

Table 7.20. Grade, recoveries and solids recoveries for flotation of Palabora ore using ligands 1, 5, 12 and 18 as co-collectors.^d

^a Grades are recorded as a percentage of the mineral(s) of value found in the concentrate.

^b Recoveries are recorded as a percentage of the mineral value in the feed that is recovered in the concentrate.

^c Solids recoveries are recorded as a percentage of the total amount of solids recovered in relation to the total mineral mass.

^d SIBX was added at 30 g ton^{-1} in all cases.

7.3. CONCLUSIONS

The froth flotation tests conducted on Amandelbult ore (UG2 reef) proved very useful to establish an experimental protocol and demonstrated that it is best to use the co-collectors as sodium salts to ensure sufficient water solubility as it is not practicable to add them as an ethanol solution.

There is no direct correlation between measured binding strengths at goethite and performance as a co-collector. However, the reagents that show benefit all have good equilibrium adsorption constants (they were selected for testing on this basis). In retrospect, it would have been useful to do a “negative control” testing one of the hydroxamates which does not bind strongly to goethite.

Benzohydroxamic acid, **5**, shows the best overall performance as a co-collector. For Kennecott ore (Monazite - MZ2HE) at 60 g ton^{-1} , it works well since for the same final *grade* as the control **5** gives a higher *recovery*. **5** also gave good results for Palabora ore giving a higher final *recovery* for an even slightly higher *grade* than the control. As discussed in Section 7.2.3.1, the positive results of **5** in both ores could be due to the special surface ligating properties that **5** showed. They involve penetration in the surface of the oxygen atom attached to the nitrogen in the hydroxamate functionality, causing the system to be more stable.

12, the phosphonic acid analogue of the commercial iron corrosion inhibitor, **1**, performed poorly in all tests, despite showing the highest equilibrium binding constant to goethite. A possible reason is that phosphonic acids are good surfactants (see Section 7.2.3.1), generating stable bubbles which enhance the transport of hydrophilic particles as well as favouring micellization. This suggests that strong binding to an iron(III) oxide surface may prove to be a necessary but not a sufficient condition for good co-collector properties.

The commercial iron corrosion inhibitor for mild steel, ligand **1**, shows a remarkable performance on Palabora ore, being the co-collector that increases the *grade* of all the concentrates most significantly.

18 (60 g ton^{-1}) offers good results for Kennecott ore, as it enhances the *recovery* for the same final *grade* relative to the control.

On the basis of the limited range of flotation tests undertaken, the original concept that *recovery* of oxidized sulfidic minerals can be enhanced by adding ligands as co-collectors with an affinity for iron(III) oxides has been demonstrated. Ligands **1**, **5** and **18** in particular appear useful in this role.

7.4. EXPERIMENTAL

7.4.1. MATERIALS

For initial crushing, some of the material was passed through a Pegson Jaw crusher. Size distributions were determined by using 8 inch wire mesh sieves. Prior to flotation tests, a rod mill was used to grind samples to final size. Froth flotation experiments were carried out in a Denver laboratory flotation machine. Dried solid samples were analysed for sulfur using a Leco SC32 sulfur analyser.

7.4.2. SOLVENTS AND REAGENTS

All commercially available materials were used as received from Dow Deutschland Inc., Senmin, QuemQuest, Aldrich, Acros, AlfaAesar, Avocado, Fluka or Ciba Specialty Chemicals Inc. Solvents were of analytical reagent grade. Water was purified before use with a Milli-Q[®] water purification system. A Platinum Group Metal (PGM) ore from Amandelbult (UG2 reef), Anglo Platinum - South Africa, supplied by University of Manchester was used to set up a test procedure. Kennecott Utah Copper ore (MZ2HE) from U.S.A. and Palabora ore from South

Africa, were supplied by Rio Tinto to represent examples of oxidised chalcopyrite ores.

7.4.3. COMPOSITION OF THE ORES

The composition of Kennecott ore (Monazite – MZ2HE) was determined by the Rio Tinto Technical Services in Melbourne:¹⁴

- Feldspar 58.2 %
- Quartz 19.7 %
- Fe Mica 16.7 %
- Chalcopyrite 1.8 %
- Pyrite 0.8 %
- Others 2.8 %

The composition of the Palabora ore was determined by University of Nottingham:¹⁵

- Calcite 70 %
- Magnetite 20 %
- Permiculite 5 %
- Pyrite/Chalcopyrite 1 – 2 %
- Others 4 – 3 %

7.4.4. CRUSHING PROCESSES

Crushing of Kennecott (Monazite - MZ2HE) ore sample was undertaken in the Department of Chemical Engineering at the University of Nottingham.

The initial size of Kennecott (MZ2HE) ore was of the region of 5-25 mm. The material was passed through a Pegson Jaw crusher with an initial close side

setting of approximately 5 mm. The material was then passed over a 4.75 mm screen, the undersize retained and the oversize passed through the jaw crusher again with a slightly reduced close side setting. The process was repeated until 25 kg of - 4.75 mm material was obtained.

There was already a sufficient quantity of -3.35 mm Palabora ore (particle size distribution was determined to check) in University of Nottingham, and further crushing was unnecessary.

Two sub-samples of each ore were obtained by riffing from 25 - 30 kg down to approximately 130 g using sample splitters of different sizes (Figure 7.9). Their size distributions were obtained by passing each sub-sample through a series of 8 inch wire mesh sieves. The sieves were vibrated for a total of twenty minutes. There was good agreement between the size distributions of the two sub-samples for each ore, and can be assumed to be a true representation of the size distribution of the ores.

7.4.5. FLOTATION EXPERIMENTAL PROCESSES

For each of the three ores studied, several trials to establish the best conditions to carry out the flotation experiments were made. Required milling times, air flowrates, amount of ore and water in the cell as well as concentration of reagents were parameters to set previous to the study of the ligands.

Froth flotation experiments were undertaken in a Denver laboratory flotation machine and a specially constructed cell designed to contain a pulp volume of approximately 1 litre. The agitator operated at a constant speed of 1500 rpm. The flotation cell is 12 cm wide and 12 cm long, with a free section of 144 cm², where the agitator is inserted. Compressed air was introduced to the system through the cell agitator at constant pressure which is regulated by an air flowrate control system. The supplied air flowrate ranged from 2 l min⁻¹ to 10 l min⁻¹.

7.4.5.1. FLOTATION TESTS WITH AMANDELBULT ORE (UG2 REEF)

The following experiments were carried out in the School of Analytical Science and Chemical Engineering at the University of Manchester. The experimental conditions and reagents (except for the ligand added) are the ones used in industrial flotation processes. The ore used was a Platinum Group Metal (PGM) ore from Amandelbult (UG2 reef), South Africa.

The ore was milled in a rod mill for 40 minutes in all tests until the size distribution was 40% passing 74 μm . The milling time required to achieve that distribution size was determined previously by the research group with which the flotation experiments were undertaken.

Three different conditions were chosen in which the concentration of the ligand tested changed as well as the air flowrate. The flowrate used was 6 l min^{-1} in most of the cases, apart from two of the tests with ligand **12** in which 2 l min^{-1} were supplied.

Because of the ligands were not water soluble and there was not any pH regulator available in that laboratory, ligands were dissolved in the minimum amount of ethanol possible. This amount of ethanol was different for each ligand and the corresponding amount of ethanol was also added to each of the control tests (containing no ligand) in order to have the same conditions for all series of tests.

Frother and collectors were used and also a depressant in order to avoid natural hydrophobic talc in the ore being floated instead of the mineral of interest. The reagents and the concentrations used are given in Table 7.21.

Type	Reagent	Concentration (g ton ⁻¹ of ore)
Collector	SIBX	50
	SENKOL 5	50
	Ligand tested	50/100
Depressant	Guar gum	100
Frother	Dow 200	40

Table 7.21. Reagents used in Amandelbult ore (UG2 reef) flotation tests.

300 g of previously milled ore and 600 ml of water were placed in the flotation cell. The agitator was turned on and the corresponding amounts of collectors, ligand (co-collector) and depressant were added. After 1 minute of conditioning time, the frother was also added, allowing an overall conditioning time of 2 minutes before the air supplied was turned on. The froth overflow to plastic containers, the concentrates were collected at timed intervals and weighed while wet. The solids were recovered by vacuum filtration, then dried in the oven at 70 °C for around 2 hours and weighed. The amount of sulfur in the dried samples was analysed using a Leco SC32 sulfur analyser.

7.4.5.2. FLOTATION TESTS WITH KENNECOTT ORE (MZ2HE)

The following experiments were carried out in the Royal School of Mines at Imperial College London. The ore used was a chalcopyrite containing ore coming from Kennecott Utah Copper ore (Monazite - MZ2HE) from U.S.A.

The ore was spread in large uncovered trays in contact with air for some days in order to be oxidized and then was milled in a rod mill for 40 minutes in all the tests until the size distribution was 50% passing 75 µm. Several tests were carried out in order to establish the milling time required to achieve that distribution size. The time was determined to be 40 minutes and was kept constant for all set of

experiments. 1 kg of ore was milled each time and divided in a rotary sample splitter into smaller samples suitable for flotation tests. Two different conditions were chosen where the concentration of ligand added was changed.

350 g of previously milled ore were placed in the flotation cell and 700 ml of water were also added. The agitator was turned on and the corresponding amounts of collector and ligand in its sodium salt form (co-collector) were added. The experimental process was undertaken from this point as explained in Section 7.4.5.1 for Amandelbult ore. The flowrate used was 10 l min^{-1} . The reagents and the concentrations used are shown in Table 7.22.

Type	Reagent	Concentration (g ton ⁻¹ of ore)
Collector	SIBX	60
	Ligand tested	60/30
Frother	Dow 200	80

Table 7.22. Reagents used in Kennecott ore (MZ2HE) flotation tests.

7.4.5.3. FLOTATION TESTS WITH PALABORA ORE

The set of experiments described in this section were run in the Royal School of Mines at Imperial College London. The ore used was a chalcopyrite containing ore from Palabora, South Africa.

As for Kennecott ore, the Palabora ore was spread in large uncovered trays in contact with air to oxidized the ore. In all the tests the mineral was milled in a rod mill for 45 minutes to get a size distribution of 50% passing 75 μm . To determine the milling time required to reach that distribution size many trials were done. The milling time for Palabora ore was established to be 45 minutes and was kept constant for all the flotation experiments.

The rest of the process was carried out as described in Section 7.4.5.2 for Kennecott ore. The aeration supplied was 6 l min^{-1} . Table 7.23 lists the reagents and the concentration used.

Type	Reagent	Concentration (g ton ⁻¹ of ore)
Collector	SIBX	30
	Ligand tested	30
Frother	MIBC	40

Table 7.23. Reagents used in Palabora ore flotation tests.

7.5. REFERENCES

- 1 W. Tolley, D. Kotlyar, and R. Van Wagoner, *Minerals Engineering*, 1996, **9**, 603.
- 2 S. Chander and A. Khan, *International Journal of Mineral Processing*, 2000, **58**, 45.
- 3 D. Fornasiero, D. Fullston, C. Li, and J. Ralston, *International Journal of Mineral Processing*, 2001, **61**, 109.
- 4 S. R. Grano, M. Sollaart, W. Skinner, C. A. Prestidge, and J. Ralston, *International Journal of Mineral Processing*, 1997, **50**, 1.
- 5 E. G. Kelly and D. J. Spottiswood, 'Introduction to mineral processing', John Wiley & Sons, New York, 1982.
- 6 N. Barbian, K. Hadler, E. Ventura-Medina, and J. J. Cilliers, *Minerals Engineering*, 2005, **18**, 317.
- 7 D. Tao, G. H. Luttrell, and R. H. Yoon, *International Journal of Mineral Processing*, 2000, **59**, 25.
- 8 V. D. Smar, R. R. Klimpel, and F. F. Aplan, *International Journal of Mineral Processing*, 1994, **42**, 225.
- 9 <http://www.sepor.com/new/sample.htm>.
- 10 R. Renz, 'Design and synthesis of benign, N- and O-containing organic ligands for surface engineering', PhD Thesis, University of Edinburgh, 2007.
- 11 Cytec Industries, 'Mining Chemicals Handbook', 2002.
- 12 E. Ventura-Medina, N. Barbian, and J. J. Cilliers, *International Journal of Mineral Processing*, 2004, **74**, 189.
- 13 G. Johansson and R. J. Pugh, *International Journal of Mineral Processing*, 1992, **34**, 1.
- 14 S. Kingman, University of Nottingham, 2006.
- 15 A. Jones, University of Nottingham, 2006.

Chapter 8

Conclusions and future work

8. CONCLUSIONS AND FUTURE WORK

The aim of this thesis was to identify ligands that will act as co-collectors in froth flotation processes to enhance the recovery of oxidized sulfidic minerals which are not effectively collected by the commercial reagents currently available. The co-collectors would be used in a blend with a conventional collector for sulfide minerals so that both the oxidized and the sulfidic surfaces of the particles are addressed. These new co-collectors must show selectivity for the oxidized particles of interest over the siliceous waste. We used adsorption isotherms to study the thermodynamic stability of complexes formed by the new ligands on iron(III) oxides surfaces (goethite) and on silica.

All the ligands studied offered good selectivity for goethite over silica. Five ligands which showed particularly strong binding and multisite attachment to goethite were tested in froth flotation tests at laboratory scale. Two different copper ores of interest for Rio Tinto were used in these experiments. Three of the tested ligands improved the recoveries of oxidized sulfidic minerals. When binding strengths were compared with performance in froth flotation tests, results suggested that strong binding to the mineral particles was necessary to obtain a good co-collector performance and could be considered as an initial criterion for selection of a co-collector but further factors such as concentration of ligand (co-collector), air flowrate and the composition of the ore to be floated were also important. As a consequence, it would be interesting to explore the effects of the different variables that affect the flotation system as well as different concentrations of ligands for both ores.

The phosphonic acid, 3-oxo-3-*p*-tolylpropylphosphonic acid, used in flotation tests proved not to be effective as a co-collector despite earlier work indicating that it had a very high affinity for goethite.

Additional work should include the tests using lower concentrations of phosphonic acids to determine whether their very strong binding abilities to iron(III)

oxides can be useful in froth flotation and their surfactant properties be minimized by using a smaller quantities and structural less likely to have an adverse effect on froth stability.

The development of formulations to address the oxidized surfaces of minerals would be best approached by collaborations between reagent-suppliers and end users. To be effective such projects will need to be focused on ores which have been shown to give poor recoveries when processed by conventional techniques and conventional collectors. As each ore body is unique, optimisation of a process will need to take account of both the collector formulation and a wide range of parameters associated with operating flotation plants.

The work undertaken in this thesis supports the concept that polynucleating or “multisite attachment” ligands can be used to control the properties of the surfaces of metal (oxide) surfaces and minerals. Identification of functionalities which lead to strong surface binding is a key to such developments in industrial process. The identification of hydroxamates as a strong ligand for iron(III) oxides (see also below) has lead to new work in Edinburgh being undertaken in collaboration with a lubricant additive supplier to develop friction modifiers which do not contain harmful elements.

The observation that simple hydroxamic acids form very stable surface complexes with iron(III) oxides rather than transfer Fe^{3+} ions to the solution phase as trishydroxamates complexes was surprising and may have implications on the roles of siderophores in biological systems. Whether iron can be sourced from solid materials *in vivo* may depend crucially on the structure of these materials, particularly their surfaces in defining whether formation of the polynuclear surface complex or mononuclear solution complex is more favourable.

Appendix

CONTENTS OF APPENDIX

All data is on the supplementary CD

CHAPTER 1

Particle size needed for adsorption isotherms.....182

CHAPTER 2

Adsorption isotherm data of **1** on goethite and silica.....184

Adsorption isotherm data of **2** on goethite and silica.....184

Adsorption isotherm data and plot of **18** on goethite185

CHAPTER 3

Adsorption isotherm data of **3** on goethite and silica.....186

CHAPTER 4

Adsorption isotherm data of **4** on goethite and silica.....186

CHAPTER 5

Adsorption isotherm data of **5** on goethite and silica.....187

Adsorption isotherm data of **6** on goethite and silica.....188

Adsorption isotherm data of **8** on goethite and silica.....188

Adsorption isotherm data of **9** on goethite and silica.....189

Adsorption isotherm data of **10** on goethite.....189

Adsorption isotherm data of **10** in presence of **5** on goethite.....189

Adsorption isotherm data of **10** in presence of **7** on goethite.....190

CHAPTER 6

Adsorption isotherm data of **11** on goethite and silica.....191

Adsorption isotherm data of **12** on goethite.....191

Adsorption isotherm data of **13** on goethite.....192

Adsorption isotherm data of **14** on goethite and silica.....192

Adsorption isotherm data of **15** on goethite.....192

Adsorption isotherm data of **16** on goethite.....193

REFERENCE.....193

Also on the supplementary CD: cif files and crystal data for:

Complex **4a**

Complex **5b**

Complex **5a**

Ligand **9**

CHAPTER 1

PARTICLE SIZE NEEDED FOR ADSORPTION ISOTHERMS

Estimate based on “known” surface area of goethite (*ca.* $20 \text{ m}^2 \text{ g}^{-1}$) used in this adsorption isotherm work.

We assume we need to grind solid $\text{Fe}_2\text{O}_3 \cdot x \text{H}_2\text{O}$, whose density is *ca.* 3.8 g cm^{-3} , into n small spheres of equal size of radius r (m).

If we take 1g of solid $\text{Fe}_2\text{O}_3 \cdot x \text{H}_2\text{O}$ and grind it into n spheres of equal size then,

Each sphere has mass = $1/n$ (g)

Each sphere has a surface area = $4\pi r^2$ (m^2)

Each sphere has volume = $\frac{3}{4 n \pi r^3}$

$$\text{Thus density} = \frac{\text{mass}}{\text{volume}} = \frac{\frac{1}{n}}{\frac{4}{3} \pi r^3} = \frac{3}{4 n \pi r^3} = 3.8 \times 10^6 \text{ g m}^{-2}$$

$$n = \frac{3}{3.8 \times 10^6 \times 4 n \pi r^2} \quad (1)$$

The total surface area of the n particles = $4n \pi r^2 = 20 \text{ m}^2$

$$n = \frac{20}{4 \pi r^2} \quad (2)$$

From (1) and (2):

$$\frac{3}{3.8 \times 10^6 \times 4 n \pi r^2} = \frac{3}{4 n \pi r^2}$$

$$r = \frac{3}{3.8 \times 10^6 \times 20} = 4 \times 10^{-8} \text{ m}$$

CHAPTER 2Adsorption isotherm data of **1** (goethite and silica)

Ligand 1 on goethite		Ligand 1 on silica	
Residual concentration (mol l ⁻¹)	Amount adsorbed (mol g ⁻¹)	Residual concentration (mol l ⁻¹)	Amount adsorbed (mol g ⁻¹)
1.04E-05	1.47E-06	9.72E-05	3.46E-07
3.88E-05	2.49E-06	1.95E-04	7.07E-07
6.08E-05	3.64E-06	2.31E-04	4.79E-07
1.04E-04	4.33E-06	3.27E-04	1.60E-07
1.82E-04	5.81E-06	3.59E-04	1.47E-06
2.24E-04	6.47E-06	4.37E-04	1.58E-06
2.67E-04	7.09E-06	4.88E-04	2.42E-06
3.14E-04	7.71E-06	5.85E-04	2.07E-06
3.92E-04	7.46E-06	8.45E-04	9.34E-07
4.47E-04	8.81E-06	9.89E-04	9.90E-07
5.66E-04	9.08E-06	1.12E-03	1.43E-06
6.37E-04	1.07E-05	1.28E-03	1.06E-06
8.01E-04	9.84E-06	1.42E-03	1.32E-06
9.33E-04	9.98E-06		
1.64E-06	2.87E-07		
6.92E-06	4.82E-07		
4.28E-06	8.78E-07		
9.31E-06	1.08E-06		
1.47E-05	1.27E-06		

Adsorption isotherm data of **2** (goethite and silica)

Ligand 2 on goethite		Ligand 2 on silica	
Residual concentration (mol l ⁻¹)	Amount adsorbed (mol g ⁻¹)	Residual concentration (mol l ⁻¹)	Amount adsorbed (mol g ⁻¹)
4.59E-07	1.58E-06	1.25E-04	1.28E-07
5.33E-06	3.04E-06	1.87E-04	1.90E-07
2.84E-05	4.07E-06	2.59E-04	2.56E-08
6.50E-05	4.77E-06	3.77E-04	3.39E-07
1.00E-04	5.47E-06	4.49E-04	1.49E-07
1.39E-04	6.15E-06	5.13E-04	1.66E-07
1.93E-04	6.35E-06	6.39E-04	2.69E-07
2.34E-04	6.97E-06	7.94E-04	9.07E-08
2.91E-04	7.04E-06	9.16E-04	3.73E-07
3.21E-04	7.87E-06	1.05E-03	4.27E-07
4.58E-04	9.26E-06	1.18E-03	5.35E-07
5.71E-04	9.88E-06	1.28E-03	1.17E-06
7.05E-04	1.00E-05		
8.01E-04	1.10E-05		

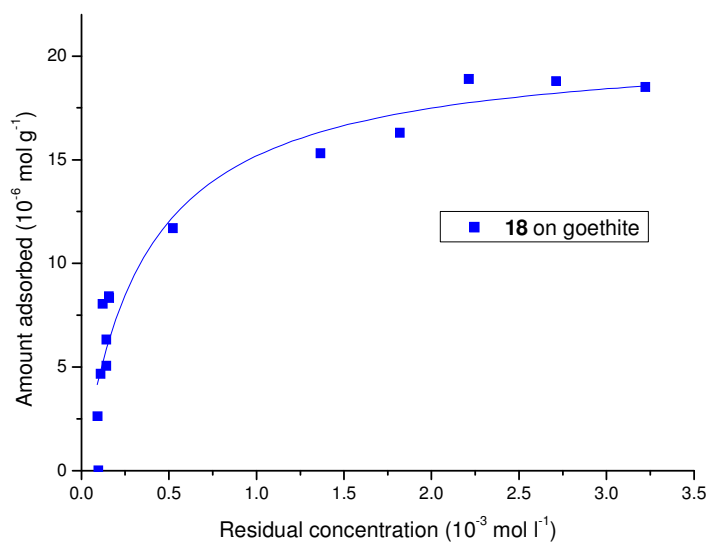
Adsorption isotherm data of **18** (goethite)

Figure 7.1. Adsorption isotherm of ligand **18** on goethite in methanol/water (95:5 v/v) at 25°C.¹

Ligand 18 on goethite	
Residual concentration (mol l ⁻¹)	Amount adsorbed (mol g ⁻¹)
9.30E-05	2.63E-06
9.85E-05	1.24E-08
1.11E-04	4.67E-06
1.23E-04	8.05E-06
1.44E-04	6.33E-06
1.44E-04	5.05E-06
1.58E-04	8.42E-06
1.61E-04	8.33E-06
5.24E-04	1.17E-05
1.37E-03	1.53E-05
1.82E-03	1.63E-05
2.21E-03	1.89E-05
2.71E-03	1.88E-05
3.22E-03	1.85E-05

Equilibrium adsorption constant (K) = $2.8(6) \times 10^3$
 Surface coverage = $21(1) \times 10^{-6} \text{ mol g}^{-1}$

CHAPTER 3Adsorption isotherm data of **3** (goethite and silica)

Ligand 3 on goethite		Ligand 3 on silica	
Residual concentration (mol l ⁻¹)	Amount adsorbed (mol g ⁻¹)	Residual concentration (mol l ⁻¹)	Amount adsorbed (mol g ⁻¹)
7.22E-05	4.67E-08	1.12E-04	1.02E-08
8.35E-05	1.42E-06	1.73E-04	7.50E-08
9.21E-05	2.95E-06	2.17E-04	7.64E-08
1.00E-04	4.54E-06	2.74E-04	2.87E-07
1.15E-04	5.91E-06	3.21E-04	8.94E-07
1.19E-04	7.59E-06	3.66E-04	1.58E-06
1.38E-04	8.86E-06	4.21E-04	1.97E-06
1.87E-04	1.11E-05	4.84E-04	2.18E-06
2.09E-04	1.24E-05	6.16E-04	6.69E-07
2.46E-04	1.31E-05	6.84E-04	7.53E-07
2.99E-04	1.51E-05	7.79E-04	1.52E-06
3.58E-04	1.68E-05	8.99E-04	2.02E-06
5.37E-04	1.55E-05	1.06E-03	1.38E-06
6.34E-04	1.64E-05	1.22E-03	9.57E-07

CHAPTER 4Adsorption isotherm data of **4** (goethite and silica)

Ligand 4 on goethite		Ligand 4 on silica	
Residual concentration (mol l ⁻¹)	Amount adsorbed (mol g ⁻¹)	Residual concentration (mol l ⁻¹)	Amount adsorbed (mol g ⁻¹)
6.32E-06	9.95E-08	6.17E-05	9.24E-08
1.21E-05	2.11E-07	1.20E-04	2.62E-07
2.09E-05	2.49E-07	1.81E-04	3.82E-07
2.85E-05	3.17E-07	2.36E-04	6.38E-07
3.34E-05	4.52E-07	3.06E-04	5.23E-07
2.97E-05	5.31E-07	3.34E-04	1.45E-06
7.16E-05	7.48E-07	3.96E-04	1.54E-06
1.14E-04	9.62E-07	4.45E-04	1.94E-06
4.26E-04	2.05E-06	4.91E-04	2.43E-06
3.59E-05	6.28E-07	5.51E-04	2.59E-06
7.69E-05	1.12E-06	7.13E-04	6.32E-07
1.34E-04	1.22E-06	7.92E-04	1.73E-06
1.67E-04	1.89E-06	9.29E-04	1.37E-06
2.25E-04	1.98E-06	1.04E-03	1.58E-06
2.83E-04	2.06E-06	1.12E-03	2.75E-06
3.36E-04	2.22E-06		
3.97E-04	2.22E-06		
4.67E-04	2.02E-06		
5.01E-04	2.69E-06		
5.87E-04	2.87E-06		

CHAPTER 5Adsorption isotherm data of **5** (goethite and silica)

Ligand 5 on goethite		Ligand 5 on silica	
Residual concentration (mol l ⁻¹)	Amount adsorbed (mol g ⁻¹)	Residual concentration (mol l ⁻¹)	Amount adsorbed (mol g ⁻¹)
3.22E-07	3.85E-06	6.94E-05	1.40E-08
4.19E-06	2.03E-06	1.45E-04	1.22E-07
6.76E-06	1.36E-06	2.17E-04	1.84E-07
7.62E-06	9.55E-07	3.02E-04	5.54E-07
8.48E-06	2.70E-06	3.47E-04	7.06E-08
8.91E-06	5.50E-06	4.13E-04	1.70E-07
9.34E-06	4.15E-06	4.88E-04	4.23E-08
1.02E-05	1.40E-06	5.08E-04	1.31E-06
1.19E-05	1.61E-06	6.12E-04	4.54E-07
1.62E-05	5.40E-06	6.76E-04	5.93E-07
1.75E-05	1.03E-06	8.18E-04	3.59E-07
2.78E-05	6.58E-06	8.97E-04	1.84E-06
4.20E-05	6.60E-06	1.02E-03	2.26E-06
4.55E-05	7.61E-06	1.19E-03	1.48E-06
5.27E-05	8.32E-06	1.28E-03	2.64E-06
6.27E-05	8.00E-06		
6.27E-05	8.59E-06		
8.25E-05	9.62E-06		
8.53E-05	9.15E-06		
1.14E-04	1.02E-05		
1.47E-04	1.10E-05		
1.53E-04	1.07E-05		
1.78E-04	1.09E-05		
2.05E-04	1.10E-05		
2.85E-04	1.17E-05		
2.85E-04	1.17E-05		
3.66E-04	1.27E-05		
3.66E-04	1.27E-05		
4.59E-04	1.35E-05		
4.62E-04	1.35E-05		
4.62E-04	1.35E-05		
5.65E-04	1.41E-05		
5.65E-04	1.41E-05		
6.88E-04	1.41E-05		
6.88E-04	1.41E-05		
8.27E-04	1.43E-05		
1.04E-03	1.50E-05		
1.27E-03	1.50E-05		

Adsorption isotherm data of **6** (goethite and silica)

Ligand 6 on goethite		Ligand 6 on silica	
Residual concentration (mol l ⁻¹)	Amount adsorbed (mol g ⁻¹)	Residual concentration (mol l ⁻¹)	Amount adsorbed (mol g ⁻¹)
4.54E-06	2.53E-06	5.43E-05	3.27E-07
3.16E-06	3.16E-06	1.20E-04	8.02E-08
7.84E-06	3.88E-06	1.76E-04	2.83E-07
2.79E-05	4.16E-06	2.01E-04	1.12E-07
3.62E-05	4.77E-06	2.56E-04	2.34E-07
5.16E-05	5.22E-06	2.66E-04	5.55E-07
6.61E-05	5.19E-06	3.40E-04	2.72E-07
7.16E-05	5.49E-06	3.63E-04	1.91E-07
8.81E-05	5.46E-06	4.39E-04	6.69E-07
9.17E-05	5.76E-06	4.95E-04	1.45E-07
1.65E-04	7.88E-06	5.75E-04	1.00E-07
2.31E-04	8.11E-06	6.53E-04	2.14E-08
2.90E-04	8.75E-06	7.55E-04	5.30E-07
3.54E-04	9.07E-06	8.06E-04	2.40E-07
4.11E-04	9.66E-06		

Adsorption isotherm data of **8** (goethite and silica)

Ligand 8 on goethite		Ligand 8 on silica	
Residual concentration (mol l ⁻¹)	Amount adsorbed (mol g ⁻¹)	Residual concentration (mol l ⁻¹)	Amount adsorbed (mol g ⁻¹)
1.17E-05	2.36E-06	6.43E-05	2.46E-07
2.13E-05	3.46E-06	1.15E-04	1.39E-07
4.04E-05	4.35E-06	1.81E-04	4.21E-07
6.70E-05	4.98E-06	2.33E-04	3.65E-07
9.57E-05	5.65E-06	2.89E-04	4.15E-07
1.39E-04	5.88E-06	3.56E-04	7.16E-07
1.83E-04	6.10E-06	4.15E-04	8.10E-07
2.20E-04	6.56E-06	4.61E-04	6.16E-07
2.58E-04	6.93E-06	4.62E-04	7.31E-07
2.69E-04	7.20E-06		
3.65E-04	7.63E-06		
4.36E-04	8.50E-06		
5.30E-04	8.95E-06		
6.49E-04	8.85E-06		
7.39E-04	9.37E-06		

Adsorption isotherm data of **9** (goethite and silica)

Ligand 9 on goethite		Ligand 9 on silica	
Residual concentration (mol l ⁻¹)	Amount adsorbed (mol g ⁻¹)	Residual concentration (mol l ⁻¹)	Amount adsorbed (mol g ⁻¹)
1.26E-04	5.53E-07	4.82E-05	5.85E-07
1.75E-04	4.89E-07	7.07E-05	5.34E-07
2.60E-04	1.30E-06	9.27E-05	4.57E-07
3.21E-04	1.53E-06	1.31E-04	2.30E-06
3.75E-04	1.58E-06	1.41E-04	1.43E-06
4.07E-04	1.08E-06	1.44E-04	4.96E-07
4.03E-04	3.15E-07	1.82E-04	8.45E-07
4.84E-04	4.12E-07	2.22E-04	1.21E-06
5.23E-04	8.53E-08		
5.00E-04	5.11E-07		

Adsorption isotherm data of **10** (goethite)

Ligand 10 on goethite	
Residual concentration (mol l ⁻¹)	Amount adsorbed (mol g ⁻¹)
2.53E-06	1.2E-06
2.59E-06	2.47E-06
2.72E-06	3.68E-06
4.55E-06	4.88E-06
6.63E-06	6.11E-06
8.56E-06	7.36E-06
1.38E-05	8.53E-06
1.93E-05	9.54E-06
3.3E-05	1.06E-05
1.55E-04	1.36E-05
2.63E-04	1.39E-05
4.76E-04	1.44E-05
5.92E-04	1.44E-05
2.48E-05	1.04E-05
7.46E-05	1.19E-05

Adsorption isotherm data of **10** in presence of **5** (goethite)

Ligand 10 in presence of 5 (goethite)	
Residual concentration (mol l ⁻¹)	Amount adsorbed (mol g ⁻¹)
7.41E-06	2.34E-06
7.97E-06	1.06E-06
8.83E-06	3.53E-06
1.02E-05	5.26E-06
1.06E-05	4.76E-06
1.71E-05	5.87E-06
2.39E-05	7.65E-06
2.97E-05	6.84E-06
6.42E-05	9.39E-06
1.20E-04	1.07E-05
2.06E-04	1.24E-05
3.97E-04	1.35E-05
5.10E-04	1.37E-05

Adsorption isotherm data of **10** in presence of **7** (goethite)

Ligand 10 in the presence of 7 (goethite)	
Residual concentration (mol l ⁻¹)	Amount adsorbed (mol g ⁻¹)
3.58E-06	1.18E-06
3.98E-06	2.4E-06
5.22E-06	3.65E-06
8.22E-06	4.81E-06
1.28E-05	5.97E-06
1.94E-05	7E-06
2.26E-05	7.71E-06
3.20E-05	7.91E-06
5.38E-05	8.66E-06
6.60E-05	9.41E-06
1.26E-04	1.07E-05
2.14E-04	1.13E-05
3.08E-04	1.17E-05
4.25E-04	1.15E-05
4.68E-04	1.17E-05

CHAPTER 6Adsorption isotherm data of **11** (goethite and silica)

Ligand 11 on goethite		Ligand 11 on silica	
Residual concentration (mol l ⁻¹)	Amount adsorbed (mol g ⁻¹)	Residual concentration (mol l ⁻¹)	Amount adsorbed (mol g ⁻¹)
5.50E-07	1.28E-06	2.63E-05	3.82E-07
1.00E-06	2.62E-06	6.86E-05	3.71E-07
1.90E-06	5.17E-06	1.61E-04	1.40E-07
3.00E-06	7.71E-06	2.54E-04	8.96E-08
3.20E-06	1.02E-05	3.17E-04	4.21E-07
3.40E-06	1.27E-05	4.2E-04	6.45E-08
3.50E-06	1.31E-05	8.91E-04	2.15E-07
4.20E-05	2.53E-05	1.27E-03	1.42E-06
3.51E-04	3.04E-05	2.20E-03	3.49E-08
8.67E-04	3.09E-05	2.45E-03	4.84E-06
1.31E-03	3.29E-05	2.93E-03	4.01E-06
1.84E-03	3.26E-05	3.42E-03	2.60E-06
2.33E-03	3.31E-05	3.90E-03	1.61E-06
3.32E-03	3.47E-05		

Adsorption isotherm data of **12** (goethite)

Ligand 12 on goethite	
Residual concentration (mol l ⁻¹)	Amount adsorbed (mol g ⁻¹)
5.50E-07	1.12E-06
7.40E-07	1.16E-05
8.40E-07	6.60E-06
8.70E-07	2.23E-06
9.00E-07	8.86E-06
9.00E-07	1.10E-05
1.20E-06	4.43E-06
3.26E-06	1.35E-05
8.55E-06	2.30E-05
2.45E-05	2.64E-05
7.67E-05	3.33E-05
2.26E-04	3.52E-05
5.91E-04	3.96E-05
1.11E-03	4.22E-05
1.51E-03	4.38E-05
1.54E-03	4.31E-05
1.99E-03	4.55E-05
2.41E-03	4.49E-05
2.55E-03	4.50E-05

Adsorption isotherm data of **13** (goethite)

Ligand 13 on goethite	
Residual concentration (mol l ⁻¹)	Amount adsorbed (mol g ⁻¹)
5.16E-06	2.54E-05
5.50E-06	1.33E-06
5.90E-06	1.29E-05
7.10E-06	4.91E-06
7.30E-06	2.58E-06
7.50E-06	7.31E-06
7.60E-06	9.69E-06
1.86E-04	3.34E-05
5.13E-04	3.80E-05
9.12E-04	4.09E-05
1.31E-03	4.35E-05
1.81E-03	4.36E-05
2.40E-03	4.50E-05
3.07E-03	4.35E-05

Adsorption isotherm data of **14** (goethite and silica)

Ligand 14 on goethite		Ligand 14 on silica	
Residual concentration (mol l ⁻¹)	Amount adsorbed (mol g ⁻¹)	Residual concentration (mol l ⁻¹)	Amount adsorbed (mol g ⁻¹)
3.23E-08	1.32E-05	5.16E-05	1.03E-06
6.45E-08	1.33E-06	9.75E-05	3.46E-06
9.68E-08	2.66E-06	1.50E-04	4.26E-06
9.68E-08	5.29E-06	2.13E-04	2.47E-06
9.68E-08	1.05E-05	2.70E-04	2.05E-06
2.58E-07	7.97E-06	3.20E-04	3.50E-06
7.10E-07	1.34E-05	3.92E-04	4.98E-07
1.92E-05	2.64E-05	4.44E-04	2.78E-07
2.06E-04	3.48E-05		
5.89E-04	3.89E-05		
1.00E-03	4.16E-05		
1.50E-03	4.26E-05		
1.97E-03	4.43E-05		
2.39E-03	4.70E-05		
2.84E-03	4.92E-05		

Adsorption isotherm data of **15** (goethite)

Ligand 15 on goethite	
Residual concentration (mol l ⁻¹)	Amount adsorbed (mol g ⁻¹)
1.48E-06	8.74E-06
1.84E-06	4.41E-06
1.84E-06	6.60E-06
1.90E-06	1.11E-05
2.35E-06	1.05E-06
7.61E-06	2.50E-05
2.02E-04	3.27E-05
5.69E-04	3.60E-05
1.02E-03	3.71E-05
1.49E-03	3.80E-05

Adsorption isotherm data of **16** (goethite)

Ligand 16 on goethite	
Residual concentration (mol l ⁻¹)	Amount adsorbed (mol g ⁻¹)
2.90E-07	1.92E-05
5.81E-07	2.42E-05
8.71E-07	9.59E-06
9.03E-07	1.44E-05
1.23E-06	2.37E-06
1.29E-06	4.75E-06
4.10E-06	2.77E-05
4.25E-04	3.54E-05
8.25E-04	3.67E-05
1.22E-03	3.86E-05
1.76E-03	3.95E-05
2.12E-03	3.91E-05
2.37E-03	3.85E-05
2.53E-03	4.00E-05
2.75E-03	4.06E-05

REFERENCES

- ¹ R. Renz. 'Design and synthesis of benign, N- and O-containing organic ligands for surface engineering'. PhD Thesis. University of Edinburgh. 2007.

Crystal Data for Complex 4a

Table 1. Crystal data and structure refinement for pt6036.

Contact Fraser J. White, f.j.white@sms.ed.ac.uk

A. CRYSTAL DATAEmpirical formula C₃₄ H₃₁ N₅ Ni₂ S₈C₂₈ H₁₆ N₄ Ni₂ S₈, Et₃N

Formula weight 883.54

Wavelength 0.71073 Å

Temperature 150(2) K

Crystal system Triclinic

Space group P -1

Unit cell dimensions a = 15.9373(3) Å alpha = 104.6310(10) deg.

b = 18.2046(4) Å beta = 90.2620(10) deg.

c = 20.2691(4) Å gamma = 94.8990(10) deg.

Volume 5667.1(2) Å³

Number of reflections for cell 6848 (2.29 < theta < 28.13 deg.)

Z 6

Density (calculated) 1.553 Mg/m³

Absorption coefficient 1.472 mm⁻¹

F(000) 2724

B. DATA COLLECTION

Crystal description black block

Crystal size 0.32 x 0.22 x 0.17 mm

Instrument Bruker Smart Apex CCD

Theta range for data collection 1.28 to 30.03 deg.

Index ranges -21 ≤ h ≤ 22, -25 ≤ k ≤ 23, -27 ≤ l ≤ 28

Reflections collected 106097

Independent reflections 30011 [R(int) = 0.0587]

Scan type Phi and Omega Scans

Absorption correction Semi-empirical from equivalents
(Tmin= 0.43, Tmax=0.78)

C. SOLUTION AND REFINEMENT.

Solution direct (Shelxs Sheldrick)

Refinement type Full-matrix least-squares on F²

Program used for refinement SHELXL-97

Hydrogen atom placement geom

Hydrogen atom treatment riding

Data / restraints / parameters 30011/ 0/ 1135

Goodness-of-fit on F^2 1.020

Conventional R [$F > 4\sigma(F)$] $R1 = 0.0598$ [20757 data]

Rw 0.1415

Final maximum Δ/σ 0.002

Weighting scheme

calc $w = 1/[\sigma^2(F_o^2) + (0.0654P)^2 + 2.0441P]$ where $P = (F_o^2 + 2F_c^2)/3$

Largest diff. peak and hole 0.967 and -0.468 e.A⁻³

Table 2. Atomic coordinates ($\times 10^4$) and equivalent isotropic displacement parameters ($\text{\AA}^2 \times 10^3$) for pt6036. $U(\text{eq})$ is defined as one third of the trace of the orthogonalized U_{ij} tensor.

	x	y	z	$U(\text{eq})$
Ni(1)	1791(1)	1940(1)	4026(1)	21(1)
Ni(2)	1808(1)	2993(1)	3390(1)	23(1)
S(11)	403(1)	1977(1)	4160(1)	26(1)
C(21)	285(2)	2884(2)	4101(2)	22(1)
N(31)	795(2)	3302(2)	3799(2)	22(1)
C(41)	512(2)	4015(2)	3834(2)	22(1)
C(51)	907(2)	4569(2)	3544(2)	30(1)
C(61)	529(2)	5246(2)	3624(2)	32(1)
C(71)	-207(2)	5379(2)	3979(2)	30(1)
C(81)	-596(2)	4834(2)	4268(2)	26(1)
C(91)	-227(2)	4136(2)	4184(2)	23(1)
S(101)	-580(1)	3343(1)	4464(1)	27(1)
S(12)	1099(1)	2175(1)	2515(1)	32(1)
C(22)	1311(2)	1317(2)	2633(2)	29(1)

N(32)	1587(2)	1177(2)	3200(2)	26(1)
C(42)	1666(2)	405(2)	3142(2)	33(1)
C(52)	1931(2)	88(2)	3656(2)	35(1)
C(62)	1946(3)	-691(2)	3522(3)	44(1)
C(72)	1714(3)	-1154(2)	2884(3)	55(1)
C(82)	1444(3)	-853(3)	2372(3)	57(1)
C(92)	1421(3)	-66(2)	2503(2)	41(1)
S(102)	1125(1)	491(1)	1972(1)	49(1)
S(13)	2494(1)	3826(1)	4272(1)	27(1)
C(23)	2233(2)	3409(2)	4922(2)	24(1)
N(33)	1972(2)	2690(2)	4865(2)	24(1)
C(43)	1829(2)	2540(2)	5503(2)	27(1)
C(53)	1548(2)	1842(2)	5616(2)	36(1)
C(63)	1432(3)	1800(3)	6285(2)	44(1)
C(73)	1577(3)	2438(3)	6826(2)	43(1)
C(83)	1864(2)	3130(3)	6725(2)	40(1)
C(93)	1987(2)	3175(2)	6054(2)	30(1)
S(103)	2327(1)	3964(1)	5758(1)	33(1)
S(14)	3176(1)	1884(1)	3880(1)	25(1)
C(24)	3354(2)	2312(2)	3224(2)	24(1)
N(34)	2846(2)	2724(2)	2989(2)	23(1)
C(44)	3189(2)	3009(2)	2463(2)	28(1)
C(54)	2812(2)	3478(2)	2127(2)	32(1)
C(64)	3256(2)	3743(2)	1637(2)	37(1)

C(74)	4069(2)	3540(2)	1482(2)	37(1)
C(84)	4449(2)	3078(2)	1805(2)	35(1)
C(94)	4001(2)	2812(2)	2303(2)	27(1)
S(104)	4321(1)	2247(1)	2818(1)	31(1)
Ni(3)	6828(1)	3117(1)	5627(1)	24(1)
Ni(4)	6741(1)	1999(1)	4563(1)	22(1)
S(15)	6065(1)	2416(1)	6193(1)	37(1)
C(25)	6168(2)	1511(2)	5725(2)	37(1)
N(35)	6463(2)	1302(2)	5095(2)	31(1)
C(45)	6467(2)	514(2)	4861(3)	40(1)
C(55)	6759(3)	117(2)	4241(3)	49(1)
C(65)	6724(3)	-668(3)	4105(4)	71(2)
C(75)	6388(4)	-1047(3)	4591(4)	76(2)
C(85)	6099(3)	-664(3)	5188(4)	72(2)
C(95)	6127(3)	129(3)	5343(3)	55(2)
S(105)	5831(1)	755(1)	6061(1)	55(1)
S(16)	5374(1)	2110(1)	4426(1)	26(1)
C(26)	5276(2)	3014(2)	4898(2)	23(1)
N(36)	5817(2)	3446(2)	5360(2)	24(1)
C(46)	5536(2)	4150(2)	5680(2)	25(1)
C(56)	5954(2)	4705(2)	6206(2)	31(1)
C(66)	5565(2)	5354(2)	6491(2)	34(1)
C(76)	4775(2)	5463(2)	6238(2)	34(1)
C(86)	4361(2)	4921(2)	5715(2)	29(1)

C(96)	4746(2)	4252(2)	5441(2)	26(1)
S(106)	4365(1)	3453(1)	4812(1)	29(1)
S(17)	7550(1)	3872(1)	5066(1)	26(1)
C(27)	7274(2)	3403(2)	4239(2)	23(1)
N(37)	6978(2)	2685(2)	4010(1)	23(1)
C(47)	6813(2)	2483(2)	3303(2)	27(1)
C(57)	6485(2)	1770(2)	2913(2)	36(1)
C(67)	6356(3)	1682(3)	2221(2)	47(1)
C(77)	6544(3)	2272(3)	1914(2)	47(1)
C(87)	6864(2)	2985(3)	2297(2)	40(1)
C(97)	7002(2)	3085(2)	2995(2)	31(1)
S(107)	7396(1)	3892(1)	3603(1)	31(1)
S(18)	8111(1)	1861(1)	4680(1)	27(1)
C(28)	8323(2)	2341(2)	5512(2)	25(1)
N(38)	7841(2)	2802(2)	5921(2)	25(1)
C(48)	8197(2)	3097(2)	6570(2)	26(1)
C(58)	7831(2)	3580(2)	7114(2)	32(1)
C(68)	8277(3)	3842(2)	7726(2)	39(1)
C(78)	9084(2)	3624(3)	7800(2)	40(1)
C(88)	9451(2)	3145(2)	7272(2)	35(1)
C(98)	9001(2)	2873(2)	6650(2)	28(1)
S(108)	9291(1)	2268(1)	5894(1)	30(1)
Ni(5)	7395(1)	5707(1)	678(1)	30(1)
Ni(6)	7617(1)	4281(1)	330(1)	30(1)

S(19)	6495(1)	4014(1)	915(1)	33(1)
C(29)	6421(2)	4878(2)	1481(2)	32(1)
N(39)	6704(2)	5560(2)	1404(2)	30(1)
C(49)	6492(2)	6160(2)	1936(2)	30(1)
C(59)	6656(2)	6925(3)	1974(2)	40(1)
C(69)	6387(3)	7449(3)	2531(2)	45(1)
C(79)	5949(3)	7206(3)	3047(2)	47(1)
C(89)	5774(2)	6440(3)	3011(2)	41(1)
C(99)	6048(2)	5912(2)	2449(2)	34(1)
S(109)	5905(1)	4927(1)	2243(1)	38(1)
S(1A)	8521(1)	5930(1)	1390(1)	36(1)
C(2A)	8587(2)	5054(2)	1528(2)	34(1)
N(3A)	8308(2)	4387(2)	1122(2)	32(1)
C(4A)	8519(2)	3770(2)	1363(2)	33(1)
C(5A)	8338(2)	3007(2)	1035(2)	38(1)
C(6A)	8589(3)	2453(3)	1340(2)	45(1)
C(7A)	9014(3)	2679(3)	1974(2)	48(1)
C(8A)	9205(3)	3425(3)	2298(2)	49(1)
C(9A)	8956(2)	3974(3)	1990(2)	39(1)
S(10A)	9104(1)	4966(1)	2265(1)	42(1)
S(1B)	8758(1)	4507(1)	-249(1)	39(1)
C(2B)	8620(2)	5390(3)	-354(2)	37(1)
N(3B)	8100(2)	5879(2)	-32(2)	33(1)
C(4B)	8175(3)	6562(3)	-222(2)	39(1)

C(5B)	7703(3)	7188(3)	26(2)	50(1)
C(6B)	7871(3)	7820(3)	-216(3)	55(1)
C(7B)	8485(4)	7844(3)	-704(3)	62(2)
C(8B)	8953(3)	7237(3)	-952(2)	56(1)
C(9B)	8787(3)	6597(3)	-706(2)	43(1)
S(10B)	9261(1)	5745(1)	-923(1)	46(1)
S(1C)	6253(1)	5529(1)	0(1)	35(1)
C(2C)	6386(2)	4657(2)	-533(2)	34(1)
N(3C)	6902(2)	4163(2)	-451(2)	33(1)
C(4C)	6807(2)	3482(2)	-962(2)	36(1)
C(5C)	7244(3)	2846(3)	-1002(2)	43(1)
C(6C)	7057(3)	2216(3)	-1536(3)	60(1)
C(7C)	6462(3)	2214(3)	-2037(2)	58(1)
C(8C)	6009(3)	2835(3)	-1999(2)	49(1)
C(9C)	6182(3)	3472(2)	-1459(2)	37(1)
S(10C)	5742(1)	4336(1)	-1270(1)	40(1)

Table 3. Bond lengths [Å] and angles [deg] for pt6036.

Ni(1)-N(32)	1.893(3)
Ni(1)-N(33)	1.895(3)
Ni(1)-S(11)	2.2340(9)
Ni(1)-S(14)	2.2363(9)
Ni(1)-Ni(2)	2.5639(6)
Ni(2)-N(31)	1.881(3)
Ni(2)-N(34)	1.895(3)
Ni(2)-S(12)	2.2358(11)
Ni(2)-S(13)	2.2403(10)
S(11)-C(21)	1.713(3)
C(21)-N(31)	1.322(4)
C(21)-S(101)	1.743(3)
N(31)-C(41)	1.396(4)
C(41)-C(91)	1.383(5)
C(41)-C(51)	1.397(5)
C(51)-C(61)	1.391(5)
C(51)-H(51)	0.9500
C(61)-C(71)	1.387(5)
C(61)-H(61)	0.9500
C(71)-C(81)	1.379(5)

C(71)-H(71)	0.9500
C(81)-C(91)	1.418(5)
C(81)-H(81)	0.9500
C(91)-S(101)	1.731(3)
S(12)-C(22)	1.701(4)
C(22)-N(32)	1.318(5)
C(22)-S(102)	1.746(4)
N(32)-C(42)	1.397(5)
C(42)-C(52)	1.392(6)
C(42)-C(92)	1.394(6)
C(52)-C(62)	1.378(5)
C(52)-H(52)	0.9500
C(62)-C(72)	1.382(7)
C(62)-H(62)	0.9500
C(72)-C(82)	1.373(7)
C(72)-H(72)	0.9500
C(82)-C(92)	1.392(6)
C(82)-H(82)	0.9500
C(92)-S(102)	1.743(5)
S(13)-C(23)	1.715(4)
C(23)-N(33)	1.317(4)
C(23)-S(103)	1.739(4)
N(33)-C(43)	1.403(5)
C(43)-C(53)	1.386(5)

C(43)-C(93)	1.394(5)
C(53)-C(63)	1.389(6)
C(53)-H(53)	0.9500
C(63)-C(73)	1.384(6)
C(63)-H(63)	0.9500
C(73)-C(83)	1.369(6)
C(73)-H(73)	0.9500
C(83)-C(93)	1.395(6)
C(83)-H(83)	0.9500
C(93)-S(103)	1.739(4)
S(14)-C(24)	1.715(4)
C(24)-N(34)	1.314(4)
C(24)-S(104)	1.748(3)
N(34)-C(44)	1.393(4)
C(44)-C(94)	1.390(5)
C(44)-C(54)	1.392(5)
C(54)-C(64)	1.381(5)
C(54)-H(54)	0.9500
C(64)-C(74)	1.393(6)
C(64)-H(64)	0.9500
C(74)-C(84)	1.367(6)
C(74)-H(74)	0.9500
C(84)-C(94)	1.399(5)
C(84)-H(84)	0.9500

C(94)-S(104)	1.743(4)
Ni(3)-N(36)	1.889(3)
Ni(3)-N(38)	1.900(3)
Ni(3)-S(15)	2.2156(11)
Ni(3)-S(17)	2.2447(10)
Ni(3)-Ni(4)	2.5586(6)
Ni(4)-N(35)	1.889(3)
Ni(4)-N(37)	1.894(3)
Ni(4)-S(16)	2.2286(9)
Ni(4)-S(18)	2.2369(10)
S(15)-C(25)	1.703(5)
C(25)-N(35)	1.336(5)
C(25)-S(105)	1.731(4)
N(35)-C(45)	1.394(5)
C(45)-C(55)	1.386(7)
C(45)-C(95)	1.422(6)
C(55)-C(65)	1.380(6)
C(55)-H(55)	0.9500
C(65)-C(75)	1.420(9)
C(65)-H(65)	0.9500
C(75)-C(85)	1.340(9)
C(75)-H(75)	0.9500
C(85)-C(95)	1.394(7)
C(85)-H(85)	0.9500

C(95)-S(105)	1.703(6)
S(16)-C(26)	1.702(4)
C(26)-N(36)	1.321(4)
C(26)-S(106)	1.744(3)
N(36)-C(46)	1.395(4)
C(46)-C(96)	1.391(5)
C(46)-C(56)	1.391(5)
C(56)-C(66)	1.377(5)
C(56)-H(56)	0.9500
C(66)-C(76)	1.405(5)
C(66)-H(66)	0.9500
C(76)-C(86)	1.374(5)
C(76)-H(76)	0.9500
C(86)-C(96)	1.398(5)
C(86)-H(86)	0.9500
C(96)-S(106)	1.736(4)
S(17)-C(27)	1.714(4)
C(27)-N(37)	1.316(4)
C(27)-S(107)	1.746(4)
N(37)-C(47)	1.405(5)
C(47)-C(57)	1.395(5)
C(47)-C(97)	1.405(5)
C(57)-C(67)	1.382(6)
C(57)-H(57)	0.9500

C(67)-C(77)	1.383(7)
C(67)-H(67)	0.9500
C(77)-C(87)	1.387(6)
C(77)-H(77)	0.9500
C(87)-C(97)	1.392(6)
C(87)-H(87)	0.9500
C(97)-S(107)	1.729(4)
S(18)-C(28)	1.711(4)
C(28)-N(38)	1.321(4)
C(28)-S(108)	1.752(4)
N(38)-C(48)	1.388(4)
C(48)-C(58)	1.390(5)
C(48)-C(98)	1.398(5)
C(58)-C(68)	1.381(5)
C(58)-H(58)	0.9500
C(68)-C(78)	1.396(6)
C(68)-H(68)	0.9500
C(78)-C(88)	1.367(6)
C(78)-H(78)	0.9500
C(88)-C(98)	1.402(5)
C(88)-H(88)	0.9500
C(98)-S(108)	1.737(4)
Ni(5)-N(3B)	1.901(3)
Ni(5)-N(39)	1.901(3)

Ni(5)-S(1C)	2.2266(11)
Ni(5)-S(1A)	2.2405(11)
Ni(5)-Ni(6)	2.5678(7)
Ni(6)-N(3A)	1.902(3)
Ni(6)-N(3C)	1.902(3)
Ni(6)-S(1B)	2.2327(11)
Ni(6)-S(19)	2.2375(10)
S(19)-C(29)	1.711(4)
C(29)-N(39)	1.331(5)
C(29)-S(109)	1.739(4)
N(39)-C(49)	1.393(5)
C(49)-C(59)	1.379(6)
C(49)-C(99)	1.406(5)
C(59)-C(69)	1.378(6)
C(59)-H(59)	0.9500
C(69)-C(79)	1.401(6)
C(69)-H(69)	0.9500
C(79)-C(89)	1.382(6)
C(79)-H(79)	0.9500
C(89)-C(99)	1.391(5)
C(89)-H(89)	0.9500
C(99)-S(109)	1.730(4)
S(1A)-C(2A)	1.700(5)
C(2A)-N(3A)	1.323(5)

C(2A)-S(10A)	1.750(4)
N(3A)-C(4A)	1.396(5)
C(4A)-C(5A)	1.385(6)
C(4A)-C(9A)	1.396(5)
C(5A)-C(6A)	1.395(6)
C(5A)-H(5A)	0.9500
C(6A)-C(7A)	1.399(6)
C(6A)-H(6A)	0.9500
C(7A)-C(8A)	1.359(7)
C(7A)-H(7A)	0.9500
C(8A)-C(9A)	1.389(6)
C(8A)-H(8A)	0.9500
C(9A)-S(10A)	1.745(5)
S(1B)-C(2B)	1.705(5)
C(2B)-N(3B)	1.320(5)
C(2B)-S(10B)	1.751(4)
N(3B)-C(4B)	1.388(5)
C(4B)-C(9B)	1.394(5)
C(4B)-C(5B)	1.407(6)
C(5B)-C(6B)	1.368(6)
C(5B)-H(5B)	0.9500
C(6B)-C(7B)	1.401(7)
C(6B)-H(6B)	0.9500
C(7B)-C(8B)	1.377(7)

C(7B)-H(7B)	0.9500
C(8B)-C(9B)	1.385(6)
C(8B)-H(8B)	0.9500
C(9B)-S(10B)	1.740(5)
S(1C)-C(2C)	1.711(4)
C(2C)-N(3C)	1.308(5)
C(2C)-S(10C)	1.752(4)
N(3C)-C(4C)	1.397(5)
C(4C)-C(5C)	1.387(6)
C(4C)-C(9C)	1.409(5)
C(5C)-C(6C)	1.374(6)
C(5C)-H(5C)	0.9500
C(6C)-C(7C)	1.386(7)
C(6C)-H(6C)	0.9500
C(7C)-C(8C)	1.379(7)
C(7C)-H(7C)	0.9500
C(8C)-C(9C)	1.385(6)
C(8C)-H(8C)	0.9500
C(9C)-S(10C)	1.733(4)
N(32)-Ni(1)-N(33)	178.41(13)
N(32)-Ni(1)-S(11)	89.80(9)
N(33)-Ni(1)-S(11)	89.10(9)
N(32)-Ni(1)-S(14)	89.28(9)

N(33)-Ni(1)-S(14)	91.82(9)
S(11)-Ni(1)-S(14)	179.00(4)
N(32)-Ni(1)-Ni(2)	91.17(9)
N(33)-Ni(1)-Ni(2)	89.98(9)
S(11)-Ni(1)-Ni(2)	90.45(3)
S(14)-Ni(1)-Ni(2)	89.95(3)
N(31)-Ni(2)-N(34)	177.64(13)
N(31)-Ni(2)-S(12)	91.13(9)
N(34)-Ni(2)-S(12)	90.68(9)
N(31)-Ni(2)-S(13)	87.79(9)
N(34)-Ni(2)-S(13)	90.39(9)
S(12)-Ni(2)-S(13)	178.83(4)
N(31)-Ni(2)-Ni(1)	90.03(9)
N(34)-Ni(2)-Ni(1)	91.49(9)
S(12)-Ni(2)-Ni(1)	89.60(3)
S(13)-Ni(2)-Ni(1)	90.85(3)
C(21)-S(11)-Ni(1)	100.41(11)
N(31)-C(21)-S(11)	126.7(3)
N(31)-C(21)-S(101)	113.6(2)
S(11)-C(21)-S(101)	119.7(2)
C(21)-N(31)-C(41)	112.4(3)
C(21)-N(31)-Ni(2)	124.4(2)
C(41)-N(31)-Ni(2)	123.2(2)
C(91)-C(41)-N(31)	113.5(3)

C(91)-C(41)-C(51)	121.2(3)
N(31)-C(41)-C(51)	125.2(3)
C(61)-C(51)-C(41)	117.4(3)
C(61)-C(51)-H(51)	121.3
C(41)-C(51)-H(51)	121.3
C(71)-C(61)-C(51)	122.0(3)
C(71)-C(61)-H(61)	119.0
C(51)-C(61)-H(61)	119.0
C(81)-C(71)-C(61)	120.6(3)
C(81)-C(71)-H(71)	119.7
C(61)-C(71)-H(71)	119.7
C(71)-C(81)-C(91)	118.1(3)
C(71)-C(81)-H(81)	120.9
C(91)-C(81)-H(81)	120.9
C(41)-C(91)-C(81)	120.5(3)
C(41)-C(91)-S(101)	110.7(3)
C(81)-C(91)-S(101)	128.8(3)
C(91)-S(101)-C(21)	89.81(16)
C(22)-S(12)-Ni(2)	102.22(13)
N(32)-C(22)-S(12)	127.2(3)
N(32)-C(22)-S(102)	112.5(3)
S(12)-C(22)-S(102)	120.2(2)
C(22)-N(32)-C(42)	113.5(3)
C(22)-N(32)-Ni(1)	123.2(3)

C(42)-N(32)-Ni(1)	123.2(3)
C(52)-C(42)-C(92)	119.8(4)
C(52)-C(42)-N(32)	126.3(4)
C(92)-C(42)-N(32)	113.8(4)
C(62)-C(52)-C(42)	119.1(4)
C(62)-C(52)-H(52)	120.5
C(42)-C(52)-H(52)	120.5
C(52)-C(62)-C(72)	120.7(5)
C(52)-C(62)-H(62)	119.6
C(72)-C(62)-H(62)	119.6
C(82)-C(72)-C(62)	121.1(4)
C(82)-C(72)-H(72)	119.5
C(62)-C(72)-H(72)	119.5
C(72)-C(82)-C(92)	118.7(4)
C(72)-C(82)-H(82)	120.6
C(92)-C(82)-H(82)	120.6
C(82)-C(92)-C(42)	120.5(4)
C(82)-C(92)-S(102)	130.2(4)
C(42)-C(92)-S(102)	109.3(3)
C(92)-S(102)-C(22)	90.89(19)
C(23)-S(13)-Ni(2)	100.63(12)
N(33)-C(23)-S(13)	127.0(3)
N(33)-C(23)-S(103)	114.1(3)
S(13)-C(23)-S(103)	118.9(2)

C(23)-N(33)-C(43)	111.9(3)
C(23)-N(33)-Ni(1)	124.6(2)
C(43)-N(33)-Ni(1)	123.5(2)
C(53)-C(43)-C(93)	119.8(4)
C(53)-C(43)-N(33)	126.0(3)
C(93)-C(43)-N(33)	114.2(3)
C(43)-C(53)-C(63)	118.2(4)
C(43)-C(53)-H(53)	120.9
C(63)-C(53)-H(53)	120.9
C(73)-C(63)-C(53)	121.3(4)
C(73)-C(63)-H(63)	119.3
C(53)-C(63)-H(63)	119.3
C(83)-C(73)-C(63)	121.2(4)
C(83)-C(73)-H(73)	119.4
C(63)-C(73)-H(73)	119.4
C(73)-C(83)-C(93)	117.7(4)
C(73)-C(83)-H(83)	121.1
C(93)-C(83)-H(83)	121.1
C(43)-C(93)-C(83)	121.7(4)
C(43)-C(93)-S(103)	109.5(3)
C(83)-C(93)-S(103)	128.8(3)
C(23)-S(103)-C(93)	90.32(18)
C(24)-S(14)-Ni(1)	102.57(12)
N(34)-C(24)-S(14)	127.2(3)

N(34)-C(24)-S(104)	113.3(3)
S(14)-C(24)-S(104)	119.4(2)
C(24)-N(34)-C(44)	113.1(3)
C(24)-N(34)-Ni(2)	123.3(2)
C(44)-N(34)-Ni(2)	123.3(2)
C(94)-C(44)-C(54)	119.9(3)
C(94)-C(44)-N(34)	113.7(3)
C(54)-C(44)-N(34)	126.3(3)
C(64)-C(54)-C(44)	119.0(4)
C(64)-C(54)-H(54)	120.5
C(44)-C(54)-H(54)	120.5
C(54)-C(64)-C(74)	120.4(4)
C(54)-C(64)-H(64)	119.8
C(74)-C(64)-H(64)	119.8
C(84)-C(74)-C(64)	121.5(4)
C(84)-C(74)-H(74)	119.3
C(64)-C(74)-H(74)	119.3
C(74)-C(84)-C(94)	118.1(4)
C(74)-C(84)-H(84)	120.9
C(94)-C(84)-H(84)	120.9
C(44)-C(94)-C(84)	121.1(4)
C(44)-C(94)-S(104)	109.9(3)
C(84)-C(94)-S(104)	129.0(3)
C(94)-S(104)-C(24)	89.99(17)

N(36)-Ni(3)-N(38)	178.42(13)
N(36)-Ni(3)-S(15)	88.33(9)
N(38)-Ni(3)-S(15)	91.12(9)
N(36)-Ni(3)-S(17)	89.07(9)
N(38)-Ni(3)-S(17)	91.43(9)
S(15)-Ni(3)-S(17)	176.95(4)
N(36)-Ni(3)-Ni(4)	90.82(9)
N(38)-Ni(3)-Ni(4)	90.66(9)
S(15)-Ni(3)-Ni(4)	90.54(3)
S(17)-Ni(3)-Ni(4)	91.11(3)
N(35)-Ni(4)-N(37)	177.66(13)
N(35)-Ni(4)-S(16)	89.32(9)
N(37)-Ni(4)-S(16)	88.61(9)
N(35)-Ni(4)-S(18)	90.46(9)
N(37)-Ni(4)-S(18)	91.59(9)
S(16)-Ni(4)-S(18)	178.59(4)
N(35)-Ni(4)-Ni(3)	90.97(10)
N(37)-Ni(4)-Ni(3)	90.13(9)
S(16)-Ni(4)-Ni(3)	90.57(3)
S(18)-Ni(4)-Ni(3)	90.82(3)
C(25)-S(15)-Ni(3)	102.64(14)
N(35)-C(25)-S(15)	126.9(3)
N(35)-C(25)-S(105)	114.2(3)
S(15)-C(25)-S(105)	118.9(3)

C(25)-N(35)-C(45)	112.1(3)
C(25)-N(35)-Ni(4)	123.1(3)
C(45)-N(35)-Ni(4)	124.5(3)
C(55)-C(45)-N(35)	126.6(4)
C(55)-C(45)-C(95)	121.5(4)
N(35)-C(45)-C(95)	112.0(4)
C(65)-C(55)-C(45)	118.1(5)
C(65)-C(55)-H(55)	120.9
C(45)-C(55)-H(55)	120.9
C(55)-C(65)-C(75)	120.1(6)
C(55)-C(65)-H(65)	120.0
C(75)-C(65)-H(65)	120.0
C(85)-C(75)-C(65)	121.8(5)
C(85)-C(75)-H(75)	119.1
C(65)-C(75)-H(75)	119.1
C(75)-C(85)-C(95)	119.7(6)
C(75)-C(85)-H(85)	120.1
C(95)-C(85)-H(85)	120.1
C(85)-C(95)-C(45)	118.8(6)
C(85)-C(95)-S(105)	129.7(5)
C(45)-C(95)-S(105)	111.4(3)
C(95)-S(105)-C(25)	90.2(2)
C(26)-S(16)-Ni(4)	102.08(11)
N(36)-C(26)-S(16)	127.3(3)

N(36)-C(26)-S(106)	112.9(3)
S(16)-C(26)-S(106)	119.8(2)
C(26)-N(36)-C(46)	113.4(3)
C(26)-N(36)-Ni(3)	123.8(2)
C(46)-N(36)-Ni(3)	122.6(2)
C(96)-C(46)-C(56)	120.7(3)
C(96)-C(46)-N(36)	113.1(3)
C(56)-C(46)-N(36)	126.1(3)
C(66)-C(56)-C(46)	118.7(3)
C(66)-C(56)-H(56)	120.7
C(46)-C(56)-H(56)	120.7
C(56)-C(66)-C(76)	120.4(4)
C(56)-C(66)-H(66)	119.8
C(76)-C(66)-H(66)	119.8
C(86)-C(76)-C(66)	121.3(4)
C(86)-C(76)-H(76)	119.4
C(66)-C(76)-H(76)	119.4
C(76)-C(86)-C(96)	118.1(3)
C(76)-C(86)-H(86)	121.0
C(96)-C(86)-H(86)	121.0
C(46)-C(96)-C(86)	120.8(3)
C(46)-C(96)-S(106)	110.3(3)
C(86)-C(96)-S(106)	128.9(3)
C(96)-S(106)-C(26)	90.29(17)

C(27)-S(17)-Ni(3)	100.56(12)
N(37)-C(27)-S(17)	127.1(3)
N(37)-C(27)-S(107)	113.7(3)
S(17)-C(27)-S(107)	119.2(2)
C(27)-N(37)-C(47)	112.4(3)
C(27)-N(37)-Ni(4)	124.8(2)
C(47)-N(37)-Ni(4)	122.7(2)
C(57)-C(47)-N(37)	126.1(3)
C(57)-C(47)-C(97)	120.3(4)
N(37)-C(47)-C(97)	113.6(3)
C(67)-C(57)-C(47)	117.8(4)
C(67)-C(57)-H(57)	121.1
C(47)-C(57)-H(57)	121.1
C(57)-C(67)-C(77)	122.1(4)
C(57)-C(67)-H(67)	118.9
C(77)-C(67)-H(67)	118.9
C(67)-C(77)-C(87)	120.7(4)
C(67)-C(77)-H(77)	119.7
C(87)-C(77)-H(77)	119.7
C(77)-C(87)-C(97)	118.1(4)
C(77)-C(87)-H(87)	120.9
C(97)-C(87)-H(87)	120.9
C(87)-C(97)-C(47)	121.0(4)
C(87)-C(97)-S(107)	129.3(3)

C(47)-C(97)-S(107)	109.8(3)
C(97)-S(107)-C(27)	90.56(18)
C(28)-S(18)-Ni(4)	102.05(12)
N(38)-C(28)-S(18)	127.3(3)
N(38)-C(28)-S(108)	113.3(3)
S(18)-C(28)-S(108)	119.4(2)
C(28)-N(38)-C(48)	112.8(3)
C(28)-N(38)-Ni(3)	123.7(2)
C(48)-N(38)-Ni(3)	123.2(2)
N(38)-C(48)-C(58)	126.0(3)
N(38)-C(48)-C(98)	114.0(3)
C(58)-C(48)-C(98)	119.9(3)
C(68)-C(58)-C(48)	119.1(4)
C(68)-C(58)-H(58)	120.4
C(48)-C(58)-H(58)	120.4
C(58)-C(68)-C(78)	120.6(4)
C(58)-C(68)-H(68)	119.7
C(78)-C(68)-H(68)	119.7
C(88)-C(78)-C(68)	121.1(4)
C(88)-C(78)-H(78)	119.5
C(68)-C(78)-H(78)	119.5
C(78)-C(88)-C(98)	118.7(4)
C(78)-C(88)-H(88)	120.6
C(98)-C(88)-H(88)	120.6

C(48)-C(98)-C(88)	120.5(4)
C(48)-C(98)-S(108)	109.8(3)
C(88)-C(98)-S(108)	129.7(3)
C(98)-S(108)-C(28)	90.08(17)
N(3B)-Ni(5)-N(39)	178.45(14)
N(3B)-Ni(5)-S(1C)	91.43(10)
N(39)-Ni(5)-S(1C)	89.56(10)
N(3B)-Ni(5)-S(1A)	89.79(10)
N(39)-Ni(5)-S(1A)	89.18(10)
S(1C)-Ni(5)-S(1A)	177.49(5)
N(3B)-Ni(5)-Ni(6)	90.49(10)
N(39)-Ni(5)-Ni(6)	90.67(10)
S(1C)-Ni(5)-Ni(6)	91.89(3)
S(1A)-Ni(5)-Ni(6)	90.29(3)
N(3A)-Ni(6)-N(3C)	178.46(13)
N(3A)-Ni(6)-S(1B)	89.87(9)
N(3C)-Ni(6)-S(1B)	91.62(10)
N(3A)-Ni(6)-S(19)	89.13(9)
N(3C)-Ni(6)-S(19)	89.37(10)
S(1B)-Ni(6)-S(19)	177.75(5)
N(3A)-Ni(6)-Ni(5)	91.00(11)
N(3C)-Ni(6)-Ni(5)	89.38(10)
S(1B)-Ni(6)-Ni(5)	91.08(4)
S(19)-Ni(6)-Ni(5)	90.96(3)

C(29)-S(19)-Ni(6)	100.87(13)
N(39)-C(29)-S(19)	127.0(3)
N(39)-C(29)-S(109)	113.0(3)
S(19)-C(29)-S(109)	119.9(2)
C(29)-N(39)-C(49)	113.1(3)
C(29)-N(39)-Ni(5)	123.9(3)
C(49)-N(39)-Ni(5)	122.9(3)
C(59)-C(49)-N(39)	126.0(3)
C(59)-C(49)-C(99)	121.0(4)
N(39)-C(49)-C(99)	113.0(4)
C(69)-C(59)-C(49)	118.8(4)
C(69)-C(59)-H(59)	120.6
C(49)-C(59)-H(59)	120.6
C(59)-C(69)-C(79)	120.5(4)
C(59)-C(69)-H(69)	119.8
C(79)-C(69)-H(69)	119.8
C(89)-C(79)-C(69)	121.2(4)
C(89)-C(79)-H(79)	119.4
C(69)-C(79)-H(79)	119.4
C(79)-C(89)-C(99)	118.3(4)
C(79)-C(89)-H(89)	120.8
C(99)-C(89)-H(89)	120.8
C(89)-C(99)-C(49)	120.2(4)
C(89)-C(99)-S(109)	129.5(3)

C(49)-C(99)-S(109)	110.3(3)
C(99)-S(109)-C(29)	90.57(19)
C(2A)-S(1A)-Ni(5)	101.18(13)
N(3A)-C(2A)-S(1A)	127.4(3)
N(3A)-C(2A)-S(10A)	112.7(3)
S(1A)-C(2A)-S(10A)	119.9(2)
C(2A)-N(3A)-C(4A)	113.0(3)
C(2A)-N(3A)-Ni(6)	123.4(3)
C(4A)-N(3A)-Ni(6)	123.5(3)
C(5A)-C(4A)-N(3A)	125.9(4)
C(5A)-C(4A)-C(9A)	119.7(4)
N(3A)-C(4A)-C(9A)	114.4(4)
C(4A)-C(5A)-C(6A)	119.4(4)
C(4A)-C(5A)-H(5A)	120.3
C(6A)-C(5A)-H(5A)	120.3
C(5A)-C(6A)-C(7A)	119.3(5)
C(5A)-C(6A)-H(6A)	120.4
C(7A)-C(6A)-H(6A)	120.4
C(8A)-C(7A)-C(6A)	122.0(4)
C(8A)-C(7A)-H(7A)	119.0
C(6A)-C(7A)-H(7A)	119.0
C(7A)-C(8A)-C(9A)	118.4(4)
C(7A)-C(8A)-H(8A)	120.8
C(9A)-C(8A)-H(8A)	120.8

C(8A)-C(9A)-C(4A)	121.2(4)
C(8A)-C(9A)-S(10A)	129.8(4)
C(4A)-C(9A)-S(10A)	109.0(3)
C(9A)-S(10A)-C(2A)	90.9(2)
C(2B)-S(1B)-Ni(6)	101.62(13)
N(3B)-C(2B)-S(1B)	128.1(3)
N(3B)-C(2B)-S(10B)	113.1(3)
S(1B)-C(2B)-S(10B)	118.7(2)
C(2B)-N(3B)-C(4B)	113.0(3)
C(2B)-N(3B)-Ni(5)	123.7(3)
C(4B)-N(3B)-Ni(5)	123.1(3)
N(3B)-C(4B)-C(9B)	114.0(4)
N(3B)-C(4B)-C(5B)	126.2(4)
C(9B)-C(4B)-C(5B)	119.9(4)
C(6B)-C(5B)-C(4B)	118.0(4)
C(6B)-C(5B)-H(5B)	121.0
C(4B)-C(5B)-H(5B)	121.0
C(5B)-C(6B)-C(7B)	121.4(5)
C(5B)-C(6B)-H(6B)	119.3
C(7B)-C(6B)-H(6B)	119.3
C(8B)-C(7B)-C(6B)	121.4(5)
C(8B)-C(7B)-H(7B)	119.3
C(6B)-C(7B)-H(7B)	119.3
C(7B)-C(8B)-C(9B)	117.4(4)

C(7B)-C(8B)-H(8B)	121.3
C(9B)-C(8B)-H(8B)	121.3
C(8B)-C(9B)-C(4B)	122.0(5)
C(8B)-C(9B)-S(10B)	128.2(4)
C(4B)-C(9B)-S(10B)	109.8(3)
C(9B)-S(10B)-C(2B)	90.1(2)
C(2C)-S(1C)-Ni(5)	100.96(14)
N(3C)-C(2C)-S(1C)	127.9(3)
N(3C)-C(2C)-S(10C)	113.5(3)
S(1C)-C(2C)-S(10C)	118.5(2)
C(2C)-N(3C)-C(4C)	113.0(3)
C(2C)-N(3C)-Ni(6)	124.9(3)
C(4C)-N(3C)-Ni(6)	121.7(3)
C(5C)-C(4C)-N(3C)	126.3(4)
C(5C)-C(4C)-C(9C)	120.1(4)
N(3C)-C(4C)-C(9C)	113.6(4)
C(6C)-C(5C)-C(4C)	118.5(4)
C(6C)-C(5C)-H(5C)	120.7
C(4C)-C(5C)-H(5C)	120.7
C(5C)-C(6C)-C(7C)	121.4(5)
C(5C)-C(6C)-H(6C)	119.3
C(7C)-C(6C)-H(6C)	119.3
C(8C)-C(7C)-C(6C)	120.8(5)
C(8C)-C(7C)-H(7C)	119.6

C(6C)-C(7C)-H(7C)	119.6
C(7C)-C(8C)-C(9C)	118.4(4)
C(7C)-C(8C)-H(8C)	120.8
C(9C)-C(8C)-H(8C)	120.8
C(8C)-C(9C)-C(4C)	120.6(4)
C(8C)-C(9C)-S(10C)	129.8(3)
C(4C)-C(9C)-S(10C)	109.5(3)
C(9C)-S(10C)-C(2C)	90.4(2)

Symmetry transformations used to generate equivalent atoms:

Table 4. Anisotropic displacement parameters ($\text{\AA}^2 \times 10^3$) for pt6036.

The anisotropic displacement factor exponent takes the form:

$$-2 \pi^2 [h^2 a^{*2} U_{11} + \dots + 2 h k a^* b^* U_{12}]$$

	U11	U22	U33	U23	U13	U12
Ni(1)	21(1)	21(1)	23(1)	8(1)	0(1)	2(1)
Ni(2)	18(1)	28(1)	28(1)	15(1)	2(1)	4(1)
S(11)	23(1)	25(1)	33(1)	13(1)	4(1)	1(1)
C(21)	17(2)	25(2)	26(2)	10(1)	-2(1)	4(1)
N(31)	19(1)	23(2)	28(2)	11(1)	0(1)	5(1)
C(41)	21(2)	21(2)	28(2)	11(1)	-3(1)	1(1)
C(51)	20(2)	36(2)	39(2)	19(2)	-1(2)	1(2)
C(61)	27(2)	26(2)	46(2)	19(2)	-4(2)	-2(2)
C(71)	26(2)	25(2)	39(2)	9(2)	-6(2)	5(2)
C(81)	20(2)	24(2)	31(2)	4(2)	-1(1)	1(1)
C(91)	21(2)	23(2)	24(2)	8(1)	-3(1)	0(1)
S(101)	23(1)	27(1)	33(1)	12(1)	7(1)	4(1)

S(12)	28(1)	43(1)	28(1)	15(1)	-4(1)	3(1)
C(22)	28(2)	35(2)	23(2)	7(2)	-1(1)	1(2)
N(32)	23(2)	26(2)	26(2)	5(1)	0(1)	1(1)
C(42)	30(2)	23(2)	43(2)	6(2)	6(2)	0(2)
C(52)	32(2)	26(2)	47(3)	12(2)	8(2)	2(2)
C(62)	41(2)	31(2)	64(3)	20(2)	9(2)	1(2)
C(72)	73(3)	22(2)	68(4)	9(2)	12(3)	-2(2)
C(82)	79(4)	30(3)	52(3)	-6(2)	7(3)	-4(2)
C(92)	49(3)	34(2)	36(2)	3(2)	2(2)	-2(2)
S(102)	64(1)	46(1)	30(1)	-1(1)	-8(1)	-3(1)
S(13)	21(1)	25(1)	38(1)	13(1)	1(1)	2(1)
C(23)	19(2)	25(2)	29(2)	6(1)	2(1)	4(1)
N(33)	20(1)	27(2)	26(2)	10(1)	1(1)	3(1)
C(43)	20(2)	38(2)	27(2)	11(2)	4(1)	8(2)
C(53)	38(2)	37(2)	36(2)	16(2)	1(2)	1(2)
C(63)	47(3)	58(3)	37(3)	32(2)	5(2)	2(2)
C(73)	34(2)	78(3)	27(2)	24(2)	7(2)	18(2)
C(83)	30(2)	60(3)	27(2)	4(2)	3(2)	10(2)
C(93)	20(2)	41(2)	30(2)	8(2)	1(1)	6(2)
S(103)	29(1)	30(1)	36(1)	-1(1)	5(1)	3(1)
S(14)	23(1)	28(1)	27(1)	13(1)	0(1)	6(1)
C(24)	19(2)	29(2)	23(2)	6(1)	1(1)	4(1)
N(34)	17(1)	28(2)	25(2)	11(1)	3(1)	2(1)
C(44)	28(2)	32(2)	26(2)	11(2)	3(1)	1(2)

C(54)	23(2)	38(2)	38(2)	19(2)	0(2)	1(2)
C(64)	31(2)	52(3)	35(2)	27(2)	-2(2)	-2(2)
C(74)	35(2)	54(3)	27(2)	21(2)	5(2)	-1(2)
C(84)	31(2)	44(2)	31(2)	11(2)	8(2)	6(2)
C(94)	28(2)	30(2)	24(2)	7(2)	0(1)	5(2)
S(104)	27(1)	39(1)	33(1)	15(1)	8(1)	13(1)
Ni(3)	17(1)	32(1)	23(1)	7(1)	2(1)	4(1)
Ni(4)	21(1)	21(1)	26(1)	9(1)	2(1)	2(1)
S(15)	26(1)	57(1)	33(1)	23(1)	7(1)	4(1)
C(25)	20(2)	53(3)	47(3)	33(2)	-4(2)	-6(2)
N(35)	22(2)	32(2)	43(2)	19(2)	2(1)	-2(1)
C(45)	29(2)	30(2)	68(3)	26(2)	-19(2)	-5(2)
C(55)	42(3)	23(2)	77(4)	8(2)	-20(2)	-2(2)
C(65)	65(3)	28(3)	110(5)	-1(3)	-42(3)	10(2)
C(75)	79(4)	23(3)	127(6)	30(3)	-60(4)	-13(3)
C(85)	60(3)	43(3)	124(6)	55(4)	-47(4)	-26(3)
C(95)	41(2)	42(3)	96(4)	51(3)	-34(3)	-15(2)
S(105)	39(1)	73(1)	69(1)	55(1)	-8(1)	-13(1)
S(16)	21(1)	27(1)	30(1)	7(1)	-1(1)	1(1)
C(26)	17(2)	34(2)	22(2)	14(2)	3(1)	3(1)
N(36)	16(1)	34(2)	22(2)	8(1)	4(1)	2(1)
C(46)	21(2)	27(2)	26(2)	8(1)	5(1)	0(1)
C(56)	19(2)	38(2)	35(2)	6(2)	1(2)	2(2)
C(66)	31(2)	31(2)	33(2)	-2(2)	6(2)	-1(2)

C(76)	30(2)	31(2)	41(2)	10(2)	14(2)	5(2)
C(86)	21(2)	33(2)	37(2)	14(2)	6(2)	4(2)
C(96)	18(2)	29(2)	31(2)	12(2)	1(1)	-2(1)
S(106)	21(1)	30(1)	35(1)	9(1)	-4(1)	3(1)
S(17)	21(1)	25(1)	31(1)	5(1)	2(1)	1(1)
C(27)	20(2)	28(2)	25(2)	10(1)	5(1)	8(1)
N(37)	23(1)	25(2)	21(2)	7(1)	2(1)	3(1)
C(47)	24(2)	32(2)	30(2)	13(2)	8(1)	6(2)
C(57)	35(2)	37(2)	34(2)	7(2)	5(2)	1(2)
C(67)	38(2)	56(3)	35(3)	-9(2)	3(2)	2(2)
C(77)	35(2)	82(4)	24(2)	14(2)	6(2)	10(2)
C(87)	26(2)	64(3)	37(2)	26(2)	3(2)	4(2)
C(97)	23(2)	38(2)	36(2)	14(2)	4(2)	6(2)
S(107)	29(1)	31(1)	39(1)	20(1)	3(1)	5(1)
S(18)	23(1)	26(1)	32(1)	7(1)	4(1)	4(1)
C(28)	19(2)	28(2)	32(2)	14(2)	1(1)	1(1)
N(38)	19(1)	33(2)	25(2)	13(1)	0(1)	2(1)
C(48)	22(2)	28(2)	29(2)	12(2)	-1(1)	-3(1)
C(58)	21(2)	44(2)	32(2)	13(2)	-1(2)	1(2)
C(68)	35(2)	52(3)	27(2)	4(2)	2(2)	1(2)
C(78)	31(2)	56(3)	33(2)	13(2)	-7(2)	-4(2)
C(88)	25(2)	43(2)	39(2)	19(2)	-7(2)	-2(2)
C(98)	23(2)	31(2)	34(2)	19(2)	-1(1)	0(2)
S(108)	24(1)	34(1)	37(1)	14(1)	-1(1)	8(1)

Ni(5)	32(1)	42(1)	18(1)	11(1)	4(1)	1(1)
Ni(6)	30(1)	43(1)	17(1)	10(1)	-1(1)	3(1)
S(19)	33(1)	44(1)	25(1)	15(1)	-2(1)	-2(1)
C(29)	24(2)	50(2)	23(2)	15(2)	1(1)	1(2)
N(39)	29(2)	43(2)	20(2)	13(1)	0(1)	0(1)
C(49)	23(2)	45(2)	23(2)	9(2)	0(1)	2(2)
C(59)	34(2)	56(3)	31(2)	13(2)	1(2)	1(2)
C(69)	34(2)	51(3)	43(3)	1(2)	-4(2)	5(2)
C(79)	32(2)	71(3)	29(2)	-5(2)	8(2)	8(2)
C(89)	27(2)	65(3)	28(2)	6(2)	8(2)	5(2)
C(99)	25(2)	55(3)	24(2)	12(2)	2(2)	0(2)
S(109)	34(1)	57(1)	28(1)	20(1)	8(1)	1(1)
S(1A)	34(1)	48(1)	23(1)	9(1)	1(1)	-5(1)
C(2A)	22(2)	60(3)	20(2)	10(2)	1(1)	-1(2)
N(3A)	28(2)	52(2)	18(2)	15(1)	0(1)	2(1)
C(4A)	23(2)	52(3)	25(2)	14(2)	4(1)	4(2)
C(5A)	35(2)	52(3)	30(2)	15(2)	0(2)	11(2)
C(6A)	37(2)	56(3)	46(3)	16(2)	4(2)	13(2)
C(7A)	32(2)	74(3)	47(3)	33(3)	-2(2)	13(2)
C(8A)	32(2)	84(4)	38(3)	31(3)	-11(2)	-1(2)
C(9A)	26(2)	65(3)	29(2)	21(2)	2(2)	0(2)
S(10A)	35(1)	66(1)	25(1)	14(1)	-8(1)	-4(1)
S(1B)	36(1)	57(1)	27(1)	15(1)	7(1)	9(1)
C(2B)	30(2)	67(3)	18(2)	18(2)	3(2)	2(2)

N(3B)	35(2)	45(2)	21(2)	15(1)	5(1)	1(2)
C(4B)	42(2)	54(3)	23(2)	16(2)	0(2)	-10(2)
C(5B)	65(3)	53(3)	34(3)	16(2)	5(2)	1(2)
C(6B)	72(3)	51(3)	47(3)	23(2)	12(2)	3(3)
C(7B)	78(4)	65(4)	50(3)	33(3)	4(3)	-13(3)
C(8B)	52(3)	82(4)	40(3)	33(3)	3(2)	-14(3)
C(9B)	39(2)	64(3)	28(2)	19(2)	-2(2)	-7(2)
S(10B)	38(1)	76(1)	31(1)	25(1)	11(1)	2(1)
S(1C)	39(1)	45(1)	25(1)	13(1)	-1(1)	7(1)
C(2C)	34(2)	50(3)	20(2)	12(2)	-2(2)	1(2)
N(3C)	35(2)	46(2)	19(2)	11(1)	1(1)	4(2)
C(4C)	36(2)	48(3)	23(2)	10(2)	1(2)	2(2)
C(5C)	50(3)	52(3)	27(2)	7(2)	-2(2)	15(2)
C(6C)	75(4)	59(3)	41(3)	1(2)	-3(3)	14(3)
C(7C)	63(3)	70(4)	33(3)	-2(2)	-3(2)	7(3)
C(8C)	42(3)	68(3)	34(3)	8(2)	-8(2)	1(2)
C(9C)	39(2)	48(3)	24(2)	11(2)	-2(2)	1(2)
S(10C)	39(1)	56(1)	27(1)	14(1)	-9(1)	4(1)

Table 5. Hydrogen coordinates ($\times 10^4$) and isotropic displacement parameters ($\text{\AA}^2 \times 10^3$) for pt6036.

	x	y	z	U(eq)
H(51)	1413	4486	3302	36
H(61)	784	5630	3428	38
H(71)	-445	5849	4025	36
H(81)	-1098	4924	4516	31
H(52)	2099	404	4093	42
H(62)	2118	-913	3871	53
H(72)	1742	-1689	2798	66
H(82)	1275	-1175	1937	69
H(53)	1438	1403	5246	43
H(63)	1249	1324	6372	53
H(73)	1475	2394	7277	52
H(83)	1975	3565	7098	48
H(54)	2257	3615	2233	38
H(64)	3005	4065	1405	44
H(74)	4365	3727	1143	44

H(84)	5003	2941	1695	42
H(55)	6976	377	3919	58
H(65)	6925	-954	3687	85
H(75)	6369	-1587	4490	91
H(85)	5876	-931	5503	86
H(56)	6497	4638	6365	37
H(66)	5832	5731	6862	40
H(76)	4523	5921	6431	40
H(86)	3827	4997	5545	35
H(57)	6354	1359	3116	43
H(67)	6131	1201	1948	56
H(77)	6452	2187	1437	56
H(87)	6987	3394	2090	48
H(58)	7282	3728	7065	38
H(68)	8033	4173	8100	47
H(78)	9383	3812	8224	48
H(88)	10000	2999	7326	41
H(59)	6949	7089	1622	48
H(69)	6499	7979	2566	54
H(79)	5769	7575	3428	56
H(89)	5474	6279	3361	49
H(5A)	8046	2863	606	46
H(6A)	8472	1927	1120	54
H(7A)	9173	2299	2185	57

H(8A)	9503	3568	2725	59
H(5B)	7280	7172	352	60
H(6B)	7564	8251	-50	66
H(7B)	8580	8289	-868	75
H(8B)	9375	7256	-1279	67
H(5C)	7662	2846	-667	52
H(6C)	7343	1773	-1563	72
H(7C)	6365	1779	-2412	70
H(8C)	5588	2827	-2335	59

Crystal Data for Complex 5a

Table 1. Crystal data and structure refinement for pt0512.

Contact Fraser J. White, f.j.white@sms.ed.ac.uk

A. CRYSTAL DATA

Empirical formula C₄₅ H₄₈ Fe₂ N₆ O₁₅
2(C₂₁ H₁₈ Fe N₃ O₆), 3(C H₄ O)

Formula weight 1024.59

Wavelength 0.71073 Å

Temperature 150(2) K

Crystal system Monoclinic

Space group P 2₁/c

Unit cell dimensions a = 20.2477(8) Å alpha = 90 deg.
b = 11.3483(4) Å beta = 115.874(2) deg.
c = 22.4035(9) Å gamma = 90 deg.

Volume 4631.8(3) Å³

Number of reflections for cell 5970 (2 < theta < 27 deg.)

Z 4

Density (calculated) 1.469 Mg/m³

Absorption coefficient 0.702 mm⁻¹

F(000) 2128

B. DATA COLLECTION

Crystal description ORANGE BLOCK

Crystal size 0.53 x 0.34 x 0.14 mm

Instrument Bruker Smart Apex CCD

Theta range for data collection 1.12 to 27.04 deg.

Index ranges	-25<=h<=25, -14<=k<=14, -28<=l<=28
Reflections collected	62262
Independent reflections	10127 [R(int) = 0.0442]
Scan type	Omega and Phi scans
Absorption correction	Semi-empirical from equivalents (Tmin= 0.74, Tmax=0.91)

C. SOLUTION AND REFINEMENT.

Solution	direct (SHELXS-97 (Sheldrick, 1990))
Refinement type	Full-matrix least-squares on F ²
Program used for refinement	SHELXL-97
Hydrogen atom placement	geom
Hydrogen atom treatment	mixed
Data / restraints / parameters	10127/ 0/ 652
Goodness-of-fit on F ²	1.086
Conventional R [F>4sigma(F)]	R1 = 0.0371 [8129 data]
Rw	0.1064
Final maximum delta/sigma	0.002

Weighting scheme
calc $w=1/[\sigma^2(F_o^2)+(0.0577P)^2+1.4434P]$ where $P=(F_o^2+2F_c^2)/3$

Largest diff. peak and hole	0.548 and -0.286 e.A ⁻³
-----------------------------	------------------------------------

Table 2. Atomic coordinates ($\times 10^4$) and equivalent isotropic displacement parameters ($\text{\AA}^2 \times 10^3$) for pt0512. $U(\text{eq})$ is defined as one third of the trace of the orthogonalized U_{ij} tensor.

	x	y	z	$U(\text{eq})$
Fe(1)	5219(1)	6773(1)	6622(1)	19(1)
Fe(2)	1283(1)	1941(1)	1136(1)	19(1)
C(1A)	2942(1)	7405(2)	5521(1)	30(1)
C(2A)	2437(1)	7744(2)	5760(1)	40(1)
C(3A)	1692(1)	7620(2)	5354(2)	51(1)
C(4A)	1449(1)	7164(2)	4722(2)	52(1)
C(5A)	1947(2)	6828(2)	4487(2)	47(1)
C(6A)	2694(1)	6940(2)	4885(1)	37(1)
C(10A)	3745(1)	7452(2)	5952(1)	25(1)
O(11A)	4190(1)	6783(1)	5848(1)	26(1)
N(11A)	4005(1)	8162(2)	6463(1)	25(1)
O(12A)	4747(1)	8106(1)	6872(1)	23(1)
C(1B)	6811(1)	8775(2)	6337(1)	22(1)
C(2B)	7503(1)	9220(2)	6750(1)	30(1)
C(3B)	7885(1)	9872(2)	6483(1)	35(1)
C(4B)	7581(1)	10097(2)	5806(1)	37(1)
C(5B)	6899(1)	9653(2)	5395(1)	35(1)
C(6B)	6518(1)	8981(2)	5657(1)	28(1)
C(10B)	6366(1)	8063(2)	6580(1)	21(1)
O(11B)	5746(1)	7649(1)	6177(1)	22(1)
N(11B)	6604(1)	7827(2)	7212(1)	24(1)
O(12B)	6167(1)	7130(1)	7393(1)	24(1)
C(1C)	5217(1)	3076(2)	6299(1)	21(1)
C(2C)	4943(1)	2141(2)	6526(1)	26(1)
C(3C)	4948(1)	1010(2)	6291(1)	29(1)
C(4C)	5218(1)	810(2)	5829(1)	30(1)
C(5C)	5473(1)	1745(2)	5591(1)	29(1)
C(6C)	5472(1)	2878(2)	5822(1)	25(1)
C(10C)	5227(1)	4298(2)	6539(1)	20(1)
O(11C)	5359(1)	5178(1)	6255(1)	22(1)
N(11C)	5076(1)	4487(1)	7046(1)	20(1)
O(12C)	5049(1)	5641(1)	7225(1)	23(1)
C(1D)	2651(1)	1248(2)	199(1)	21(1)
C(2D)	3370(1)	866(2)	422(1)	27(1)
C(3D)	3664(1)	696(2)	-24(1)	27(1)
C(4D)	3246(1)	897(2)	-693(1)	27(1)
C(5D)	2524(1)	1273(2)	-919(1)	31(1)
C(6D)	2232(1)	1456(2)	-474(1)	28(1)

C(10D)	2301(1)	1428(2)	649(1)	21(1)
O(11D)	1725(1)	2073(1)	484(1)	22(1)
N(11D)	2575(1)	924(2)	1230(1)	23(1)
O(12D)	2233(1)	1113(1)	1633(1)	23(1)
C(1E)	67(1)	-484(2)	1696(1)	23(1)
C(2E)	-253(1)	-1561(2)	1432(1)	28(1)
C(3E)	-546(1)	-2253(2)	1767(1)	33(1)
C(4E)	-515(1)	-1890(2)	2366(1)	37(1)
C(5E)	-186(2)	-835(2)	2631(1)	45(1)
C(6E)	104(1)	-131(2)	2301(1)	36(1)
C(10E)	403(1)	281(2)	1372(1)	22(1)
O(11E)	868(1)	1076(1)	1694(1)	24(1)
N(11E)	234(1)	147(2)	744(1)	25(1)
O(12E)	587(1)	837(1)	472(1)	27(1)
C(1F)	1713(1)	5280(2)	2089(1)	24(1)
C(2F)	1308(1)	6310(2)	2009(1)	39(1)
C(3F)	1610(1)	7250(2)	2437(1)	44(1)
C(4F)	2314(1)	7181(2)	2934(1)	34(1)
C(5F)	2719(1)	6167(2)	3009(1)	32(1)
C(6F)	2420(1)	5219(2)	2590(1)	27(1)
C(10F)	1414(1)	4231(2)	1665(1)	22(1)
O(11F)	1728(1)	3228(1)	1837(1)	23(1)
N(11F)	827(1)	4304(2)	1098(1)	25(1)
O(12F)	578(1)	3272(1)	743(1)	25(1)
O(1S)	205(1)	3957(2)	9487(1)	32(1)
C(1S)	879(1)	4461(2)	9556(1)	42(1)
O(2S)	3406(1)	10156(1)	6707(1)	36(1)
C(2S)	2912(1)	10868(2)	6186(1)	38(1)
O(3S)	3598(1)	5658(2)	6959(1)	37(1)
C(3S)	3307(1)	6279(2)	7340(1)	36(1)

Table 3. Bond lengths [Å] and angles [deg] for pt0512.

Fe(1)-O(12B)	1.9843(14)
Fe(1)-O(12A)	1.9966(14)
Fe(1)-O(12C)	2.0015(14)
Fe(1)-O(11B)	2.0118(14)
Fe(1)-O(11A)	2.0486(14)
Fe(1)-O(11C)	2.0588(14)
Fe(2)-O(12E)	1.9853(14)
Fe(2)-O(12D)	1.9878(14)
Fe(2)-O(12F)	1.9988(14)
Fe(2)-O(11D)	2.0234(14)
Fe(2)-O(11E)	2.0382(14)
Fe(2)-O(11F)	2.0439(14)
C(1A)-C(6A)	1.393(3)
C(1A)-C(2A)	1.401(3)
C(1A)-C(10A)	1.485(3)
C(2A)-C(3A)	1.387(4)
C(2A)-H(2A)	0.9500
C(3A)-C(4A)	1.380(4)
C(3A)-H(3A)	0.9500
C(4A)-C(5A)	1.381(4)
C(4A)-H(4A)	0.9500
C(5A)-C(6A)	1.385(3)
C(5A)-H(5A)	0.9500
C(6A)-H(6A)	0.9500
C(10A)-O(11A)	1.274(3)
C(10A)-N(11A)	1.310(3)
N(11A)-O(12A)	1.378(2)
N(11A)-H(11A)	0.86(3)
C(1B)-C(6B)	1.393(3)
C(1B)-C(2B)	1.394(3)
C(1B)-C(10B)	1.480(3)
C(2B)-C(3B)	1.381(3)
C(2B)-H(2B)	0.9500
C(3B)-C(4B)	1.389(4)
C(3B)-H(3B)	0.9500
C(4B)-C(5B)	1.379(4)
C(4B)-H(4B)	0.9500
C(5B)-C(6B)	1.384(3)
C(5B)-H(5B)	0.9500
C(6B)-H(6B)	0.9500
C(10B)-O(11B)	1.273(2)
C(10B)-N(11B)	1.309(3)
N(11B)-O(12B)	1.373(2)
N(11B)-H(11B)	0.80(3)

C(1C)-C(6C)	1.391(3)
C(1C)-C(2C)	1.394(3)
C(1C)-C(10C)	1.485(3)
C(2C)-C(3C)	1.389(3)
C(2C)-H(2C)	0.9500
C(3C)-C(4C)	1.384(3)
C(3C)-H(3C)	0.9500
C(4C)-C(5C)	1.385(3)
C(4C)-H(4C)	0.9500
C(5C)-C(6C)	1.386(3)
C(5C)-H(5C)	0.9500
C(6C)-H(6C)	0.9500
C(10C)-O(11C)	1.275(2)
C(10C)-N(11C)	1.315(3)
N(11C)-O(12C)	1.379(2)
N(11C)-H(11C)	0.88(3)
C(1D)-C(2D)	1.388(3)
C(1D)-C(6D)	1.391(3)
C(1D)-C(10D)	1.477(3)
C(2D)-C(3D)	1.382(3)
C(2D)-H(2D)	0.9500
C(3D)-C(4D)	1.382(3)
C(3D)-H(3D)	0.9500
C(4D)-C(5D)	1.390(3)
C(4D)-H(4D)	0.9500
C(5D)-C(6D)	1.377(3)
C(5D)-H(5D)	0.9500
C(6D)-H(6D)	0.9500
C(10D)-O(11D)	1.287(2)
C(10D)-N(11D)	1.305(3)
N(11D)-O(12D)	1.373(2)
N(11D)-H(11D)	0.87(3)
C(1E)-C(6E)	1.385(3)
C(1E)-C(2E)	1.389(3)
C(1E)-C(10E)	1.473(3)
C(2E)-C(3E)	1.386(3)
C(2E)-H(2E)	0.9500
C(3E)-C(4E)	1.379(3)
C(3E)-H(3E)	0.9500
C(4E)-C(5E)	1.372(3)
C(4E)-H(4E)	0.9500
C(5E)-C(6E)	1.382(3)
C(5E)-H(5E)	0.9500
C(6E)-H(6E)	0.9500
C(10E)-O(11E)	1.276(2)
C(10E)-N(11E)	1.305(3)
N(11E)-O(12E)	1.370(2)
N(11E)-H(11E)	0.80(2)

C(1F)-C(6F)	1.382(3)
C(1F)-C(2F)	1.395(3)
C(1F)-C(10F)	1.478(3)
C(2F)-C(3F)	1.385(3)
C(2F)-H(2F)	0.9500
C(3F)-C(4F)	1.375(3)
C(3F)-H(3F)	0.9500
C(4F)-C(5F)	1.381(3)
C(4F)-H(4F)	0.9500
C(5F)-C(6F)	1.381(3)
C(5F)-H(5F)	0.9500
C(6F)-H(6F)	0.9500
C(10F)-O(11F)	1.278(2)
C(10F)-N(11F)	1.309(3)
N(11F)-O(12F)	1.381(2)
N(11F)-H(11F)	0.89(3)
O(1S)-C(1S)	1.424(3)
O(1S)-H(1S)	0.76(3)
C(1S)-H(11)	0.9800
C(1S)-H(12)	0.9800
C(1S)-H(13)	0.9800
O(2S)-C(2S)	1.412(3)
O(2S)-H(2S)	0.76(3)
C(2S)-H(21)	0.9800
C(2S)-H(22)	0.9800
C(2S)-H(23)	0.9800
O(3S)-C(3S)	1.419(3)
O(3S)-H(3S)	0.78(2)
C(3S)-H(31)	0.9800
C(3S)-H(32)	0.9800
C(3S)-H(33)	0.9800
O(12B)-Fe(1)-O(12A)	89.99(6)
O(12B)-Fe(1)-O(12C)	85.92(6)
O(12A)-Fe(1)-O(12C)	92.92(6)
O(12B)-Fe(1)-O(11B)	79.09(6)
O(12A)-Fe(1)-O(11B)	100.83(6)
O(12C)-Fe(1)-O(11B)	159.56(6)
O(12B)-Fe(1)-O(11A)	167.38(6)
O(12A)-Fe(1)-O(11A)	78.35(6)
O(12C)-Fe(1)-O(11A)	99.36(6)
O(11B)-Fe(1)-O(11A)	98.19(6)
O(12B)-Fe(1)-O(11C)	106.17(6)
O(12A)-Fe(1)-O(11C)	160.89(6)
O(12C)-Fe(1)-O(11C)	78.46(5)
O(11B)-Fe(1)-O(11C)	92.36(6)
O(11A)-Fe(1)-O(11C)	86.18(6)
O(12E)-Fe(2)-O(12D)	108.51(6)

O(12E)-Fe(2)-O(12F)	90.57(6)
O(12D)-Fe(2)-O(12F)	159.09(6)
O(12E)-Fe(2)-O(11D)	84.14(6)
O(12D)-Fe(2)-O(11D)	79.32(6)
O(12F)-Fe(2)-O(11D)	94.69(6)
O(12E)-Fe(2)-O(11E)	78.94(6)
O(12D)-Fe(2)-O(11E)	89.18(6)
O(12F)-Fe(2)-O(11E)	103.19(6)
O(11D)-Fe(2)-O(11E)	155.37(6)
O(12E)-Fe(2)-O(11F)	163.33(6)
O(12D)-Fe(2)-O(11F)	85.04(6)
O(12F)-Fe(2)-O(11F)	77.84(5)
O(11D)-Fe(2)-O(11F)	108.47(6)
O(11E)-Fe(2)-O(11F)	91.95(6)
C(6A)-C(1A)-C(2A)	119.9(2)
C(6A)-C(1A)-C(10A)	118.8(2)
C(2A)-C(1A)-C(10A)	121.1(2)
C(3A)-C(2A)-C(1A)	119.2(3)
C(3A)-C(2A)-H(2A)	120.4
C(1A)-C(2A)-H(2A)	120.4
C(4A)-C(3A)-C(2A)	120.7(3)
C(4A)-C(3A)-H(3A)	119.6
C(2A)-C(3A)-H(3A)	119.6
C(3A)-C(4A)-C(5A)	120.1(2)
C(3A)-C(4A)-H(4A)	119.9
C(5A)-C(4A)-H(4A)	119.9
C(4A)-C(5A)-C(6A)	120.2(3)
C(4A)-C(5A)-H(5A)	119.9
C(6A)-C(5A)-H(5A)	119.9
C(5A)-C(6A)-C(1A)	119.9(3)
C(5A)-C(6A)-H(6A)	120.0
C(1A)-C(6A)-H(6A)	120.0
O(11A)-C(10A)-N(11A)	118.65(19)
O(11A)-C(10A)-C(1A)	121.38(19)
N(11A)-C(10A)-C(1A)	119.92(19)
C(10A)-O(11A)-Fe(1)	112.88(13)
C(10A)-N(11A)-O(12A)	117.34(17)
C(10A)-N(11A)-H(11A)	124.6(17)
O(12A)-N(11A)-H(11A)	117.1(17)
N(11A)-O(12A)-Fe(1)	111.42(11)
C(6B)-C(1B)-C(2B)	119.4(2)
C(6B)-C(1B)-C(10B)	117.20(19)
C(2B)-C(1B)-C(10B)	123.41(19)
C(3B)-C(2B)-C(1B)	119.8(2)
C(3B)-C(2B)-H(2B)	120.1
C(1B)-C(2B)-H(2B)	120.1
C(2B)-C(3B)-C(4B)	120.4(2)
C(2B)-C(3B)-H(3B)	119.8

C(4B)-C(3B)-H(3B)	119.8
C(5B)-C(4B)-C(3B)	120.0(2)
C(5B)-C(4B)-H(4B)	120.0
C(3B)-C(4B)-H(4B)	120.0
C(4B)-C(5B)-C(6B)	119.9(2)
C(4B)-C(5B)-H(5B)	120.0
C(6B)-C(5B)-H(5B)	120.0
C(5B)-C(6B)-C(1B)	120.4(2)
C(5B)-C(6B)-H(6B)	119.8
C(1B)-C(6B)-H(6B)	119.8
O(11B)-C(10B)-N(11B)	118.36(18)
O(11B)-C(10B)-C(1B)	120.68(18)
N(11B)-C(10B)-C(1B)	120.94(18)
C(10B)-O(11B)-Fe(1)	113.72(12)
C(10B)-N(11B)-O(12B)	117.22(17)
C(10B)-N(11B)-H(11B)	124.5(18)
O(12B)-N(11B)-H(11B)	118.2(18)
N(11B)-O(12B)-Fe(1)	111.26(11)
C(6C)-C(1C)-C(2C)	119.80(19)
C(6C)-C(1C)-C(10C)	118.64(18)
C(2C)-C(1C)-C(10C)	121.54(19)
C(3C)-C(2C)-C(1C)	119.7(2)
C(3C)-C(2C)-H(2C)	120.2
C(1C)-C(2C)-H(2C)	120.2
C(4C)-C(3C)-C(2C)	120.4(2)
C(4C)-C(3C)-H(3C)	119.8
C(2C)-C(3C)-H(3C)	119.8
C(3C)-C(4C)-C(5C)	119.9(2)
C(3C)-C(4C)-H(4C)	120.1
C(5C)-C(4C)-H(4C)	120.1
C(4C)-C(5C)-C(6C)	120.3(2)
C(4C)-C(5C)-H(5C)	119.9
C(6C)-C(5C)-H(5C)	119.9
C(5C)-C(6C)-C(1C)	119.9(2)
C(5C)-C(6C)-H(6C)	120.0
C(1C)-C(6C)-H(6C)	120.0
O(11C)-C(10C)-N(11C)	118.94(18)
O(11C)-C(10C)-C(1C)	121.46(18)
N(11C)-C(10C)-C(1C)	119.58(17)
C(10C)-O(11C)-Fe(1)	113.12(12)
C(10C)-N(11C)-O(12C)	117.37(16)
C(10C)-N(11C)-H(11C)	127.6(16)
O(12C)-N(11C)-H(11C)	114.4(16)
N(11C)-O(12C)-Fe(1)	111.87(11)
C(2D)-C(1D)-C(6D)	119.39(19)
C(2D)-C(1D)-C(10D)	122.57(18)
C(6D)-C(1D)-C(10D)	118.04(18)
C(3D)-C(2D)-C(1D)	119.9(2)

C(3D)-C(2D)-H(2D)	120.0
C(1D)-C(2D)-H(2D)	120.0
C(2D)-C(3D)-C(4D)	120.6(2)
C(2D)-C(3D)-H(3D)	119.7
C(4D)-C(3D)-H(3D)	119.7
C(3D)-C(4D)-C(5D)	119.6(2)
C(3D)-C(4D)-H(4D)	120.2
C(5D)-C(4D)-H(4D)	120.2
C(6D)-C(5D)-C(4D)	119.9(2)
C(6D)-C(5D)-H(5D)	120.1
C(4D)-C(5D)-H(5D)	120.1
C(5D)-C(6D)-C(1D)	120.6(2)
C(5D)-C(6D)-H(6D)	119.7
C(1D)-C(6D)-H(6D)	119.7
O(11D)-C(10D)-N(11D)	118.21(19)
O(11D)-C(10D)-C(1D)	121.88(18)
N(11D)-C(10D)-C(1D)	119.91(18)
C(10D)-O(11D)-Fe(2)	112.49(13)
C(10D)-N(11D)-O(12D)	118.08(17)
C(10D)-N(11D)-H(11D)	127.7(17)
O(12D)-N(11D)-H(11D)	113.7(17)
N(11D)-O(12D)-Fe(2)	110.39(11)
C(6E)-C(1E)-C(2E)	119.2(2)
C(6E)-C(1E)-C(10E)	118.17(19)
C(2E)-C(1E)-C(10E)	122.61(19)
C(3E)-C(2E)-C(1E)	119.9(2)
C(3E)-C(2E)-H(2E)	120.1
C(1E)-C(2E)-H(2E)	120.1
C(4E)-C(3E)-C(2E)	120.7(2)
C(4E)-C(3E)-H(3E)	119.6
C(2E)-C(3E)-H(3E)	119.6
C(5E)-C(4E)-C(3E)	119.2(2)
C(5E)-C(4E)-H(4E)	120.4
C(3E)-C(4E)-H(4E)	120.4
C(4E)-C(5E)-C(6E)	120.8(2)
C(4E)-C(5E)-H(5E)	119.6
C(6E)-C(5E)-H(5E)	119.6
C(5E)-C(6E)-C(1E)	120.2(2)
C(5E)-C(6E)-H(6E)	119.9
C(1E)-C(6E)-H(6E)	119.9
O(11E)-C(10E)-N(11E)	118.30(19)
O(11E)-C(10E)-C(1E)	121.55(18)
N(11E)-C(10E)-C(1E)	120.14(18)
C(10E)-O(11E)-Fe(2)	113.18(12)
C(10E)-N(11E)-O(12E)	118.15(17)
C(10E)-N(11E)-H(11E)	127.4(17)
O(12E)-N(11E)-H(11E)	114.4(17)
N(11E)-O(12E)-Fe(2)	111.39(11)

C(6F)-C(1F)-C(2F)	119.23(19)
C(6F)-C(1F)-C(10F)	118.09(18)
C(2F)-C(1F)-C(10F)	122.68(19)
C(3F)-C(2F)-C(1F)	120.0(2)
C(3F)-C(2F)-H(2F)	120.0
C(1F)-C(2F)-H(2F)	120.0
C(4F)-C(3F)-C(2F)	120.4(2)
C(4F)-C(3F)-H(3F)	119.8
C(2F)-C(3F)-H(3F)	119.8
C(3F)-C(4F)-C(5F)	119.8(2)
C(3F)-C(4F)-H(4F)	120.1
C(5F)-C(4F)-H(4F)	120.1
C(4F)-C(5F)-C(6F)	120.3(2)
C(4F)-C(5F)-H(5F)	119.8
C(6F)-C(5F)-H(5F)	119.8
C(5F)-C(6F)-C(1F)	120.3(2)
C(5F)-C(6F)-H(6F)	119.8
C(1F)-C(6F)-H(6F)	119.8
O(11F)-C(10F)-N(11F)	118.11(18)
O(11F)-C(10F)-C(1F)	120.81(18)
N(11F)-C(10F)-C(1F)	121.08(18)
C(10F)-O(11F)-Fe(2)	114.14(12)
C(10F)-N(11F)-O(12F)	116.97(17)
C(10F)-N(11F)-H(11F)	128.0(16)
O(12F)-N(11F)-H(11F)	115.0(16)
N(11F)-O(12F)-Fe(2)	112.07(11)
C(1S)-O(1S)-H(1S)	110(2)
O(1S)-C(1S)-H(11)	109.5
O(1S)-C(1S)-H(12)	109.5
H(11)-C(1S)-H(12)	109.5
O(1S)-C(1S)-H(13)	109.5
H(11)-C(1S)-H(13)	109.5
H(12)-C(1S)-H(13)	109.5
C(2S)-O(2S)-H(2S)	104(2)
O(2S)-C(2S)-H(21)	109.5
O(2S)-C(2S)-H(22)	109.5
H(21)-C(2S)-H(22)	109.5
O(2S)-C(2S)-H(23)	109.5
H(21)-C(2S)-H(23)	109.5
H(22)-C(2S)-H(23)	109.5
C(3S)-O(3S)-H(3S)	113.3(18)
O(3S)-C(3S)-H(31)	109.5
O(3S)-C(3S)-H(32)	109.5
H(31)-C(3S)-H(32)	109.5
O(3S)-C(3S)-H(33)	109.5
H(31)-C(3S)-H(33)	109.5
H(32)-C(3S)-H(33)	109.5

Symmetry transformations used to generate equivalent atoms:

Table 4. Anisotropic displacement parameters ($\text{Å}^2 \times 10^3$) for pt0512.
 The anisotropic displacement factor exponent takes the form:
 $-2 \pi^2 [h^2 a^{*2} U_{11} + \dots + 2 h k a^* b^* U_{12}]$

	U11	U22	U33	U23	U13	U12
Fe(1)	21(1)	15(1)	21(1)	0(1)	9(1)	-1(1)
Fe(2)	19(1)	20(1)	17(1)	-2(1)	7(1)	-1(1)
C(1A)	25(1)	19(1)	39(1)	2(1)	7(1)	1(1)
C(2A)	30(1)	33(1)	49(2)	2(1)	11(1)	0(1)
C(3A)	28(1)	44(2)	78(2)	6(2)	18(1)	1(1)
C(4A)	26(1)	39(1)	70(2)	3(1)	0(1)	-6(1)
C(5A)	38(2)	31(1)	48(2)	-1(1)	-5(1)	-2(1)
C(6A)	35(1)	24(1)	40(1)	1(1)	6(1)	3(1)
C(10A)	26(1)	17(1)	29(1)	3(1)	10(1)	0(1)
O(11A)	24(1)	24(1)	27(1)	-4(1)	7(1)	2(1)
N(11A)	22(1)	18(1)	32(1)	-1(1)	10(1)	2(1)
O(12A)	21(1)	18(1)	26(1)	-3(1)	8(1)	1(1)
C(1B)	26(1)	18(1)	26(1)	0(1)	13(1)	2(1)
C(2B)	33(1)	29(1)	30(1)	-5(1)	15(1)	-7(1)
C(3B)	33(1)	32(1)	47(2)	-8(1)	23(1)	-10(1)
C(4B)	45(1)	27(1)	54(2)	5(1)	36(1)	-1(1)
C(5B)	43(1)	32(1)	37(1)	11(1)	25(1)	5(1)
C(6B)	28(1)	30(1)	27(1)	3(1)	13(1)	1(1)
C(10B)	23(1)	17(1)	23(1)	-1(1)	11(1)	1(1)
O(11B)	22(1)	24(1)	20(1)	0(1)	8(1)	-3(1)
N(11B)	22(1)	26(1)	22(1)	1(1)	8(1)	-6(1)
O(12B)	26(1)	25(1)	22(1)	4(1)	10(1)	-5(1)
C(1C)	19(1)	20(1)	20(1)	0(1)	5(1)	1(1)
C(2C)	32(1)	22(1)	25(1)	-1(1)	12(1)	-1(1)
C(3C)	35(1)	18(1)	28(1)	1(1)	8(1)	-3(1)
C(4C)	32(1)	20(1)	28(1)	-7(1)	6(1)	3(1)
C(5C)	30(1)	29(1)	28(1)	-8(1)	12(1)	2(1)
C(6C)	23(1)	24(1)	26(1)	-2(1)	9(1)	-1(1)
C(10C)	17(1)	20(1)	21(1)	1(1)	6(1)	0(1)
O(11C)	28(1)	17(1)	24(1)	0(1)	14(1)	-1(1)
N(11C)	26(1)	13(1)	23(1)	-1(1)	12(1)	-1(1)
O(12C)	32(1)	13(1)	28(1)	-3(1)	18(1)	-2(1)
C(1D)	24(1)	18(1)	22(1)	-1(1)	11(1)	-2(1)
C(2D)	25(1)	29(1)	22(1)	0(1)	8(1)	0(1)

C(3D)	24(1)	27(1)	32(1)	-4(1)	13(1)	0(1)
C(4D)	35(1)	25(1)	30(1)	-3(1)	21(1)	-4(1)
C(5D)	35(1)	39(1)	22(1)	6(1)	13(1)	3(1)
C(6D)	26(1)	32(1)	27(1)	4(1)	12(1)	4(1)
C(10D)	22(1)	17(1)	22(1)	-3(1)	8(1)	-3(1)
O(11D)	21(1)	23(1)	21(1)	2(1)	9(1)	3(1)
N(11D)	24(1)	22(1)	23(1)	2(1)	12(1)	5(1)
O(12D)	24(1)	28(1)	20(1)	3(1)	12(1)	5(1)
C(1E)	21(1)	24(1)	24(1)	-1(1)	11(1)	0(1)
C(2E)	32(1)	26(1)	21(1)	1(1)	8(1)	-1(1)
C(3E)	36(1)	27(1)	32(1)	5(1)	10(1)	-5(1)
C(4E)	43(1)	36(1)	40(1)	7(1)	27(1)	-4(1)
C(5E)	64(2)	49(2)	40(1)	-9(1)	39(1)	-14(1)
C(6E)	48(2)	34(1)	37(1)	-12(1)	29(1)	-15(1)
C(10E)	21(1)	23(1)	22(1)	-2(1)	10(1)	0(1)
O(11E)	26(1)	27(1)	20(1)	-6(1)	11(1)	-8(1)
N(11E)	29(1)	27(1)	19(1)	-4(1)	10(1)	-12(1)
O(12E)	31(1)	31(1)	20(1)	-5(1)	12(1)	-13(1)
C(1F)	25(1)	23(1)	24(1)	-3(1)	11(1)	-2(1)
C(2F)	33(1)	31(1)	38(1)	-11(1)	0(1)	7(1)
C(3F)	43(2)	27(1)	49(2)	-11(1)	7(1)	9(1)
C(4F)	40(1)	26(1)	32(1)	-8(1)	10(1)	-6(1)
C(5F)	29(1)	29(1)	31(1)	-2(1)	5(1)	-5(1)
C(6F)	27(1)	22(1)	29(1)	1(1)	10(1)	1(1)
C(10F)	22(1)	23(1)	23(1)	-2(1)	11(1)	1(1)
O(11F)	22(1)	20(1)	22(1)	-3(1)	5(1)	2(1)
N(11F)	26(1)	21(1)	22(1)	-3(1)	7(1)	4(1)
O(12F)	23(1)	24(1)	23(1)	-6(1)	5(1)	1(1)
O(1S)	34(1)	33(1)	22(1)	1(1)	5(1)	8(1)
C(1S)	42(2)	40(1)	37(1)	6(1)	13(1)	3(1)
O(2S)	35(1)	25(1)	34(1)	-6(1)	2(1)	8(1)
C(2S)	38(1)	37(1)	34(1)	4(1)	12(1)	9(1)
O(3S)	25(1)	41(1)	47(1)	-19(1)	18(1)	-10(1)
C(3S)	32(1)	40(1)	38(1)	-12(1)	16(1)	-4(1)

Table 5. Hydrogen coordinates ($\times 10^4$) and isotropic displacement parameters ($\text{Å}^2 \times 10^3$) for pt0512.

	x	y	z	U(eq)
H(2A)	2602	8055	6195	48
H(3A)	1346	7851	5512	62
H(4A)	938	7082	4449	63
H(5A)	1778	6519	4050	57
H(6A)	3036	6699	4724	44
H(2B)	7711	9076	7214	36
H(3B)	8358	10168	6764	42
H(4B)	7844	10557	5627	44
H(5B)	6690	9809	4932	42
H(6B)	6054	8658	5370	33
H(2C)	4753	2276	6840	31
H(3C)	4765	370	6448	35
H(4C)	5229	33	5676	35
H(5C)	5649	1610	5268	35
H(6C)	5644	3517	5655	30
H(2D)	3660	721	881	32
H(3D)	4158	439	131	33
H(4D)	3452	778	-997	33
H(5D)	2232	1403	-1379	38
H(6D)	1741	1727	-629	34
H(2E)	-271	-1823	1022	33
H(3E)	-769	-2984	1583	40
H(4E)	-720	-2365	2593	44
H(5E)	-157	-587	3047	54
H(6E)	328	599	2490	43
H(2F)	824	6367	1661	47
H(3F)	1330	7946	2386	53
H(4F)	2520	7829	3224	41
H(5F)	3206	6121	3350	39
H(6F)	2701	4522	2647	32
H(11)	1046	5047	9914	62
H(12)	805	4844	9139	62
H(13)	1250	3841	9663	62
H(21)	2642	11380	6355	57
H(22)	2565	10365	5833	57
H(23)	3186	11352	6009	57
H(31)	3516	5962	7792	55
H(32)	2772	6189	7137	55
H(33)	3431	7117	7354	55

H(11F)	563(13)	4940(20)	909(12)	34(7)
H(11E)	-53(13)	-310(20)	491(12)	26(6)
H(11D)	2923(14)	400(20)	1383(13)	41(7)
H(11B)	6977(14)	8080(20)	7499(12)	29(7)
H(11A)	3767(14)	8740(20)	6523(13)	38(7)
H(11C)	5052(13)	3960(20)	7327(12)	34(7)
H(3S)	4026(14)	5700(20)	7102(12)	26(7)
H(1S)	256(15)	3680(30)	9815(14)	42(9)
H(2S)	3607(17)	10590(30)	6990(15)	55(10)

Crystal Data for Complex 5b

data_pt0510

_audit_creation_method SHELXL-97
_chemical_name_systematic ?

_publ_contact_author_name 'Fraser J. White'
_publ_contact_author_email f.j.white@sms.ed.ac.uk
_chemical_compound_source 'Iria Rio'
_exptl_crystal_recrystallization_method 'Recrystallised from MeOH/MeCN solution'

_chemical_name_common ?
_chemical_melting_point ?
_chemical_formula_moiety 'C14 H12 Br Fe N2 O4'
_chemical_formula_sum 'C14 H12 Br Fe N2 O4'
_chemical_formula_weight 408.02

loop_

_atom_type_symbol
_atom_type_description
_atom_type_scatter_dispersion_real
_atom_type_scatter_dispersion_imag
_atom_type_scatter_source
C C 0.0033 0.0016 'International Tables Vol C Tables 4.2.6.8 and 6.1.1.4'
H H 0.0000 0.0000 'International Tables Vol C Tables 4.2.6.8 and 6.1.1.4'
Br Br -0.2901 2.4595 'International Tables Vol C Tables 4.2.6.8 and 6.1.1.4'
Fe Fe 0.3463 0.8444 'International Tables Vol C Tables 4.2.6.8 and 6.1.1.4'
N N 0.0061 0.0033 'International Tables Vol C Tables 4.2.6.8 and 6.1.1.4'
O O 0.0106 0.0060 'International Tables Vol C Tables 4.2.6.8 and 6.1.1.4'

_symmetry_cell_setting monoclinic
_symmetry_space_group_name_H-M 'C 2/c'
_symmetry_int_tables_number 15
_symmetry_space_group_name_Hall '-C 2yc'

loop_

_symmetry_equiv_pos_as_xyz
'x, y, z'
'-x, y, -z+1/2'
'x+1/2, y+1/2, z'
'-x+1/2, y+1/2, -z+1/2'
'-x, -y, -z'
'x, -y, z-1/2'
'-x+1/2, -y+1/2, -z'
'x+1/2, -y+1/2, z-1/2'

```
_cell_length_a      14.5538(9)
_cell_length_b      16.2543(10)
_cell_length_c      12.9684(8)
_cell_angle_alpha   90.00
_cell_angle_beta    91.814(4)
_cell_angle_gamma   90.00
_cell_volume        3066.3(3)
_cell_formula_units_Z  8
_cell_measurement_temperature 150(2)
_cell_measurement_reflns_used 5257
_cell_measurement_theta_min 2.5
_cell_measurement_theta_max 28.5

_exptl_crystal_description  block
_exptl_crystal_colour      black
_exptl_crystal_size_max    0.37
_exptl_crystal_size_mid    0.18
_exptl_crystal_size_min    0.14
_exptl_crystal_density_meas  ?
_exptl_crystal_density_diffn  1.768
_exptl_crystal_density_method 'not measured'
_exptl_crystal_F_000      1624
_exptl_absorpt_coefficient_mu  3.608
_exptl_absorpt_correction_type multi-scan
_exptl_absorpt_correction_T_min 0.46
_exptl_absorpt_correction_T_max 0.6
_exptl_absorpt_process_details 'SADABS 2004/1'

_exptl_special_details
;
?
;

_diffrn_ambient_temperature 150(2)
_diffrn_radiation_probe      ?
_diffrn_radiation_type       MoK\alpha
_diffrn_radiation_wavelength 0.71073
_diffrn_source                'fine-focus sealed tube'
_diffrn_radiation_monochromator graphite
_diffrn_measurement_device_type 'Bruker Smart APex CCD'
_diffrn_measurement_method    '\w + \o scans'
_diffrn_detector_area_resol_mean ?
_diffrn_standards_number      ?
_diffrn_standards_interval_count ?
_diffrn_standards_interval_time ?
_diffrn_standards_decay_%     ?
_diffrn_reflns_number         43236
_diffrn_reflns_av_R_equivalents 0.0422
```

```

_diffrn_reflms_av_sigmaI/netI  0.0346
_diffrn_reflms_limit_h_min     -20
_diffrn_reflms_limit_h_max     20
_diffrn_reflms_limit_k_min     -23
_diffrn_reflms_limit_k_max     22
_diffrn_reflms_limit_l_min     -18
_diffrn_reflms_limit_l_max     18
_diffrn_reflms_theta_min       1.88
_diffrn_reflms_theta_max       30.57
_reflms_number_total           4680
_reflms_number_gt              3511
_reflms_threshold_expression    >2sigma(I)

_computing_data_collection     SMART
_computing_cell_refinement     SAINT
_computing_data_reduction      SAINT
_computing_structure_solution  'SHELXS-97 (Sheldrick, 1990)'
_computing_structure_refinement 'SHELXL-97 (Sheldrick, 1997)'
_computing_molecular_graphics  XP
_computing_publication_material 'PLATON, ENCIFER, XCIF'

```

```
_refine_special_details
```

```
;
```

Refinement of F^2 against ALL reflections. The weighted R-factor wR and goodness of fit S are based on F^2 , conventional R-factors R are based on F, with F set to zero for negative F^2 . The threshold expression of $F^2 > 2\sigma(F^2)$ is used only for calculating R-factors(gt) etc. and is not relevant to the choice of reflections for refinement. R-factors based on F^2 are statistically about twice as large as those based on F, and R-factors based on ALL data will be even larger.

```

041_ALERT_1_C Calc. and Rep. SumFormula Strings Differ .... ?
045_ALERT_1_C Calculated and Reported Z Differ by ..... 0.50 Ratio
042_ALERT_1_C Calc. and Rep. MoietyFormula Strings Differ .... ?

```

Zcalc is half that of Zrep, but the reported formula is half that of calculated thus these cancel.

```
094_ALERT_2_C Ratio of Maximum / Minimum Residual Density .... 2.18
```

No action taken, these are small and next to the Fe atom

```

220_ALERT_2_C Large Non-Solvent C Ueq(max)/Ueq(min) ... 3.22 Ratio
241_ALERT_2_C Check High Ueq as Compared to Neighbors for C5B
241_ALERT_2_C Check High Ueq as Compared to Neighbors for C6B
242_ALERT_2_C Check Low Ueq as Compared to Neighbors for C1B
242_ALERT_2_C Check Low Ueq as Compared to Neighbors for C4B

```

Atoms C5B and C6B have small q peaks near them suggesting disorder in this phenyl ring also, they are however not sufficient to attempt to model this disorder and so I opted to model this with slightly raised ADPs. Atoms C5B and C4B are neighbours thus two alerts for one problem. Same goes for C6B and C1B.

301_ALERT_3_C Main Residue Disorder 21.00 Perc.
 779_ALERT_2_C Suspect or Irrelevant (Bond) Angle in CIF 2.60 Deg.
 C1A -C11A -C1A' 1.555 1.555 1.555

noted, there is a phenyl ring torsionally disordered and slightly displaced over two positions, C1A and C1A' are the same atom in the two parts, both are attached to C11A giving rise to the angle.

720_ALERT_4_C Number of Unusual/Non-Standard Label(s) 16

No action taken

912_ALERT_3_C # Missing FCF Reflections Above STH/L=0.6 33

See completeness stats below

INTENSITY STATISTICS FOR DATASET # 1 pt0510.hkl

Resolution	#Data	#Theory	%Complete	Redundancy	Mean I	Mean I/s	R(int)	Rsigma
Inf - 1.94	246	246	100.0	21.91	748.7	68.11	0.0267	0.0133
1.94 - 1.53	245	245	100.0	21.18	364.8	59.67	0.0325	0.0127
1.53 - 1.33	252	252	100.0	16.73	226.3	45.93	0.0390	0.0151
1.33 - 1.20	264	264	100.0	14.83	176.0	40.89	0.0470	0.0174
1.20 - 1.11	264	264	100.0	13.29	139.2	33.05	0.0529	0.0204
1.11 - 1.04	276	276	100.0	11.13	116.3	28.68	0.0589	0.0249
1.04 - 0.98	299	299	100.0	9.80	88.6	23.41	0.0729	0.0298
0.98 - 0.93	302	302	100.0	9.27	73.5	20.06	0.0782	0.0366
0.93 - 0.89	316	316	100.0	7.98	54.0	15.48	0.1027	0.0497
0.89 - 0.86	261	261	100.0	6.77	51.7	13.91	0.1057	0.0570
0.86 - 0.83	303	303	100.0	5.85	35.1	9.49	0.1396	0.0872
0.83 - 0.80	358	358	100.0	5.45	36.9	9.14	0.1331	0.0911
0.80 - 0.78	252	252	100.0	5.30	32.2	7.95	0.1462	0.1068
0.78 - 0.76	309	309	100.0	5.06	22.1	5.76	0.1964	0.1631
0.76 - 0.74	308	310	99.4	3.30	23.3	4.55	0.1900	0.2126
0.74 - 0.72	377	383	98.4	2.04	19.0	2.74	0.1938	0.3597
0.72 - 0.70	198	224	88.4	1.67	20.7	2.86	0.2106	0.3512

0.80 - 0.70	1576	1610	97.9	3.61	24.2	5.04	0.1716	0.2093
Inf - 0.70	4830	4864	99.3	9.07	120.6	21.72	0.0415	0.0338

;

```

_refine_ls_structure_factor_coef Fsqd
_refine_ls_matrix_type full
_refine_ls_weighting_scheme calc
_refine_ls_weighting_details
'calc w=1/[\s^2^(Fo^2^)+(0.0466P)^2^+0.6372P] where P=(Fo^2^+2Fc^2^)/3'
_atom_sites_solution_primary direct
_atom_sites_solution_secondary difmap
_atom_sites_solution_hydrogens geom
_refine_ls_hydrogen_treatment mixed
_refine_ls_extinction_method none
_refine_ls_extinction_coef ?
_refine_ls_number_reflns 4680
_refine_ls_number_parameters 238
_refine_ls_number_restraints 0
_refine_ls_R_factor_all 0.0545
_refine_ls_R_factor_gt 0.0336
_refine_ls_wR_factor_ref 0.0848
_refine_ls_wR_factor_gt 0.0794
_refine_ls_goodness_of_fit_ref 1.052
_refine_ls_restrained_S_all 1.052
_refine_ls_shift/su_max 0.001
_refine_ls_shift/su_mean 0.000

```

loop_

```

_atom_site_label
_atom_site_type_symbol
_atom_site_fract_x
_atom_site_fract_y
_atom_site_fract_z
_atom_site_U_iso_or_equiv
_atom_site_adp_type
_atom_site_occupancy
_atom_site_symmetry_multiplicity
_atom_site_calc_flag
_atom_site_refinement_flags
_atom_site_disorder_assembly
_atom_site_disorder_group
Br1 Br 0.250463(14) 0.023188(13) 0.535902(15) 0.03275(8) Uani 1 1 d . . .
Fe1 Fe 0.10027(2) 0.013713(16) 0.44680(2) 0.02451(8) Uani 1 1 d . . .
O1 O 0.04096(10) -0.02073(7) 0.58526(10) 0.0265(3) Uani 1 1 d . . .
O1B O 0.13729(10) 0.02019(8) 0.30339(10) 0.0282(3) Uani 1 1 d . . .
O11A O 0.07530(9) 0.13565(8) 0.44766(10) 0.0281(3) Uani 1 1 d . A .

```

O11B O 0.09843(10) -0.10657(8) 0.40870(10) 0.0328(3) Uani 1 1 d . . .
N1B N 0.14551(13) -0.05632(10) 0.26152(13) 0.0303(4) Uani 1 1 d . . .
N2 N 0.06205(12) -0.09957(10) 0.61771(12) 0.0283(4) Uani 1 1 d . . .
C1A C -0.02492(16) 0.24333(13) 0.3888(2) 0.032(3) Uani 0.688(7) 1 d PG A 1
C2A C 0.04532(13) 0.30126(17) 0.3883(3) 0.0401(10) Uani 0.688(7) 1 d PG A 1
H2A H 0.1077 0.2838 0.3897 0.048 Uiso 0.688(7) 1 calc PR A 1
C3A C 0.02436(18) 0.38468(15) 0.3857(4) 0.0587(17) Uani 0.688(7) 1 d PG A 1
H3A H 0.0724 0.4243 0.3853 0.070 Uiso 0.688(7) 1 calc PR A 1
C4A C -0.0668(2) 0.41017(12) 0.3836(3) 0.053(3) Uani 0.688(7) 1 d PG A 1
H4A H -0.0812 0.4672 0.3818 0.064 Uiso 0.688(7) 1 calc PR A 1
C5A C -0.13709(15) 0.35225(16) 0.3841(3) 0.0502(12) Uani 0.688(7) 1 d PG A 1
H5A H -0.1994 0.3697 0.3827 0.060 Uiso 0.688(7) 1 calc PR A 1
C6A C -0.11613(14) 0.26883(15) 0.3867(3) 0.0374(9) Uani 0.688(7) 1 d PG A 1
H6A H -0.1641 0.2292 0.3871 0.045 Uiso 0.688(7) 1 calc PR A 1
C1A' C -0.0242(4) 0.2453(3) 0.3935(4) 0.024(7) Uani 0.312(7) 1 d PG A 2
C2A' C 0.0294(5) 0.3026(4) 0.4475(6) 0.044(2) Uani 0.312(7) 1 d PG A 2
H2A1 H 0.0787 0.2847 0.4918 0.053 Uiso 0.312(7) 1 calc PR A 2
C3A' C 0.0108(6) 0.3861(3) 0.4369(7) 0.066(4) Uani 0.312(7) 1 d PG A 2
H3A1 H 0.0474 0.4253 0.4738 0.080 Uiso 0.312(7) 1 calc PR A 2
C4A' C -0.0613(5) 0.4124(3) 0.3722(7) 0.075(8) Uani 0.312(7) 1 d PG A 2
H4A1 H -0.0740 0.4694 0.3649 0.090 Uiso 0.312(7) 1 calc PR A 2
C5A' C -0.1149(5) 0.3551(4) 0.3181(7) 0.063(3) Uani 0.312(7) 1 d PG A 2
H5A1 H -0.1642 0.3730 0.2739 0.075 Uiso 0.312(7) 1 calc PR A 2
C6A' C -0.0963(4) 0.2716(3) 0.3287(6) 0.045(2) Uani 0.312(7) 1 d PG A 2
H6A1 H -0.1330 0.2324 0.2918 0.055 Uiso 0.312(7) 1 calc PR A 2
C1B C 0.13670(15) -0.20485(12) 0.27856(15) 0.0316(4) Uani 1 1 d . . .
C2B C 0.1766(2) -0.22146(15) 0.1858(2) 0.0532(7) Uani 1 1 d . . .
H2CA H 0.1928 -0.1776 0.1416 0.064 Uiso 1 1 calc R . .
C3B C 0.1930(2) -0.30205(16) 0.1570(2) 0.0615(8) Uani 1 1 d . . .
H3CA H 0.2216 -0.3131 0.0937 0.074 Uiso 1 1 calc R . .
C4B C 0.16837(18) -0.36565(15) 0.2188(2) 0.0496(6) Uani 1 1 d . . .
H4CA H 0.1804 -0.4208 0.1989 0.059 Uiso 1 1 calc R . .
C5B C 0.1270(3) -0.35007(16) 0.3078(2) 0.0805(11) Uani 1 1 d . . .
H5CA H 0.1096 -0.3945 0.3507 0.097 Uiso 1 1 calc R . .
C6B C 0.1092(3) -0.26918(15) 0.3382(2) 0.0715(10) Uani 1 1 d . . .
H6CA H 0.0781 -0.2589 0.4001 0.086 Uiso 1 1 calc R . .
C11A C -0.00135(13) 0.15712(12) 0.40631(13) 0.0254(4) Uani 1 1 d . . .
C11B C 0.12487(14) -0.12041(12) 0.31764(14) 0.0282(4) Uani 1 1 d . . .
H2 H 0.1153(19) -0.1035(18) 0.653(2) 0.063(9) Uiso 1 1 d . . .
H3 H 0.1581(16) -0.0547(15) 0.2002(19) 0.039(7) Uiso 1 1 d . . .

loop_

_atom_site_aniso_label
_atom_site_aniso_U_11
_atom_site_aniso_U_22
_atom_site_aniso_U_33
_atom_site_aniso_U_23
_atom_site_aniso_U_13

_atom_site_aniso_U_12

Br1 0.02986(13) 0.04159(14) 0.02690(12) 0.00371(8) 0.00218(8) 0.00466(8)
 Fe1 0.03259(17) 0.02071(15) 0.02038(14) -0.00111(10) 0.00301(11) 0.00040(11)
 O1 0.0350(8) 0.0221(7) 0.0224(6) 0.0015(5) 0.0015(5) -0.0033(6)
 O1B 0.0423(9) 0.0207(7) 0.0218(7) -0.0013(5) 0.0030(6) 0.0028(6)
 O11A 0.0278(7) 0.0236(7) 0.0325(7) -0.0034(5) -0.0030(6) 0.0021(6)
 O11B 0.0519(9) 0.0228(7) 0.0241(7) -0.0019(5) 0.0092(6) 0.0010(6)
 N1B 0.0475(11) 0.0240(9) 0.0194(8) -0.0012(6) 0.0019(7) 0.0073(8)
 N2 0.0337(9) 0.0260(9) 0.0247(8) 0.0030(6) -0.0039(7) -0.0025(7)
 C1A 0.029(7) 0.039(6) 0.028(5) 0.000(4) 0.003(4) -0.005(4)
 C2A 0.0321(19) 0.0273(17) 0.060(3) 0.0031(17) -0.0062(17) 0.0006(14)
 C3A 0.041(3) 0.032(2) 0.101(5) 0.005(2) -0.019(3) -0.0057(19)
 C4A 0.046(5) 0.027(5) 0.086(5) 0.005(4) -0.006(4) 0.011(4)
 C5A 0.032(2) 0.042(2) 0.076(3) -0.005(2) -0.0106(19) 0.0116(17)
 C6A 0.0311(19) 0.0317(17) 0.049(2) -0.0014(16) -0.0041(15) -0.0002(14)
 C1A' 0.030(14) 0.010(8) 0.033(11) 0.005(6) -0.005(8) 0.009(8)
 C2A' 0.046(5) 0.029(4) 0.059(6) -0.005(4) -0.001(4) 0.001(3)
 C3A' 0.048(6) 0.023(5) 0.127(13) -0.002(5) 0.004(7) -0.003(4)
 C4A' 0.059(15) 0.029(13) 0.14(2) 0.013(11) -0.018(13) 0.000(11)
 C5A' 0.032(5) 0.041(5) 0.115(10) 0.027(6) -0.004(5) 0.013(4)
 C6A' 0.025(4) 0.039(5) 0.072(7) 0.019(4) -0.010(4) -0.004(3)
 C1B 0.0413(12) 0.0258(10) 0.0273(10) -0.0034(8) -0.0026(8) 0.0050(9)
 C2B 0.082(2) 0.0314(12) 0.0477(15) -0.0110(10) 0.0283(13) -0.0029(13)
 C3B 0.086(2) 0.0387(14) 0.0616(18) -0.0196(12) 0.0326(16) -0.0026(14)
 C4B 0.0617(17) 0.0286(12) 0.0581(16) -0.0142(11) -0.0038(12) 0.0079(11)
 C5B 0.165(4) 0.0249(13) 0.0530(17) 0.0037(11) 0.0282(19) 0.0096(17)
 C6B 0.146(3) 0.0318(14) 0.0384(14) -0.0005(11) 0.0304(16) 0.0094(16)
 C11A 0.0307(10) 0.0255(10) 0.0201(9) -0.0012(7) 0.0033(7) -0.0007(8)
 C11B 0.0352(11) 0.0256(10) 0.0238(9) -0.0012(7) -0.0007(8) 0.0057(8)

_geom_special_details

;

All esds (except the esd in the dihedral angle between two l.s. planes) are estimated using the full covariance matrix. The cell esds are taken into account individually in the estimation of esds in distances, angles and torsion angles; correlations between esds in cell parameters are only used when they are defined by crystal symmetry. An approximate (isotropic) treatment of cell esds is used for estimating esds involving l.s. planes.

;

loop_

_geom_bond_atom_site_label_1
 _geom_bond_atom_site_label_2
 _geom_bond_distance
 _geom_bond_site_symmetry_2
 _geom_bond_publ_flag
 Br1 Fe1 2.4448(4) . ?
 Fe1 O1B 1.9554(13) . ?

Fe1 O11A 2.0152(13) . ?
Fe1 O11B 2.0166(13) . ?
Fe1 O1 2.0873(15) 5_556 ?
Fe1 O1 2.0930(13) . ?
O1 N2 1.380(2) . ?
O1 Fe1 2.0873(15) 5_556 ?
O1B N1B 1.364(2) . ?
O11A C11A 1.271(2) . ?
O11B C11B 1.274(2) . ?
N1B C11B 1.311(3) . ?
N1B H3 0.82(2) . ?
N2 C11A 1.317(2) 5_556 ?
N2 H2 0.89(3) . ?
C1A C2A 1.3900 . ?
C1A C6A 1.3900 . ?
C1A C11A 1.459(3) . ?
C2A C3A 1.3900 . ?
C2A H2A 0.9500 . ?
C3A C4A 1.3900 . ?
C3A H3A 0.9500 . ?
C4A C5A 1.3900 . ?
C4A H4A 0.9500 . ?
C5A C6A 1.3900 . ?
C5A H5A 0.9500 . ?
C6A H6A 0.9500 . ?
C1A' C2A' 1.3900 . ?
C1A' C6A' 1.3900 . ?
C1A' C11A 1.480(4) . ?
C2A' C3A' 1.3900 . ?
C2A' H2A1 0.9500 . ?
C3A' C4A' 1.3900 . ?
C3A' H3A1 0.9500 . ?
C4A' C5A' 1.3900 . ?
C4A' H4A1 0.9500 . ?
C5A' C6A' 1.3900 . ?
C5A' H5A1 0.9500 . ?
C6A' H6A1 0.9500 . ?
C1B C6B 1.368(3) . ?
C1B C2B 1.378(3) . ?
C1B C11B 1.475(3) . ?
C2B C3B 1.385(3) . ?
C2B H2CA 0.9500 . ?
C3B C4B 1.362(4) . ?
C3B H3CA 0.9500 . ?
C4B C5B 1.344(4) . ?
C4B H4CA 0.9500 . ?
C5B C6B 1.399(4) . ?
C5B H5CA 0.9500 . ?

C6B H6CA 0.9500 . ?
C11A N2 1.317(2) 5_556 ?

loop_
_geom_angle_atom_site_label_1
_geom_angle_atom_site_label_2
_geom_angle_atom_site_label_3
_geom_angle
_geom_angle_site_symmetry_1
_geom_angle_site_symmetry_3
_geom_angle_publ_flag
O1B Fe1 O11A 90.43(5) . . ?
O1B Fe1 O11B 79.69(5) . . ?
O11A Fe1 O11B 162.54(6) . . ?
O1B Fe1 O1 96.13(6) . 5_556 ?
O11A Fe1 O1 76.75(5) . 5_556 ?
O11B Fe1 O1 89.93(5) . 5_556 ?
O1B Fe1 O1 164.55(5) . . ?
O11A Fe1 O1 100.31(5) . . ?
O11B Fe1 O1 87.03(5) . . ?
O1 Fe1 O1 75.83(6) 5_556 . ?
O1B Fe1 Br1 100.20(5) . . ?
O11A Fe1 Br1 95.40(4) . . ?
O11B Fe1 Br1 100.46(4) . . ?
O1 Fe1 Br1 161.95(4) 5_556 . ?
O1 Fe1 Br1 89.90(4) . . ?
N2 O1 Fe1 108.63(11) . 5_556 ?
N2 O1 Fe1 114.59(11) . . ?
Fe1 O1 Fe1 104.17(6) 5_556 . ?
N1B O1B Fe1 111.09(11) . . ?
C11A O11A Fe1 115.07(12) . . ?
C11B O11B Fe1 113.35(12) . . ?
C11B N1B O1B 118.62(16) . . ?
C11B N1B H3 128.7(17) . . ?
O1B N1B H3 112.4(17) . . ?
C11A N2 O1 116.51(16) 5_556 . ?
C11A N2 H2 129.5(19) 5_556 . ?
O1 N2 H2 113.9(19) . . ?
C2A C1A C6A 120.0 . . ?
C2A C1A C11A 118.82(18) . . ?
C6A C1A C11A 120.60(17) . . ?
C1A C2A C3A 120.0 . . ?
C1A C2A H2A 120.0 . . ?
C3A C2A H2A 120.0 . . ?
C4A C3A C2A 120.0 . . ?
C4A C3A H3A 120.0 . . ?
C2A C3A H3A 120.0 . . ?
C5A C4A C3A 120.0 . . ?

C5A C4A H4A 120.0 .. ?
C3A C4A H4A 120.0 .. ?
C4A C5A C6A 120.0 .. ?
C4A C5A H5A 120.0 .. ?
C6A C5A H5A 120.0 .. ?
C5A C6A C1A 120.0 .. ?
C5A C6A H6A 120.0 .. ?
C1A C6A H6A 120.0 .. ?
C2A' C1A' C6A' 120.0 .. ?
C2A' C1A' C11A 118.2(4) .. ?
C6A' C1A' C11A 121.8(4) .. ?
C3A' C2A' C1A' 120.0 .. ?
C3A' C2A' H2A1 120.0 .. ?
C1A' C2A' H2A1 120.0 .. ?
C2A' C3A' C4A' 120.0 .. ?
C2A' C3A' H3A1 120.0 .. ?
C4A' C3A' H3A1 120.0 .. ?
C3A' C4A' C5A' 120.0 .. ?
C3A' C4A' H4A1 120.0 .. ?
C5A' C4A' H4A1 120.0 .. ?
C6A' C5A' C4A' 120.0 .. ?
C6A' C5A' H5A1 120.0 .. ?
C4A' C5A' H5A1 120.0 .. ?
C5A' C6A' C1A' 120.0 .. ?
C5A' C6A' H6A1 120.0 .. ?
C1A' C6A' H6A1 120.0 .. ?
C6B C1B C2B 118.8(2) .. ?
C6B C1B C11B 118.55(19) .. ?
C2B C1B C11B 122.6(2) .. ?
C1B C2B C3B 120.1(2) .. ?
C1B C2B H2CA 120.0 .. ?
C3B C2B H2CA 120.0 .. ?
C4B C3B C2B 120.6(2) .. ?
C4B C3B H3CA 119.7 .. ?
C2B C3B H3CA 119.7 .. ?
C5B C4B C3B 119.7(2) .. ?
C5B C4B H4CA 120.1 .. ?
C3B C4B H4CA 120.1 .. ?
C4B C5B C6B 120.7(3) .. ?
C4B C5B H5CA 119.6 .. ?
C6B C5B H5CA 119.6 .. ?
C1B C6B C5B 120.0(2) .. ?
C1B C6B H6CA 120.0 .. ?
C5B C6B H6CA 120.0 .. ?
O11A C11A N2 118.54(17) . 5_556 ?
O11A C11A C1A 121.89(18) .. ?
N2 C11A C1A 119.52(19) 5_556 . ?
O11A C11A C1A' 120.3(3) .. ?

N2 C11A C1A' 121.0(3) 5_556 . ?
C1A C11A C1A' 2.6(3) . . ?
O11B C11B N1B 117.11(17) . . ?
O11B C11B C1B 121.66(17) . . ?
N1B C11B C1B 121.15(17) . . ?

_diffn_measured_fraction_theta_max 0.993
_diffn_reflns_theta_full 30.57
_diffn_measured_fraction_theta_full 0.993
_refine_diff_density_max 0.695
_refine_diff_density_min -0.319
_refine_diff_density_rms 0.089

Crystal Data for Ligand 9

Table 1. Crystal data and structure refinement for pt7034.

Contact Fraser J. White, f.j.white@sms.ed.ac.uk

A. CRYSTAL DATA

Empirical formula	C12 H17 N O2 S
	C12 H17 N O2 S
Formula weight	239.33
Wavelength	0.71073 Å
Temperature	150(2) K
Crystal system	Monoclinic
Space group	P 21/c
Unit cell dimensions	a = 8.0333(4) Å alpha = 90 deg.
	b = 15.6823(6) Å beta = 96.860(3) deg.
	c = 9.8325(4) Å gamma = 90 deg.

Volume	1229.84 (9) Å ³
Number of reflections for cell	3535 (2.4575 < theta < 28.38 deg.)
Z	4
Density (calculated)	1.293 Mg/m ³
Absorption coefficient	0.249 mm ⁻¹
F(000)	512

B. DATA COLLECTION

Crystal description	colourless block
Crystal size	0.43 x 0.20 x 0.12 mm
Instrument	Bruker Smart Apex CCD
Theta range for data collection	2.46 to 29.66 deg.
Index ranges	-11<=h<=11, -21<=k<=20, -13<=l<=13

Reflections collected	9829
Independent reflections	3247 [R(int) = 0.0303]
Scan type	Omega Scans (cosmo)
Absorption correction	Semi-empirical from equivalents (Tmin= 0.8199, Tmax=0.9697)
C. SOLUTION AND REFINEMENT.	
Solution	direct (Shelxs Sheldrick)
Refinement type	Full-matrix least-squares on F ²
Program used for refinement	SHELXL-97
Hydrogen atom placement	geom
Hydrogen atom treatment	mixed
Data / restraints / parameters	3247/ 0/ 148

Goodness-of-fit on F^2 1.033

Conventional R [$F > 4\sigma(F)$] $R_1 = 0.0417$ [2619 data]

Rw 0.1119

Final maximum Δ/σ 0.000

Weighting scheme

calc $w = 1 / [\sigma^2(F_0^2) + (0.0660P)^2 + 0.1724P]$ where $P = (F_0^2 + 2F_c^2) / 3$

Largest diff. peak and hole 0.381 and $-0.264 \text{ e.}\text{\AA}^{-3}$

Table 2. Atomic coordinates ($\times 10^4$) and equivalent isotropic displacement parameters ($\text{\AA}^2 \times 10^3$) for pt7034. $U(\text{eq})$ is defined as one third of the trace of the orthogonalized U_{ij} tensor.

	x	y	z	$U(\text{eq})$
C(1)	7849(2)	264(1)	4015(1)	22(1)
C(2)	8822(2)	-6(1)	3018(1)	24(1)
C(3)	9257(2)	-856(1)	2916(1)	23(1)
C(4)	8722(2)	-1456(1)	3816(1)	19(1)
C(5)	7751(2)	-1190(1)	4822(1)	22(1)
C(6)	7319(2)	-336(1)	4916(1)	23(1)
C(11)	7372(2)	1191(1)	4081(1)	26(1)
S(12)	5643(1)	1403(1)	2760(1)	27(1)
C(13)	5861(2)	2543(1)	2555(1)	29(1)
C(14)	5574(2)	3078(1)	3789(2)	35(1)
C(15)	5676(2)	4025(1)	3478(2)	37(1)
C(41)	9193(2)	-2368(1)	3626(1)	20(1)
O(42)	9484(1)	-2656(1)	2511(1)	27(1)
N(43)	9256(2)	-2854(1)	4755(1)	24(1)

O (44)	9748 (1)	-3703 (1)	4673 (1)	22 (1)
C (45)	8296 (2)	-4223 (1)	4301 (2)	28 (1)

Table 3. Bond lengths [Å] and angles [deg] for pt7034.

C (1) - C (2)	1.3906 (19)
C (1) - C (6)	1.3933 (19)
C (1) - C (11)	1.5064 (18)
C (2) - C (3)	1.3845 (19)
C (2) - H (2)	0.9500
C (3) - C (4)	1.3942 (18)
C (3) - H (3)	0.9500
C (4) - C (5)	1.3952 (18)
C (4) - C (41)	1.4965 (18)
C (5) - C (6)	1.3899 (19)
C (5) - H (5)	0.9500
C (6) - H (6)	0.9500
C (11) - S (12)	1.8156 (14)
C (11) - H (11A)	0.9900
C (11) - H (11B)	0.9900
S (12) - C (13)	1.8103 (15)
C (13) - C (14)	1.515 (2)
C (13) - H (13A)	0.9900
C (13) - H (13B)	0.9900
C (14) - C (15)	1.521 (2)

C (14) -H (14A)	0.9900
C (14) -H (14B)	0.9900
C (15) -H (15A)	0.9800
C (15) -H (15B)	0.9800
C (15) -H (15C)	0.9800
C (41) -O (42)	1.2333 (15)
C (41) -N (43)	1.3426 (16)
N (43) -O (44)	1.3938 (14)
N (43) -H (43)	0.828 (16)
O (44) -C (45)	1.4344 (16)
C (45) -H (45A)	0.9800
C (45) -H (45B)	0.9800
C (45) -H (45C)	0.9800
C (2) -C (1) -C (6)	118.83 (12)
C (2) -C (1) -C (11)	119.44 (12)
C (6) -C (1) -C (11)	121.72 (13)
C (3) -C (2) -C (1)	120.84 (12)
C (3) -C (2) -H (2)	119.6
C (1) -C (2) -H (2)	119.6
C (2) -C (3) -C (4)	120.27 (12)
C (2) -C (3) -H (3)	119.9
C (4) -C (3) -H (3)	119.9
C (3) -C (4) -C (5)	119.30 (12)

C (3) -C (4) -C (41)	117.66 (12)
C (5) -C (4) -C (41)	123.02 (12)
C (6) -C (5) -C (4)	120.00 (12)
C (6) -C (5) -H (5)	120.0
C (4) -C (5) -H (5)	120.0
C (5) -C (6) -C (1)	120.76 (12)
C (5) -C (6) -H (6)	119.6
C (1) -C (6) -H (6)	119.6
C (1) -C (11) -S (12)	108.81 (9)
C (1) -C (11) -H (11A)	109.9
S (12) -C (11) -H (11A)	109.9
C (1) -C (11) -H (11B)	109.9
S (12) -C (11) -H (11B)	109.9
H (11A) -C (11) -H (11B)	108.3
C (13) -S (12) -C (11)	100.61 (6)
C (14) -C (13) -S (12)	115.59 (10)
C (14) -C (13) -H (13A)	108.4
S (12) -C (13) -H (13A)	108.4
C (14) -C (13) -H (13B)	108.4
S (12) -C (13) -H (13B)	108.4
H (13A) -C (13) -H (13B)	107.4
C (13) -C (14) -C (15)	111.26 (13)
C (13) -C (14) -H (14A)	109.4
C (15) -C (14) -H (14A)	109.4

C (13) -C (14) -H (14B)	109.4
C (15) -C (14) -H (14B)	109.4
H (14A) -C (14) -H (14B)	108.0
C (14) -C (15) -H (15A)	109.5
C (14) -C (15) -H (15B)	109.5
H (15A) -C (15) -H (15B)	109.5
C (14) -C (15) -H (15C)	109.5
H (15A) -C (15) -H (15C)	109.5
H (15B) -C (15) -H (15C)	109.5
O (42) -C (41) -N (43)	122.31 (12)
O (42) -C (41) -C (4)	122.54 (11)
N (43) -C (41) -C (4)	115.14 (11)
C (41) -N (43) -O (44)	118.57 (11)
C (41) -N (43) -H (43)	124.8 (12)
O (44) -N (43) -H (43)	115.2 (12)
N (43) -O (44) -C (45)	109.26 (10)
O (44) -C (45) -H (45A)	109.5
O (44) -C (45) -H (45B)	109.5
H (45A) -C (45) -H (45B)	109.5
O (44) -C (45) -H (45C)	109.5
H (45A) -C (45) -H (45C)	109.5
H (45B) -C (45) -H (45C)	109.5

Symmetry transformations used to generate equivalent atoms:

Table 4. Anisotropic displacement parameters ($\text{\AA}^2 \times 10^3$) for pt7034.

The anisotropic displacement factor exponent takes the form:

$$-2 \pi^2 [h^2 a^{*2} U_{11} + \dots + 2 h k a^* b^* U_{12}]$$

	U ₁₁	U ₂₂	U ₃₃	U ₂₃	U ₁₃	U ₁₂
C(1)	25(1)	18(1)	21(1)	-1(1)	-3(1)	0(1)
C(2)	31(1)	21(1)	23(1)	4(1)	5(1)	-3(1)
C(3)	29(1)	23(1)	19(1)	-1(1)	7(1)	-1(1)
C(4)	23(1)	19(1)	16(1)	-1(1)	1(1)	0(1)
C(5)	26(1)	21(1)	19(1)	1(1)	4(1)	0(1)
C(6)	27(1)	23(1)	20(1)	-3(1)	4(1)	2(1)
C(11)	32(1)	19(1)	24(1)	-2(1)	-2(1)	1(1)
S(12)	28(1)	21(1)	31(1)	-1(1)	-3(1)	0(1)
C(13)	36(1)	25(1)	26(1)	4(1)	3(1)	4(1)
C(14)	45(1)	25(1)	34(1)	0(1)	11(1)	3(1)
C(15)	41(1)	22(1)	49(1)	-2(1)	6(1)	-1(1)
C(41)	23(1)	19(1)	17(1)	-1(1)	2(1)	-1(1)
O(42)	41(1)	23(1)	17(1)	0(1)	7(1)	5(1)
N(43)	41(1)	16(1)	15(1)	-2(1)	4(1)	4(1)

O(44)	28(1)	16(1)	21(1)	0(1)	2(1)	2(1)
C(45)	30(1)	22(1)	33(1)	-2(1)	0(1)	-2(1)

Table 5. Hydrogen coordinates ($\times 10^4$) and isotropic displacement parameters ($\text{\AA}^2 \times 10^3$) for pt7034.

	x	y	z	U (eq)
H(2)	9193	398	2400	29
H(3)	9923	-1031	2230	28
H(5)	7385	-1594	5444	26
H(6)	6655	-159	5602	28
H(11A)	8343	1554	3937	31
H(11B)	7034	1324	4994	31
H(13A)	7005	2661	2323	35
H(13B)	5059	2729	1768	35
H(14A)	6427	2932	4565	41
H(14B)	4456	2946	4063	41
H(15A)	5474	4355	4289	56
H(15B)	4828	4171	2713	56
H(15C)	6793	4160	3231	56
H(43)	9230 (20)	-2670 (11)	5541 (17)	29
H(45A)	8638	-4820	4241	43

H (45B)	7733	-4037	3411	43
H (45C)	7525	-4167	4997	43